Functional Analysis of a Reticulon Protein from *Arabidopsis thaliana*

A thesis submitted to
The University of Warwick
for the degree of
Doctor of Philosophy

Nicholas Joseph Tolley
Department of Biological Sciences
University of Warwick
March 2010

Contents

List of figures

List of tables

List of abbreviations

Å	Angstrom(s)
AAA	ATPases associated with diverse cellular activites
Acetosyringone	3,5-dimethoxy-4-hydroxy-acetophenone
AFVY	C-terminal vacuolar sorting signal of phaseolin
ALS	Amyotrophic lateral sclerosis
AMV	Avian myeloblastosis virus
AP-2	Clathrin adaptor protein complex 2
APS	Ammonium persulphate
6-BAP	6-benzylaminopurine
BACE-1	β-site of APP cleaving enzyme, β-Secretase
BAP	Bacterial alkaline phosphatase
ATP	Adenosine triphosphate
BFA	Brefeldin A
BiFC	Bimolecular fluorescence complementation
BiP	Binding protein
BSA	Bovine serum albumin
CaMV	Cauliflower mosaic virus
CDC48	Cell division control protein 48
cDNA	Complementary DNA
CLIMP-63	Cytoskeleton linking membrane protein – 63 kDa
Col-0	Arabidopsis thaliana ecotype Columbia
COPI	Coat protein complex I
COPII	Coat protein complex II
C-terminal	Carboxy-terminal
$DiOC_6$	3,3'-dihexyloxacarbocyanine iodide
DMSO	Dimethyl sulfoxide
DNA	Deoxyribonucleic acid
dNTP	Deoxyribonucleoside 5'-triphosphate
dsDNA	Double-stranded DNA
DTT	Dithiothreitol
EDTA	Diaminoethane-tetraacetic acid
ECL	Enhanced chemiluminescence
EM	Electron microscopy
ER	Endoplasmic reticulum
ERAD	ER-associated degradation
ERES	ER-exit sites
FRAP	Fluorescence recovery after photobleaching
g	Gram(s)
g	Unit of gravitational field
GC	Gas chromatography
GEF	Guanine nucleotide exchange factor
GFP	Green fluorescent protein
GST	Glutathione-S-transferase
GTP	Guanosine triphosphate
h	Hour(s)
HEPES	4-(2-hydroxyethyl)-1-piperazineethanesulfonic acid
H/KDEL	Tetrapeptide ER-retrieval motif

Hsc	Heat shock cognate
Hsp	Heat shock protein
IgG	Immunoglobulin class G
IRE1	Inositol requirement 1
kb	Kilobase(s)
kDa	Kilo-Dalton(s)
KKXX	Tetrapeptide ER-retrieval motif
l	Litre(s)
LB	Luria-Bertani
LINC	Linker of the nucleoskeleton and cytoskeleton
M	Molar
MeOH	Methanol
MES	Morpholineethansulfonic acid monohydrate
min	Minute(s)
mg	Milligram(s)
ml	Millilitre(s)
mm	Millimetre(s)
mM	Millimolar
MS	Murashige and Skoog
NAA	α-naphtalenacetic acid
NgR	Nogo-66 receptor
Nogo	Rtn4 (synonym)
Nogo-66	Hydrophilip loop region of Rtn4
ng	Nanogram(s)
nm	Nanometre(s)
NSF	N-ethylmaleimide sensitive factor
N-terminal	Amino-terminal
OCS	Octopine synthase
OD	Optical density
OST	Oligosaccharyltransferase
PAC	Precursor accumulating vesicles
PAGE	Polyacrylamide electrophoresis
pah	Phosphatidic acid hydrolase
PCR	Polymerase chain reaction
PBS	Phosphate buffered saline
PDI	Protein disulfide isomerase
PEG	Polyethylene glycol
PK	Proteinase K
pmole	Pico-mole(s)
psi	Pounds per square inch
PSV	Protein storage vacuole
PVDF	Polyvinylidene fluoride
PVP	Polyvinylpyrrolidone
RER	Rough ER
RER1	Retention in ER 1 protein
RFP	Red fluorescent protein
RHD	Reticulon homology domain
RHD3	Root hair defective 3
RNA	Ribonucleic acid
RoGFP	Redox sensitive GFP

rpm	Revolution(s) per minute
RTN	Reticulon
RTNL	Reticulon-like
RTNLB	Reticulon-like, non-chordate taxa, class B
RT-PCR	Reverse transcriptase PCR
s	Second(s)
S	Svedberg unit, sedimentation coefficient
SDS	Sodium dodecyl sulphate
SDW	Sterile distilled water
SER	Smooth ER
SNAREs	Soluble NSF attachment proteins receptors
SP	Signal peptide
SRI	*Nicotiana tabacum* cv. Petit Havana
SRP	Signal recognition particle
SR	SRP-receptor
ST	Sialyl-transferase
SUN	Sad1p, UNC-84
TAG	Triacylglycerol
TBE	Tris, Borate, EDTA
TCM	Tris, Calcium, Magnesium
TEMED	NNN'N'-tetramethylethylenediamine
TIP	Tonoplast intrinsic protein
T_m	Melting temperature
TM	Transmembrane
Tris	Tris (hydroxymethyl) aminomethane
Triton X-100	Iso-octylphenoxypolyethoxethanol
Tween 20	Polyoxyethylenesorbitan monolaurate
U	Unit(s)
UPR	Unfolded protein response
V	Volt(s)
v/v	Volume per volume
w/v	Weight per volume
YFP	Yellow fluorescent protein
YC	C-terminal fragment of YFP, residues 155-239
YN	N-terminal fragment of YFP, residues 1-154
°C	Degrees celsius
µCi	Microcurie(s)
µg	Microgram(s)
µl	Microlitre(s)
µM	Micromolar
µg	Microgram(s)
×*g*	Times greater than gravity
%	Percent
~	Approximately

List of amino acid abbreviations

Amino Acid	Single letter code	Abbreviation
Alanine	A	Ala
Cysteine	C	Cys
Aspartic acid	D	Asp
Glutamic acid	E	Glu
Phenylalanine	F	Phe
Glycine	G	Gly
Histidine	H	His
Isoleucine	I	Ile
Lysine	K	Lys
Leucine	L	Leu
Methionine	M	Met
Asparagine	N	Asn
Proline	P	Pro
Glutamine	Q	Gln
Arginine	R	Arg
Serine	S	Ser
Threonine	T	Thr
Valine	V	Val
Tryptophan	W	Trp
Tyrosine	Y	Tyr

Acknowledgements

I would like to thank my supervisor, Dr Lorenzo Frigerio, for his support and guidance throughout the course of this project. I would also like to thank all of those in the Molecular Cell Biology Lab C46 past and present, especially Christian Craddock, James Nuttall, Paul Hunter and Richard Marshall, for their training and their patience. Thanks to Sara Di Benedetto, Alice De Porcellinis, Alessandro Consonni, Philip Hart, Stefano Gattolin, Mathias Sorieul and Hannah Lee for making my time in (and out of) the lab so enjoyable.

I would like to thank Chris Hawes and Imogen Sparkes at Oxford-Brookes University and Peter Eastmond at Warwick HRI for their collaborative efforts.

Finally, I would to thank my family for their continuous support and most of all, I would like to dearly thank my fiancée Eilish McCann for her endless encouragement, and for traversing the PhD process with me.

Declaration

The data presented in this thesis represent original work conducted by myself, unless otherwise specified, under the supervision of Dr Lorenzo Frigerio at the University of Warwick. This research was funded by a BBSRC studentship. All sources of information have been acknowledged by means of a reference. None of this work has been used in any previous application for a degree.

Some of the work presented in this thesis has been published in the following journals:

Tolley, N., Sparkes, I. A., Hunter, P. R., Craddock, C. P., Nuttall, J., Roberts, L. M., Hawes, C., Pedrazzini, E. and Frigerio, L. (2008) Overexpression of a plant reticulon remodels the lumen of the cortical endoplasmic reticulum but does not perturb protein transport. *Traffic* **9**:94-102.

Sparkes, I. A., Frigerio, L., Tolley, N. and Hawes, C. (2009) The plant endoplasmic reticulum: a cell-wide web. *Biochem J* **423**(2):145-55.

Sparkes, I., Tolley, N., Aller, I., Svozil, J., Osterrieder, A., Botchway, S., Mueller, C., Frigerio, L. and Hawes, C. (2010) Five plant reticulon isoforms share ER localisation, topology, ER membrane shaping properties and the ability to form both homo- and heterotypic interactions. *Plant Cell* **In press**.

Tolley, N., Sparkes, I, Craddock, C. P., Eastmond, P. J., Hawes, C. and Frigerio, L. (2010) Transmembrane domain length is responsible for the ability of a plant reticulon to shape ER tubules in vivo. **Submitted**.

Nicholas Joseph Tolley

March 2010

Summary

While our knowledge of the functional properties of eukaryotic cellular organelles is quite comprehensive, the mechanisms by which organelles achieve their varied shapes remain poorly understood. By categorising the components which contribute to the architecture of the cell, relationships between structure and function can be established.

Many mechanisms have been proposed which try to account for the shape and structure of complex organelles such as mitochondria and, more recently, the endoplasmic reticulum (ER); an organelle which comprises multiple domains, both structurally and functionally.

Recently, a class of membrane proteins – the reticulons – have received renewed attention as they are thought to shape the tubular ER through their wedge-like insertion into the lipid bilayer and the formation of scaffolds through homo- and hetero-oligomerisation. Reticulons and reticulon-like proteins have been implicated in many cellular processes and have key roles in many disease states – for which they have received much attention.

As much of the research on reticulons has focused on mammals and yeast, the functions of reticulons in plants are poorly characterised. The model organism, *Arabidopsis thaliana*, contains 21 reticulon genes, expressed throughout all tissues and developmental stages of the plant.

This thesis focuses on the ER-shaping properties of a seed-specific reticulon - RTNLB13. Its expression and unique topology were found to contribute to the formation of ER tubules in plants by inducing curvature in the ER membrane. RTNLB13 is restricted to tubular ER and its over-expression induces constrictions within the ER membrane which affects both soluble and membrane protein diffusion. RTNLB13 sits in a ‘w’ conformation in the membrane with its N- and C-termini facing the cytosol. The length and orientation of its transmembrane domains play an important role in protein localisation and inducing membrane curvature. In its native organism, *Arabidopsis thaliana*, RTNLB13 is expressed during the late stages of embryonic maturation, although a *rtn13* knockout yielded no observable phenotype.

Chapter 1: Introduction

1.1 Preface

The endoplasmic reticulum (ER) is one of the largest organelles in the eukaryotic cell and is continuous with the nuclear envelope, forming an intricate network of sheets and tubules. It can be divided into 'rough' and 'smooth' ER, and is responsible for protein synthesis, folding, modification, quality control, degradation and export, and is also responsible for lipid metabolism and calcium homeostasis. It is the port of entry for the secretory pathway, and all proteins destined to be secreted or targeted to the secretory pathway pass through the ER. It is in contact with many other organelles which may facilitate the exchange of lipids and the delivery of proteins.

Early work on the ER began in 1943, when, through the use of ultracentrifugation, Albert Claude separated a fraction termed 'microsomes' (Claude, 1943). It was only when cell sections were viewed using electron microscopy (EM) in 1945 that Claude, along with Keith Porter and Ernest Fullham recognised a 'connected system of lace-like reticulum' (Porter *et al*., 1945). The name 'endoplasmic reticulum' was coined by Porter in 1952 and it was noticed that microsomes were more prevalent in cells actively synthesising proteins. Porter also noted the close proximity of the ER to the nuclear envelope and proposed that they were continuous with one another. Similarly, he described how the smooth ER seemed to merge with the Golgi, and how the ER appeared to operate as part of a larger system.

Although much research has been carried out on the ER since its discovery, many questions remain. Why does the ER display this unique reticular shape? It has been proposed (based on EM observation) that the ER can be divided into several subdomains (Staehelin, 1997), although the extent and functional significance of this subcompartmentalisation remains to be established. The fluorescent reporter GFP-HDEL highlights the lumen of the ER (Haseloff *et al*., 1997), and does not seem to discriminate between different domains, including the nuclear envelope. A more obvious and less extensive morphological distinction can be made between reticular and cisternal ER (Sparkes *et al*., 2010). This distinction is likely to depend on the membrane protein and lipid composition of the ER. A class of membrane proteins that regulate the shape of the ER – the reticulons - is the focus of the work presented in this thesis.

1.2 Functions of the endoplasmic reticulum

This introduction is primarily designed to discuss the shape of the ER and the factors which are thought to contribute to this. The functions of the ER are deliberately discussed in brief, only in order to relate ER structure to its function. Where possible, the description of the ER is specific to plants, and descriptions of eukaryotic, mammalian or yeast systems are clearly indicated in the text.

1.2.1 Protein synthesis

Eukaryotic cells have developed specific systems which allow them to import proteins from the cytosol into the ER. Newly synthesised polypeptides are recognised in the cytosol, then targeted to the ER membrane and recognised by specific components on the surface of the ER. These proteins are then translocated across the membrane (Palade, 1975) into the lumen, or laterally into the membrane of the ER.

All soluble proteins destined to reside in the cytosol are synthesised by 'free' ribosomes. During protein synthesis, cytosolic proteins interact with a variety of molecular chaperones that guide the folding process, such as Hsp70 and chaperonins (Hartl & Hayer-Hartl, 2002).

The studded appearance of ribosomes attached to the surface of the ER has led to the classification of a domain known as 'rough' ER. The binding of ribosomes to the surface of the ER is thought to induce flat sheeted regions (Puhka *et al*., 2007). ER which is not studded with ribosomes is simply known as 'smooth' ER and is thought to be the site of lipid metabolism and protein export from the ER. However, the simplicity of these labels hardly reflects the complex nature of this organelle.

Proteins destined for secretion or residence within the secretory pathway are translocated into the lumen of the ER, upon which the proteins are folded and modified by virtue of ER-resident chaperones and the oxidising environment of the ER lumen. For this process to happen, nascent proteins carry a specific signal at their N-terminus (Blobel & Sabatini, 1971), termed the signal peptide (SP), which is

recognised by a signal recognition particle (SRP) while the protein is actively being synthesised. The SRP directs the ribosome-nascent peptide complex to the translocation pore within the membrane of the ER, allowing transport into the lumen. The SRP binds to both the signal peptide of the nascent protein and the large subunit of the ribosome, causing a pause in protein synthesis (Lauring *et al*., 1995; Halic *et al*., 2004), while the SP-SRP complex is delivered to the translocation pore where it is recognised by the SRP-receptor (SR) on the membrane of the ER and subsequently the signal peptide is transferred from the SRP to the translocation site (Grudnik *et al*., 2009).

This process is common to most eukaryotic organisms and is known as co-translational translocation. Although not well characterised in plants, in several instances proteins can be synthesised fully and released from the ribosome, before being targeted to the ER membrane for translocation. This post-translational pathway is thought to operate to some extent in all eukaryotes (Rapoport, 2007).

The translocation pore consists of a heterotrimeric protein complex composed of Sec61α, Sec61β and Sec61γ. The Sec61α subunit forms the aqueous channel (Mothes *et al*., 1994) and is divided into two halves, with the joining region in between serving as a hinge region which forms a lateral gate – essential for the insertion of transmembrane domains into the lipid bilayer. The Sec61γ subunit is located at the hinge region of Sec61α and links the two halves of Sec61α at the back by extending one transmembrane segment diagonally across their interface. The dispensable Sec61β subunit lies at the periphery of the complex and its role is less well defined (Becker *et al*., 2009). Homologues of Sec61β and Sec61γ have been identified in plants (Hartmann *et al*., 1994).

1.2.2 Insertion of membrane proteins into the ER lipid bilayer

Membrane proteins are inserted into the lipid bilayer of the ER by virtue of the lateral gate formed at the hinge region of the Sec61α subunit. The transmembrane domains of these proteins move laterally from the aqueous interior of the translocation pore into the membrane. The Sec61α channel is much larger than the minimum space required to allow passage of a single polypeptide chain (Hamman *et*

al., 1997), therefore transmembrane domains may exit the channel either alone or in pairs (Rapoport, 2007; Becker *et al*., 2009).

Membrane-spanning proteins can be classified into different types based on how they are recognised and their final orientation in the membrane (Spiess, 1995). Type I membrane proteins have their N-terminus in the lumen and their C-terminus in the cytosol. They contain a cleavable signal peptide and a stop-transfer signal, allowing a pause for lateral movement into the membrane. Type II membrane proteins are oriented with their N-terminus in the cytosol and their C-terminus in the lumen, and type III have a similar topology to type I, although these proteins contain signal-anchor sequences, whereby sequences within or near to the transmembrane domains determine the topology of the protein. Multi-spanning membrane proteins can also be classified as type I, II or III and often the first transmembrane domain determines the orientation of the subsequent ones (Wessels & Spiess, 1988).

A further class of membrane proteins are tail-anchored proteins. These proteins contain a C-terminal hydrophobic transmembrane domain which inserts into membranes of various organelles in a post-translational manner by virtue of the composition and length of the transmembrane domains (Pedrazzini, 2009). Most research has been focused on the mammalian model tail-anchored protein – cytochrome b5 (D'Arrigo *et al*., 1993). Tail-anchor insertion is thought to be mediated by three different mechanisms. The first mechanism involves the spontaneous, translocon-independent insertion of the tail-anchor into the membrane. This process is mediated by the presence of a mildly hydrophobic transmembrane domain which prevents aggregation upon protein synthesis (Brambillasca *et al*., 2006). The second mechanism involves an ATP-dependent transmembrane-recognition complex which binds to transmembrane domains with high hydrophobicity and inserts them into the target membrane (High & Abell, 2004; Schuldiner *et al*., 2008). The third mechanism involves the chaperones Hsc70 and Hsp40 which prevent aggregation and are thought to facilitate the ATP-dependent insertion of tail-anchored proteins described previously (Abell *et al*., 2007).

1.2.3 Protein folding, modification and quality control

Once proteins have successfully translocated into the lumen of the ER, they are folded and modified by a range of chaperones which prevent incorrect folding and aggregation, aid in tertiary and quaternary protein assembly and protein glycosylation (Vitale & Denecke, 1999).

Once the translocating polypeptide chain has begun to emerge into the lumen of the ER, the chaperone BiP (Binding immunoglobulin Protein, GRP78), a member of the Hsp70 family, is required for the complete transport of proteins into the ER and is thought to reel in the nascent chain as it enters the ER lumen (Matlack *et al*., 1999; Schatz & Dobberstein, 1996). This process may only be required for post-translationally translocated proteins, as the drive of protein synthesis from the ribosome is thought to be enough to push the nascent chain into the lumen of the ER during co-translational translocation (Matlack *et al*., 1999). BiP interacts with the Sec61 translocon (Young *et al*., 2001; Brodsky and Schekman, 1993) and acts as a gate on the luminal side of the channel acting in an ATP-dependent manner (Alder *et al*., 2005; Hamman *et al*., 1998). BiP then interacts with the nascent chain as it emerges from the translocon to prevent misfolding, and this interaction may persist after the protein has been fully translocated to prevent protein aggregation through the exposure of hydrophobic regions of the protein (Gething, 1999). BiP has also been implicated in the assembly of proteins to achieve their quaternary structure. For example, the storage protein phaseolin transiently associates with BiP before being assembled into trimers and exported to the Golgi (Vitale *et al*., 1995). As the protein enters the ER lumen, the hydrophobic signal peptide is then cleaved by signal peptidase, which is located at the site of the translocon (Tuteja, 2005; Evans *et al*., 1986).

An early event in the synthesis of many eukaryotic proteins is the addition of sugar residues in a process known as asparagine-linked glycosylation. In plants, N-glycosylation has been implicated in many cellular processes (Pattison & Amtmann, 2009). N-glycosylation takes place in the ER and involves the transfer of a lipid-linked oligosaccharide precursor to an asparagine residue (in the sequon Asn-X-Ser/Thr, where X is any amino acid except proline) by the oligosaccharyltransferase

(OST) complex. The sugar residues are subsequently processed by a series of enzymes present in both the ER and Golgi. After the successful transfer of the oligosaccharide, proteins may undergo a quality control step by entering the calnexin-calreticulin cycle whereby, following the trimming of glucose residues, a further glucose residue is re-added by glucosyltransferase until the protein is deemed fully folded (Helenius & Aebi, 2001; Pattison & Amtmann, 2009). Once correctly folded, following the necessary number of passes through the calnexin-calreticulin cycle, the glucose residue is not re-added to the glycan and the protein is exported from the ER.

The oxidising environment of the ER allows the formation of disulfide bonds between cysteine residues. The formation of these bonds is regulated by a family of ER resident oxidoreductases, with protein disulfide isomerase (PDI) being the best studied member. The ability of PDI to bind nascent proteins and the catalysis of disulfide bond formations are however thought to be two distinct properties of the protein (Noiva *et al*., 1993; Riemer *et al*., 2009).

Another, lesser studied chaperone of the ER (at least in plants) is endoplasmin. This protein is part of the Hsp90 family and is thought to act in a similar manner to BiP. Endoplasmin has been shown to interact with a number of newly synthesised proteins in mammals, but seems much less promiscuous than BiP (Argon & Simen, 1999). Plant endoplasmin is regulated by the unfolded protein response (UPR) (Martinez & Chrispeels, 2003) which enables the cell to cope with the accumulation of unfolded or misfolded proteins in the ER (Klein *et al*., 2006).

In the event that a protein misfolds, cells possess a quality control system which allows for the removal and degradation of aberrant proteins (Anelli & Sitia, 2008). This system is linked to the UPR which controls the transcriptional and translational levels of protein production so that the ER can cope with overloading of misfolded proteins (Malhotra & Kaufman, 2007). In mammalian and yeast cells, aberrant proteins are usually retrotranslocated from the ER lumen to the cytosol and degraded by proteasomes in a process called ER-associated degradation (ERAD, Romisch, 2005).

A similar pathway has been proposed to exist in plants and has been exemplified by the retrotranslocation of the catalytic subunit of the A-B plant toxin ricin (Di Cola *et al*., 2001). It has since been shown that this event requires the participation of an AAA-ATPase complex called CDC48, which is thought to use its ATPase activity to sequester ubiquitinated ERAD substrates and extract them from the ER membrane (Marshall *et al*., 2008). When unfolded proteins accumulate in the ER, sensors such as inositol-requiring enzyme-1 (IRE1) interact with chaperones and initiate phosphorylation signalling cascades (Malhotra & Kaufman, 2007). Plant IRE1 can functionally replace its yeast homologue (Koizumi *et al*., 2001), but its downstream targets remain unknown.

1.2.4 Protein retention in the ER

The final destination of many proteins synthesised in the ER is within the ER itself. Therefore, these proteins require a signal which will retain them in the ER, generally found at the C-terminus. Soluble proteins retained in the ER display a C-terminal tetrapeptide motif (K/HDEL) which is conserved across many organisms (Munro & Pelham, 1987), of which a receptor has been identified in plants (Lee *et al*., 1993). Although some plasma membrane and vacuolar resident proteins have been identified bearing the K/HDEL motif, it is thought these C-terminal retention signals are cleaved in order to regulate the trafficking of these proteins (Okamoto *et al*., 1994; Okamoto *et al*., 2003).

Many type I membrane spanning proteins with their C-terminus facing the cytosol are retrieved to the ER through the detection of another well characterised tetrapeptide motif – the dilysine motif (KKXX), positioned as the last four residues of the protein (Teasdale & Jackson, 1996). These residues are thought to be recognised by α and β' COP protein components of COPI machinery and transported back to the ER (Lee *et al*., 2004; McMahon & Mills, 2004). This protein retrieval process is also present in plants (Benghezal *et al*., 2000).

Retrieval of type II membrane proteins, where their C-terminus is in the lumen, was originally thought to be regulated by the presence of a double-arginine motif in the cytosolically oriented N-terminus (Gomord *et al*., 1999). However, it is now

generally accepted that double-arginine motifs (RR, RxR and RxxR) are found in a variety of cytosolic positions, including polytopic loops, and within the C- and N-termini of type I and type II membrane proteins, respectively (Michelsen *et al*., 2005). More recently, luminal signals of type II membrane proteins have also been shown to contribute to ER retrieval (Boulaflous *et al*., 2009).

A less well defined ER-retrieval signal has also been described. It has been suggested that ER resident membrane proteins are retrieved from the Golgi by means of detection by the Rer1 protein family. These proteins recognise and retrieve mislocalised ER membrane proteins by means of a motif found within the transmembrane domains of ER resident proteins (Sato *et al*., 1999). Similar to a motif found in yeast (Sato *et al*., 1996), this plant motif consists of a leucine residue separated from a tyrosine residue by a stretch of 11 amino acids, located within the transmembrane domain. However, the presence of this motif is based solely on sequence comparison with its homologues in yeast, and therefore the function of this motif has not been tested experimentally in *Arabidopsis*. Recently, a more refined motif has been proposed in yeast, comprising of a 6-residue highly hydrophobic region flanked by the polar residues - tyrosine and serine, mutations of which have been shown to influence the efficiency of the Rer1 receptor (Sato *et al*., 2003).

To some extent, the length of the transmembrane domains of a protein also plays a role in protein localisation. The thickness of the lipid bilayer increases the further along the secretory pathway an organelle is located (Brandizzi *et al*., 2002). The typical span of amino acids in the ER or Golgi is 17 residues, compared to ~20 residues in the plasma membrane (Munro, 1995; Pedrazzini, 2009). Therefore, the composition of amino acids in the transmembrane domain somewhat defines the compartment to which a protein is targeted, which can be demonstrated experimentally by altering the length of transmembrane domains and determining its effect on localisation (Ronchi *et al*., 2008).

1.2.5 Lipid synthesis in the ER

Cellular membranes have a unique and specific lipid composition which contribute to their identity. Lipid composition may differ within subdomains of organelles (Moreau *et al*., 1998). The synthesis of one such lipid, glycerolipid, occurs mainly in

the plastid envelope and ER membranes (Jouhet *et al*., 2007). Not only does the ER synthesise lipids involved in membrane and organelle homeostasis, but it is also the site of triacylglycerol (TAG) synthesis – a major lipid storage compound. A unique step in TAG synthesis is catalyzed by the ER-membrane bound diacylglycerol acyltransferase, which localises to the rough ER (Murphy *et al*., 1993).

In seeds, lipid bodies are formed when membrane proteins called oleosins encapsulate TAGs in a lipid monolayer which originates from the ER (Napier *et al*., 1996). Containing two transmembrane domains, oleosins span the lipid monolayer, with their N- and C-termini facing the cytosol and a hydrophobic loop region containing a proline-knot (Tzen *et al*., 1992) embedded in the TAG core of the lipid bodies (Napier *et al*., 1996). Oleosins are targeted to the lipid bodies via the ER and their specific topology is a necessary requirement for correct localisation (Abell *et al*., 2004). Oleosins are abundantly expressed in plants, and oleosin knockout plants display unregulated lipid body size (Shimada *et al*., 2008).

1.2.6 Protein storage within the ER

In addition to lipid bodies, plant cells accumulate proteins which are assembled into ER-derived organelles known as ER bodies, which are thought to originate from tubular ER (Herman, 2008). ER protein bodies accumulate storage protein precursors, cysteine proteases and cereal prolamins. The mechanisms by which some of the storage proteins are retained in the ER are not yet known as prolamins, for example, do not contain an ER retrieval signal (Galili *et al*., 1998). However, cysteine proteases do carry an ER-retrieval motif which is thought to be cleaved, allowing transport to the vacuole (Toyooka *et al*., 2000). Acting as intermediate storage compartments, the ER bodies are then transferred to the vacuole, bypassing the Golgi (Herman & Schmidt, 2004), although some ER bodies have been found to remain as cytoplasmic organelles (Herman, 2008). Other storage protein precursors, such as those of pumpkin albumins, have been found to exit the ER in precursor-accumulating (PAC) vesicles which also bypass the Golgi (Hara-Nishimura *et al*., 1998). The existence of a PAC-vesicle mediated transport route however appears to be strictly species-specific (Joliffe *et al*., 2004).

1.3 Structure of the ER in plants

The peripheral ER (comprises all ER other than the nuclear envelope) is connected to the nuclear envelope and consists of sheet-like cisternae and an extensive polygonal network of tubules connected by three-way junctions, which spread throughout the cytosol forming a single contiguous luminal space (Boevink *et al*., 1996). At a simplified level, the ER membrane offers a divide between the reducing environment of the cytosol and the oxidative environment of the ER lumen. In plant cells, the desmotubules, low-diameter ER tubules across plasmodesmata (Oparka, 2005) and ER-derived organelles such as lipid bodies, ER protein bodies and PAC vesicles, can also be considered structural components of the ER (Herman, 2008).

The ER has traditionally been classified into two domains, rough and smooth ER, depending on the presence of membrane-bound ribosomes, and it is these terms which are typically used to describe the organelle (Sparkes *et al*., 2009a). The predominant network of tubular ER is often visualised as either cortical ER, due to the turgor pressure of the central vegetative vacuole forcing the ER into the almost two-dimensional space between the tonoplast and the plasma membrane (Hepler, 1981; Bouchekhima *et al*., 2009), or as cytosolic ER, where the ER is seen as streaming through trans-vacuolar strands (Quader *et al*., 1989).

Whereas the ER of mammalian cells is linked to microtubules, plant ER is associated with the actin cytoskeleton (Boevink *et al*., 1998) and the movement of ER membrane proteins has been shown to be actin-dependent (Runions *et al*., 2006). However, the depolymerisation of the actin cytoskeleton using drugs such as latrunculin B, inhibits ER movement but does not disrupt the reticular architecture of the tubular ER network (Boevink *et al*., 1998; Runions *et al*., 2006), suggesting that factors other than the cytoskeleton are responsible for the regulation of the shape of the ER.

Within the polygonal network of cortical ER, individual tubules can be seen to extend and retract, while other regions, termed anchor/growth sites, remain relatively immotile. Tubule movement is attributed to an association with the actin cytoskeleton connected via myosin proteins, and can be described as elongating,

shrinking and sliding between fixed anchor/growth sites, often visualised as three-way junctions (Sparkes *et al*., 2009c).

In plants, the transition between tubular and cisternal ER is linked with development, whereby sheets are most often found in elongating cells, whereas tubular ER is found in more mature cells (Ridge *et al*., 1999). The actin cytoskeleton, to some extent, is thought to be responsible for the transition between sheets and tubules, and depolymerisation of the actin cytoskeleton with latrunculin results in an increase in cisternal ER (Sparkes *et al*., 2009c).

Due to the pleomorphic nature of the ER and the abundance of ER tubules (Staehelin, 1997), plant cells offer a beneficial model in order to study the morphology of the ER using light microscopy, although the links between the functions of this organelle and its dynamic structure are still poorly understood.

1.3.1 Structural domains of the plant ER

The unique extensive reticular network of the ER allows it to associate closely with nearly every other organelle in the cell. Staehelin, (1997) attributes 16 subdomains to the plant ER based on their structural and functional properties. In addition to the nuclear envelope, cisternal sheets (rough ER) and tubular ER (smooth ER), the author describes specialised regions of the ER which mediate ER-to-Golgi transport (described in the following section), lipid body (section 1.2.5), ER protein body (section 1.2.6) and vacuole formation, cell-to-cell communication via plasmodesma and attachment domains to mitochondria, the cytoskeleton, vacuole and plasma membrane. However, the manner by which the composition and protein complement of these proposed ER domains is regulated has yet to be understood. Although some protein partitioning in the ER is evident (Nikonov *et al*., 2002), the luminal reporter GFP-HDEL does not discriminate between nuclear envelope, cisternal and tubular ER (Boevink *et al*., 1996) and therefore an attempt to visualise these domains may prove difficult.

1.3.2 ER-exit sites and ER-Golgi interactions

The ER is the port of entry of the secretory pathway, and following synthesis, folding and modification, nascent proteins are transported to downstream organelles via the Golgi. The regions of the ER where both membrane and soluble cargo are transported from the ER are known as ER-exit sites (ERES). Protein cargo is transported to the Golgi via COPII coated vesicles and retrograde transport from the Golgi back to the ER is mediated by COPI vesicles (Hawes *et al*., 2008).

The formation of COPII vesicles requires the activation of the GTPase, Sar1, which then recruits the structural components of the vesicle to the ER membrane. Sar1 is activated via a guanine-nucleotide exchange factor (GEF) anchored to the ER membrane, Sec12. Two heterodimeric complexes are then recruited to Sar1. Firstly, Sec23/24 binds to Sar1 and secondly, Sec13/31 completes the coat. The assembly of the coat proteins on the membrane permits cargo selection and causes membrane curvature and the subsequent budding of the vesicle (Hanton *et al*., 2005).

However, the precise physical nature of ERES-Golgi transport in plants has only been resolved recently. It was proposed that the ERES and Golgi exist as a close motile unit embedded in the ER membrane (DaSilva *et al*., 2004). It has since been confirmed that components of COPII maintain a constant association with the Golgi (Hanton *et al*., 2008). The connection of the two compartments can be visualised as Golgi movement mirrors the ER, and vice versa (Boevink *et al*., 1998*;* Sparkes *et al*., 2009a). Using laser-trapping technology (Wright *et al*., 2007), Sparkes *et al*., (2009b) observed that Golgi appear to be attached to the ER, whereby the trapped Golgi could pull an ER tubule, and if the connection was lost, the Golgi body could be re-attached by docking the Golgi to the tip of an ER tubule. The question then remains whether the ER follows the Golgi, or the Golgi follows the ER or a combination of both.

1.3.3 Linking structure to function: sheets versus tubules

1.3.3.1 Different structures within the ER

Typically, ER sheets are thought to correspond to rough ER, and tubules to smooth ER. Differential levels of sheets and tubules are found in certain cell types where cells display a specialised function (Shibata *et al*., 2006). It is currently unknown as to whether tubules are actively shaped and sheets are the default conformation of the ER, or whether sheets are also actively shaped and there is a dynamic equilibrium between the two states. The latter would involve (perhaps separate) mechanisms which regulate both ER sheets and tubules, indicating that the transition between the two states is a complex process (Shibata *et al*., 2009).

1.3.3.2 Advantages of sheets and tubules

The conservation of sheets and tubules across all eukaryotic organisms indicates they have functional significance. Sheets may offer the most efficient platform for polysomes to bind the ER surface, and the resulting uninterrupted volume of space (compared to tubules) could provide optimal conditions for the folding and modification of nascent proteins. It has been proposed that the binding of ribosomes to the ER membrane is entirely responsible for the induction of sheets (Puhka *et al*., 2007), although this seems unlikely based on recent evidence for sheet-maintaining mechanisms (discussed below). Tubular ER would therefore provide a separate domain of the ER more suitable for enzymes which synthesise lipids or components involved in vesicle trafficking (Shibata *et al*., 2006). This raises the question of how proteins are segregated within a single organelle containing varied structural regions – a process which is currently poorly understood.

1.4 Mechanisms regulating organelle shape

Eukaryotic organelles have characteristic shapes. Spherical organelles, such as vesicles, endosomes and vacuoles, are likely to reside in their most thermodynamically and energetically favourable state. Other organelles, such as the ER, Golgi and mitochondria, are arranged into more complex structures, and it is the

mechanism by which these structures are generated which is central to a new field of research into organelle shape-function relationships (Dreier & Rapoport, 2000). Although the functional significance behind the morphology of the ER is at present unclear, based on current understanding of membrane architecture, many different mechanisms have been proposed which try to rationalise how membrane curvature of organelles is achieved. At a basic level, membrane curvature is attributed either to specialised proteins which insert into, or form scaffolds between membranes, lipid composition and membrane tethering (Voeltz & Prinz, 2007).

Firstly, protein insertion into membranes, also known as the bilayer coupling effect, is where wedge-shaped proteins are inserted into at least one, if not both leaflets of the lipid bilayer. Due to the wedge-like or conical shape of the protein, the outer monolayer of the membrane increases in surface area in relation to the inner monolayer, therefore inducing positive curvature of the membrane (Sheetz & Singer, 1974; Zimmerberg & Kozlov, 2006). It has been proposed that this mechanism is responsible for shaping the tubular ER (Voeltz *et al*., 2006), which is discussed in more detail in later sections.

Another mechanism is the oligomerisation of proteins into a scaffold which interacts with, and subsequently induces curvature in, lipid membranes (Farsad & De Camilli, 2003). COPI, COPII and clathrin machinery complexes are thought to provide scaffolds for spherical curvature, and dynamin (involved in vesicle budding) and BAR-domain-containing proteins are thought to provide scaffolds for cylindrical curvature (Chernomordik & Kozlov, 2003). Such proteins are thought to form transient, rigid oligomers which bend membranes. N-BAR-domain proteins form banana-like dimers which interact with the head groups of phospholipids in the membrane and subsequently induce membrane curvature (Zimmerberg & Kozlov, 2006). Several types of BAR domain have now been identified. F-BAR domains induce lower curvature than that of N-BAR domains, and I-BAR domains form a convex surface and induce negative curvature (Shibata *et al*., 2009). Another example, caveolin, oligomerises at the plasma membrane forming localised invaginations known as caveolae (Bauer & Pelkmans, 2006). In addition, some proteins can promote tubulation by inducing lipid reorganisation (Romer *et al*., 2007).

Lipids themselves are also believed to induce positive and negative curvature when they are asymmetrically distributed between the two leaflets of the lipid bilayer (Voeltz & Prinz, 2007). The size of polar head groups of lipids in relation to their tails becomes important when considering membrane curvature. If the sizes were comparable, then a relatively flat membrane would result. However, larger head groups and small tails located in one leaflet of the bilayer could induce curvature (Farsad & De Camilli, 2003). Enzymes which transfer lipids between bilayer leaflets in an ATP-dependent manner– flippases – have been implicated in the regulation of membrane curvature (Poulsen *et al*., 2008). However, there is little evidence for the regulation of lipids across the entire surface of an organelle, and it is thought that energy-independent flippases equilibrate lipids in the ER membrane (Pomorski *et al*., 2004). Although lipid composition may contribute to the overall bending of the membrane, the lipid composition of cell membranes alone is thought not to be sufficient to shape organelles (van Meer *et al*., 2008).

Another mechanism of organelle regulation is tethering of the organelle in question to either the cytoskeleton or another membrane. Many organelles, such as the ER, mitochondria and the Golgi, bind to the cytoskeleton. However, these interactions are thought to regulate the overall movement of organelles, rather than their morphology. In the case of the ER, this is supported by the use of depolymerising agents which disrupt the cytoskeleton, whereby the ER retains its reticular structure and its morphology is thought to be largely unaffected by the depolymerisation of actin (plants) or microtubules (mammals) (Boevink *et al*., 1998; Voeltz *et al*., 2002). Indeed, mammalian ER tubules have successfully been formed *in vitro* in the absence of microtubules (Dreier & Rapoport, 2000), indicating ER morphology is not dependent on an intact cytoskeleton. However, this is not the case *in vivo*, whereby inhibiting kinesin-I or dynein leads to a striking increase in lamellar ER (Wozniak *et al*., 2009).

Intermembrane tethering is also thought to help determine organelle shape. This would allow membranes to form closely apposing surfaces, as exemplified by the layering of ER cisternae seen in some cell types (Voeltz & Prinz, 2007). Low-affinity interactions between cytosolic domains of ER membrane proteins have been proposed to promote the formation of stacked ER cisternae (Snapp *et al*., 2003).

A combination of both cytoskeletal and intermembrane tethering is also possible. The LINC (linker of nucleoskeleton and cytoskeleton) complex of the nuclear envelope encompasses such a concept. Here, the SUN proteins span the inner nuclear membrane and interact with both lamins in the nucleus and the nesprin proteins in the perinuclear space. The nesprin proteins then span the outer nuclear membrane and interact with the cytoskeleton (Ostlund *et al*., 2009).

Although these mechanisms may facilitate the regulation of organelle morphology, multiple mechanisms may be required in order to shape a multi-structural organelle such as the ER, and more specifically the nuclear envelope, sheets and tubules. Putative models propose a combination of a selective diffusion barrier within regions of the ER (Luedeke *et al*., 2005) coupled with differential membrane tethering, the latter being a mechanism suggested to regulate the shape of the nuclear envelope (Mattaj, 2004). Further to this, segregation of ER domains may be achieved by membrane proteins which are targeted to more energetically favourable regions of the membrane, be it flat or tubular. This theme is discussed in more detail in the following sections.

1.4.1 Maintenance of ER sheets

The mechanisms by which cisternal sheets of the ER are formed are largely unknown. In the case of maintaining sheets, membrane curvature must be reduced in order to obtain a flattened region. As the size of sheets vary, the space separating the two bilayers must be kept constant over a large area. The luminal spacing is approximately 50-100 nm, similar to the diameter of an ER tubule, and the curvature at the edge of sheets is also similar to that of tubules. With this in mind, it has been speculated that structural elements are also required to actively flatten membranes (Shibata *et al*., 2006).

In mammals, one such proposed mechanism is intra-luminal bridging, a candidate of which is CLIMP-63 which is thought to both stabilise and induce proliferation of ER sheets (Korkhov & Zuber, 2009). Another mechanism may be the formation of a scaffold on the cytosolic face of the ER. Over-expression of a cytosol-facing membrane protein, p180, has been shown to induce the formation of sheets in the ER

(Benyamini *et al*., 2009). However, such mechanisms have not yet been discovered in plants.

Continuous with the ER, the nuclear envelope is considered to be a flattened sheet. The distance between the inner and outer membranes is similar to that of ER sheets (~50 nm). As mentioned previously, the nuclear envelope is thought to be stabilised by a combination of luminal bridging by the SUN and nesprin proteins (Worman & Gundersen, 2006) and the regular occurrence of nuclear pores (Shibata *et al*., 2009).

1.4.2 Protein-induced membrane curvature of ER tubules

1.4.2.1 Reticulons and reticulon-like proteins

One class of proteins thought to be responsible for inducing curvature of ER tubules are reticulons. These are thought to operate by inserting into the outer leaflet of the membrane in a wedge-like manner and oligomerising to form a scaffold within the tubular membrane of the ER.

In recent years, three key publications from the Rapoport group have addressed the structural properties of mammalian and yeast reticulons and reticulon-like proteins. Reticulons are highly conserved, abundant membrane proteins which localise to regions of tubular ER and have been shown *in vitro* and *in vivo* to oligomerise and form a scaffold thought to maintain the structure of tubular ER (Voeltz *et al*., 2006). Reticulon proteins were initially associated with tubular ER using *in vitro* recapitulation of an ER network from the eggs of *Xenopus laevis*. Through the application of cysteine-modifying reagents, network formation was inhibited and the target was identified as Rtn4a (Dreier & Rapoport, 2000), a finding confirmed using inhibitory Rtn4a antibodies (Voeltz *et al*., 2006).

Four reticulon genes are present in mammals, and many isoforms of each gene exist due to alternative splicing (Oertle *et al*., 2003b). There are two reticulon genes present in yeast (*Saccharomyces cerevisiae*), and it is these two organisms in which reticulon research has been mainly focused. The deletion of Rtn1p and Rtn2p in yeast only results in a small increase in cisternal sheets, indicating additional proteins

may be involved in structuring tubular ER (Voeltz *et al*., 2006). Accordingly, pull-down experiments revealed interacting partners for mammalian Rtn4a – DP1, and the yeast reticulons – Yop1p. These proteins (hereafter referred to as 'reticulon-like' proteins) do not share any primary sequence homology with reticulons, but do contain a conserved C-terminal hydrophobic region common to all reticulons – the reticulon homology domain (RHD), which is thought to insert into the ER membrane and induce curvature to form tubules.

Reticulons and DP1/Yop1p localise exclusively to tubular ER and are excluded from ER sheets (except at the edges – where reticulons and tubule-branching atlastins localise (Hu *et al*., 2009)) and the nuclear envelope by an unknown mechanism (Voeltz *et al*., 2006). The specific topology and oligomerisation of reticulons are thought to contribute to their ability to curve membranes. Their protein structure consists of a variable-length N-terminus, followed by the conserved 200 residue-long RHD containing two long hydrophobic regions, possibly configured as 2-4 transmembrane domains. The N- and C-termini both face the cytosol and, depending on the topology of reticulon, a central loop region could either face the ER lumen (indicating a 'v' topology), or the cytosol (indicating a 'w' topology). At present, it is this latter conformation which is thought to represent the topology and orientation of 'structural' reticulons (Voeltz *et al*., 2006; He *et al*., 2007; Figure 1.1).

The 'w' conformation in the membrane is proposed to act as a wedge inserting into (at least) the outer leaflet of the ER lipid bilayer and therefore inducing positive curvature by increasing the surface area relative to the inner leaflet (English *et al*., 2009). This hypothesis is supported by over-expression and deletion studies in mammals and yeast, whereby deletion of reticulons results in an increase in peripheral sheets, and their over-expression leads to an increase in ER tubules (Voeltz *et al*., 2006; Anderson & Hetzer, 2008).

It is unlikely that reticulon monomers would curve the ER membrane enough to form tubules. Therefore it has been proposed that reticulons form a scaffold in the membrane in a ring or spiral conformation (Voeltz & Prinz, 2007), although this doesn't take into account how membrane proteins could freely diffuse along the tubules. In order to form a tubular structure rather than a spherical vesicle, reticulons

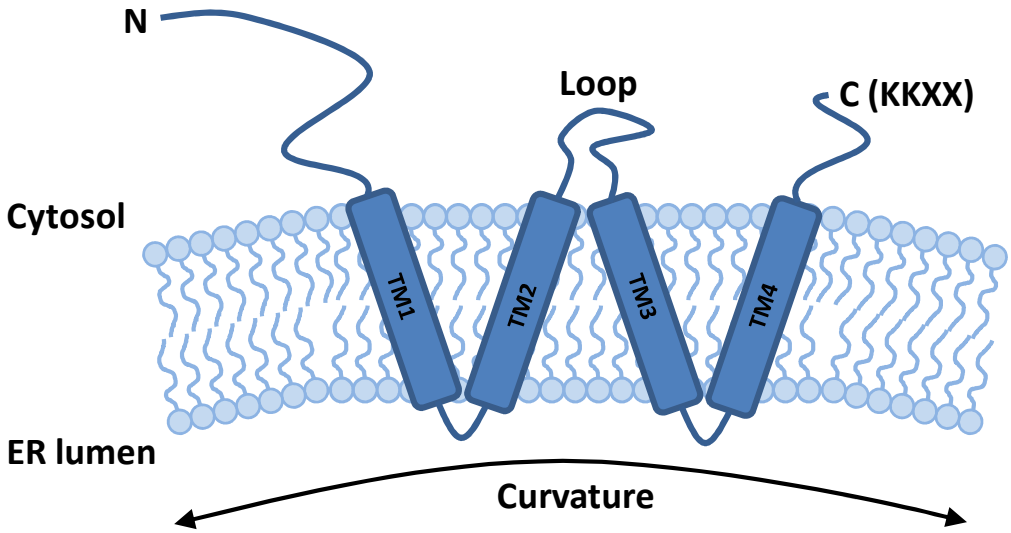

Figure 1.1 Putative structure and topology of reticulons. 2-4 predicted transmembrane domains are thought to insert into the ER membrane causing positive curvature, with the variable-length N-terminus and short C-terminus facing the cytosol. The orientation of the loop region, either cytosolic (shown here), or luminal, would dictate the structural conformation of reticulon in the membrane as either a ‘v’ or a ‘w’, respectively.

are thought to assemble in only one dimension (Shibata *et al*., 2006), possibly forming arcs of reticulon oligomers, which would also allow diffusion of membrane proteins (Shibata *et al*., 2009). The assembly and disassembly of arc-like scaffolds may be an ATP-dependent process, as the depletion of ATP in mammalian and yeast cells reduces the diffusional mobility of reticulon and reticulon-like proteins in the membrane (Shibata *et al*., 2008).

Through fluorescence recovery after photo-bleaching (FRAP), sucrose gradients and cross-linking studies, reticulons have been shown to form immobile homo- and hetero-oligomers in the membrane. Interestingly, RHD mutants which no longer localise exclusively to tubular ER and cannot form tubules are more mobile and cannot form oligomers, indicating that the RHD alone is responsible for localisation and oligomerisation (Shibata *et al*., 2008).

Reconstitution of yeast Rtn1p and Yop1p into proteoliposomes generates narrow tubules (20 nm), the diameter of which is dependent of the expression levels of reticulon. Again, it has been shown that the RHD alone is sufficient to form tubules (Hu *et al*., 2008). Together, these data indicate that reticulon and reticulon-like proteins are important components of ER tubule formation, although their precise mechanism remains unclear.

1.4.2.2 Dissecting the role of the RHD

As indicated previously, the conserved reticulon homology domain retains many of the key properties of ER tubule formation and localisation.

In mammals, the RHD of Rtn1 has been shown to be critical for ER localisation (van de Velde *et al.,* 1994), and although both hydrophobic regions can determine ER localisation individually (Iwahashi *et al*., 2007), a single hydrophobic region is sufficient to target Rtn1 to the ER (Chen *et al*., 2000). Disruption of the first hydrophobic region of Rtn3 results in misfolding and incorrect insertion of Rtn3 into the ER membrane (He *et al*., 2007) and deletion of the entire RHD abolishes all association with the ER (Chen *et al*., 2000). Within the RHD, the second hydrophobic region is the most highly conserved, followed by the first (Yang &

Strittmatter, 2007), although the second hydrophobic region of Rtn3 is not required for ER localisation (He *et al*., 2007).

However, there is no conclusive evidence as to the orientation of the hydrophobic regions or the number of membrane spanning segments in reticulons. The first hydrophobic region of the RHD may contain up to two transmembrane domains (TM1, TM2), and similarly for the second hydrophobic region (TM3, TM4). A proposed structure of reticulon is presented in Figure 1.1.

The two hydrophobic regions of reticulons are also unusually long to span the ER membrane (approximately 40 residues each), raising the question of whether the length of these domains has any significance for the function of reticulons (Yang & Strittmatter, 2007). When the first hydrophobic region of Rtn1 is split in two, neither half is sufficient for ER localisation and both are mistargeted to the Golgi (Iwahashi *et al*., 2007). The second hydrophobic region of Rtn3 is thought to contain two smaller TM domains separated by a 3 residue linker (He *et al*., 2007).

Flanked by the two hydrophobic regions of the RHD is a 60-70 amino acid hydrophilic loop which is thought to be exposed to the cytosol. Two independent studies on mammalian reticulons have revealed that the N-terminus and the loop region, at least, face the cytosol, indicating a 'w' orientation in the membrane (Voeltz *et al*., 2006; He *et al*., 2007). In mammals, the loop of Rtn4a (also known as Nogo) has been shown to interact with a receptor, termed Nogo-66 receptor (NgR) which is involved in the inhibition of axonal regeneration after injury (Fournier *et al*., 2002).

Many reticulons display a C-terminal extension, extending beyond the RHD, and often contain dilysine ER-retrieval motifs (KKXX). However, this motif seems redundant as its removal from Rtn1 and Rtn4c still permits steady-state ER localisation (Sironen *et al*., 2004; Iwahashi *et al*., 2007).

1.4.2.3 Reticulon function

The discovery of novel properties of reticulons and reticulon-like proteins has been extended to isoforms present in many eukaryotic organisms. Through differential promoter usage and alternative splicing (Oertle *et al*., 2003a), the four mammalian reticulon genes encode multiple isoforms, namely: Rtn1a-c, Rtn2a-c, Rtn3-a1 and Rtn4a-c.

Reticulons have been implicated in many cellular processes such as intracellular trafficking (Yang & Strittmatter, 2007), apoptosis (Teng & Tang, 2008a), nuclear envelope formation (Anderson & Hetzer, 2008) and the inhibition of axonal regeneration in neuroendocrine cells (Yan *et al*., 2006) – a phenomenon which involves recognition of the loop region of Rtn4a (Nogo-66) by the Nogo receptor (NgR) (Teng & Tang, 2008b).

Mammalian reticulons have also been affiliated with several major disease states such as Alzheimer's disease (Wildasin, 2004; He *et al*., 2006), cancer (Watari & Yutsudo, 2003), the motor neurone disease: amyotrophic lateral sclerosis (ALS; Teng & Tang, 2008b), schizophrenia (Novak *et al*., 2002) and atherosclerosis (Rodreguez-Feo *et al*., 2007).

Many interactions between reticulons and other proteins have been identified (Oertle & Schwab, 2003), and the repertoire of cellular processes and diseases associated with reticulons is growing rapidly. Recent research has also addressed reticulon expression in fish (RTN1-4, Diekmann *et al*., 2005), *Caenorhabditis elegans* (nRTNa-c, Iwahashi *et al*., 2002), *Drosophila* (RTNL-1, Wakefield & Tear, 2006) and *Xenopus* (XRTN1a, 1b, 2, 3, Park *et al*., 2005; Park *et al*., 2007).

One of the reticulon-related processes perhaps most applicable to plants is the intracellular trafficking of proteins. Reticulons have been found to affect the trafficking of proteins (Liu *et al*., 2008), specifically between the ER and Golgi (Wakana *et al*., 2005), which may involve SNAREs (Steiner *et al*., 2004; Martin *et al*., 2006) and Rab proteins associated with Golgi biogenesis (Haas *et al*., 2007). Reticulons in *C. elegans* are thought to be involved in endocytosis during

embryogenesis (Iwahashi *et al*., 2002). Mammalian Rtn1a and Rtn1b have also been found to interact with a subunit of the AP-2 adaptor complex which is involved in endocytosis and clathrin-mediated vesicular transport. Nziengui & Schoefs, (2008) postulate that many of the plant reticulons contain putative tyrosine sorting motifs (Ohno *et al*., 1995) at their N-terminus, which may be involved in the recognition and recruitment of the AP-2 complex and clathrin coat machinery.

In addition to mammalian reticulon research hinting on what is yet to be discovered in plants, plant reticulon research may prove invaluable to eukaryotic research as a whole, and finding parallels between the two systems can only strengthen knowledge of ancestral lineages in eukaryotes.

1.4.2.4 Atlastins

Recent developments in research into the formation and maintenance of ER tubules has identified a candidate for the regulation of tubule fusion and fission in mammals and yeast. Atlastins are membrane-bound GTPases (Rismanchi *et al*., 2008) which belong to the dynamin superfamily of GTPases involved in membrane fusion and fission events (Praefcke & McMahon, 2004). A related GTPase has been identified in yeast – Sey1p, which, while not sharing any sequence homology with mammalian atlastin, belongs to the same dynamin-like family and contains the conserved N-terminal GTPase domain and two C-terminal transmembrane domains (Hu *et al*., 2009). Atlastin/Sey1p is involved in the homotypic fusion of ER membranes and the generation of the tubular network and localise to discrete points of tubule growth and fusion (Hu *et al*., 2009, Muriel *et al*., 2009). A similar role for atlastins in *Drosophila* has recently been established (Orso *et al*., 2009). Atlastin/Sey1p localises to ER tubules and has been found to interact with reticulons and DP1/Yop1p. Over-expression of atlastin/Sey1p results in long, unbranched ER tubules and their inhibition/deletion results in strong defects in ER morphology (Hu *et al*., 2009).

A common mutation found in atlastin proteins causes the most frequent form of early onset hereditary spastic paraplegia (HSP) - a group of neuronal disorders marked by the progressive spasticity and weakness of the lower limbs. This suggests that defects

in ER morphology may be the underlying cause of neurodegenerative disorders (Salinas *et al*., 2008).

Hu *et al*., (2009) identified an atlastin homologue in *Arabidopsis thaliana*, denoted RHD3 (root hair defective). A knockout mutant of RHD3 was originally isolated in *Arabidopsis* exhibiting short roots and short wavy root hairs (Schiefelbein & Somerville, 1990). RHD3 is an 89 kDa protein with a putative N-terminal GTP-binding motif (Wang *et al*., 1997) which is expressed in all major *Arabidopsis* organs with multiple levels of regulation (Wang *et al*., 2002). The absence of RHD3 causes an unbranched, cable-like ER network (Zheng *et al*., 2004). This indicates that ER tubule-forming mechanisms similar to those found in mammals and yeast may also be present in plants.

1.5 Reticulons in *Arabidopsis*

Very little is known about the function of reticulons in plants. Over 250 reticulon-like (RTNL) genes were identified in deeply diverging eukaryotes by Oertle *et al*., (2003b) and plant reticulons were classified as reticulon-like non-chordate taxa class B (hence RTNLB). Of more than 180 plant reticulons, at least 15 were attributed to *Arabidopsis thaliana*, of which low homology was found between the N-termini. Due to a lack of experimental evidence of the function of plant reticulons, many of their properties were assumed to be similar to that of mammals and yeast due to the overall similarities in gene organisation. Concurrent with the literature, three reticulon isoforms (RTNLB1, 3 and 5) were identified as being associated with the ER in a large-scale screen of the *Arabidopsis* organelle proteome (Dunkley *et al*., 2006), although RTNLB1 and RTNLB6 have also been found in plasma membrane-rich fractions (Marmagne *et al*., 2004).

Hwang & Gelvin, (2004) initiated a search for interacting partners of VirB2, the major component of the *Agrobacterium tumefaciens* T-pilus, which is involved in *Agrobacterium*-mediated transformation of plants. Through yeast two-hybrid screening and GST pull-down assays, the authors identified three interacting proteins, later revealed as RTNLB1, 2 and 4. Antisense and RNAi experiments

indicated that more than one of the RTNLB genes contributed to the transformation competence of the plant. Early evidence of reticulon homo- and hetero-oligomersisation was apparent when yeast two-hybrid experiments showed that the three proteins could interact with themselves and each other, and it was suggested that they may form a multimeric complex inside the plants. Low magnification microscopy of GFP-tagged forms of these reticulon proteins localised to a not-better-defined cell periphery, but were absent from the cell wall.

More recently, Nziengui *et al*., (2007) extended the *Arabidopsis* reticulon family number to 21 isoforms (the phylogenetic relationship of which is demonstrated in Figure 1.2), including five genes with long N-termini (RTNLB17-21), of which one (RTNLB19) has been shown to have 3*β*-hydroxysteroid dehydrogenase/C-4 decarboxylase activity involved in sterol synthesis, which is functional as a cytosolic protein regardless of the presence of its RHD (Rahier *et al*., 2006). In this study, the authors also investigated the subcellular localisation of RTNLB2 and RTNLB4, which were shown to localise to several subcompartments of the ER; tubular, cisternal and chloroplast-associated ER.

Of the 21 reticulon isoforms identified in *Arabidopsis*, mRNA expression data is available for all but 5 genes (eFP Browser, Winter *et al*., 2007). Expression profiles display either ubiquitous expression throughout the plant or tissue/development specific expression (see Appendix Figure A8). For example, RTNLB1-4, 8, 19 and 20 all display ubiquitous expression and RTNLB9, 14, 15 and 18 are expressed to low levels. However, RTNLB5, 10 and 11 are expressed highly in pollen, and RTNLB 1, 2 and 13 are expressed to high levels in the seed, where RTNLB13 is expressed solely in the late maturing embryo. It is unclear why there are so many reticulons expressed so thoroughly throughout the plant, although this may indicate that each isoform retains a specific function – perhaps attributed to the highly differentiated N-terminal domain.

1.5.1 Reticulons in plants – a wider perspective

Although plant reticulon research has been initiated in the model organism *Arabidopsis*, reticulons have been identified in other plant species (Oertle *et al*., 2003b; Nziengui & Schoefs, 2008; Sparkes *et al*., 2009a). In addition to the 21 isoforms found in *Arabidopsis*, reticulons have been identified in *Glycine max* (1), *Hordeum vulgare* (1), *Solanum tuberosum* (1), *Oryza sativa* (17) and *Vitis vinifera* (6). These plant reticulons have been characterised into four groups based on the lengths of their N- and C-terminal domains (Nziengui & Schoefs, 2008). However, evolutionary insights into the development of plants can often be found by studying less complex, divergent plant species (Lang *et al*., 2008). Accordingly, reticulon genes have been identified in early plants such as the green alga *Chlamydomonas reinhardtii* (1), the moss *Physcomitrella patens* (9) and the spikemoss *Selaginella moellendorffii* (5), of which there is evidence of N-terminal enzyme linked isoforms (Figure 1.2; Sparkes *et al*., 2009a).

1.6 Introduction to the project

A triple knockout of Rtn1p, Rtn2p and Yop1p in yeast results in only a moderate growth defect, raising the question of the importance of an intact tubular ER (Voeltz *et al*., 2006). However, the deletion of reticulon and reticulon-like proteins in *C. elegans* results in a drastic reduction in embryonic viability (Audhya *et al*., 2007), indicating that the presence of tubular ER in higher eukaryotes is important. With the majority of reticulon research focused in mammals and yeast, plant reticulons have received little attention. However, the ER of plants is enriched in cortical tubules, usually the only flattened region being the nuclear envelope (Hepler, 1981). The role of reticulons in plants and their contribution to the formation of tubular ER are therefore unknown at present.

1.6.1 RTNLB13

Reticulons have varying length N-termini (Oertle *et al.*, 2003b) and this is also true for reticulons in plants (Nziengui *et al*., 2007). Therefore, this study will concentrate on one of the smallest of the plant reticulons, RTNLB13. This protein has an

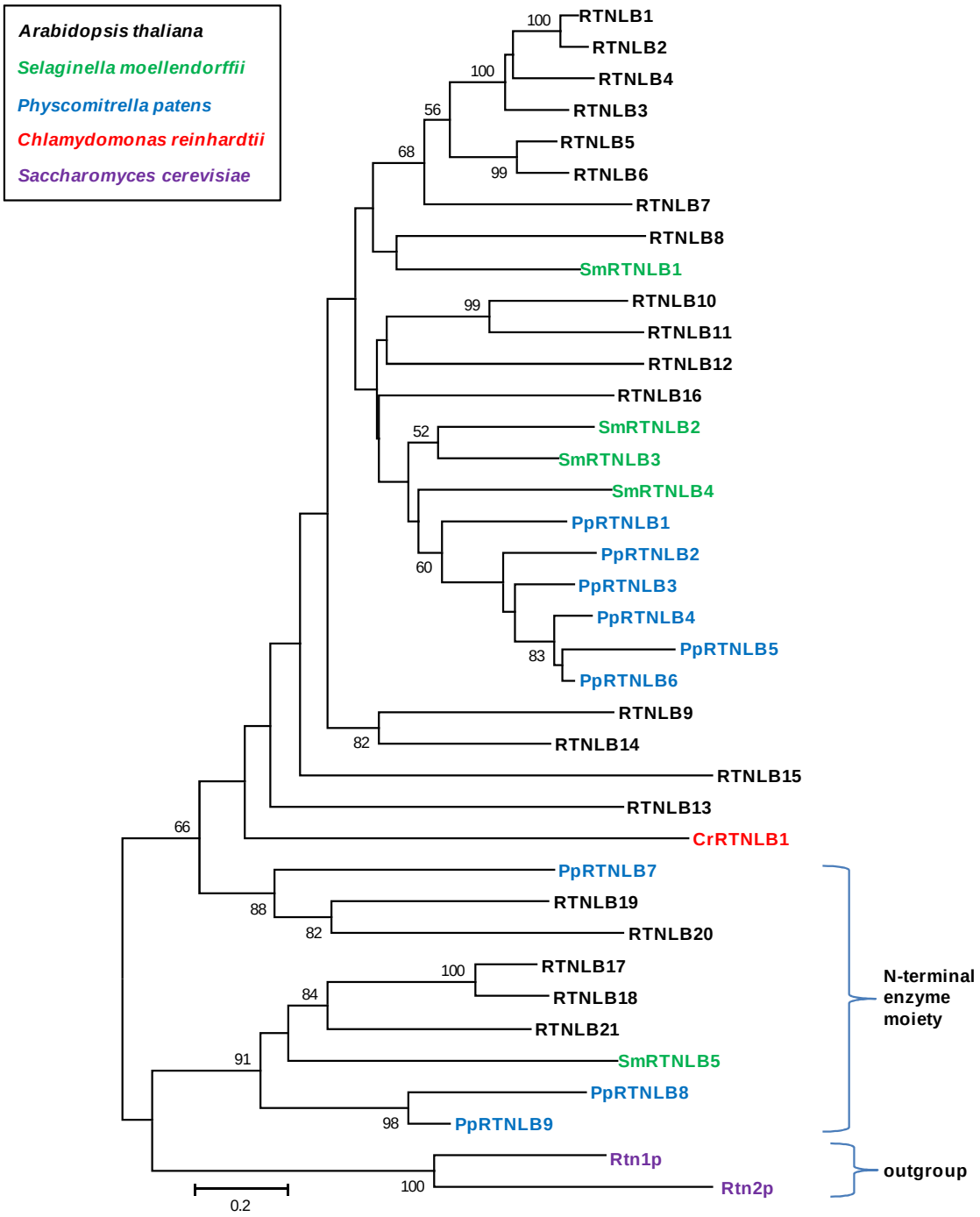

Figure 1.2 Evolutionary relationships of plant RHDs. A phylogenetic comparison between the RHD sequences of *A. thaliana* (RTNLB), *P. patens* (PpRTNLB), *S. moellendorffii* (SmRTNLB) and *C. reinhardtii* (CrRTNLB). Yeast Rtn1p and Rtn2p were used as the outgroup. Figure modified from Sparkes *et al.*, (2009a).

extremely short N-terminus and comprises little more than the RHD (see Appendix Figure A11 for sequence). Consequently, RTNLB13 proves a good starting point for studying the putative structural role of this novel protein family in plants.

The expression of RTNLB13 is seed-specific, and is not detected in any other tissue of the plant (eFP Browser – enhanced fluorescence pictograph indicating expression levels of genes, Winter *et al*., 2007). With regards to the ubiquitous expression of other reticulons expressed (partially) in the seed, this property makes RTNLB13 an interesting candidate for studying the regulation of ER morphology in developing seeds; an area of plant biology mainly based on EM observation.

1.6.2 Aims & experimental approach

In order to analyse the function of RTNLB13, the cDNA sequence will be cloned in frame with a fluorescent protein and the localisation and effect of over-expression determined. RTNLB13 will be co-expressed with an array of molecular markers, including fluorescent protein fusions targeted to the ER, Golgi and the vacuole, to investigate any effect on protein trafficking and organelle dynamics. Both confocal microscopy and biochemical techniques will be carried out, initially in tobacco, in order to establish if and how RTNLB13 localises to the ER membrane, how different domains of RTNLB13 may relate to function and the orientation of which RTNLB13 inserts into the membrane; a pressing question in the reticulon field. Expression will also be analysed in *Arabidopsis thaliana* using a native promoter and cellular processes such as vacuole and lipid body formation, ER morphology and storage protein processing will be compared between wild type *Arabidopsis* and a knockout of RTNLB13.

Chapter 2: Materials & Methods

2.1 Suppliers of Chemicals and Regents

Reagents used were of analytical grade if available, and were obtained from the following sources:

3M (UK): Micropore tape.

AMS Biotechnology (UK): Macerozyme R-10, Cellulase Onozuka R-10.

B & Q (UK): Compost.

BDH (UK): 40% acrylamide solution, NN'-methylene bis-acrylamide, calcium chloride 2-hydrate, ethanol, glucose, glycerol, isopropanol, mannitol, methanol, polyethylene glycol-4000, orthoboric acid, tri-sodium orthophosphate.

BioRad (UK): M17 tungsten particles.

Difco (USA): Bacto-agar, Bacto-tryptone.

Fermentas (UK): Generuler^{TM} 1kb DNA ladder.

Fisher Scientific (UK): Acetic acid (glacial), acetone, EDTA, glycine, hydrochloric acid, potassium hydroxide, sodium chloride, sodium dodecyl sulphate, sucrose, Tris, Tris-buffered phenol.

Fujifilm (Germany): Super RX X-ray film.

GE Healthcare (UK): Amplify™, ammonium persulphate, bromophenol blue, ECL developing reagents, Hybond-P PVDF, [^{35}S]-methionine and cysteine (Promix, 1000 Ci/mmol), Protein A-Sepharose beads, ultra-pure dNTPs.

Gibco BRL (USA): Agarose.

Hycor Biomedical (USA): Glasstic® heamocytometer slides.

Invitrogen (USA): Bacterial alkaline phosphatase, Cloned AMV Reverse Transcriptase Kit, Restriction endonucleases, REact™ buffers, SeeBlue® Plus2 pre-stained markers, T4 DNA ligase, T4 DNA ligase buffer, *taq* DNA polymerase, custom primers.

Kodak (UK): Biomax MR-1 X-ray film.

Loveland Industries (UK): Silwet L-77.

Oxoid (UK): Yeast extract.

Promega (USA): Anti-mouse IgG horseradish peroxidase conjugate.

Qiagen (Germany): QIAprep Spin Plasmid kit, QIAprep Maxi Plasmid kit, QIAprep Gel Extraction kit.

Rathburn (UK): Hexane

Roche (Germany): Complete protease inhibitor cocktail tablets, proteinase K, *Pwo* DNA polymerase.

Sigma-Aldrich (UK): Acetosyringone, ammonium nitrate, anti-rabbit IgG horseradish peroxidase conjugate, β-mercaptoethanol, bovine serum albumin, brefeldin A, calcium nitrate, Coomassie R-250, L-cysteine, disodium hydrogen orthophosphate, $DiOC_6(3)$, DMSO, EDTA, ethidium bromide, Gamborg's B5 basal medium with minimal organics, gelatin, HEPES, kanamycin, latrunculin B, magnesium chloride, L-methionine, Murashige and Skoog basal medium, Nile Red, potassium chloride, polyvinylpyrrolidone, potassium dihydrogen phosphate, rifampicin, spermidine, sodium azide, TEMED, tetracycline, tripentadecanoin (15:0 TAG), Triton X-100, Tween-20, W1 detergent, xylose.

Sinclair (UK): Vermiculite.

Tesco (UK): Marvel dried milk powder.

USB (USA): Nonidet P-40.

Whatman (UK): 3MM chromatography paper.

2.2 Maintenance, preparation and transformation of competent *Escherichia coli* and *Agrobacterium tumefaciens*

2.2.1 Maintenance of *Escherichia coli* and *Agrobacterium tumefaciens* strains

E. coli strain DH5α and *A. tumefaciens* strain C58 harbouring the pSOUP helper plasmid were maintained on Luria-Bertani (LB) agar (10 g/l bacto-tryptone, 5g/l yeast extract, 10 g/l sodium chloride, 2% (w/v) bacto-agar) containing the appropriate antibiotics by streaking and subsequent incubation at 37°C overnight. Overnight cultures (5 ml LB medium containing appropriate selective antibiotics) were inoculated with either *E. coli* or *A. tumefaciens* and incubated at 37°C or 28°C, respectively, in a shaking incubator for approximately 16 hours. Glycerol stocks of each strain and subsequent transformed strains were prepared using a 1:1 ratio of overnight culture to sterile 80% glycerol, thoroughly mixed and stored at -80°C.

2.2.2 Preparation of chemically competent *Escherichia coli* DH5α cells

5 ml LB medium (10 g/l bacto-tryptone, 5 g/l yeast extract, 10 g/l sodium chloride) was inoculated with 10 µl of DH5α (in 50 mM $CaCl_2$, 20% (v/v) glycerol), and incubated for 16 h at 37°C shaking at 250 rpm. 1 ml of this culture was then used to inoculate 100 ml of LB sterilised in a 1 l conical flask. A zero time measurement of OD_{600} was taken (Biochrom Ultrospec 3300 Pro Spectrophotometer) using LB as a blank. This zero measurement was then used as a blank for subsequent measurements. The cells were incubated at 25°C shaking at 250 rpm until the culture had reached an OD_{600} between 0.3 and 0.4. The culture was then cooled on ice for 30 minutes, and transferred to two sterile 50 ml Falcon tubes. Cells were harvested by centrifugation at 2000×*g* (3000 rpm, Beckman GPR bench centrifuge) at 4°C for 10 minutes. The supernatant was discarded, and the pellets were re-suspended in 25 ml cold 50 mM $CaCl_2$. The cells were then held on ice for a further 30 minutes before harvesting as before, but for 5 minutes only. The supernatant was discarded and the

pellets were gently re-suspended in 3 ml cold 50 mM $CaCl_2$, 20% (v/v) glycerol. After gently mixing, cells were transferred to pre-cooled 1.5 ml Eppendorf tubes in 100 µl aliquots. These were immediately frozen in liquid nitrogen, and stored at –80°C.

2.2.3 Transformation of chemically competent *Escherichia coli* DH5α cells

Approximately 5 ng of DNA in 100 µl TCM (10 mM Tris.HCl pH 7.5, 10 mM $CaCl_2$, 10 mM $MgCl_2$) was mixed with 100 µl competent cells in a 1.5 ml Eppendorf tube, and incubated on ice for 30 minutes. Cells were then incubated at room temperature for 10 minutes, before adding 800 µl of pre-warmed LB and incubating at 37°C shaking at 250 rpm for either 30 minutes or 1 hour, depending on whether the antibiotics ampicillin or kanamycin were used, respectively. Cells were harvested by centrifugation at 3000 rpm (Eppendorf bench microfuge) for 5 minutes. Following this, 800 µl of the supernatant was removed, and the pellet was re-suspended in the remaining broth and plated on LB-agar plates containing the appropriate selective antibiotic(s). Plates were incubated inverted at 37°C overnight.

2.2.4 Preparation of chemically competent *Agrobacterium tumefaciens* C58 cells

5 ml LB medium containing rifampicin (50 µg/ml, stock 50 mg/ml in methanol) and tetracycline (5 µg/ml stock 12 mg/ml in ethanol) was inoculated with 10 µl of *A. tumefaciens* strain C58 harbouring pSOUP (in 20 mM $CaCl_2$, 20% (v/v) glycerol), and incubated overnight at 28°C, shaking at 250 rpm. 1 ml of this culture was then used to inoculate 50 ml of LB in a 250 ml conical flask. A zero time measurement of OD_{600} was taken (Biochrom Ultrospec 3300 Pro Spectrophotometer) against LB as a blank. This zero measurement was then used as a blank for subsequent measurements. The cells were incubated at 25°C shaking at 250 rpm until the culture had reached an OD_{600} between 0.5 and 1. The culture was then cooled on ice for 30 minutes and transferred to a sterile 50 ml Falcon tube. Cells were harvested by centrifugation at 2000×*g* (3000 rpm, Beckman GPR bench centrifuge) at 4°C for 10 minutes. The supernatant was discarded, and the pellets re-suspended in 10ml ice-cold 20 mM $CaCl_2$. The re-suspended cells were kept on ice for 30 minutes before harvesting as before, but for 5 minutes only. The supernatant was discarded, and the

pellet was gently re-suspended in 3 ml cold 20 mM $CaCl_2$, 20% (v/v) glycerol. After mixing, cells were transferred to pre-cooled 1.5 ml Eppendorf tubes in 100 µl aliquots. These were immediately frozen in liquid nitrogen, and stored at –80°C.

2.2.5 Transformation of chemically competent *Agrobacterium tumefaciens* C58 cells

Between 0.1 µg and 1 µg plasmid DNA was added to a frozen 100 µl aliquot of competent C58 cells in a 1.5 ml Eppendorf tube. The cells were thawed by incubating at 37°C for 5 minutes, and then flash-frozen in liquid nitrogen. Cells were thawed again by incubating at 37°C for 5 minutes, before adding 1 ml of pre-warmed LB and incubating at 28°C shaking at 250 rpm for a minimum of 2 hours. Cells were harvested by centrifugation at 3000 rpm (Eppendorf bench microfuge) for 5 minutes, 900 µl of the supernatant was removed, and the pellet was re-suspended in the remaining medium and plated onto selective LB agar plates (LB, 2% (w/v) bacto-agar, rifampicin 50 µg/ml (stock 50 mg/ml in methanol), tetracycline 5 µg/ml (stock 12 mg/ml in ethanol), kanamycin 50 µg/ml (stock 100 mg/ml in SDW)). Plates were incubated inverted at 28°C for 2 days.

2.3 Nucleic acid techniques

2.3.1 Preparation of total RNA from *Arabidopsis thaliana* seeds

To isolate total RNA from *Arabidopsis thaliana* seeds, the protocol from Birtic & Kranner, (2006) was followed. In order to quantify the amount of RNA, samples were analysed using a Thermo Scientific NanoDrop 1000.

2.3.1.1 Reverse-transcriptase PCR

Reverse-transcriptase PCR was carried out using the Invitrogen Cloned AMV Reverse Transcriptase Kit. All quantities of RNA, reagents and PCR parameters were followed as per the manufacturer’s instructions.

2.3.2 Preparation of genomic DNA from *Arabidopsis thaliana* leaves

A rapid extraction protocol was utilised to isolate DNA from plant tissue which was required for PCR screening. 10-20 mg of plant leaf tissue was ground in a 1.5 ml Eppendorf tube using a 1 ml pipette tip with the end melted over as a pestle. 400 µl of extraction buffer (250 mM NaCl, 25 mM EDTA, 200 mM Tris.HCl pH 7.5, 0.5% w/v SDS) was added and the samples vortexed for 15 s and centrifuged at 20,000×*g* (Eppendorf benchtop centrifuge) for 5 min. 300 µl of the supernatant was transferred to a new 1.5 ml Eppendorf tube containing 300 µl of room temperature isopropanol. The samples were mixed and incubated at room temperature for 5 min. The mixture was centrifuged at 20,000×*g* for 10 min and the supernatant removed by pipette. The pellet was dried on a hot block at 37°C and re-suspended in 50 µl SDW buffered to pH 8.0.

2.3.3 Amplification of DNA by conventional PCR

DNA fragments required for cloning purposes were typically amplified from plant genomic DNA or from a vector containing the desired region of DNA using conventional PCR. PCR was carried out with *Pwo* DNA polymerase, using a Hybaid OmniGene Thermal Cycler. A typical PCR reaction mixture contained 0.5 ng template DNA, 50 pmol of each primer, 50 µM of each dNTP, 1× PCR buffer (+$MgCl_2$) and 0.5 µl *Pwo* DNA polymerase (5 U/µl), made to a final volume of 50 µl with SDW. Reactions were incubated at 94°C for 1 min and then subjected to 30 cycles of PCR (94°C (denaturing) for 15 s, 55°C (annealing) for 15 s, and 72°C (extension) for 60 s). A final extension period of 10 min at 72°C was performed and the PCR product was analysed by agarose gel electrophoresis (section 2.3.7). The times and temperatures of the PCR cycles varied depending on the size of the PCR product and the T_m of the primers.

To fuse two fragments of DNA, as opposed to inserting a restriction site between them, firstly, the two individual fragments were amplified by PCR, in the case of the first fragment, using a conventional forward primer and a reverse primer, half of which is complementary to the first fragment, and the other half complementary to the second. This technique was repeated for the second fragment, then the two

products were combined with the outer forward and reverse primers in a PCR reaction with an appropriate extension time, to yield the full-length fused construct.

2.3.4 Screening plant genomic DNA by PCR

The presence of a recombinant protein within the *Arabidopsis* genome of potential transgenic plants was verified using a PCR-based approach. Crude *Arabidopsis* genomic DNA (section 2.3.2) was subjected to *taq* polymerase based PCR (30 cycles, 94°C – 15 s, 55°C – 15 s, 72 °C – 60 s, in the presence of 1.5 mM $MgCl_2$ and 0.05% W1 detergent) using gene specific primers.

2.3.5 Preparation of plasmid DNA from *Escherichia coli* DH5α

2.3.5.1 Small-scale preparation of plasmid DNA

Mini-preparation of plasmid DNA was performed using the QIAprep Spin Plasmid Kit. A culture of the plasmid-containing *E. coli* was prepared by inoculating 5 ml LB containing the appropriate selective antibiotic with the colony of interest and incubating at 37°C for 16 hours, shaking at 250 rpm. The following day, cells were harvested by centrifugation at 1500×*g* (2500 rpm, Beckman GPR bench centrifuge) at 4°C for 5 minutes. The supernatant was discarded, and DNA from the resulting cell pellet was extracted according to manufacturer's protocol. The DNA was recovered in 50 µl SDW, and either used immediately or stored at –20°C.

2.3.5.2 Large-scale preparation of plasmid DNA

Large scale preparation of plasmid DNA was achieved using the QIAprep Maxi Plasmid Kit. A culture of the plasmid-containing *E. coli* was prepared by inoculating 2 ml LB containing the appropriate selective antibiotic with a fresh colony, and incubating at 37°C for 8 hours, shaking at 250 rpm. 1 ml of this culture was then used to inoculate 200 ml of LB containing the same concentration of the selective antibiotic, which was incubated in a sterile 1 l conical flask under the same conditions for 16 hours. Cells were harvested by centrifugation at 6000×*g* (6000 rpm,

Beckman J2-21M/E centrifuge) at 4°C for 15 minutes. The supernatant was decanted, and the pellet was used immediately according to manufacturer's protocol. Plasmid DNA was ultimately recovered in 500 µl SDW, and stored at −20°C. DNA concentration was determined using a Thermo Scientific NanoDrop 1000.

2.3.6 Restriction endonuclease digestion of DNA

Restriction endonucleases were used to digest DNA constructs in order to confirm the insertion of DNA or prepare them for ligation (section 2.3.9). Typically, 500 ng DNA was incubated with the appropriate REact™ buffer to a final concentration of 1× in the presence of 1 µl enzyme (5-10 U/µl) in a total volume of 20 µl at the recommended temperature for 2 hours. Resulting DNA fragments were analysed by agarose gel electrophoresis (section 2.3.7). When more than one enzyme was used to digest DNA, if the enzymes did not have compatible REact™ buffers, the cut DNA was isolated and purified after agarose gel electrophoresis (section 2.3.8) between each digestion. When plasmid DNA was cut using blunt-ended restriction enzymes in preparation for the ligation of an insert, it was de-phosphorylated by incubation with 1 µl (150 U/µl) bacterial alkaline phosphatase (BAP) for 1 hour at 65°C, before being isolated and purified (section 2.3.8).

2.3.7 Agarose gel electrophoresis of DNA

Agarose gels were prepared with 0.8-2% (w/v) agarose dissolved in 1× TBE buffer (89 mM Tris, 89 mM H_3BO_3, 20 mM EDTA pH 8.0) containing 0.05% (w/v) ethidium bromide, to stain the DNA. DNA samples were mixed with 6× DNA sample buffer (40% (w/v) sucrose, 0.25% (w/v) bromophenol blue) to a final concentration of 1× buffer, and the mixture loaded into the wells. DNA was electrophoresed at 100 V/cm submerged in 1× TBE for a suitable length of time. The DNA was visualised by placing the gels on a short wave ultra-violet trans-illuminator, and digital images recorded using a GDS8000 Documentation and Analysis System.

2.3.8 Isolation and purification of DNA from agarose gels

DNA digests and DNA amplification by PCR were carried out (sections 2.3.6 and 2.3.3 respectively) and run on agarose gels (section 2.3.7). Fragments were excised from the gel using a scalpel blade under short wave ultra-violet illumination, keeping exposure time to a minimum, and transferred to 1.5 ml Eppendorf tubes. DNA was then either stored in the gel fragment at –20°C, or purified immediately, according to the manufacturer's protocol, using a QIAprep Gel Extraction Kit. DNA was typically recovered in 30 µl SDW, and either used immediately or stored at –20°C.

2.3.9 Ligation of DNA fragments

DNA ligations were performed using T4 DNA ligase, either blunt-ended or following restriction endonuclease digestion and subsequent generation of sticky DNA ends (section 2.3.6). DNA fragments, typically in a 4:1 ratio of insert to vector, were mixed with 2 µl of 5× T4 DNA ligase buffer (250 mM Tris.HCl pH 7.6, 50 mM $MgCl_2$, 5 mM ATP, 5 mM DTT, 25% (w/v) polyethylene-glycol 8000) and 1 µl T4 DNA ligase (1 U/µl), and made up to a total volume of 10 µl with SDW. The mixture was normally incubated for 2 hours at room temperature or at 4°C overnight. Ligated DNA was then transformed into *E. coli* DH5α cells as described in section 2.2.3.

2.3.10 Automated sequencing of plasmid DNA

Automated sequencing of constructs was performed by the Molecular Biology Service at the Department of Biological Sciences, University of Warwick, using ABI® BigDye™ terminator chemistry and an ABI PRISM 3130xl Genetic Analyser™, using protocols and conditions recommended by the manufacturer. Sequencing reactions were specified to use 5.5 pmole primer and 250 ng dsDNA.

2.4 Cloning & Constructs

All constructs generated in this study were synthesised using oligonucleotide primers (Appendix Table A1) and cloned either directly into their destination vector, or

indirectly via a sub-cloning vector. With the exception of two constructs, the restriction sites *XbaI* and *SacI* were exclusively used throughout this study due to their reliable cutting efficiency and the absence of these sites within the DNA coding sequence of RTN13, the myc-epitope and YFP. Unless otherwise stated, all constructs are driven by a 35S CaMV promoter. All vectors used are listed in table 2.1.

2.4.1 Sub-cloning

To facilitate the cloning process, constructs were regularly cloned first into the sub-cloning vectors pBluescript (Stratagene) and 35S-CaMV (Hellens *et al*., 2000). Both vectors are approximately 3kb (Appendix Figures A1-A2, respectively) and contain multiple cloning sites. The orientation in which the constructs were cloned in was irrelevant due to the digestion and re-cloning of the constructs once successfully inserted into the sub-cloning vector. Sequencing primers were designed to surround the multiple cloning sites.

2.4.2 Destination vectors

Following successful sub-cloning and sequencing, constructs were cloned into their final expression vectors. In the case of PEG-mediated protoplast transfections, constructs were cloned into the 35S-CaMV vector downstream of the 35S promoter (Hellens *et al*., 2000). The binary vectors pVKH18-En6 (Moore *et al*., 1998), pGreenII-0029 (Hellens *et al*., 2000) and pLH7000 (Hausmann & Töpfer, 1999) were used for *Agrobacterium*-mediated plant transformation. pVKH18-En6 (Appendix Figure A3) was the main vector used. It contains only two restriction sites, *XbaI* and *SacI*. It has hygromycin resistance in plants for use when making transgenic *Arabidopsis*. pGreenII-0029 (Appendix Figure A4) was only used in one instance, whereby the native promoter and genomic sequence of RTN13 was cloned upstream of YFP-OCS (octopine synthase terminator) for use in localising RTN13 expression in its native tissue. The wide range of restriction sites already available in pGreenII-0029 remained intact upstream of the YFP-OCS insertion. The binary vector pLH7000 (Appendix Figure A6) was used for expression exploiting the Bi-molecular Fluorescence Complementation (BiFC) system (kindly donated by Dr

Eugene Savenkov, Uppsala BioCenter SLU, Sweden). RTN13 and YFP fragment fusions were cloned to include a 35S promoter, and inserted upstream of a 35S terminator. All binary vectors were transformed into *Agrobacterium tumefaciens* strain C58 harbouring the pSoup helper plasmid (Appendix Figure A5). These constructs were then co-expressed with constructs previously made (listed in table 2.2) either to exert an effect on cells, or to be used as fluorescent organelle markers.

Table 2.1 Vectors used in the generation of constructs

Vector	**Application**	**Resistance**	**Reference**
pBluescript KS	Sub-cloning	Ampicillin (100 μg/ml)	Stratagene (Appendix Figure A1)
35S-CaMV cassette vector	Sub-cloning and PEG-mediated transfection	Ampicillin (100 μg/ml)	Hellens *et al*., 2000 (Appendix Figure A2)
pVKH18-En6	*Agrobacterium*-mediated plant transformation (binary vector)	Kanamycin (50 μg/ml – bacteria) Hygromycin (20 μg/ml – *Arabidopsis*)	Moore *et al*., 1998 (Appendix Figure A3)
pGreenII-0029 YFP-OCS	*Agrobacterium*-mediated plant transformation (binary vector)	Kanamycin (50 μg/ml – bacteria) Kanamycin (50 μg/ml – *Arabidopsis*)	Hellens *et al*., 2000 (Appendix Figure A4)
pSoup	Helper plasmid for *Agrobacterium*-mediated plant transformation	Tetracycline (4 μg/ml – bacteria)	Hellens *et al*., 2000 (Appendix Figure A5)
pLH7000	*Agrobacterium*-mediated plant transformation (binary vector)	Streptomycin (100 μg/ml – bacteria) Spectinomycin (100 μg/ml – bacteria)	Hausmann & Töpfer, 1999 (Appendix Figure A6)

Table 2.2 Previously generated 35S-driven constructs used in this study

Construct	Application	Reference
GFP-HDEL	Luminal ER marker	Batoko *et al*., 2000
RFP-HDEL	Luminal ER marker	Proprietary
ST-RFP	Golgi marker	Saint-Jore *et al*., 2002
GFP-calnexin	ER-membrane marker	Irons *et al*., 2003
αTIP-GFP	Tonoplast marker	Hunter *et al*., 2007
γTIP-GFP	Tonoplast marker	Hunter *et al*., 2007
SP:RFP:AFVY	Vacuolar marker	Hunter *et al*., 2007
YN	Residues 1-154 of YFP expressed cytosolically.	Zamyatnin *et al*., 2006
YC	Residues 155-239 of YFP expressed cytosolically.	Zamyatnin *et al*., 2006
YN-ER	Residues 1-154 of YFP targeted to the ER by means of a signal peptide and HDEL retention motif.	Zamyatnin *et al*., 2006
YC-ER	Residues 155-239 of YFP targeted to the ER by means of a signal peptide and HDEL retention motif.	Zamyatnin *et al*., 2006
Phaseolin Δ418	Truncated, secreted version of the vacuolar storage protein phaseolin.	Frigerio *et al*., 1998
Sec12	Guanine nucleotide exchange factor – over-expression inhibits initiation of transport of COPII vesicles from the ER and blocks secretion.	Phillipson *et al*., 2001
YFP-RTN1	N-terminally tagged AtRTNLB1	Courtesy of Professor Chris Hawes, Oxford-Brookes University, UK
RTN1-YFP	C-terminally tagged AtRTNLB1	
YFP-RTN2	N-terminally tagged AtRTNLB2	
RTN2-YFP	C-terminally tagged AtRTNLB2	
YFP-RTN3	N-terminally tagged AtRTNLB3	
RTN3-YFP	C-terminally tagged AtRTNLB3	
YFP-RTN4	N-terminally tagged AtRTNLB4	
RTN4-YFP	C-terminally tagged AtRTNLB4	

2.4.3 Designing constructs

When designing the constructs used in this study (listed in table 2.3) consideration was taken to minimise the effect of the tag on the correct folding of proteins. In most cases, established tags, such as YFP and the myc-epitope, were fused at either the N-

or C-terminus of the protein to determine any effect the orientation may have. Where possible, an untagged form of the protein was also made. Constructs were usually made in two forms: one with a myc-tag for use in biochemical experiments, and one tagged with YFP for use with confocal microscopy, although both tags were used for both purposes. When truncations were implemented, conscious efforts were made to ensure that the truncated region was replaced, rather than left 'free-standing', usually with a myc-tag, which consists of a small, 10-residue stretch of amino acids.

Table 2.3 Constructs generated and used during the course of this study

Construct	Vector	Description
RTN untagged	pVKH18-En6	The full length cDNA of RTN13 cloned in frame with a myc-epitope tag at either the N- or C-terminus or untagged (Fig. 3.6 onwards).
RTN-myc	pVKH18-En6 35S-CaMV	
myc-RTN	pVKH18-En6 35S-CaMV	
RTN-myc-KKSE	pVKH18-En6	As with RTN-myc, but the ER-retrieval motif has been transposed to the C-terminus of the myc-epitope tag.
YFP-RTN	pVKH18-En6	The full length cDNA of RTN13 cloned in frame with YFP at either the N- or C-terminus.
RTN-YFP	pVKH18-En6	
RTN-YFP-KKSE	pVKH18-En6	As with RTN-YFP, but the ER-retrieval motif has been transposed to the C-terminus of YFP.
myc-RTN-ΔKKSE	35S-CaMV	Myc-epitope tagged RTN13 mutant lacking the ER-retrieval motif, residues 203-206 (KKSE).
myc-RTN-ΔC	35S-CaMV	Myc-epitope tagged RTN13 mutant lacking the C-terminus, residues 157-206.
ΔN-RTN-myc	35S-CaMV	Myc-epitope tagged RTN13 mutant lacking the N-terminus, residues 1-22.
ΔN-RRKK-RTN-myc	35S-CaMV	Myc-epitope tagged RTN13 mutant lacking the N-terminus, but retaining hypothetical stop-transfer signal, residues 23-26 (RRKK).
YFP-RTN-ΔKKSE	pVKH18-En6	As with myc-RTN-ΔKKSE, but tagged with YFP.
YFP-RTN-ΔC	pVKH18-En6	As with myc-RTN-ΔC, but tagged with YFP.
ΔN-RTN-YFP	pVKH18-En6	As with ΔN-RTN-myc, but tagged with YFP.
ΔN-RRKK-RTN-YFP	pVKH18-En6	As with ΔN-RRKK-RTN-myc, but tagged with YFP.
myc-RTN–ΔLoop	35S-CaMV	Myc-epitope tagged RTN13 mutant - the loop (residues 75-107) have been replaced with 2x myc-epitope tags.
YFP-RTN –ΔLoop	pVKH18-En6	YFP-tagged RTN13 mutant - the loop (residues 75-107) have been replaced with 2x myc-epitope tags.

Table 2.3 (continued)

YFP-RTN –ΔTM1	pVKH18-En6	YFP-RTN13 mutant - the first trans-membrane domain has been shortened, residues 44-48.
YFP-RTN –ΔTM2	pVKH18-En6	YFP-RTN13 mutant - the first and second trans-membrane domains have been shortened, residues 52-57.
YFP-RTN –ΔTM3	pVKH18-En6	YFP-RTN13 mutant - the first, second and third trans-membrane domains have been shortened, residues 125-130.
YFP-RTN –ΔTM4	pVKH18-En6	YFP-RTN13 mutant - all four trans-membrane domains have been shortened, residues 134-139.
YN-RTN	pLH7000	Residues 1-154 of YFP fused to the N-terminus of RTN13.
YC-RTN	pLH7000	Residues 155-239 of YFP fused to the N-terminus of RTN13.
RTN-YN	pLH7000	Residues 1-154 of YFP fused to the C-terminus of RTN13.
RTN-YC	pLH7000	Residues 155-239 of YFP fused to the C-terminus of RTN13.
RTN –YC–RTN	pLH7000	Residues 155-239 of YFP inserted in the loop region of RTN13 between residues 91-92.
Native-RTN-YFP	pGreenII-0029 YFP-OCS	The genomic sequence of RTN13 cloned with the native promoter and in frame with YFP at the C-terminus.

2.5 Growth, maintenance, and manipulation of *Arabidopsis thaliana* and *Nicotiana tabacum*

2.5.1 *Arabidopsis* ecotype

The *Arabidopsis thaliana* ecotype Columbia (Col-0, used in the *Arabidopsis* Genome Initiative, 2000) was used exclusively in this work.

2.5.2 *Arabidopsis* seed sterilisation, germination and maintenance

Arabidopsis seeds were incubated in 1 ml 70% (v/v) ethanol and mixed for 1 min in a 1.5 ml Eppendorf tube. Seeds were then pelleted at 16,000×*g* for 20 s. The supernatant, along with any floating seeds was removed and discarded, and 1 ml 50% (v/v) bleach added to the pellet. The seeds were then incubated, with continual

agitation, for 5 min. Seeds were pelleted and the supernatant discarded as before, and seeds washed with 1 ml SDW 3 times, spinning between washes. Seeds were then plated, in the last water wash, onto 100 mm petri dishes containing MS-agar (Murashige & Skoog, 1962). Post-sterilisation seeds were sown onto MS-agar plates (Murashige and Skoog (MS) basal medium (4.4 g/l) supplemented with 20 g/l sucrose, adjusted to pH 5.8 with 1 M KOH, and containing 0.8% (w/v) bacto agar and a selective antibiotic if desired). Plates were closed with micropore tape and the seeds vernalised lid-upwards at 4°C for 2 days to promote consistent germination. Seeds were germinated under artificial illumination (12 h light/dark cycle) at a constant temperature of 23°C. Plants were transferred 2 weeks after germination to seed trays filled with a pre-soaked mixture of 50% compost and 50% vermiculite and cultivated in a designated transgenic greenhouse facility in conditions of 16 h light/8 h dark at a constant temperature of 18ºC.

2.5.3 Transformation of *Arabidopsis thaliana*

Arabidopsis seedlings were cultivated in a transgenic greenhouse facility. Plants were transformed, by the method of Clough & Bent, (1998), when 20-50% of the flowers have begun to open. A 5 ml culture of *A. tumefaciens* harbouring the relevant plasmid construct was grown at 28°C in the presence of the appropriate antibiotics. The surfactant Silwet L-77 was added at a concentration of 0.01% immediately prior to *Arabidopsis* transformation. The culture was then pipetted onto the flowers. Plants treated with *A. tumefaciens* culture were sealed in plastic sleeves to maintain humidity and virulence of *A. tumefaciens* for 2 days. Development was then allowed to occur until senescence and watering halted for approximately 2 weeks before seed collection. The seed was harvested, and stored in a 1.5 ml Eppendorf tube, a portion of which was then sterilised (section 2.5.2). Sterilised seeds were plated on MS-agar plates in the presence of the appropriate antibiotic as determined by the plasmid used. Seedlings that germinated and reached at least the 2 rosette leaf stage were deemed putative transformants. Leaf tissue samples were taken to allow PCR, Western blot, or fluorescence analysis to be completed. Following confirmation of successful transformation, transgenic plants were transferred to soil.

2.5.4 Biolistic transformation of *Arabidopsis thaliana*

Arabidopsis thaliana leaves were transiently transformed using a Bio-Rad Biolistic® PDS-1000/He Particle Delivery System. 60 mg of M17 tungsten particles were added to a 1.5 ml Eppendorf tube and washed with freshly prepared 70% (v/v) ethanol, vortexed for 5 minutes and incubated at room temperature for 15 minutes. The particles were pelleted by brief centrifugation at full speed in a benchtop centrifuge and the ethanol discarded. 1 ml of SDW was added followed by vortexing for 1 minute, allowing particles to settle and brief centrifugation at full speed. The liquid was then removed and discarded and this wash step was repeated three times. 1 ml of sterile 50% (v/v) glycerol was added, followed by vortexing and brief centrifugation at full speed. This was repeated, and the particles washed with SDW three times as before. The tungsten pellet was stored at -20°C.

To prepare for transformation, the tungsten pellet was vortexed for 5 minutes and 50 µl was transferred to a 1.5 ml Eppendorf tube. Whilst vortexing, 1 µg of DNA, 50 µl 2.5 M $CaCl_2$ and 20 µl 0.1M spermidine were added to the particles separately. Vortexing continued for 3 minutes, and the particles allowed to settle for 1 minute before brief centrifugation at full speed in a benchtop centrifuge. The supernatant was gently removed and discarded. 140 µl 70% (v/v) ethanol was added without disturbing the pellet and subsequently removed and replaced with 140 µl 100% ethanol. This again was carefully removed and replaced with 48 µl 100% ethanol. The particles were re-suspended in the ethanol by gentle vortexing, 6 µl of which was spread onto a macro-carrier. The components of the apparatus were assembled and the particles shot into the leaves at 1100 psi, with conditions and protocols recommended by the manufacturer.

2.5.5 Isolation of *Arabidopsis* embryos

Embryos from various stages of development were dissected using fine forceps (Sigma-Aldrich No. 5). Siliques from relevant stages were removed from plants to dissect developing embryos. Alternatively, dry seeds were imbibed in SDW for 1 h to dissect mature embryos. For developing embryos, siliques were opened with a scalpel blade and seeds removed. Embryos at all stages were extracted from the testa

and any remaining endosperm by making an incision near the position of the micropyle and applying gentle pressure from the opposite end of the seed. Dissected embryos were then mounted in SDW for imaging on a slide with double sided tape under a coverslip.

2.5.6 Maintenance of *Nicotiana tabacum* plants

2.5.6.1 Tobacco seed sterilisation and germination

Seeds were sterilised in 1.5 ml Eppendorf tubes. Seeds were incubated with 1 ml 70% (v/v) ethanol and mixed for 1 minute before being pelleted at 16,000×*g* (benchtop microfuge) for 20 seconds. The supernatant, along with floating seeds, was removed and discarded, and 1 ml 10% (v/v) bleach was added to the pellet. The seeds were incubated, with continual agitation, in the presence of this bleach for 10 minutes. Seeds were pelleted and the supernatant discarded as before, and washed with 1 ml SDW 5 times, spinning between washes. Seeds were then plated, in the last water wash, onto 100 mm petri dishes containing MS-agar agar (Murashige and Skoog (MS) basal medium (4.4 g/l) supplemented with 20 g/l sucrose, adjusted to pH 5.8 with 1 M KOH, and containing 0.8% (w/v) bacto agar). Petri dishes were incubated in 12 h light/dark cycle at a constant temperature of 26°C and, once germinated, seedlings were transferred one per jar.

2.5.6.2 Maintenance of *Nicotiana tabacum* plants in growth room conditions

The tobacco plants used as the source of protoplasts for the transient expression of DNA constructs (section 2.6), was *Nicotiana tabacum* cv. Petit Havana SRI (Maliga *et al*., 1973). Plants were grown in glass Weck jars, sterilised overnight at 180°C before use, containing 80 ml MS-agar (Murashige and Skoog (MS) basal medium (4.4 g/l) supplemented with 20 g/l sucrose, adjusted to pH 5.8 with 1 M KOH, and containing 0.8% (w/v) bacto agar). When in use, jars were closed with micropore tape. All plants were maintained under artificial illumination (12 h light/dark cycle) at a constant temperature of 26°C. All procedures which involved containing vessels being opened were performed in class two sterile hoods.

2.5.6.3 Maintenance of *Nicotiana tabacum* plants in greenhouse conditions

Nicotiana tabacum cv. Petit Havana SRI were grown from seed in a 50:50 mix of compost and vermiculite in a greenhouse. Plants were maintained at a constant temperature of 18°C and illuminated with a regime of 16 h light/8 h dark.

2.5.7 Transformation of *Nicotiana tabacum* leaf cells by *Agrobacterium* infiltration

A 5 ml overnight culture of *A. tumefaciens* was grown to an OD of 0.5–1.5 at 28°C, shaking at 250 rpm. 1 ml of the culture was centrifuged in a 1.5 ml Eppendorf tube at 5000×*g* in a benchtop microfuge for 5 min. The pellet was re-suspended in 500 µl of infiltration media (50 mM MES, pH5.6; 0.5% glucose (w/v); 2 mM Na_3PO_4; 100 µM acetosyringone (1 M in DMSO stock)). The cells were pelleted as before and re-suspended again by vortexing in 500 µl of infiltration media. The OD_{600} of the suspension was adjusted to an appropriate value between 0.1 by dilution in infiltration media. A small needle was used to make a wound in the lower epidermis of the leaf and the agrobacteria pressure injected using a 1 ml disposable syringe. Multiple-construct transformation was achieved by mixing relevant cultures prior to infiltration. The plant was then incubated under a 12 h light/dark cycle at room temperature for 2-6 days prior to analysis.

2.6 Transient expression in tobacco protoplasts

2.6.1 Preparation of protoplasts from tobacco leaves

All operations in which samples or solutions were opened were carried out in class two sterile hoods. All solutions were stored at −20°C when not in use and, with the exception the DNA, filter sterilised. 10× enzyme mix (Macerozyme R-10 (2% (w/v)), Cellulase Onozuka R-10 (4% (w/v)) in K3 medium (3.78 g/l Gamborg's B5 basal medium with minimal organics, 750 mg/l $CaCl_2.2H_2O$, 250 mg/l NH_4NO_3, 136.2 g/l sucrose, 250 mg/l xylose, 1 mg/l 6-benzylaminopurine (6-BAP), 1 mg/l α-naphtalenacetic acid (NAA)) was diluted to a final concentration of 1× with K3

immediately before use, and poured into 100 mm petri dishes in 7 ml aliquots. 4 to 6 week old green leaves were cut from a sterile plant and carefully scarified on their underside using a sterilised scalpel. The mid-ribs were removed, and the scarified leaves were transferred such that the wounded face was in contact with the enzyme mix. Plates were filled by adding fragments of scarified tissue, and incubated overnight in the dark at 26°C. The following morning, the digestion mix was carefully removed using a sterile Pasteur pipette and discarded, with the protoplasts still attached to the leaves. 3 ml of K3 was added drop wise over the leaves, and the plates gently agitated in order to release the protoplasts. The resulting protoplast solution was removed, using a fresh sterile Pasteur, and filtered through a 100 µm brass sieve, flamed and wet with K3 before use. A further 3 ml K3 was added to the leaves, and any further protoplasts released by this second wash were transferred as before. The harvested, filtered protoplasts were centrifuged in 50 ml sterile Falcon tubes at 100×*g* (600 rpm, Beckman GPR bench centrifuge) for 20 minutes at room temperature, in order to separate broken from viable protoplasts. The pellet of broken protoplasts and most of the K3 above it was removed, using a Pasteur pipette connected to a 25 ml pipette, typically leaving 5ml K3 containing the floating layer of viable protoplasts. After mixing gently to redistribute this floating layer, 4 volumes of W5 medium (9 g/l NaCl, 0.37 g/l KCl, 18.37 g/l $CaCl_2.2H_2O$, 0.9 g/l glucose) was added drop-wise down the wall of the tube. The solution was gently mixed until the protoplasts were evenly distributed within the new volume. Protoplasts were pelleted by centrifugation at 100×*g* (600 rpm, Beckman GPR bench centrifuge) for 10 minutes at room temperature, and the supernatant aspirated off and discarded. The resulting pellet was gently re-suspended after the drop-wise addition of W5 to the same total volume as in the previous step. Protoplasts were pelleted again and the supernatant was once more discarded. Finally, protoplasts were carefully re-suspended up to 10 ml W5 and incubated in the dark for 30 minutes at room temperature. A 50 µl sample was removed, using a cut P200 tip, for counting.

2.6.2 Protoplast counting

A 50 µl sample of the protoplast solution in W5 was taken, using a cut P200 tip, and diluted in 450 µl K3. Protoplasts were gently mixed, and aliquots of 10 µl were

loaded onto 0.9 µl Hycor Glasstic® haemocytometer slides using a cut tip. Slides were observed at 40× magnification, and only those protoplasts appearing round were counted as viable.

2.6.3 Protoplast transfection

After the 30 minute dark incubation, protoplasts were pelleted by centrifugation at 100×*g* (600 rpm, Beckman GPR bench centrifuge) for 5 minutes at room temperature, and the supernatant removed and discarded. The resulting pellet was gently re-suspended in MaCa (0.5 M mannitol, 20 mM $CaCl_2$, 0.1% (v/v) MES pH 5.7) in a total volume yielding a final protoplast concentration of 1 million/ml. Protoplasts were heat-shocked at 45°C for 5 minutes, and allowed to cool at room temperature for at least 10 minutes. 15 ml sterile Falcon tubes containing the DNA for transfection (typically 20-40 µg per million cells) were prepared, and 1 ml aliquots of protoplasts gently transferred to each, using cut P1000 tips. Tubes were mixed, then tilted, and 1 ml 40% (w/v) PEG (40g polyethylene-glycol 4000 dissolved in 60 ml of 0.1 M $Ca(NO_3)_2.4H_2O$, 0.4 M mannitol, pH adjusted to between 8 and 10 with dilute KOH, and volume brought to 100 ml) was added drop wise down the walls of the tube, using a cut P1000 tip, with gentle but thorough mixing before incubating at room temperature for 30 minutes. Protoplasts were washed by filling the tubes with W5, which was achieved over a minimum period of 15 minutes, to avoid shocking the cells. W5 was added drop-wise down the tube walls in 3 ml aliquots and the tubes mixed gently but thoroughly between each addition. Protoplasts were pelleted by centrifugation at 100×*g* (600 rpm, Beckman GPR bench centrifuge) for 10 minutes at room temperature, the supernatant removed and discarded, and the pellet carefully re-suspended in 1ml K3. Protoplasts were then allowed to recover overnight in the dark at 26°C.

2.6.4 Radioactive labelling of protoplasts

For pulse-chase experiments, transfected protoplasts were labelled in 2 ml safe-lock Eppendorf tubes in a volume of 150 µl per time-point. The volume of the transfected protoplasts was reduced as necessary by carefully removing the subnatent,

facilitating the removal of any material which had pelleted overnight. The floating layer was redistributed in the new volume, and transferred to the Eppendorf using a cut P1000 tip. Viable protoplasts were allowed to float again during a short incubation in the dark at 26°C. 150 mg/ml bovine serum albumin (BSA, stock 4 mg/ml in K3) and 100 mCi/ml ^{35}S-Promix (14.5 mCi/ml) were then added below this floating layer, which was gently but thoroughly redistributed, and incubated in the dark at 26°C for 1 hour. The chase was performed by adding 'cold' unlabelled methionine and cysteine to a final concentration of 10 and 5 mM, respectively. The zero time-point was taken by removing 150 µl of protoplasts with a cut P200 tip, immediately after mixing, to a fresh, pre-cooled 1.5 ml Eppendorf containing 3 volumes of W5. After careful but thorough mixing, the protoplasts were pelleted by centrifugation at 100×*g* (600 rpm, Beckman GPR bench centrifuge) at 4°C for 10 minutes. The supernatant, containing any proteins secreted to the medium, was carefully transferred to a pre-cooled 2 ml Eppendorf. The resulting protoplast pellet was immediately frozen on dry ice. The saved supernatant was spun as before, in order to precipitate any protoplasts inadvertently carried over from the pellet, and finally transferred to a further pre-cooled 2 ml Eppendorf and frozen on dry ice. Any subsequent time-points were taken in this manner, and samples were again stored at –80°C until use.

For simple pulse-screening, a specific number of protoplasts (typically ~330,000) were labelled, in the manner detailed above. All protoplasts were harvested and frozen at the end of the pulse, without prior addition of unlabelled amino acids, and all supernatants were discarded.

2.6.5 Pre-clearance of antibodies

Antibodies were pre-exposed to unlabelled, cross-reacting contaminants, so as to reduce background contamination when the antibody is subsequently exposed to the radioactively-labelled sample. Leaf tissue of a similar quantity and age to that used in the pulse-chase experiment, was collected in a pre-chilled mortar and ground in liquid nitrogen until a fine powder was produced. 2 ml of ice-cold protoplast homogenisation buffer (150 mM Tris.HCl pH7.5, 150 mM NaCl, 1.5% (v/v) Triton X-100, supplemented immediately before use with 'complete' protease inhibitor

cocktail) was added to the powder. After defrosting, the homogenate was reground thoroughly and then filtered through a nylon mesh to remove any remaining large pieces of material. The homogenate was transferred to a pre-cooled 50 ml Falcon tube and centrifuged at 3,500 rpm (Beckman GPR bench centrifuge) at 4°C for 15 minutes, to remove any insoluble debris. The supernatant was then carefully transferred to a fresh, pre-cooled Falcon tube. NET-gel buffer (50 mM Tris.HCl pH7.5, 150 mM NaCl, 1 mM EDTA, 0.1% (v/v) Nonidet P-40, 0.25% (w/v) gelatine, 0.02% (w/v) NaN_3) was added such that the total volume equated to 650 µl per immunoprecipitation, and antiserum or antibody added to the required concentration (typically 1 or 2 µl per sample). The homogenate was then incubated on ice for a minimum of 2 hours, before being used, in place of NET-gel, to increase the total volume of the homogenised cell samples to 1 ml in the immunoprecipitation protocol.

2.6.6 Immunoprecipitation of radiolabelled samples

Frozen cell pellets and supernatants (section 2.6.4) were homogenised on ice by the addition of 350 µl of cold protoplast homogenisation buffer, or 2 volumes of the same buffer containing 0.25% (w/v) gelatin, respectively (both buffers supplemented immediately before use with 'complete' protease inhibitor cocktail) and promptly vortexed. The homogenised cell samples were brought to a total volume of 1 ml with either NET-gel buffer or NET-gel buffer supplemented with pre-cleared antibody, as appropriate (section 2.6.5), and mixed well. All samples were centrifuged twice at 25,000×*g* (Eppendorf 5417R refrigerated microcentrifuge) at 4°C for 4 minutes, transferring the supernatants to fresh, pre-cooled Eppendorf tubes after each spin, in order to remove any insoluble debris. Antiserum or antibody was added as appropriate, before all samples were mixed and incubated on ice for 2 hours. Tubes were centrifuged again briefly to draw samples out of the lids before opening after this incubation. 100 µl of a 10% (swelled bead w/v) suspension of Protein-A Sepharose in NET buffer (50 mM Tris.HCl pH 7.5, 150 mM NaCl, 1 mM EDTA, 0.1% (w/v) Nonidet P-40) was added to each sample, before vortexing briefly and incubating on a rotating wheel at 4°C for 2 hours. Beads were pelleted by centrifugation at 25,000×*g* (Eppendorf 5417R refrigerated microcentrifuge) for 1

minute at 4°C, the supernatant aspirated (or removed and saved in the case of immunoprecipitation with a second antisera or antibody) and the pellet re-suspended in 1 ml NET-gel buffer by brief vortexing. Beads were pelleted again, and washed in the same manner twice more. After the removal of the last supernatant, beads were stored frozen at −20°C or immediately prepared for separation by SDS-polyacrylamide gel electrophoresis (section 2.7.1).

2.6.7 Preparation of microsomes

Protoplast pellets (typically from between 333,000 to 667,000 cells) obtained at the desired time point during pulse-chase were kept on ice until they were re-suspended in 140 µl of sucrose buffer (100 mM Tris.HCl pH7.6, 10 mM KCl, 1 mM EDTA, 12% (w/v) sucrose, supplemented immediately before use with 'complete' protease inhibitor cocktail), and homogenised by pipetting up and down 50 times through a P200 tip. The homogenate was then centrifuged at 500×g (Eppendorf 5417R refrigerated microcentrifuge) to pellet any intact cells and debris. 128 µl of the supernatant was loaded on top of a 17% (w/v) sucrose pad and centrifuged at 100,000×g (55,000 rpm, Beckman TL-100 ultracentrifuge) for 30 min at 4°C. Pellets (microsomes) and supernatants (soluble proteins) were diluted in protoplast homogenisation buffer and subject to immunoprecipitation (section 2.6.6).

2.7 Protein resolution and detection

2.7.1 Separation of proteins by SDS-polyacrylamide gel electrophoresis (SDS-PAGE)

SDS-polyacrylamide gels for pulse-chase, Coomassie and western blot experiments were cast and run using the Bio-Rad Protean II gel electrophoresis system, according to the manufacturer’s instructions. All protein samples for SDS-PAGE analysis were combined with Laemmli loading dye (0.5 M Tris.HCl pH 6.8, 4.4% (w/v) SDS, 20% (v/v) glycerol, 0.036% bromophenol blue in SDW). The reducing agent β-mercaptoethanol was added at a concentration of 2% (v/v) to all protein samples unless otherwise indicated.

Typically, 15% acrylamide gels (15% (w/v) acrylamide, 0.15% (w/v) bis-acrylamide, 375 mM Tris.HCl pH 8.8, 0.1% (w/v) SDS, 0.05% (w/v) APS and 0.005% (v/v) TEMED) were used to resolve most proteins. In the case of resolving *Arabidopsis* seed storage proteins, a higher concentration of 20% (w/v) acrylamide and 0.625% (w/v) bis-acrylamide were used. Stacking gels consisted of 4.5% (w/v) acrylamide, 0.8% (w/v) bis-acrylamide, 50 mM Tris.HCl pH 6.8, 0.o4% (w/v) SDS, 0.045% (w/v) APS and 0.0045% (v/v) TEMED.

2.7.2 Fluorography, drying, and autoradiography of protein gels

2.7.2.1 Amplify™ treatment of SDS-polyacrylamide gels

Gels were incubated in fixative (40% (v/v) methanol, 10% (v/v) acetic acid) with continual agitation for at least 30 minutes. The fixative was poured off and discarded, and replaced with enough Amplify™ to cover the gel surface. Gels were incubated in Amplify™ for 20 minutes, before being rinsed with SDW, placed on dampened 3MM paper with a dry layer underneath, and covered with cling film. Gels were then dried, exposed, and the film developed. The relative intensities of radioactive bands on autoradiographs were quantified using TotalLab (2003) software. Care was taken to ensure that exposures quantified were within the linear range of the film.

2.7.2.2 Gel drying and autoradiography

Gels were vacuum dried at 80°C using either a Whatman Biometra gel drier, before being exposed to X-ray sensitive film (Kodak BioMax MR) in a light-proof cassette under dark room conditions, and stored at −80°C for an appropriate length of time (typically 1-4 weeks). Films were developed using the Agfa Curix 60 automatic developer, with conditions and protocols recommended by the manufacturer.

2.7.3 Coomassie staining of SDS-polyacrylamide gels

SDS-PAGE gels were incubated with staining solution (40% (v/v) methanol, 10% (v/v) acetic acid, 2.5% Coomassie R250) for ~1 hour on a shaking platform. Gels

were then destained for up to 2 hours with frequent changes of destain (40% (v/v) methanol, 10% (v/v) acetic acid), again on a shaking platform, or overnight, in 50% destain solution and 50% SDW. In cases where results were required in a shorter timeframe, the efficiency of the initial Coomassie and destain treatments was increased by heating the gel in solution in a microwave for approximately 1 min.

2.7.4 Western blotting of SDS-polyacrylamide gels

2.7.4.1 Protein transfer and immunodetection

Protein samples separated by SDS-PAGE (section 2.7.1) were transferred from the gel onto PVDF membrane (prepared by soaking briefly in methanol and then for 2 minutes in transfer buffer (25 mM Tris, 192 mM glycine, 20% methanol)) using Sigma-Aldrich techware Semi-dry blot apparatus under a constant current of 200 mA for 2 hours. The membrane was then blocked in phosphate-buffered saline (PBS (137 mM NaCl, 0.27 mM KCl, 10.4 mM disodium hydrogen phosphate, 1.8 mM potassium dihydrogen phosphate)) containing 5% (w/v) skimmed milk powder and 0.1% Tween-20 with agitation for 2 hours at room temperature, or at 4°C overnight. The block was discarded and the membrane incubated, with continual agitation, in 20 ml PBS-Tween-Milk containing the primary antibody (typically at a 1:1000 dilution) for 1 hour. The membrane was washed in PBS-Tween (two quick rinses followed by six subsequent incubations of 5 minutes) before incubation in 20 ml PBS-Tween-Milk containing a horseradish peroxidase-conjugated secondary antibody (at a dilution specified by the manufacturer, typically 1:10,000) for 1 hour, again under continual agitation. The membrane was then washed in PBS-Tween exactly as before, and detection of immunoreactive bands performed using the Amersham ECL kit (Enhanced chemiluminescence), according to the manufacturer's instructions, and recorded by exposing to X-ray film (Fujifilm Super RX) in a light-proof cassette for an appropriate length of time. Films were developed as in section 2.7.2.2.

2.7.4.2 Antibodies

The antisera presented in Table 2.4 were employed in this work.

Table 2.4 Antibodies

Antibody	Animal, Class	Antigen	Concentration	Reference
Anti-GFP	Rabbit, polyclonal	GFP, YFP	Western blot: 1:1000	A gift from Liwen Jiang, Chinese university of Hong Kong
Anti-myc	Mouse, monoclonal	Myc-epitope, (EQKLISEEDL)	Western blot: 1:1000 Immunoprecipitation: 1µl per sample	Jarvis JM, MRC LMB, Cambridge
Anti-BiP	Rabbit, polyclonal	Binding Protein (BiP)	Immunoprecipitation: 1µl per sample	Pedrazzini *et al*., 1997
Anti-Rabbit (Secondary)	Goat	Rabbit antibody	Western blot: 1:10000	Sigma-Aldrich (USA)
Anti-Mouse (Secondary)	Goat	Mouse antibody	Western blot: 1:10000	Promega (USA)

2.7.5 Protein Extraction from *Arabidopsis thaliana* seeds

Proteins were extracted from 1 g starting material of *Arabidopsis thaliana* seeds using the protocol from Isaacson *et al*., (2006). Protein concentration was determined using a Thermo Scientific NanoDrop 1000.

2.8 Microscopy

2.8.1 Confocal microscopy

Tissue samples from transgenic *Arabidopsis* or infiltrated tobacco leaves were examined using either an upright Leica DRM TCS SP2 or an inverted Leica TCS SP5 confocal microscope. Images of seed embryos and leaves were collected using a 63× oil objective lens (NA 1.40). Samples were mounted in SDW either directly on

the surface of a microscope slide, or adhered with double sided tape, with a coverslip on top. Fluorophores were excited and detected at their excitation/emission peaks (Table 2.5). Where significant overlap existed between the excitation spectra of multiple fluorophores present in the tissue sample, separation was achieved by detection of fluorescence from each protein in turn between sequential frame scanning. Image processing facilities were provided by Leica Confocal Software.

Table 2.5 Excitation and emission values of fluorophores and auto-fluorescent cellular material

Fluorophore	Excitation (nm)	Emission range (nm)	Type	Reference
eYFP	514	519 - 590	Protein	Clontech Laboratories, Palo Alto, CA
RFP	543 or 561	592 - 635	Protein	Clontech Laboratories, Palo Alto, CA
mGFP	488	508 - 535	Protein	Haseloff *et al.*, 1997
Chlorophyll	488 or 514	660 - 700	Autofluorescent porphyrin pigment	-
Storage vacuole metabolites	405	450 - 510	Autofluorescent material	Hunter *et al.*, 2007
Nile Red	488	525	Lipophilic dye	Hawes & Satiat-Jeunemaitre, 2001
LD540	514	548	Lipophilic dye	Spandl *et al.*, 2009
$DiOC_6$ (3)	488	511	Fluorochrome	Quader & Schnepf, 1986

2.8.2 Staining lipids with Nile Red

Arabidopsis embryos were dissected (section 2.5.5) and incubated for 1 hour in the dark at room temperature in 1% Nile Red in SDW from a stock of 1 mg/ml in acetone stored at 4°C. The embryos were washed with SDW before mounting on a

slide. At this concentration, neutral lipids can be visualised when excited at 488 nm and detected at 525 nm using confocal microscopy (section 2.8.1).

2.8.3 Staining lipids with LD540

Arabidopsis embryos were dissected (section 2.5.5) and incubated for 30 minutes in the dark at room temperature in 1 µg/ml LD540 in SDW from a stock of 0.5 mg/ml in ethanol stored at 4°C. The embryos were washed with SDW before mounting on a slide. At this concentration, lipids can be visualised when excited at 514 nm and detected at 548 nm using confocal microscopy (section 2.8.1).

2.8.4 Staining the Endoplasmic Reticulum with $DiOC_6$

Arabidopsis embryos were dissected (section 2.5.5) and incubated for 1 hour in 5 µg/ml $DiOC_6$ (3) (3,3'-dihexyloxacarbocyanin-iodide) from a stock of 5 mg/ml in DMSO (dimethylsulphoxide) stored at 4°C. At this concentration, the ER can be visualised when excited at 488 nm and detected at 511 nm using confocal microscopy (section 2.8.1).

2.8.5 Fluorescence recovery after photobleaching (FRAP)

Fluorescence recovery after photobleaching studies were performed on leaf segments treated with 10 mM latrunculin B for 30 minutes using a Zeiss LSM510 Meta equipped with a 63× oil objective lens (NA 1.40) using 514 nm/458 nm excitation and beam splitters for detection of YFP and GFP, respectively. GFP was bleached within a defined region of interest with 10 iterations of 100% 405 nm laser power and subsequent recovery monitored. The bleach area was constant in all experiments (190 μm^2). Relative levels of fluorescence were normalized to 100% prior to bleach and subsequent recovery plotted as a percentage of pre-bleaching fluorescence intensity.

2.8.6 Treatment of cells with BFA

To induce sheets within the ER, infiltrated leaf sections were incubated for 1 hour in the presence of the fungal antibiotic brefeldin A (BFA) at a concentration of 50 μg/ml from a stock of 5 mg/ml in DMSO. The leaf sectors were mounted on a slide and cells were visualised using confocal microscopy (section 2.8.1).

2.9 Lipid analysis of *Arabidopsis thaliana* seeds using gas chromatography

100 *Arabidopsis* seeds were counted into a 1.5 ml glass screw cap vial. 10 μl of 15:0 TAG internal standard (25 mg/ml tripentadecanoin in chloroform) were added to each vial, followed by 0.5 ml of 1M MeOH.HCl. The vials were capped firmly, vortexed briefly and transferred to an 85°C oven and incubated overnight, shaking periodically. The following day, the vials were removed from the oven and allowed to cool to room temperature at which point, 250 μl of 0.9% (w/v) KCl, followed by 800 μl of hexane, were added to the vials. The vials were capped, vortexed briefly and incubated at room temperature for 10 minutes to allow the two phases to separate. The upper phase contained the fatty acid methyl esters. The GC auto-sampler was programmed to sample directly from this upper phase avoiding the lower phase.

2.10 Protease protection assay

Cut pipette tips were used at all stages. 4 - 8 *Agrobacterium*-infiltrated leaf sectors containing construct of study were ground with a chilled mortar and pestle in 4 ml extraction buffer (10 mM KCl, 1 mM $MgCl_2$, 0.4 mM sucrose, 0.4% PVP, 40 mM HEPES.KOH, pH 7.5 (Brach *et al*., 2008)) for 3 minutes. The homogenate was transferred to two pre-chilled 2 ml Eppendorf tubes. The samples were centrifuged at 1000×*g* for 5 minutes at 4°C, and the supernatants transferred to a fresh tube on ice.
A sucrose pad was set up in 4 ml ultracentrifuge tube. 750 μl of 20% sucrose in extraction buffer was carefully layered on top of 750 μl of 60% sucrose in extraction buffer. Finally, 2 ml of sample was carefully added to the sucrose pad, and

centrifuged at 55,000 rpm for 30 minutes at 4°C in a Beckman TL-100 ultracentrifuge.

The microsomes form an interphase between the 20 and 60% sucrose layers. The majority of the upper phases were removed by aspiration, and 200 µl of the microsomes recovered and gently re-suspended in a fresh tube. Four 0.5 ml Eppendorf tubes were set up for each sample containing the components listed in table 2.6. At this stage, 25 µl of the sample was pre-incubated with 20 mM $CaCl_2$, PK buffer (50 mM Tris.HCl pH 8.0, 1 mM $CaCl_2$) and triton X-100 for 15 minutes on ice to ensure membranes are disrupted (Ma *et al*., 2006), before adding 5 µl of 0.5 µg/ml of Proteinase K, and incubating at 30°C for 30 minutes.

To terminate the reaction, one Complete-mini protease inhibitor cocktail tablet was dissolved in 1 ml SDW and 10 µl of this was added to each reaction tube. 60 µl of loading dye was added and the samples were boiled for 5 minutes before loading the samples to be resolved by SDS-PAGE.

Table 2.6 Reaction conditions for protease protection assay

Proteinase K		-	+	+	-
Triton X-100		-	-	+	+
$CaCl_2$		5µl	5µl	5µl	5µl
PK Buffer		20µl	15µl	5µl	10µl
PK		-	5µl	5µl	-
Triton		-	-	10µl	10µl

Chapter 3: Analysis of RTN13 over-expression in tobacco

3.1 Introduction

Originally known as neuroendocrine-specific proteins (NSPs), reticulon proteins were first identified in 1994 and found to localise to the ER, closely associated with smooth ER (van de Velde *et al*., 1994). Antibodies raised against NSP-A and NSP-C (later termed Rtn1a/c) both stain the ER (Senden *et al*., 1996) and associate with a 'calreticulin negative' domain of the ER (Steiner *et al*., 2004). Human Rtn4, known as Nogo, localises to the ER (Grandpre *et al*., 2000) and, as do many other reticulons, contains an ER-retrieval motif (Watari *et* al., 2003) and is thought to reside in regions of high curvature (Kiseleva *et al*., 2007).

In other organisms, reticulons have also been found to localise to the ER. A reticulon homologue in Rat, vp20, contains an ER-retrieval motif and is reported to be abundant in cells enriched in ER (Morris *et al*., 1999). In *Drosophila*, RTNL-1 is associated with the ER and Golgi (Wakefield *et al*., 2006), specifically a subset of the ER associated with SER. The *Xenopus* XRTN1a and XRTN1c localise to the ER and also contain ER-retrieval motifs (Park *et al*., 2005; Park *et al*., 2007). In plants, *Arabidopsis thaliana* contains 21 reticulon genes, 16 of which contain an ER-retrieval motif at the C-terminus. Of these, RTNLB1 is reported to localise to the cell periphery (Hwang & Gelvin, 2004) and both RTNLB2 and RTNLB4 localise to the ER (Nziengui *et al*., 2007).

It has been suggested that reticulons further localise to specific subdomains of the ER. Rtn2b is thought to localise to ER-exit sites (ERES) and may therefore be involved in protein transport to the cell surface (Liu *et al*., 2008). The *Drosophila* RTNL-1 localises to a distinct region of the ER which differentially interacts with microtubules (Pokrywka *et al*., 2009).

Rtn4 and its associated homologues DP1/Yop1p all localise specifically to tubular ER (Shnyrova *et al*., 2008). Further to this, Rtn4a is thought to localise to a sub-domain of tubular ER, distinct from that of ER which associates with mitochondria (Goetz *et al*., 2007). It has been suggested by Voeltz *et al*., (2006) that Rtn4 and its homologues are restricted to tubular ER due to their distinct protein structure.

When over-expressed, Rtn4 induces the formation of long, un-branched ER tubules (Voeltz *et al*., 2006). Interestingly, the over-expression of Rtn3 inhibits ER-to-Golgi trafficking (Wakana *et al*., 2005), whereas over-expressed Rtn1c increases protein secretion (Steiner *et al*., 2004). This supports the notion that, although reticulon proteins share a homology domain, their variable N-terminal region may interact with and regulate many different cellular processes.

Due to the close proximity of the ER to other organelles, and the fact that ERES and Golgi may be physically associated in plants, it seems logical to hypothesise that over-expression of reticulon would affect downstream trafficking in the secretory pathway, most notably transport to the Golgi. For example, mammalian Rtn3 has been implicated in ER-to-Golgi trafficking (Wakana *et al*., 2005) and a series of reticulon interacting partners have been associated with the Golgi including proteins contributing to organelle morphology (Haas *et al*., 2007), SNAREs and vesicle fusion (Steiner *et al*., 2004; Martin *et al*., 2006).

There is great divergence within the super-family of reticulon proteins, and due to the varying range of information available it is difficult to ascertain structural and functional properties of reticulons from a comparative perspective alone. Therefore, this thesis aims at investigating the structure and function of the smallest, seed-specific reticulon of *Arabidopsis thaliana*, RTNLB13. Little is known about the *Arabidopsis* reticulon family, or indeed the function of these proteins in plants. Of the 21 reticulon genes in *Arabidopsis*, RTNLB13 is the smallest, comprising little more than the RHD. Therefore, any structural and functional information contained within the gene must be encoded within this region. RTNLB13 is expressed in the final stages of seed maturation, and its study may provide insights into the state of the ER during this stage of development, and how reticulons may contribute to the storage of proteins, formation of lipid bodies and aid in the desiccation of the seed as it prepares for dormancy.

3.1.1 Aims & experimental approach

The focus of this chapter is to analyse the subcellular localisation of RTNLB13 using 35S-driven expression in tobacco, establish any phenotype of over-expression and

any subsequent effect on transport within the ER and to other compartments further along the secretory pathway. By creating constructs bearing myc- or YFP-tags, RTNLB13 can be analysed both by confocal microscopy and biochemically. In order to do so, tobacco leaves were transiently transformed via agro-infiltration. Typically, the concentration of agrobacteria was adjusted to an OD_{600} of 0.1 and visualised 4-5 days post infiltration. Tobacco protoplasts were tranfected by PEG-mediated transfection, radiolabelled and subject to immunoprecipitation and SDS-PAGE.

3.1.2 Cloning and construct design

The cDNA sequence of RTNLB13 was modified by means of tagging with either a myc-epitope tag or yellow fluorescent protein (YFP) and cloned, using the restriction endonucleases *XbaI* and *SacI*, into appropriate expression vectors. Constructs used for *Agrobacterium*-mediated infiltration were inserted into the plant binary vector pVKH18-En6 (Moore *et al*., 1998). Constructs used for PEG-mediated transfections in tobacco protoplasts were inserted into a small 35S-CaMV vector (Hellens *et al*., 2000). When tagging RTNLB13, variations of each construct were designed to minimise the effect of the tag's position within the protein (Figure 3.1). To improve clarity within the text, the *Arabidopsis thaliana* reticulon protein RTNLB13 is referred to as 'RTN13' and in figures simply as 'RTN'. Any reference to other reticulon isoforms is clearly indicated.

3.2 Over-expression of variably tagged RTN13 induces severe morphological changes in the structure of the ER

In order to characterise the expression of RTN13, varying myc-tagged forms were co-expressed with the ER reporter, GFP-HDEL, in tobacco leaves using agro-infiltration. This was undertaken to determine any phenotype when RTN13 is over-expressed, using soluble GFP-HDEL to highlight the lumen of the ER. Several constructs were designed, taking into account any effect of the position of the myc-tag. These included an untagged form, the myc-tag positioned at either the N- or C-terminus of RTN13 and a C-terminal myc-tag with the last four residues of RTN13 (KKSE) transposed downstream of the myc-tag in order to retain exposure of the

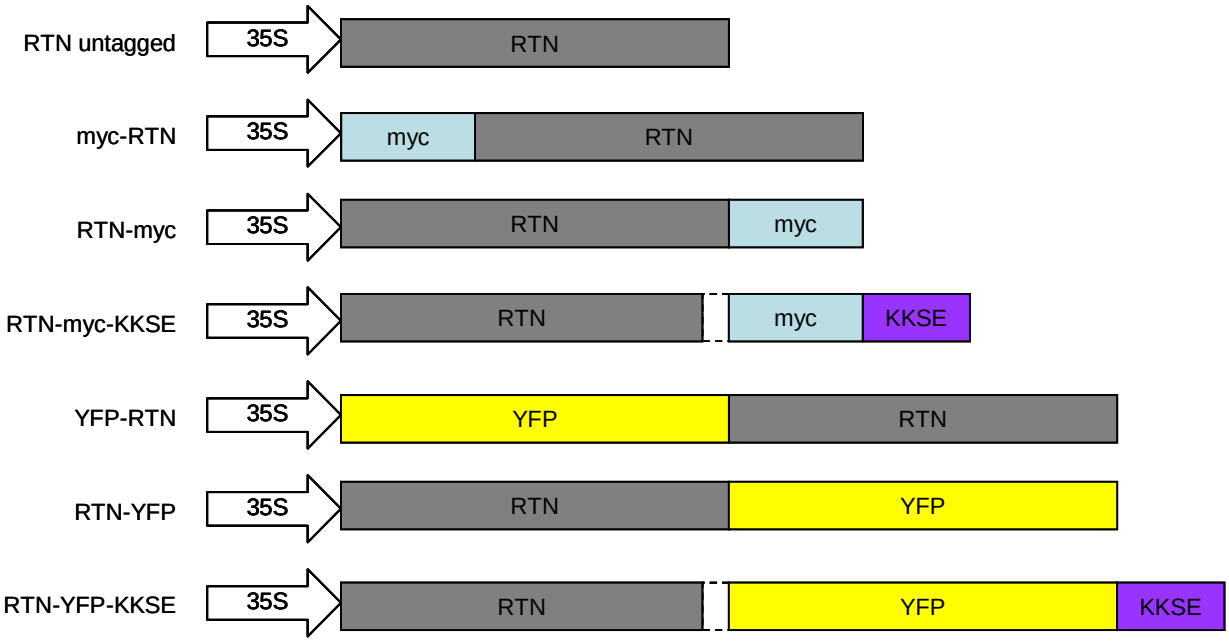

Figure 3.1 Constructs used in the over-expression of RTN13 in tobacco.
35S driven RTN13 constructs untagged, or tagged with either a myc-epitope or YFP. Tags are positioned at either N- or C-terminus. The ER-retrieval motif (KKSE) is transposed downstream of the C-terminal myc- or YFP tag. Dotted lines indicate the position of residues KKSE in wild-type RTN13. Diagrams are not drawn to scale.

retrieval motif (Figure 3.1). RTN13 was originally tagged with the myc-epitope for use in biochemical experiments which would then be comparable to any fluorescence data generated. When the untagged RTN13 was co-expressed with GFP-HDEL, cells were observed to have a re-distribution of GFP-HDEL into small punctae (Figure 3.2 A). The same phenotype was seen with the myc-RTN13, RTN13-myc (Figure 3.2 B-C) and RTN13-myc-KKSE constructs (data not shown), indicating that the orientation of the myc-tag does not seem to have an effect on the ER phenotype. From these results, no comment could be made regarding the structure of the ER when RTN13 is over-expressed. Depending on the length of time before examining leaf samples, or the concentration of *Agrobacterium* used, varying degrees of this phenotype were seen.

3.3 The induction of phenotype caused by RTN13 over-expression can be observed over time

A time-course experiment was carried out to observe the induction of the phenotype caused when over-expressing RTN13, and also to determine whether the phenotype observed becomes more severe over time in accordance with the accumulation of RTN13. Tobacco leaves were infiltrated with GFP-HDEL, followed by a second infiltration of the same leaf sector 24 h later with untagged RTN13. The leaf sectors were then observed using confocal microscopy at 48, 72 and 96 hours post-infiltration. At 48 h, the ER structure, as represented by GFP-HDEL showed classical reticular morphology (Figure 3.3 A). At 72 h, an intermediate phenotype was reached whereby, although the tubular pattern of the ER was still visible, the luminal fluorescence was beginning to show discontinuity (Figure 3.3 B). By 96 h, GFP-HDEL was completely fragmented into distinct punctae (Figure 3.3 C).

3.4 YFP-tagging of RTN13 reveals localisation to the ER

RTN13 was tagged with YFP in order to localise the protein within the cell. Multiple constructs were designed, again, to determine if the orientation of YFP affects the localisation of RTN13 and whether the C-terminal retrieval motif needs to be exposed (Figure 3.1). Using GFP-HDEL as a comparison, YFP-RTN13, RTN13-YFP and RTN13-YFP-KKSE were expressed in tobacco cells and all localised to the

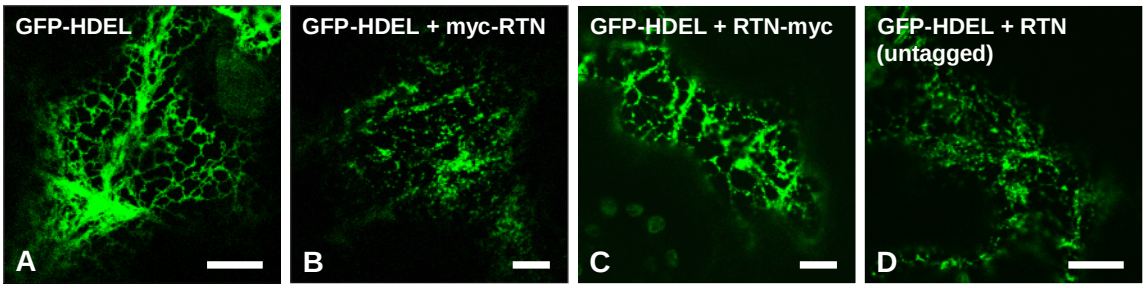

Figure 3.2 Over-expression of either myc-tagged or untagged RTN13, in the presence of the ER reporter GFP-HDEL, reveals drastic remodelling of the ER. Confocal images of *Agrobacterium*-infiltrated tobacco leaf epidermal cells transiently expressing (A) GFP-HDEL control (green), (B) GFP-HDEL co-infiltrated with N-terminally myc-tagged RTNLB13, (C) GFP-HDEL co-infiltrated with C-terminally myc-tagged RTNLB13 and (D) GFP-HDEL co-infiltrated with untagged RTNLB13. Scale bars = 20 µm.

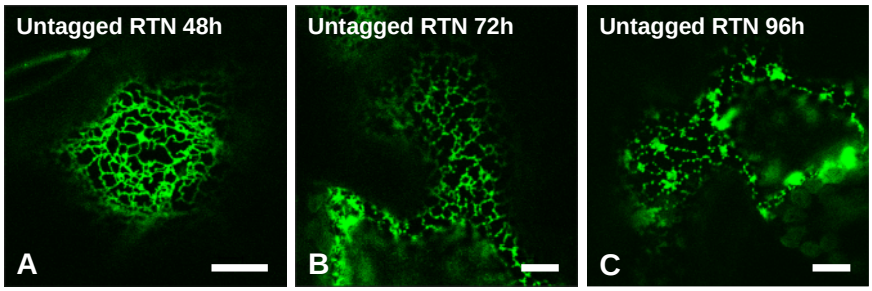

Figure 3.3 The induction of phenotype of RTN13 over-expression can be observed over time. Confocal images of *Agrobacterium*-infiltrated tobacco leaf epidermal cells transiently expressing (A) GFP-HDEL (green) infiltrated leaf sectors co-infiltrated with untagged RTN13 24 h later and visualised at 48 h, (B) 72 h and (C) 96 h. Scale bars = 20 µm.

ER (Figure 3.4 B-D). The orientation of the YFP-tag, as with the myc-tag, seemed to have no effect on localisation. Although the nucleus can be visualised using YFP-tagged RTN13, its distribution is different to that of GFP-HDEL, and often ER tubules can be seen surrounding the nuclear envelope (data not shown).

3.5 Co-expression of RFP-HDEL and RTN13 indicates super-structure of ER remains intact and that the soluble contents forms constrictions within the lumen of the ER

The YFP-tagged constructs were co-expressed with RFP-HDEL in order to assess possible co-localisation with the ER marker. Although RFP-HDEL is a classical marker for the ER lumen, and YFP-RTN13 gives a pattern which is morphologically similar to an ER network, it was necessary to determine where the two fluorescent proteins were in relation to one another. When expressed in the same cell, the fragmented phenotype can be observed only with RFP-HDEL, whereas YFP-RTN13 highlights a typical ER structure, indicating that when RTN13 is over-expressed, the super-structure of the ER remains intact and it is the luminal contents of the ER, as labelled by RFP-HDEL, which form distinct pockets of accumulation along the ER network (Figure 3.5 A-C). The same phenotype was seen regardless of the position of the YFP-tag (data not shown). This suggests that RTN13 has the capacity to constrict ER tubules leading to the accumulation of luminal material in discrete regions.

3.6 Co-expression of RTN13 with ER-membrane proteins displays differential phenotypes

In order to determine whether the over-expression of RTN13 had an effect on the distribution of proteins within the ER, YFP-RTN13 was co-expressed with membrane proteins either resident in the ER, or trafficked through the ER, namely calnexin, αTIP and γTIP, respectively. These markers were tagged with GFP either on the luminal or cytosolic face of the ER and their possible re-distribution when co-expressed with RTN13 was compared with that of the soluble, luminal marker, GFP-HDEL.

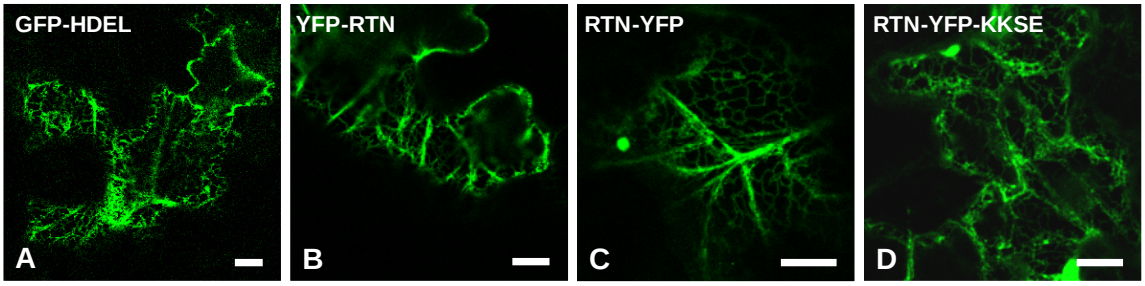

Figure 3.4 YFP-tagged RTN13 localises to the ER, regardless of the position of the ER-retrieval motif (KKSE). Confocal images of *Agrobacterium*-infiltrated tobacco leaf epidermal cells transiently expressing (A) GFP-HDEL control (green), (B) N-terminally YFP-tagged RTN13 (green), (C) C-terminally YFP-tagged RTN13 and (D) C-terminally YFP-tagged RTN13 with the ER-retrieval motif (KKSE) transposed to the C-terminus of YFP. Scale bars = 20 µm.

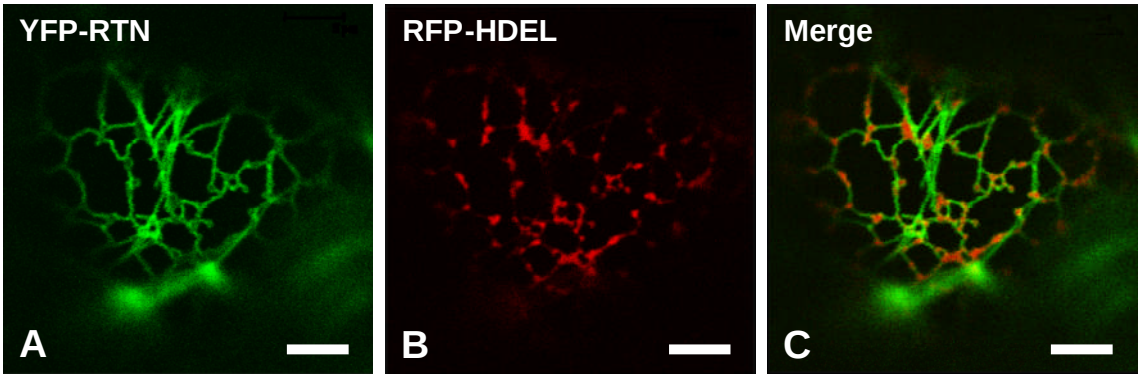

Figure 3.5 Co-expression of YFP-RTN13 and RFP-HDEL reveals that the super-structure of the ER remains intact, whilst the ER lumen is constricted. Confocal images of *Agrobacterium*-infiltrated tobacco leaf epidermal cells transiently expressing (A) YFP-RTN13 (green), (B) the ER luminal marker RFP-HDEL (red) and (C) the merged image of (A) and (B). Scale bars = 5 µm.

3.6.1 GFP-calnexin

YFP-tagged RTN13 was over-expressed with the ER membrane marker, GFP-calnexin (Irons *et al*., 2003) to compare any phenotype seen with that of the luminal GFP-HDEL. Calnexin has a single transmembrane domain with a short C-terminal extension facing the cytosol and an N-terminal region facing the lumen of the ER, to which GFP is appended. Upon over-expression, GFP-calnexin induces sheet formation in the ER membrane which is thought to be due to accommodation of over-expressed transmembrane domains in the membrane (Runions *et al*., 2006). When co-expressed with YFP-RTN13, a similar phenotype to that of GFP-HDEL can be seen with GFP-calnexin, although the fluorescent punctae seem to have thin strand like connections between them (Figure 3.6.1 A-C).

3.6.2 αTIP-GFP and γTIP-GFP

Tonoplast intrinsic proteins (TIPs) are transmembrane proteins of the vacuolar membrane. They contain six transmembrane regions and the N- and C-termini face the cytosol. In contrast to GFP-calnexin, in αTIP-GFP and γTIP-GFP, GFP is cytosolic and may be affected differently when co-expressed with RTN13. Although they are targeted to the tonoplast, TIPs are first translocated into the ER membrane, and can be seen to highlight the ER for the first few days post infiltration. YFP-RTN13 was co-expressed with both αTIP-GFP and γTIP-GFP, and visualised by confocal microscopy 2-3 days after infiltration. Both αTIP-GFP and γTIP-GFP localised to the ER membrane with very little transport to the tonoplast. However, the over-expression of RTN13 did not result in the formation of small punctae. Instead, the pattern of αTIP-GFP and γTIP-GFP was identical to that of RTN13 (Figure 3.6.2 A-F). This may reflect the orientation of GFP at the C-terminus facing the cytosol and the fact that, like RTN13, both TIPs are multi-spanning membrane proteins.

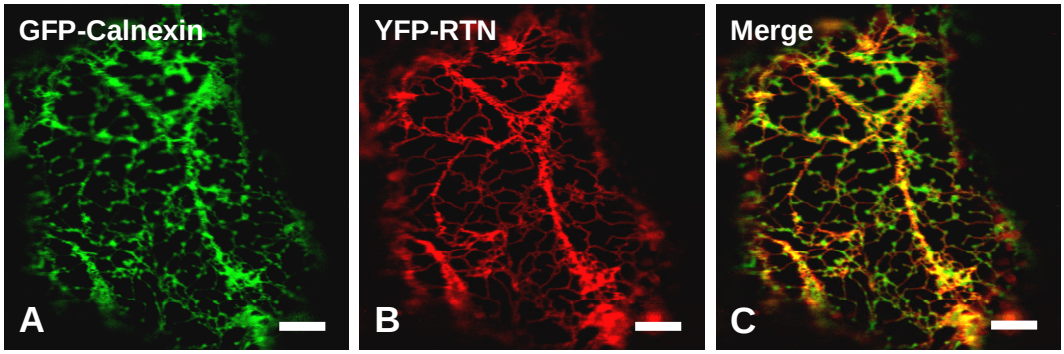

Figure 3.6.1 Co-expression of YFP-RTN13 and GFP-calnexin reveals residual continuity within the ER lumen. Confocal images of *Agrobacterium*-infiltrated tobacco leaf epidermal cells transiently expressing (A) GFP-calnexin (green), (B) YFP-RTN13 (red) and (C) the merged image of (A) and (B). Over-expression of GFP-calnexin induces the formation of small sheets within the ER membrane. Scale bars = 20 µm.

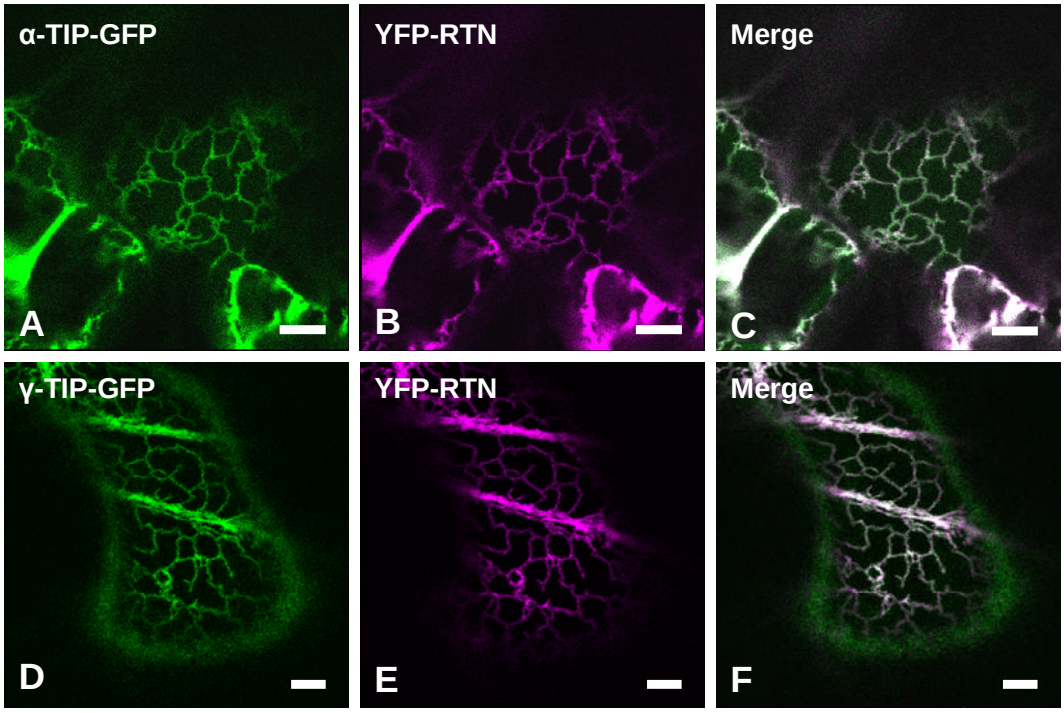

Figure 3.6.2 Co-expression of YFP-RTN13 with cytosolically tagged TIPs exhibits normal reticular pattern. Confocal images of *Agrobacterium*-infiltrated tobacco leaf epidermal cells transiently expressing (A) αTIP-GFP (green), (B) YFP-RTN13 (magenta) and (C) the merged image of (A) and (B), (D) γTIP-GFP, (E) YFP-RTN13 and (F) the merged images of (D) and (E). Scale bars =10 µm.

3.7 Fluorescence recovery after photo-bleaching reveals that RTN13 over-expression inhibits protein diffusion within the ER lumen

To assess the effect of RTN13 on the dynamics of the ER, the ER markers GFP-HDEL and GFP-calnexin were utilised in fluorescence recovery after photobleaching (FRAP) experiments, either expressed alone, or in the presence of YFP-RTN13. Movement of the actin cytoskeleton was inhibited by using the drug latrunculin B. Once bleached, the recovery of the ER markers was measured over time (Figure 3.7 A-E). When YFP-RTN13 was co-expressed with GFP-HDEL, there was a substantial lag in fluorescence recovery compared with cells expressing GFP-HDEL alone (Figure 3.7 F). Similarly, when YFP-RTN13 was co-expressed with GFP-calnexin, there was also a delay in recovery, but to a lesser extent (Figure 3.7 G). This indicates that the over-expression of RTN13 inhibits protein diffusion within both the lumen and membrane of the ER.

3.8 RTN13 localises to tubular ER and not to sheets

To further characterise the localisation of RTN13 within the ER, brefeldin A (BFA) was used to induce sheets within the ER. It is thought that sheets form as a result of the Golgi collapsing into the ER and causing newly synthesised proteins to accumulate (Boevink *et al*., 1999). When YFP-RTN13 and GFP-HDEL were co-expressed tobacco leaves which were subsequently incubated in BFA, RTN13 was largely restricted to the tubular ER, whereas GFP-HDEL localised to the BFA-induced sheets and punctae within the tubules (Figure 3.8 A-C).

3.9 Biochemical analysis of RTN13 size, stability and sub-cellular localisation

Leaf sectors expressing myc-tagged RTN13 were resolved by SDS-PAGE and subject to western blotting to establish the size and expression level of the protein. Depending on the orientation of the tag, the proteins ran at slightly different sizes (N-terminally tagged myc-RTN13 runs approximately 1 kDa higher than RTN13-myc), but overall they expressed consistently and ran at approximately 25 kDa when resolved by SDS-PAGE, concurrent with their predicted size (Figure 3.9 A).

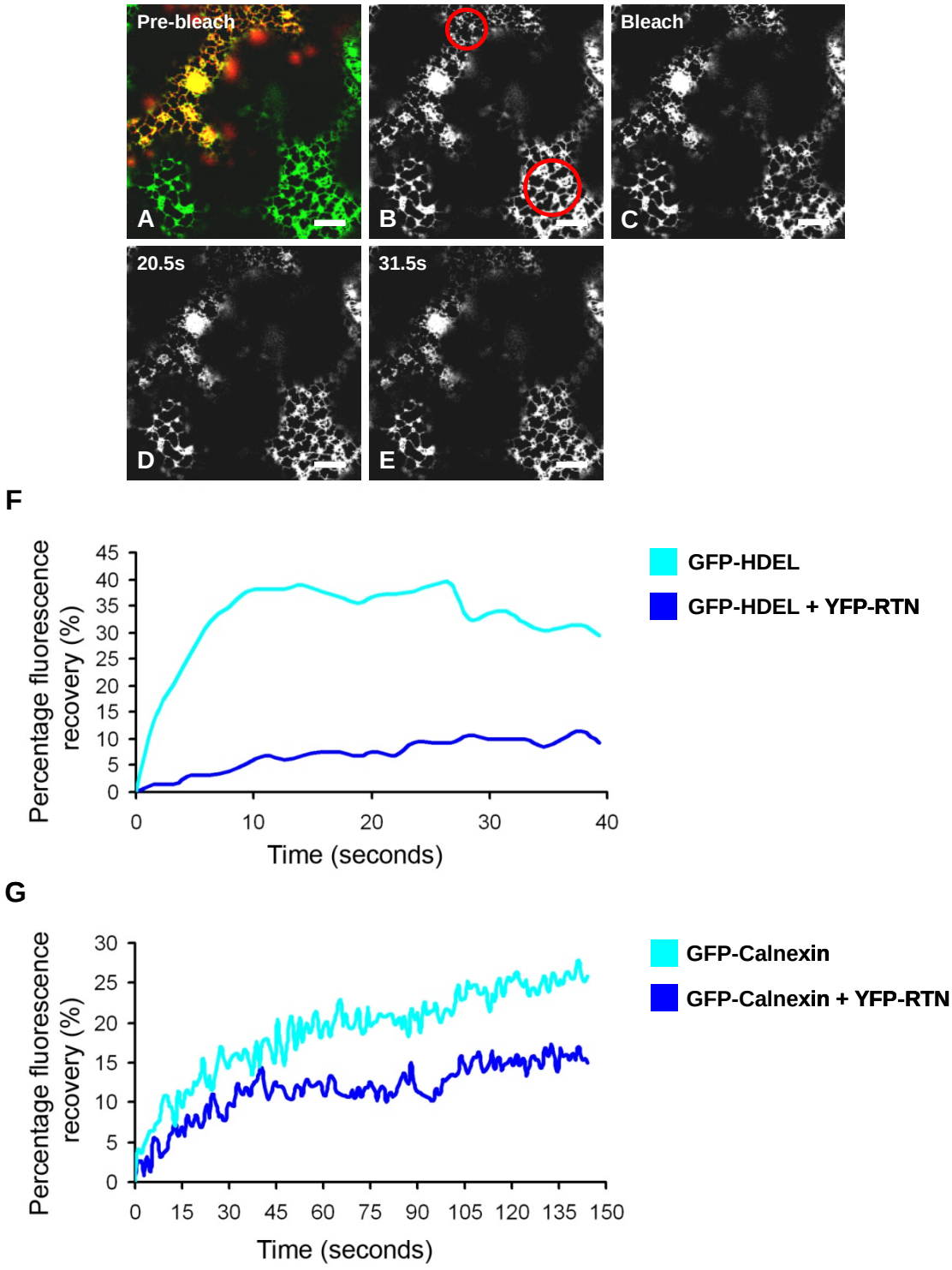

Figure 3.7 Protein diffusion within the ER is altered when GFP-HDEL and GFP-calnexin are co-expressed with YFP-RTN13 as measured by FRAP. Confocal images of *Agrobacterium*-infiltrated tobacco leaf epidermal cells transiently expressing GFP-HDEL (green) and YFP-RTN13 (red) in (A)-(B) a pre-bleached state, (C) photo-bleached, (D) 20.6 seconds after recovery and (E) 31.6 seconds after recovery. Areas bleached can be seen in (B). Scale bar = 40 µm. (F) Recovery curves of GFP-HDEL and YFP-RTN13 and (G) GFP-calnexin and YFP-RTN13.

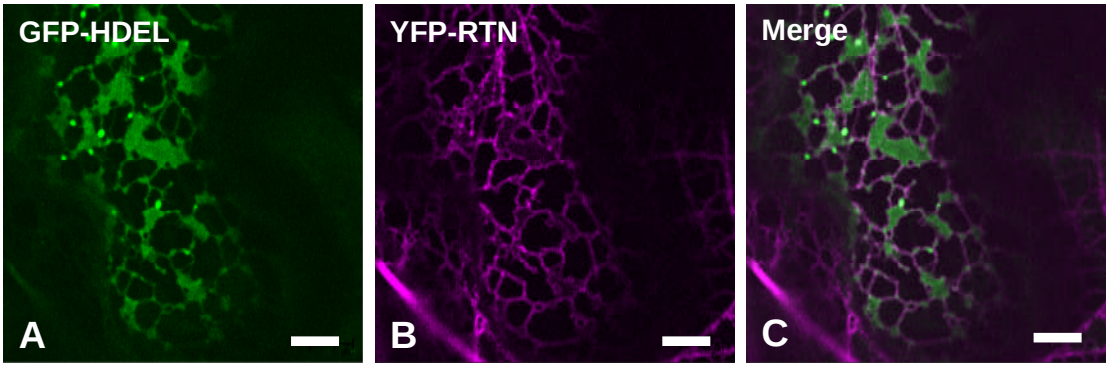

Figure 3.8 RTN13 is restricted to tubular ER when sheets are induced by incubation with BFA. Confocal images of *Agrobacterium*-infiltrated tobacco leaf epidermal cells transiently co-expressing (A) GFP-HDEL (green), (B) YFP-RTN13 (magenta) and (C) the merged image of (A) and (B). Leaf sectors incubated in 50µg/ml for 1 hour. Scale bars = 20 µm.

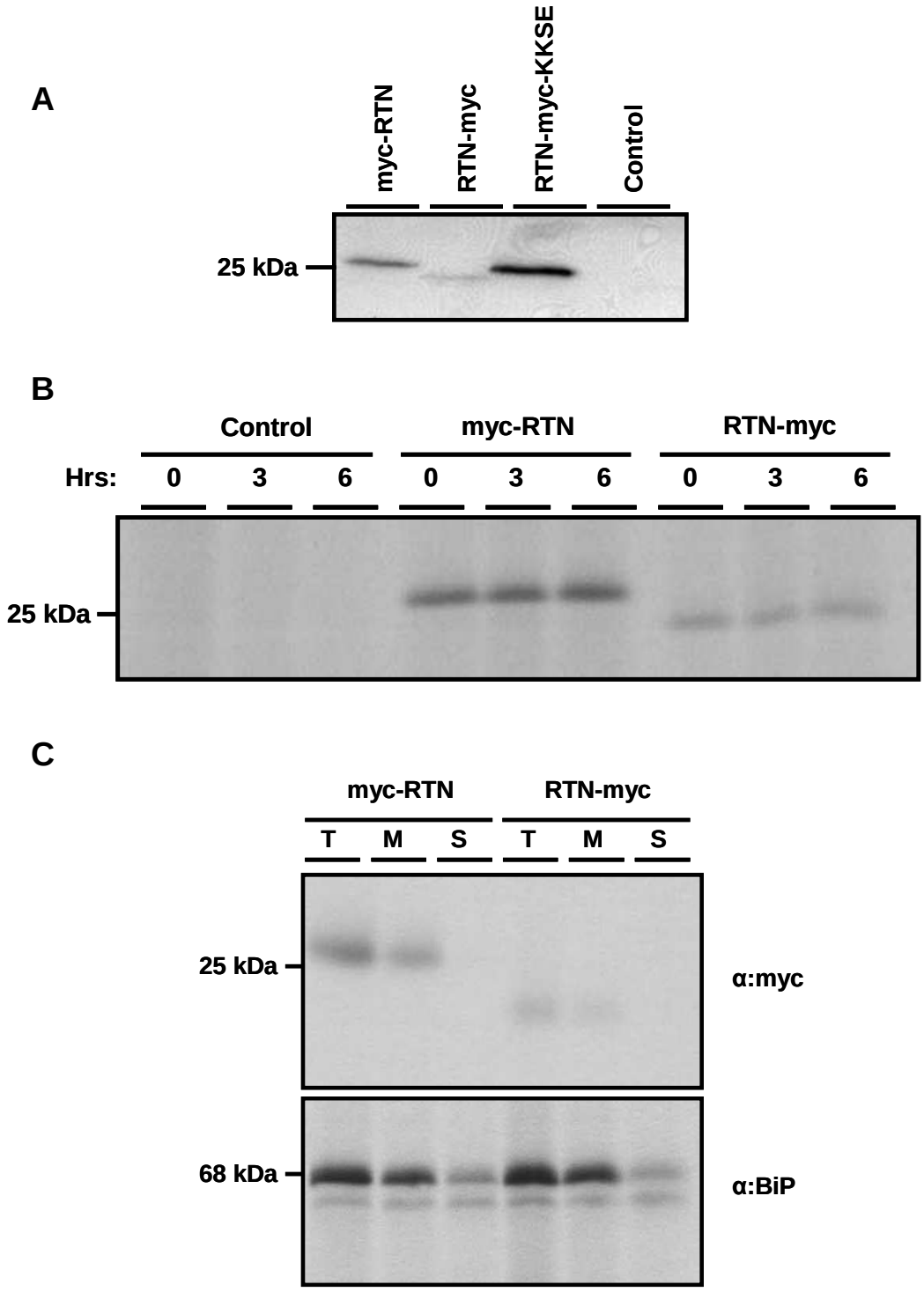

Figure 3.9 Biochemical analysis of RTN13: size, stability and localisation.
(A) Western blot of agro-infiltrated tobacco leaf sectors using anti-myc antibody following resolution of myc-tagged RTN13 variants by SDS-PAGE. Protein bands migrate at approximately 25kDa. (B) Pulse-chase of radiolabelled tobacco protoplasts immunoprecipitated with anti-myc antibody. The fate of myc-RTN13 and RTN13-myc is followed over 6 hours. (C) Microsomal fractionation of radiolabelled tobacco protoplasts expressing myc-RTN13 and RTN13-myc. Samples divided into total (T), membrane (M) and soluble (S) and immunoprecipitated with anti-myc antibody. Binding protein (BiP) was used as a microsome-bound control, although some protein is evident in the soluble fraction due to microsome breakage.

Myc-tagged RTN13 was also expressed in tobacco protoplasts and subsequently radiolabelled (pulse) to follow the fate of the protein over time (chase) to determine the stability of the protein. RTN13 was stable over a 6 h chase period and showed no sign of degradation (Figure 3.9 B).

In a similar manner, radiolabelled protoplasts were subjected to a 'pulse' only, then fractionated into soluble and membrane constituents to test which fraction RTN13 localised to. BiP was used as a control, of which the majority was found in the microsomal fraction. RTN13 was found in the microsomal fraction only, and absent from the soluble fraction, indicating that RTN13 is, at least, found within the membranes of the endomembrane system (Figure 3.9 C).

3.10 Over-expression of RTN13 causes inhibition of transport to the tonoplast, but no effect on Golgi, vacuolar or secreted cargo

Due to the remodelling of the ER caused by RTN13 over-expression, transport to compartments downstream of the ER in the secretory pathway was tested in order to determine any defects in transport of Golgi, vacuolar and secreted cargo. Both confocal microscopy and biochemical techniques were used to evaluate defects in protein transport.

The Golgi marker sialyl-transferase (ST) tagged with red fluorescent protein (RFP), which highlights Golgi stacks (Saint-Jore *et al*., 2002), was used to measure the effect of over-expression of RTN13 on protein transport to the Golgi. Expression in tobacco leaves revealed numerous discrete punctae within the cell and small amounts of secretion into the apoplast; an artefact of over-expression (Runions *et al*., 2006). Co-expression with either myc-RTN13 (Figure 3.10 A-C) or RTN13-myc (Figure 3.10 D-F) had no effect on the distribution, size or number of Golgi using qualitative analysis of confocal microscopy images.

To determine whether secretion was affected by RTN13 over-expression, RTN13 was co-expressed with a secreted variant of the vacuolar storage protein phaseolin Δ418 from *Phaseolus vulgaris* (Frigerio *et al*., 1998) in tobacco protoplasts. Specific antibodies were used in immunoprecipitation experiments to follow the secretion of

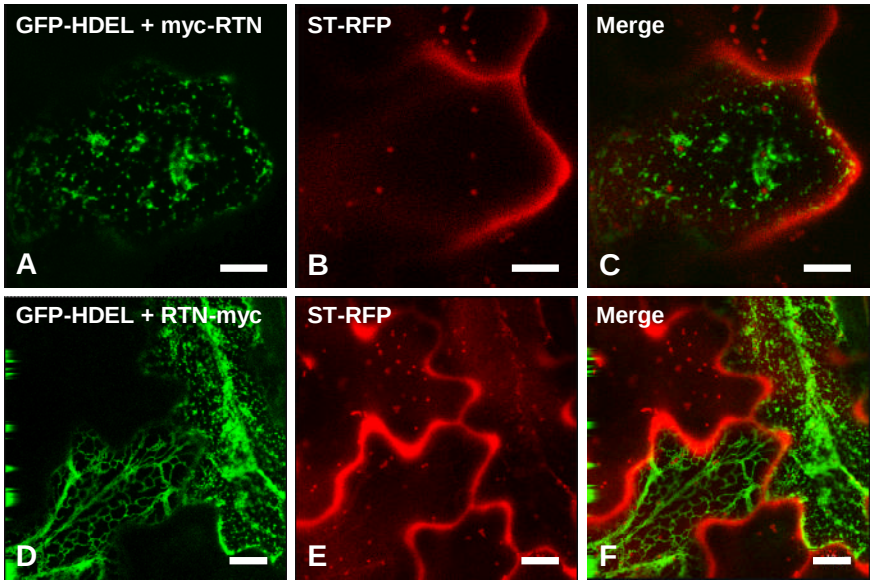

Figure 3.10 Co-expression of RTN13 with ST-RFP reveals that Golgi size, shape and number remain unaffected. Confocal images of *Agrobacterium*-infiltrated tobacco leaf epidermal cells transiently expressing (A) GFP-HDEL (green) and myc-RTN13, (B) ST-RFP (red), (C) merged images of (A) and (B), (D) GFP-HDEL and RTN13-myc, (E) ST-RFP and (F) the merged images of (D) and (E). Scale bar = 20 µm.

radio-labelled phaseolin over time from cells into the medium. As a control, over-expression of Sec12, a component for COPII coat assembly, was used to inhibit ER-to-Golgi transport and block secretion (Phillipson *et al*., 2001). Regardless of the position of the myc-tag, neither myc-RTN nor RTN-myc had any effect on the secretion of phaseolin. Samples were re-probed with anti-myc antibodies to confirm their expression (Figure 3.11). Although constriction of the ER lumen has been observed in protoplasts derived from agro-infiltrated leaves (data not shown), microscopic examination of PEG-transfected protoplasts with RTN13 and GFP-HDEL was not tested.

Three markers of the vacuole were used to investigate whether the over-expression of RTN13 had any effect on the transport of vacuolar proteins. SP:RFP:AFVY is a soluble protein targeted to the lumen of the vacuole (Hunter *et al*., 2007). It contains the signal peptide of phaseolin appended to the N-terminus of RFP, which is proceeded by the C-terminal vacuolar sorting signal of phaseolin, the tetrapeptide AFVY (Frigerio *et al.,* 1998). αTIP-GFP and γTIP-GFP are both tonoplast intrinsic proteins tagged with GFP at their C-terminus. It is thought that γTIP-GFP traffics via the Golgi and αTIP-GFP is transported to the tonoplast via a Golgi-independent route (Oufattole *et al*., 2005). It is for this reason that they were used to determine whether RTN13 over-expression affects the transport of TIPs trafficking via the Golgi or a Golgi-independent route. The aforementioned constructs were co-expressed in tobacco with RTN13 and their subsequent transport to the tonoplast observed. When co-expressing SP:RFP:AFVY, there was no difference in trafficking times when expressed in the presence or absence of RTN13 (Figure 3.12 A-F). However, when co-expressed with YFP-RTN13, αTIP-GFP and γTIP-GFP were still present in the ER, compared to cells expressing αTIP-GFP and γTIP-GFP alone, where they had already reached the tonoplast. αTIP-GFP generally took longer to traffic to the tonoplast. By 10 days post infiltration, αTIP-GFP was visible in the tonoplast, but remained in the ER in cells expressing RTN13, with only low levels detected on the vacuolar membrane (Figure 3.12 G-L). γTIP-GFP reached the tonoplast after 6-7 days post infiltration. Again, in cells expressing RTN13, γTIP-GFP remained in the ER, with only low levels detected on the tonoplast (Figure 3.12 M-R).

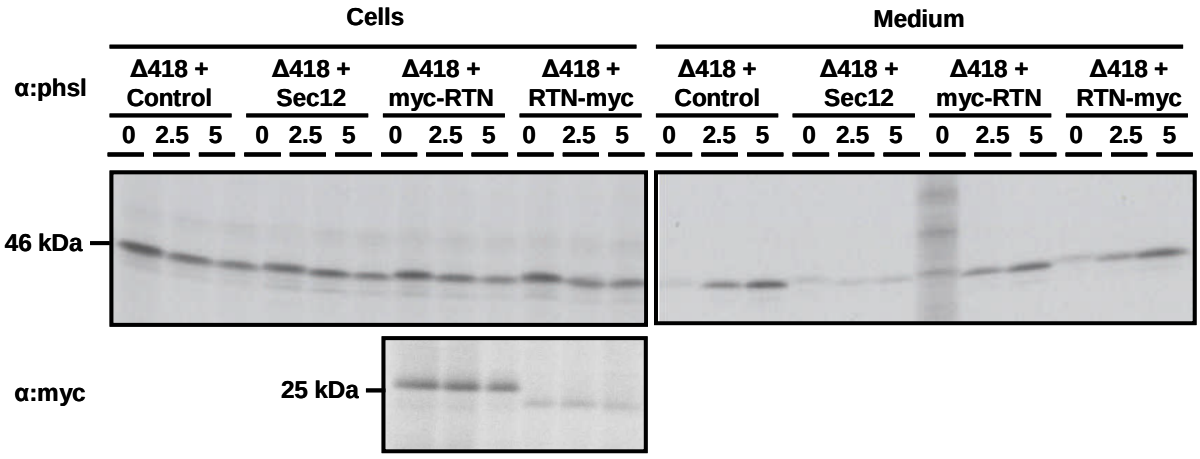

Figure 3.11 Over-expression of RTN13 does not perturb protein secretion from the cell. The secreted variant of phaseolin Δ418 was co-transfected with (1) empty vector, (2) Sec12, (3) myc-RTN13 and (4) RTN13-myc into tobacco protoplasts. Proteins were radiolabelled and immunoprecipitated with either anti-phaseolin or anti-myc antibodies and subject to SDS-PAGE. In control conditions, phaseolin Δ418 is secreted from the cells into the medium over 5 hours. Expression of sec12 blocks protein secretion. Expression of N- and C-terminally myc-tagged RTN13 has no effect on protein secretion.

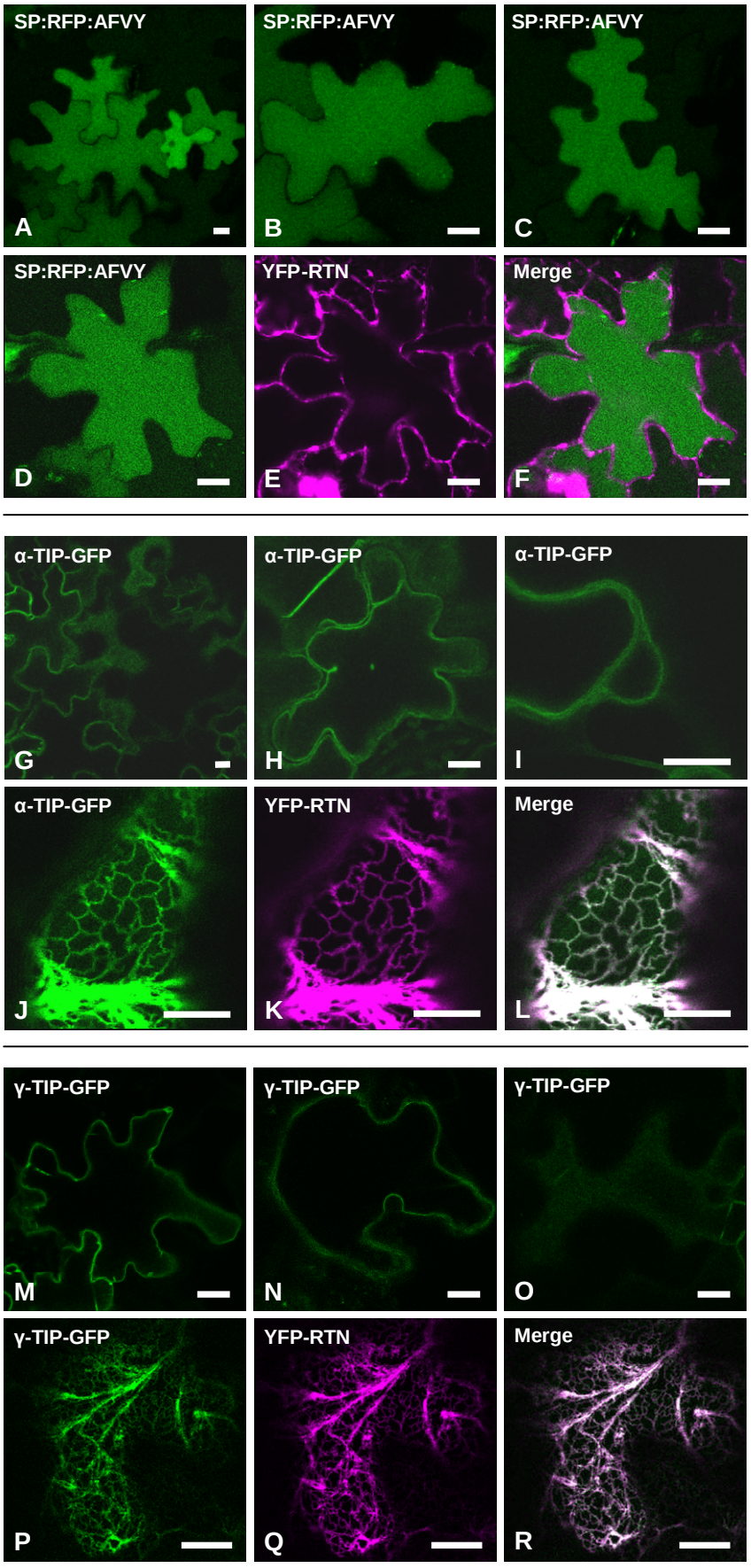
SP:RFP:AFVY
A
SP:RFP:AFVY
B
SP:RFP:AFVY
C
SP:RFP:AFVY
D
YFP-RTN
E
Merge
F
α-TIP-GFP
G
α-TIP-GFP
H
α-TIP-GFP
I
α-TIP-GFP
J
YFP-RTN
K
Merge
L
γ-TIP-GFP
M
γ-TIP-GFP
N
γ-TIP-GFP
O
γ-TIP-GFP
P
YFP-RTN
Q
Merge
R

Figure 3.12 Co-expression of RTN13 with fluorescent vacuolar markers does not affect transport to the lumen, but inhibits trafficking to the tonoplast.
(A)-(F) Confocal images of *Agrobacterium*-infiltrated tobacco leaf epidermal cells transiently expressing (A)-(C) SP:RFP:AFVY alone (green), (D) co-expressing SP:RFP:AFVY, (E) YFP-RTN13 (magenta) and (F) merged images of (D) and (E) 5 days post-infiltration. (G)–(L) Confocal images of *Agrobacterium*-infiltrated tobacco leaf epidermal cells transiently expressing (G)-(I) αTIP-GFP (green), (J) co-expressing αTIP-GFP, (K) YFP-RTN13 (magenta) and (L) merged images of (J) and (K) 10 days post-infiltration. (M)–(R) Confocal images of *Agrobacterium*-infiltrated tobacco leaf epidermal cells transiently expressing (M)-(O) γTIP-GFP (green), (P) co-expressing γTIP-GFP, (Q) YFP-RTN13 (magenta) and (R) merged images of (P) and (Q) 6-7 days post-infiltration. Scale bar = 40 μm.

3.11 Discussion

When over-expressed in tobacco leaf epidermal cells, RTN13 localises to tubular ER and forms constrictions within the lumen of the ER, resulting in a re-distribution of the luminal protein GFP-HDEL. Due to variation in expression levels and the severity of constriction increasing with time, this phenotype may be dose-dependent, which is consistent with RTN13 being a stable protein over a relatively long time (Figures 4.7; 4.9). Luminal dynamics are perturbed upon RTN13 over-expression, although cytosolically tagged membrane protein distribution is not affected. Only transport of membrane proteins to the tonoplast seems to be retarded, while transport to the Golgi, vacuole lumen and apoplast remain unaffected. Whether this reflects a different transport route for tonoplast proteins remains to be established (Oufattole *et al*., 2005).

These data indicate that RTN13 may be involved in ER tubule formation and maintenance, and that the diameter of ER tubules is important for luminal diffusion and potentially protein export. A correlation between mammalian reticulon expression and tubule diameter has already been established *in vitro* using proteoliposomes whereby increasing expression levels results in the formation of narrower tubules (Hu *et al*., 2008).

RTN13 was over-expressed under a 35S constitutive promoter, primarily to determine the localisation of the protein and furthermore investigate the effect of its over-expression within the cell. Both YFP and myc-tagged variants of RTN13 were co-expressed with the established luminal ER marker, GFP-HDEL. This revealed that RTN13 not only localises to the ER, but also affects the distribution of GFP-HDEL within the lumen. Considering the hypothesis that reticulons are curvature-inducing proteins, it can be postulated that the over-expression of RTN13 reduces the diameter of ER tubules and forces the luminal contents into small constrictions, often located near three-way junctions and extending tubules. The orientation by which RTN13 has been tagged does not seem to affect its ability to induce constrictions, and it seems that the ER-retrieval motif is either unnecessary, or does not need to be exposed in order for RTN13 to be retained in the ER. The fact that the constricted ER pattern depends on RTN13 over-expression is further supported by the induction of this phenotype over time. Three clear stages can be identified ranging between wild-type ER, intermediate constriction and fully constricted ER (Figure 3.3). The distribution of GFP differs slightly when attached to the membrane protein, GFP-calnexin, rather than a soluble protein. Although constrictions are still formed, thin strand-like connections can still be seen between the constrictions, hinting that the over-expression of RTN13 differentially affects the distribution of soluble and membrane proteins. This is reinforced by FRAP analysis, whereby the soluble GFP-HDEL recovers more slowly than the membrane bound GFP-calnexin. However, in the case of GFP-calnexin, the constriction phenotype seen may be due to the fact that GFP faces the lumen of the ER, and as the ER is being remodelled, calnexin is compelled to relocate to the constricted regions of the ER lumen. When cytosolically tagged αTIP-GFP and γTIP-GFP are co-expressed with RTN13 in the ER, the constricted phenotype is no longer visible, indicating this phenotype may only be visible with a luminal marker.

It has previously been reported that reticulons localise to tubular ER (Voeltz *et al*., 2006), but the mechanism by which this happens remains unclear. When sheets are artificially induced using the fungal metabolite brefeldin A, RTN13 is largely excluded from the sheets, and almost exclusively locates to the tubules. GFP-HDEL, however, localises to the flattened cisternae, and is also found at constricted points in the tubules. This suggests an inherent property of the structure of RTN13 to

preferentially insert into high-curvature membranes. However, at this stage, the functional relevance of this characteristic, and indeed its mechanism, remain unclear.

In parallel with the over-expression of fluorescently tagged RTN13, some basic features of the protein were also determined. The myc-tagged RTN13 constructs were expressed in tobacco leaves and subjected to SDS-PAGE and western blot analysis to determine their size - which was consistent with the predicted molecular weight of approximately 25 kDa. Using pulse-chase analysis, the protein was observed to be stable over at least six hours as there was no evidence of the formation of any degradation products. Under reducing conditions, the formation of higher molecular weight oligomers was not observed. The over-expression of a stable protein could imply that it accumulates in the ER and therefore super-imposes membrane curvature on the ER membrane and is responsible for the remodelling of the ER tubules. This could also explain why there is a seemingly dose-dependent phenotype in cells expressing RTN13 at varying levels. The fractionation of transfected protoplasts revealed RTN13 is present in microsomal membranes. This is concurrent with its predicted transmembrane domain structure and ER-localisation when fluorescently tagged.

With such a striking affect on the morphology of the ER, it would follow that downstream processes in the secretory pathway would also be hindered in some way. Using a comprehensive array of fluorescent and biochemical markers, the transport of proteins to the Golgi (ST-RFP), vacuole (SP:RFP:AFVY), tonoplast (αTIP-GFP and γTIP-GFP) and apoplast (phaseolin Δ418) were investigated upon RTN13 over-expression. Surprisingly, transport to the Golgi, vacuole lumen and the apoplast was not affected by the over-expression of RTN13. Although the markers were measured in the scale of hours and days, it would be expected that some evidence of delayed protein transport could be detected, at least at the level of ER exit or ER-to-Golgi transport. However, transport to the tonoplast was hindered. The majority of the tonoplast-targeted reporter membrane proteins, TIPs, were trapped in the ER, with only a small proportion reaching the tonoplast. It is possible that the over-expression of RTN13 provokes a re-distribution of ER-exit sites. However, as plant ERES are thought to be in very close association with Golgi bodies (Hanton *et al*., 2008), transport to the Golgi (as highlighted by ST-RFP) should also be affected, but this

does not seem to be the case. Therefore, at this stage it is only possible to speculate that TIPs may traffic to the tonoplast via a Golgi-independent route (Oufattole *et al*., 2005).

Over-expression of RTN13 in tobacco causes constrictions within the lumen of the ER, a phenotype previously unreported with reticulon over-expression in other organisms. Compared with mammalian and yeast reticulons, where over-expression causes extension of un-branched tubules (Voeltz *et al*., 2006), only recently has a similar phenotype been observed in mammals. When Rtn4a is over-expressed with ER chaperone markers such as protein disulfide isomerase (PDI), the latter are re-distributed to punctate structures (Yang *et al*., 2009). The authors attribute this phenotype to the re-distribution of proteins containing the KDEL ER-retention motif, in particular chaperones, with the KDEL-negative calnexin remaining unaffected. However, in accordance with the findings presented in this chapter, GFP-K/HDEL is not used as a control in their study, and may have also re-distributed to punctate structures. Therefore, either reticulon over-expression only affects proteins bearing the K/HDEL motif, or the data presented by Yang *et al*., (2009) are to be interpreted with caution. Seeing as the dynamics of GFP-calnexin are affected by the over-expression of RTN13, and that the GFP moiety of GFP-calnexin also forms constrictions (Figure 3.6.1), it is seems unlikely that K/HDEL-motif proteins alone are re-distributed by reticulons.

This preliminary insight into the characterisation of RTN13 raises many questions. Primarily, how do the different domains of RTN13 contribute to its structure and function (addressed in chapter 5), and how is RTN13 arranged in the ER membrane? The predicted topology of RTN13 using TOPCONS places the N- and C-termini and the loop facing the cytosol, which is concurrent with the hypothesised ‘w’ structure imposing positive curvature on the ER membrane (Voeltz *et al*., 2006; He *et al*., 2007). However, the topology of reticulons has not yet been fully proven and as such, the topologies of five *Arabidopsis* isoforms of reticulon are investigated in the following chapter.

Chapter 4: Establishing the topology of plant reticulons

4.1 Introduction

In order for reticulon proteins to induce curvature on membranes, the shape and structure of the protein is an important factor. The topology of reticulons, the number of transmembrane domains and their orientation within the ER membrane all contribute to their membrane shaping ability. At a basic level, the two hydrophobic stretches are expected to sit in the membrane. However, the number of predicted transmembrane domains directly dictates the number of passes through the membrane, and ultimately, the orientation of the protein.

He *et al*., (2007) investigated the topology of mammalian Rtn3. Computer algorithms predict that the N- and C-termini are cytosolic and through protease protection assays (using proteases such as proteinase K and trypsin) the authors determined that the N-terminus and the loop region linking the two hydrophobic regions both face the cytosol, but their data for the C-terminal hydrophobic region are unclear. They conclude that reticulons could either sit in the membrane in a 'v' or 'w' conformation (see Appendix Figure A12), and the central loops of these conformations, luminal and cytosolic respectively, may themselves embed into the membrane, as they believe is the case with Rtn3.

Voeltz *et al*., 2006 took a different approach to determine the topology of Rtn4c and the related DP1. They introduced cysteine residues into the hydrophilic regions of the protein, then permeabilised the plasma membrane using digitonin and added membrane impermeant maleimide-PEG, a compound which modifies the cysteine residues and increases the overall molecular weight of the protein by 5 kDa. Using this method, they determined that for both Rtn4c and DP1, the N-terminus and loop both face the cytosol. However, the data for the C-terminus were again inconclusive.

Early research on reticulons led to the over-simplified conclusion that these proteins could adopt a 'v' or 'horseshoe' conformation in order to carry out their function (Grandpre *et al.,* 2000; Oertle *et al.,* 2003b), and this has since expanded to include a 'w' confirmation as a possible topology (Bauer & Pelkmans, 2006; He *et al.*, 2007). In the plant reticulon family, all but one of the 21 isoforms are predicted by topology algorithms to have a 'w' topology, apart from RTNLB8, which, using certain

prediction algorithms, is thought to be shaped as a 'v' (Nziengui *et al.,* 2007; see Appendix A8).

In one case, a reticulon protein has been detected at the plasma membrane (Dodd *et al*., 2005) where its conformation in the membrane may differ to that of the ER. The functional relevance of this is not yet understood. However, it is known that membranes of the secretory pathway become thicker and more rigid further along the pathway nearer the cell surface (Brandizzi *et al.,* 2002; Ronchi *et al.,* 2008).

Topological analysis of reticulon proteins is far from complete, and the lack of compelling evidence for the orientation of the C-terminus means no firm conclusions can be drawn on the shape of reticulons in the membrane.

4.1.1 Aims & experimental approach

Over-expression of RTN13 results in the formation of constrictions of the ER lumen and it is hypothesised that the shape and orientation of the protein contribute to this phenotype. The purpose of this chapter is to determine the topology of RTN13, and compare this to other plant reticulon isoforms. Using constructs previously described, YFP-tagged RTN proteins were agro-infiltrated into tobacco and their topology determined experimentally using protease protection and bimolecular fluorescence complementation (BiFC). Predicted structure, transmembrane domains and amino acid sequence are shown in Figure 1.1 and Appendix Figure A11, respectively.

Protease protection consists of the preparation of microsomes from tobacco leaves, which are subjected to proteinase K treatment in the presence or absence of a detergent (Triton X-100). The ability of reticulon to resist digestion implies protection by the membrane and ultimately, allows for the determination of the topology of the protein.

Bimolecular fluorescence complementation exploits the plant-specific phenomenon that YFP can be divided into two non-fluorescent fragments which become fluorescent when in close proximity to one another (Zamyatnin *et al*., 2006).

Originally used to study protein-protein interactions, BiFC was tested with mammalian cells where the efficient reassembly of YFP required formation of a complex between interacting proteins fused to both YFP fragments (Hu *et al*., 2002). However, when tested in plant cells, the YFP fragments strongly associated with each other without being fused to interacting proteins (Walter *et al*., 2004). Therefore, reticulon proteins can be tagged with one fragment of YFP, and the complementary fragment targeted to the cytosol or ER lumen. Any resulting fluorescence will indicate the compartment of residence of the YFP fragment and therefore the topology of the protein.

4.1.2 Constructs

Firstly, YFP-RTN13 and RTN13-YFP were infiltrated into tobacco leaves using GFP-calnexin as a control, where GFP faces the ER lumen (Irons *et al*., 2003). These proteins were subjected to protease protection to determine their topology biochemically. The *Arabidopsis* reticulons RTNLB1-4, tagged at either terminus with YFP were also tested to identify whether other plant reticulons share the same topology.

Using bimolecular fluorescence complementation, RTNLB13 was tagged at either the N-or C-terminus with either YN (N-terminal fragment, residues 1-154 of YFP) or YC (C-terminal fragment, residues 155-239) and subsequently co-expressed with the opposing cytosolic YN or YC, or ER-targeted YN or YC by virtue of a signal peptide and C-terminal HDEL sequence. A further construct was made where YC is inserted into the central hydrophilic region of RTNLB13 to determine the orientation of the loop between the two hydrophobic regions (Figure 4.1).

4.2 Determining the topology of RTN13 using protease protection

YFP-RTN13, RTN13-YFP and GFP-calnexin constructs were agro-infiltrated into tobacco leaves and, following 4-5 days of expression, microsomes were prepared from the infiltrated leaf samples. These microsomes were then subjected to proteinase K digestion (Figure 4.2). Compared with an untreated control, microsomes were subjected to proteinase K digestion in the presence or absence of

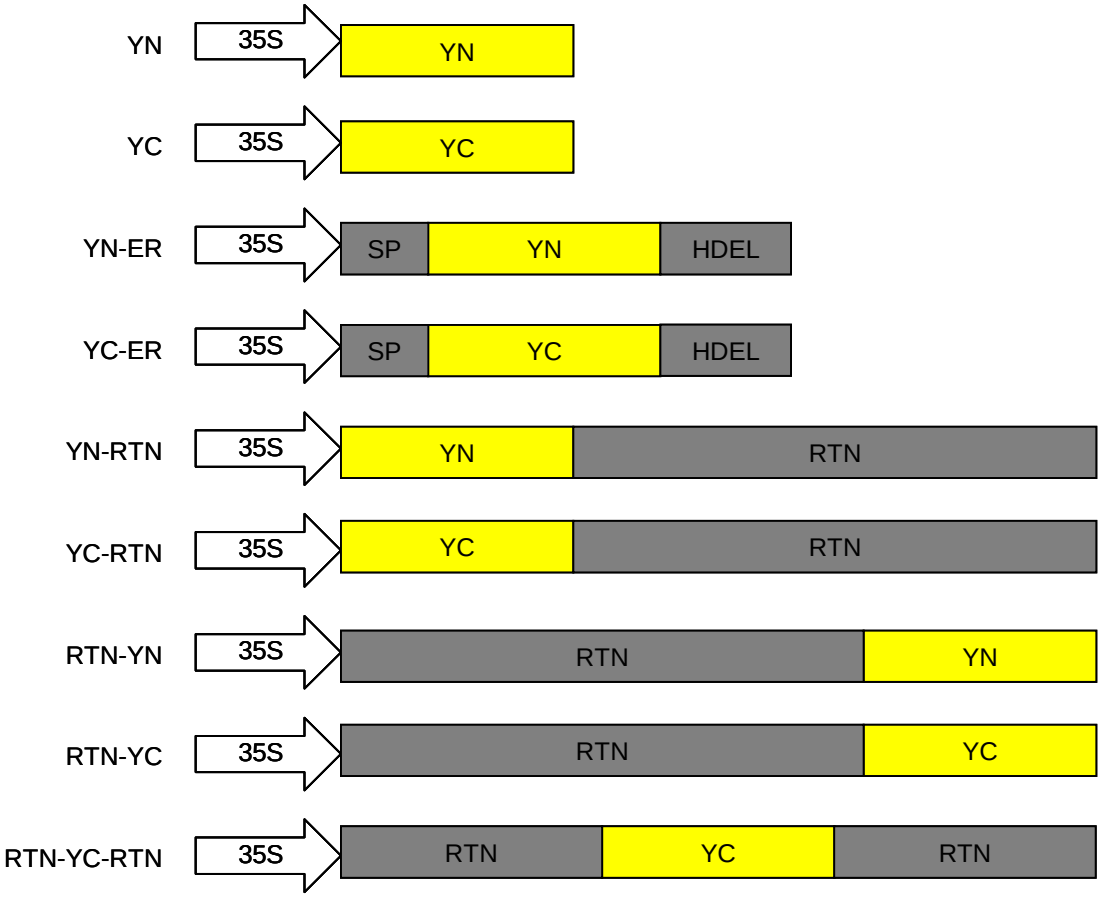

Figure 4.1 Constructs used for bimolecular fluorescence complementation (BiFC). 35S driven RTN13 constructs tagged with either YN or YC fragments. Tags are positioned at either N- or C-terminus or in the RTN13 loop region between Val91 and Val92.

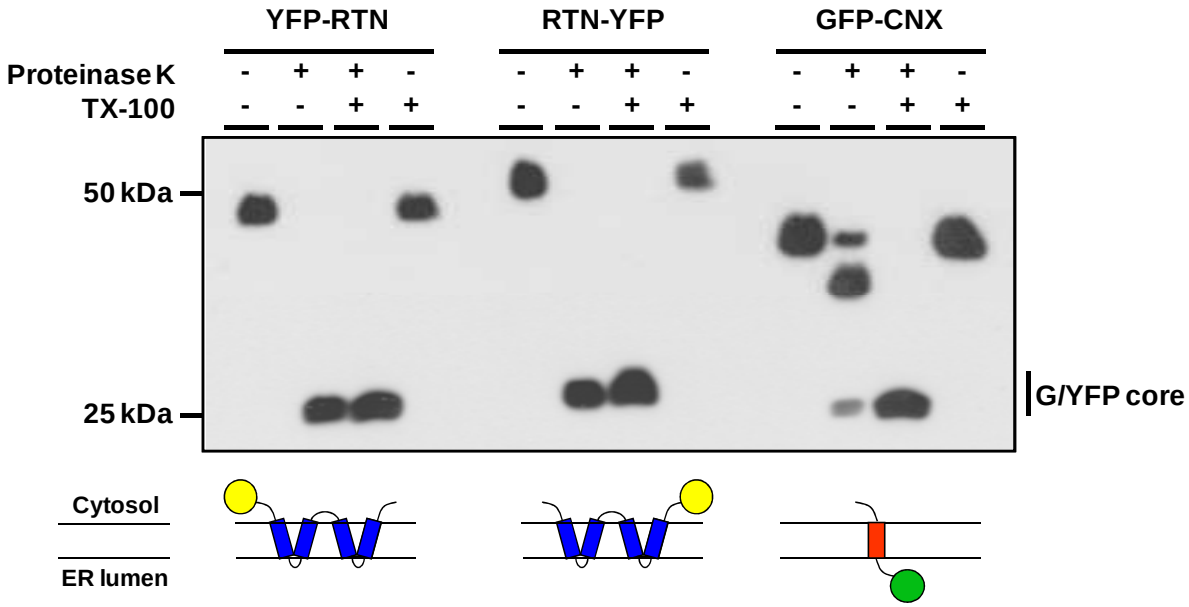

Figure 4.2 Protease protection assay of N- and C-terminally YFP tagged RTN13 to determine topology. Western blot of agro-infiltrated tobacco leaf sectors using anti-GFP antibody following protease protection assay using proteinase K. N- and C-terminally YFP-tagged RTN13 and GFP-calnexin were tested and subsequently resolved by SDS-PAGE. Full-length protected protein bands detected at approximately 50 kDa and degraded GFP core at 25 kDa. Proposed topology of proteins illustrated beneath.

the detergent Triton X-100 to solubilise the microsomes, to show that the samples were indeed susceptible to proteinase K digestion under these conditions. Microsomes were also treated with detergent alone as a further control in order to show that neither the sample nor the detergent contained any proteases. Both YFP-RTN13 and RTN13-YFP microsomes yielded a ~25 kDa polypeptide immunoreactive to GFP antiserum when exposed to proteinase K. This is likely to be the protease resistant 'core' of variants derived from and including GFP (Bokman & Ward, 1981; Chiang *et al*., 2002). In contrast, only the cytosolic tail of GFP-calnexin was trimmed as the majority appeared to be protected in the lumen of the microsomes. Upon the addition of Triton, GFP-calnexin was readily digested. These data indicate that both the N- and C-termini of RTN13 face the cytosol, as predicted by the topology consensus software TOPCONS (Figure 5.6, Bernsel *et al*., 2009).

4.3 Determining the topology of RTN1-4 using protease protection

To determine whether the topology of RTN13 is a shared feature across the *Arabidopsis* reticulon family, four reticulon proteins were subject to topological analysis. In a similar manner to RTN13, N- and C-terminally YFP tagged forms of RTN1-4 were expressed in tobacco leaves and microsomes were harvested. Following proteinase K digestion, it was determined that the N- and C-termini of RTN1-4 all face the cytosol (Figure 4.3). GFP-calnexin was again used as a control to validate the experimental procedure (data not shown). YFP-tagged RTN1-4 have also been shown to form constrictions in the ER lumen similar to that of RTN13 (Sparkes *et al*., 2010; see Appendix Figure A7).

4.4 Determining the topology of RTN13 using bimolecular fluorescence complementation

By virtue of the versatility of fluorescent molecules such as YFP, the topology of RTN13 was verified using bimolecular fluorescence complementation. The individual N- or C-terminal fragments of YFP were cloned in frame with RTN13 at either the N- or C-terminus, then subsequently expressed with either a cytosolic or ER lumen targeted counterpart. If the two halves were able to come in close proximity to one another, they would fluoresce. This method was used to determine

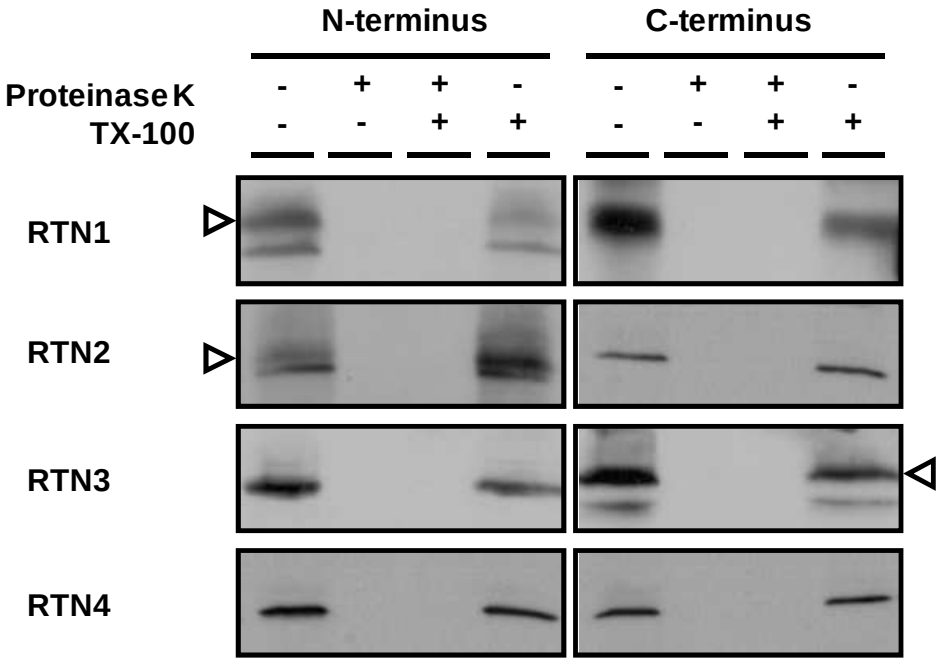

Figure 4.3 Protease protection assay of N- and C-terminally YFP tagged RTN1-4 to determine topology. Western blot of agro-infiltrated tobacco leaf sectors using anti-GFP antibody following protease protection assay using proteinase K. N- and C-terminally full-length protected protein bands migrated at approximately 50 kDa. Arrowheads indicate relevant protein bands where multiple bands are present.

the topology of the N- and C-termini and the loop of RTN13. Different combinations of YN and YC were used as it has been reported that the efficiency of fluorescence can vary between the YFP fragments (Zamyatnin *et al.*, 2006).

4.4.1 Bimolecular fluorescence complementation

As a control, YN was co-expressed with YC and similarly, YN-ER was co-expressed with YC-ER to validate the BiFC system. Both sets of reporters showed a fluorescent signal either in the cytosol or the lumen of the ER, respectively (Figure 4.4 A-B). Expression of YN and YC-ER (and vice versa) was tested and yielded no fluorescence (data not shown). Each tagged variation of RTN13 was co-expressed with its reciprocal marker targeted to either the cytosol or the ER lumen. In each case, N-terminally tagged YN- or YC-RTN13 only fluoresced with their cytosolic counterpart. Similarly, only when expressed with either YN or YC did the C-terminally tagged RTN13 fluoresce (Figure 4.4 C-J). These results indicate that the N- and C-termini face the cytosol, which is in agreement with the protease protection results.

In order to test the topology of the loop of RTN13, the YC fragment was cloned in between Val91 and Val92 in the centre of the loop and co-expressed with both YN and YN-ER. Albeit with low expression levels, fluorescence was only seen when RTN-YC-RTN was co-expressed with cytosolic YN (Figure 4.4 K-L), indicating that the loop of RTN13 is likely to face the cytosol and that the protein may sit in a ‘w’ conformation in the ER membrane.

4.4.2 Validation of BiFC

To test whether the addition of YN/YC to RTN13 had any effect on its ability to constrict the ER lumen, tagged RTN13 was co-expressed with RFP-HDEL. Expression of cytosolic YN, YC-RTN13 and RFP-HDEL, for example, was attempted, but the probability of finding a cell expressing all three constructs was low. Therefore, only RTN13 tagged with the YFP fragments were co-expressed with RFP-HDEL and cells were selected by the constriction pattern seen with RFP-HDEL. Constricted phenotypes could be found for the constructs YN-RTN13, YC-

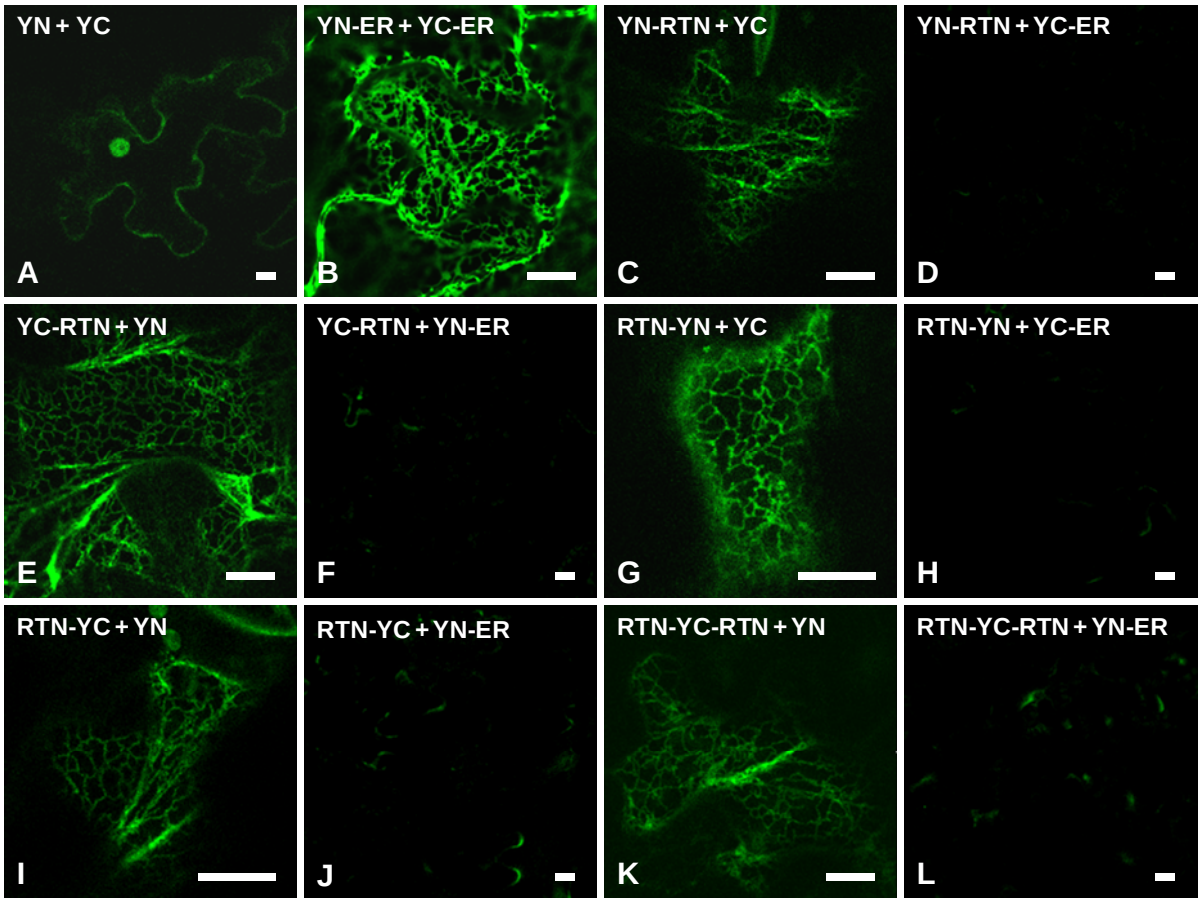

Figure 4.4 Bimolecular fluorescence complementation reveals topology of RTN13 N-, C-terminus and loop. Confocal images of *Agrobacterium*-infiltrated tobacco leaf epidermal cells transiently expressing (A) cytosolic YN and YC (green), (B) ER-targeted YN-ER and YC-ER, (C) YN-RTN13 and cytosolic YC and (D) the reciprocal expression of YN-RTN13 and ER-targeted YC-ER. (E) YC-RTN13 and YN and (F) YC-RTN13 and YN-ER. (G) RTN13-YN and YC, (H) RTN13-YN and YC-ER, (I) RTN13-YC and YN, (J) RTN13-YC and YN-ER, (K) RTN-YC-RTN and YN and (L) RTN-YC-RTN and YN-ER. Scale bar = 20 μm.

RTN13, RTN13-YN and RTN13-YC (Figure 4.5 B-E) which show varying levels of constriction (usually owing to expression levels) compared to the RFP-HDEL control (Figure 4.5 A). Due to the low expression levels of RTN-YC-RTN, a constricted phenotype could not be found. Therefore, the structural stability of RTN13, as determined by its ability to form constrictions, cannot be accounted for in this case, and the topology of the loop will need to be confirmed by other means.

4.5 Discussion

The topology of five plant reticulons was investigated to ascertain any relationship between the structure and function of these curvature inducing proteins. Using protease protection, the topologies of RTN13 and RTN1-4 were determined.

RTN1-4 and 13 were tagged with YFP at either the N- or C-terminus and expressed in tobacco leaves. Microsomes were prepared from the infiltrated leaves and subjected to proteinase K digestion using the luminal GFP-calnexin as a control. As predicted by TOPCONS, the N- and C-termini of the five reticulon isoforms were readily degraded by proteinase K, whereas GFP-calnexin was protected by the microsomal membrane, and only susceptible to degradation upon membrane permeabilisation with the detergent Triton.

The topology of RTN13 was also determined using bimolecular fluorescence complementation. This method utilises the innate ability of YFP, when divided into two non-fluorescent fragments, to non-covalently reform and restore fluorescence. This technique, initially used to detect protein-protein interactions, was further developed to ascertain the topology of proteins in plants (Zamyatnin *et al*., 2006). The YFP fragments, termed YN and YC, were targeted to either the cytosol or the ER lumen and co-expressed with RTN13 tagged at either the N- or C-terminus with either YN or YC. All combinations of YFP fragments with RTN13 were tested. Fluorescence was only observed when RTN13 was expressed with a YFP fragment targeted to the cytosol, thus confirming that both the N- and C-termini of RTN13 face the cytosol. A further construct was tested whereby the YC fragment was cloned into the centre of the loop region of RTN13 (RTN-YC-RTN) in order to determine

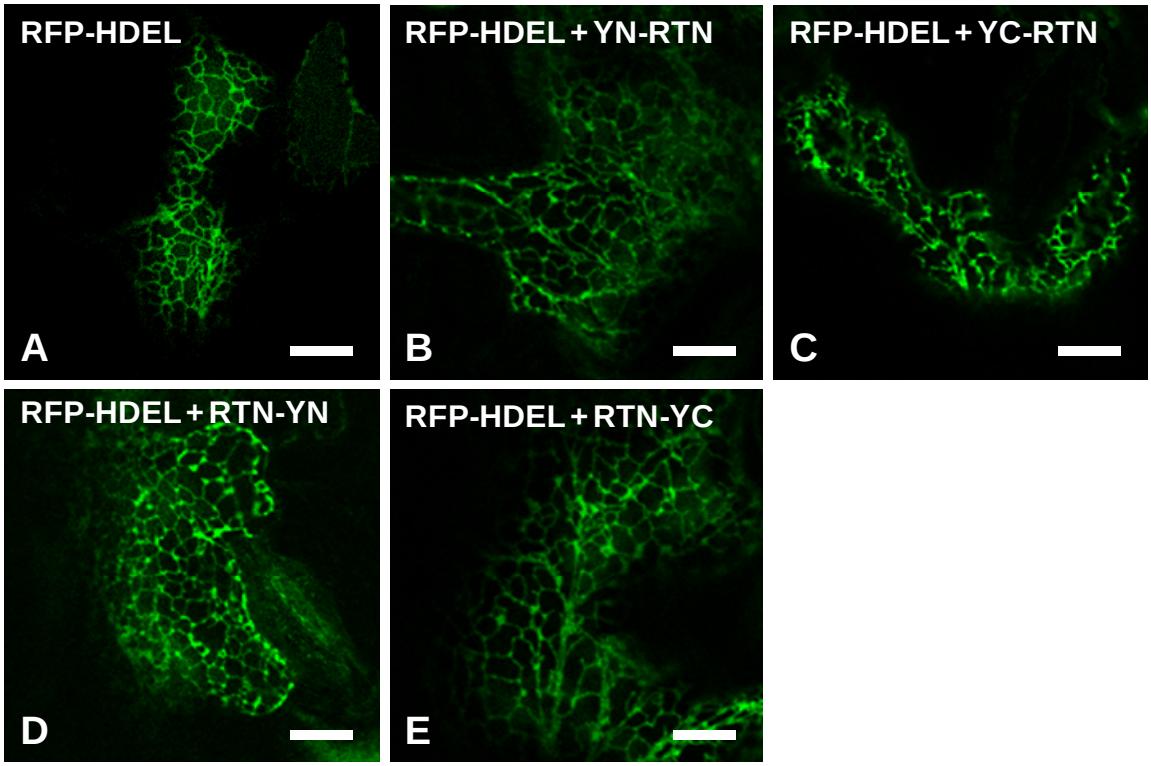

Figure 4.5 YN and YC tagged RTN13 still constrict the lumen of the ER. The green fluorescence indicates RFP expression. Confocal images of *Agrobacterium*-infiltrated tobacco leaf epidermal cells transiently expressing (A) RFP-HDEL alone, (B) RFP-HDEL and YN-RTN13, (C) RFP-HDEL and YC-RTN13, (D) RFP-HDEL and RTN13-YN and (E) RFP-HDEL and RTN13-YC. Scale bars = 10 µm.

the topology of the loop. Again, fluorescence was only detected when RTN13 was expressed with the corresponding YN fragment targeted to the cytosol, indicating that the loop of RTN13 also faces the cytosol.

Presuming that the addition of the YFP fragments to RTN13 would not alter its structure, especially in the case of RTN-YC-RTN construct, YN/YC RTN13 fusions were co-expressed with RFP-HDEL to determine whether they retained the ability to constrict ER tubules – an attribute which, in this case, would indicate that RTN13 was correctly folded. The constricted phenotype was observed for all N- and C-terminal fusions, although, due to low expression levels, a constricted tubular ER could not be found for RTN-YC-RTN. Therefore, the validity of the topology of RTN-YC-RTN, while confirmed by TOPCONS predictions (data not shown), cannot be conclusively established and the orientation of the loop region should be confirmed by other means. This may be achieved by adapting the method of Voeltz *et al*., (2006) whereby maleimide PEG modification of cysteine residues was used to map the orientation of Rtn4c.

This topological analysis of *Arabidopsis* reticulons indicates that the N- and C-termini face the cytosol and, in the case of RTN13, the loop region also faces the cytosol. This results in a 'w' structure in the ER membrane which is postulated to impose curvature on the lipid bilayer and aid the formation of tubular ER. The topology of *Arabidopsis* RTN1-4 and 13 has since been confirmed using redox-sensitive GFP (RoGFP) fusions (Sparkes *et al*., 2010). RoGFP fusions were expressed in tobacco leaves and imaged with 405nm and 488nm lasers to detect oxidised and reduced forms respectively, and subjected to ratiometric analysis (Brach *et al*., 2008). This method was also used to confirm the cytosolic localisation of the loop region of RTN1-4 and 13, which is consistent with the BiFC results presented here and the topological studies of the mammalian Rtn3 and Rtn4c (Voeltz *et al*., 2006; He *et al*., 2007). These data represent the first evidence of the topology of plant reticulon proteins.

Using the model of RTN13 arranged in a 'w' conformation in the ER membrane, questions regarding the different domains of RTN13 can be addressed. What is responsible for the localisation of RTN13 to the ER? Although it contains an ER-

retrieval motif, many of the reticulons in *Arabidopsis* do not. Which domains of RTN13 are responsible for inducing constrictions in the ER lumen? What is the relevance of the variable N- and C-termini and the conserved reticulon homology domain? By dissecting the functions of the individual domains of RTN13, parallels may then be drawn with the other isoforms of reticulon in *Arabidopsis* and other species.

Chapter 5: Analysis of mutant forms of RTN13

5.1 Introduction

Reticulon proteins are composed of variable length N-termini and a conserved C-terminal reticulon homology domain (RHD) composed of two hydrophobic stretches flanking a hydrophilic loop region. The majority of reticulon proteins are thought to localise to the ER and it is hypothesised that the RHD is responsible for this. Indeed, similar to RTNLB13 in *Arabidopsis*, the human Rtn4c consists of little more than the RHD, yet still localises to the ER (Voeltz *et al*., 2006).

The variable N-terminal regions of reticulons are thought to interact with proteins involved in various cellular processes (Iwahashi *et al*., 2007) and for anchoring and modulating enzymatic activity (Nziengui *et al*., 2007). For example, the RTNLB proteins, RTNLB1, RTNLB2 and RTNLB4, are able to interact *in vitro* with each other, and with the *Agrobacterium* VirB2 protein (Hwang & Gelvin, 2004). Therefore, this divergence seen in the N-termini of reticulons appears to carry out species- and cell-specific roles, whereas the RHD may carry out more basic cellular functions (Di Scala *et al*., 2005).

The RHD of Rtn1 is critical for ER localisation (van de Velde *et al*., 1994), and although both hydrophobic regions can determine ER localisation (Iwahashi *et al*., 2007), a single hydrophobic region is sufficient to target a fluorescent protein fusion to the ER (Chen *et al*., 2000). Disruption of the first hydrophobic region of Rtn3 results in misfolding and incorrect insertion into the ER membrane (He *et al*., 2007) and deletion of the RHD abolishes all association with the ER (Chen *et al*., 2000). Within the RHD, the second hydrophobic region is the most highly conserved, followed by the first (Yang & Strittmatter, 2007), although the second hydrophobic region of Rtn3 is not required for ER localisation (He *et al*., 2007).

Members of reticulon family, DP1 in mammals, and Yop1p in yeast were found to be sufficient to generate membrane tubules when purified proteins were incorporated into proteoliposomes, whereby the diameter of these tubules is dependent on the level of expression (Hu *et al*., 2008). Oligomerisation of reticulon proteins is thought to aid ER localisation and tubulation. The RHD alone is sufficient to localise to

tubular ER and form oligomers, although oligomerisation alone may not be sufficient to form tubules (Shibata *et al*., 2008).

The hydrophobic regions of reticulons are also unusually long to span the ER membrane. It takes approximately 20 residues to span a lipid bilayer, but in reticulon proteins, the two hydrophobic regions are approximately 40 residues long, raising the question as to whether this length has any significance to the function of reticulons (Yang & Strittmatter, 2007). When the first hydrophobic region of Rtn1 is split in two, neither half is sufficient for ER localisation and both are mistargeted to the Golgi (Iwahashi *et al*., 2007). The second hydrophobic region of Rtn3 is thought to contain two smaller transmembrane domains separated by a 3-residue linker. Increasing or shortening the length of this linker affects the latter transmembrane domain and Rtn3 can no longer interact with BACE-1 (He *et al*., 2007). If these longer hydrophobic stretches do represent multiple transmembrane domains, then their lengths (~20 residues) remain unusually long and indicative of a plasma membrane resident protein, with ER and Golgi transmembrane domains typically measuring 17-19 residues (Munro, 1995).

The RHD is often described as the C-terminal domain of reticulon proteins, but in plants and yeast, reticulon proteins display a C-terminal extension beyond the RHD (Nziengui & Schoefs, 2008; Sparkes *et al*., 2009a). It is in this C-terminal region where the dilysine ER retrieval motif (KKXX) is found. The KKXX motif is used for retrieval of type I and type III membrane proteins whereby components of COPI machinery recognise the motif on the cytosolic facing tail of ER-destined proteins (Jackson *et al*., 1990). Although only present in some reticulons, the KKXX motif seems unnecessary as its removal from Rtn1 and Rtn4c still permits steady state ER localisation (Iwahashi *et al*., 2007; Sironen *et al*., 2004), although visualisation of reticulon escape to the Golgi may prove difficult experimentally.

Within the RHD, flanked by the two hydrophobic regions is the 60-70 amino acid hydrophilic loop, although this region is smaller in plant reticulons. In mammals, the loop of Rtn4a (Nogo-66) is thought to interact with a receptor, termed Nogo-66 receptor (NgR) which is involved in the inhibition of axonal regeneration after injury

(Fournier *et al*., 2001). There is no known homologue of this receptor in plants (Nziengui & Schoefs, 2008).

5.1.1 Aims & experimental approach

Over-expressed full-length RTN13 localises to the ER and results in constriction of the ER lumen. The purpose of this chapter is to determine how RTN13 localises to ER, and which domains of the protein are responsible for correct targeting and expression. The ability of RTN13 to induce tubulation is also addressed. Two types of mutations were made to full-length RTN13 – truncations to the hydrophilic regions (N-, C-termini and loop) and shortenings of the transmembrane domains. YFP and myc-tagged variants were made of all constructs. Both tobacco and *Arabidopsis* plants were transiently transformed by means of *Agrobacterium*-infiltration and biolistic gene delivery, respectively.

5.1.2 Cloning & construct design

Constructs were cloned using the restriction endonucleases *XbaI* and *SacI* into appropriate expression vectors. Constructs used for *Agrobacterium*-mediated infiltration and biolistic gene delivery were inserted into the plant binary vector pVKH18-En6. Constructs used for PEG-mediated transfections in tobacco protoplasts were inserted into a 35S-CaMV vector. All mutants are shown diagrammatically in Figure 5.1.

First, truncations were made to the ER-retrieval motif, the entire C-terminus, the N-terminus and an N-terminal variant retaining a possible stop-transfer signal (Cocquerel *et al*., 2000). In all of these mutants, the predicted RHD remained intact. The RHD is proposed to be the domain responsible for ER retention, as only a proportion of reticulons contain an ER-retrieval motif, yet still localise to the ER.

The first mutant, termed RTN13-ΔKKSE, lacked the final four residues of RTN13 (KKSE) – the potential ER-retrieval motif. Next, a mutant (RTN13-ΔC) was made lacking the entire C-terminus following the final transmembrane domain of the RHD. Similarly, a mutant (ΔN-RTN13) was made lacking the entire N-terminus up to the

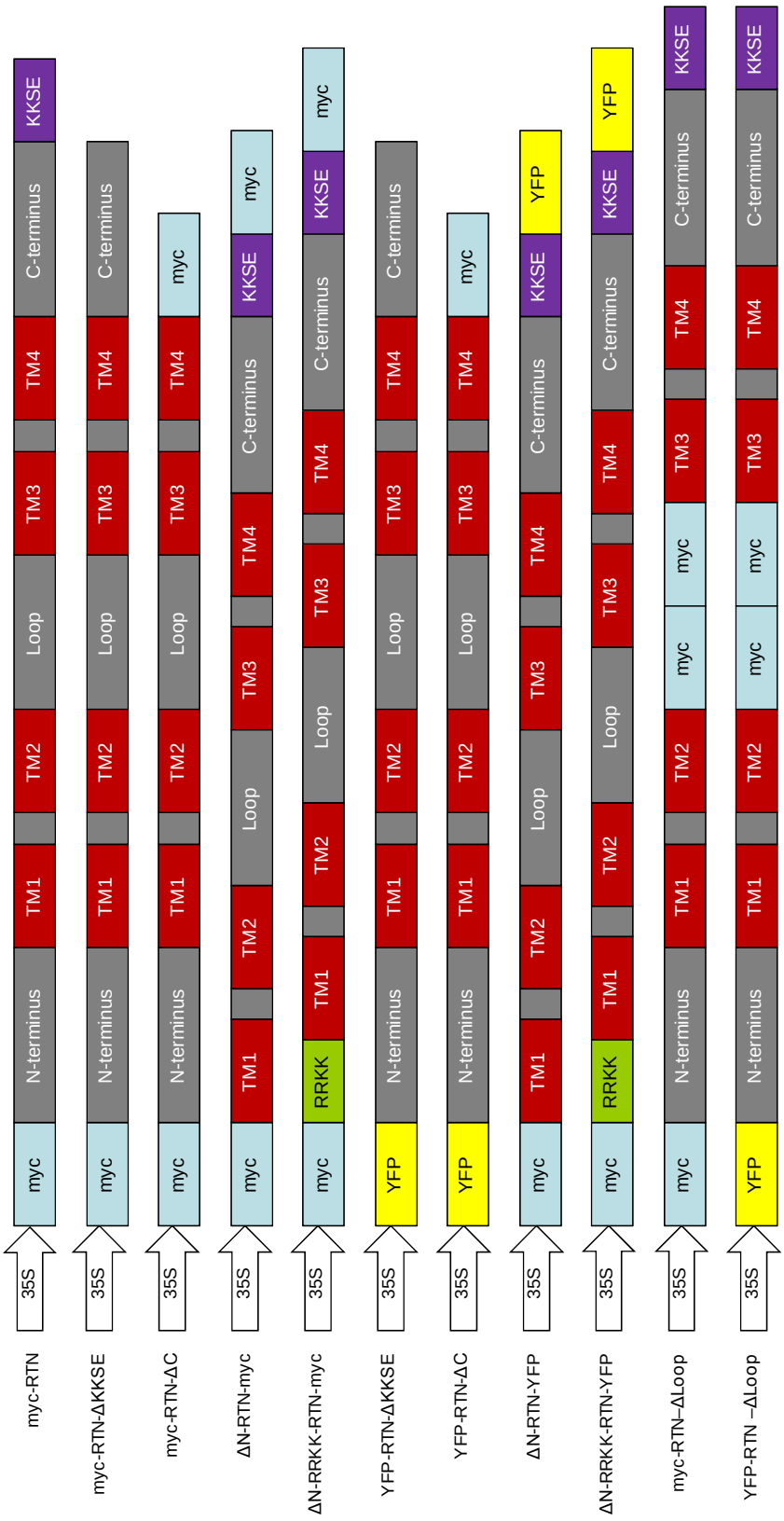

Figure 5.1 Constructs used in the over-expression of RTN13 mutants in Tobacco. 35S driven RTN13 constructs tagged with either a myc-epitope or YFP. Tags are positioned at either N- or C-terminus, usually opposite where a mutation has been made. Deletions have been made of the N- and C-terminus, the ER retrieval motif and the loop. Wild-type myc-RTN13 is shown as a comparison.

first transmembrane domain of the RHD. An additional mutant was made lacking the majority of the N-terminus, but retaining four residues upstream of the first transmembrane domain, RRKK – a potential stop-transfer signal. This was termed ΔN-RRKK-RTN13. In addition to these deletion mutants being tagged with a myc-epitope or YFP, the deleted regions were replaced with a myc-tag as a 'spacer' sequence, so as to maintain the distance between transmembrane domains and allow them to insert correctly into the membrane.

A separate deletion mutant was also made, termed RTN13-ΔLoop, where the 33 residue loop was replaced with a double myc-tag (20 residues) in order to assess the function of the loop region, without disturbing the structure and topology of RTN13.

In a second set of mutants (ΔTM), the four transmembrane domains of RTN13 were sequentially and cumulatively shortened from their unusually long 22-24 residue length, to 17 residues, which is the length required to span the plant ER membrane (Moreau *et al*., 2007). This was undertaken to investigate whether the length of the transmembrane domains contributes to ER localisation, and also their ability to impose membrane curvature.

Full-length RTN13, along with the ΔTM mutants were then expressed in *Arabidopsis* in a *pah1pah2* mutant background. *pah1pah2* is a double knockout of two genes involved in lipid metabolism, which encode phosphatidic acid hydrolase (Nakamura *et al*., 2009). The subsequent phenotype results in the abundance of sheets within the ER membrane, with almost no tubular ER remaining (Dr Peter Eastmond, personal communication). Wild-type and mutant leaves were transfected with DNA using biolistic gene delivery and examined using confocal microscopy 48 h post-transfection.

5.2 Removal of the ER-retrieval motif has no effect on RTN13 localisation

More than half of reticulon proteins in *Arabidopsis* have a C-terminal ER retrieval motif (KKXX), including RTN13 (Nziengui *et al*., 2007). A mutant form of RTN13 was made in order to determine whether this motif is necessary for steady state ER localisation. Upon removal of the KKSE ER-retrieval motif from YFP-RTN13, the

protein still localised to the ER and when co-expressed with RFP-HDEL, retained the ability to form constrictions within the ER lumen when visualised by confocal microscopy

(Figure 5.2 A-C). No additional cellular compartments were highlighted by YFP-RTN13-ΔKKSE and no apparent co-localisation between the mutant and the Golgi marker ST-RFP were observed (Figure 5.2 D-F). This suggests that another mechanism may be responsible for retaining RTN13 in the ER.

5.3 Removal of the N- or C-terminus affects RTN13 protein stability but not ER residence

In order to determine which domains of RTN13 are functionally necessary, independent truncations of the N- and C-termini were made. In the mammalian Rtn4a, the RHD alone is sufficient for ER localisation and insertion into the membrane (Shibata *et al.*, 2008). When visualised with confocal microscopy, a RTN mutant lacking its C-terminal region (residues 156-206) co-localised with RFP-HDEL (Figure 5.3 A-C). However, constrictions in the ER lumen were not apparent, perhaps owing to reduced levels of YFP-RTN13-ΔC expression. The absence of the C-terminal region may impede the correct folding of RTN13, possibly disrupting its insertion into the ER membrane. No co-localisation was observed upon co-expression with ST-RFP (Figure 5.3 D-F).

Removal of the N-terminal region (residues 1-26) in the construct ΔN-RTN13-YFP also highlighted the ER and resulted in reduced expression levels (Figure 5.4 A-C). Constrictions were not observed upon over-expression, indicating that this phenotype may be dependent on high expression levels, as variable levels of constriction have been seen previously in this study. Again, there was no co-localisation when this mutant was co-expressed with ST-RFP (Figure 5.4 D-F).

In a similar mutant, ΔN-RRKK-RTN13-YFP (residues 1-22), the four residues (RRKK) preceding the first predicted transmembrane domain of RTN13 were retained, as they are thought to encode a stop-transfer signal which helps the protein insert into the membrane. This mutant had increased expression levels compared

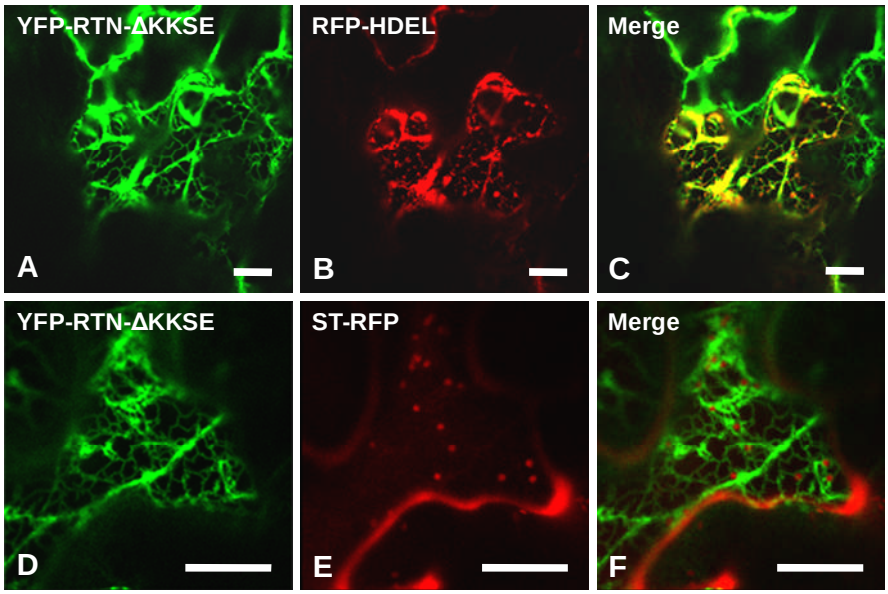

Figure 5.2 Removal of the ER retrieval motif of RTN13 does not affect its localisation to the ER. Confocal images of *Agrobacterium*-infiltrated tobacco leaf epidermal cells transiently expressing (A) YFP-RTN13-ΔKKSE (green), (B) RFP-HDEL (red) and (C) merged image of (A) and (B), (D) YFP-RTN13-ΔKKSE, (E) ST-RFP and (F) the image of (D) and (E). Scale bars = 10 µm.

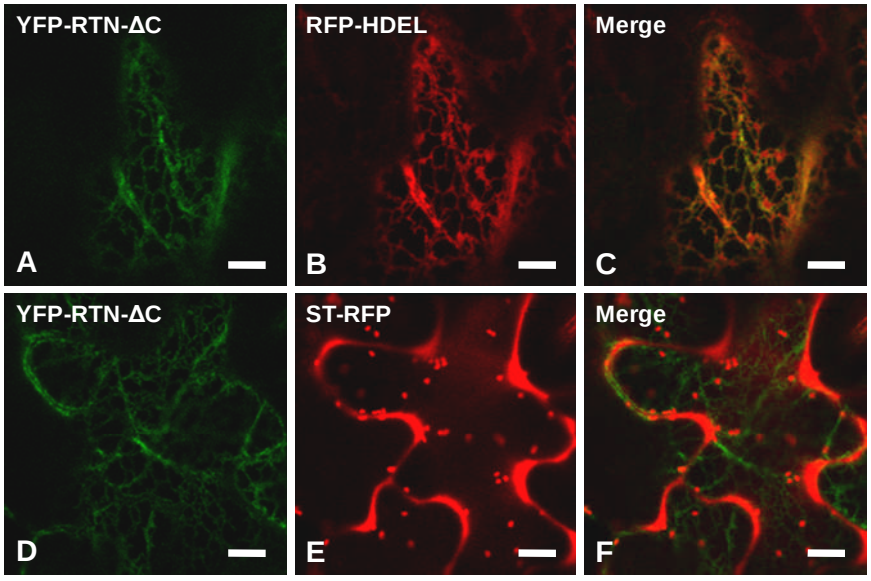

Figure 5.3 Removal of the C-terminus of RTN13 results in a loss of both expression and constriction of the ER lumen. Confocal images of *Agrobacterium*-infiltrated tobacco leaf epidermal cells transiently expressing (A) YFP-RTN13-ΔC (green), (B) RFP-HDEL (red) and (C) the merged image of (A) and (B), (D) YFP-RTN13-ΔC, (E) ST-RFP and (F) the image of (D) and (E). Scale bars = 5 µm.

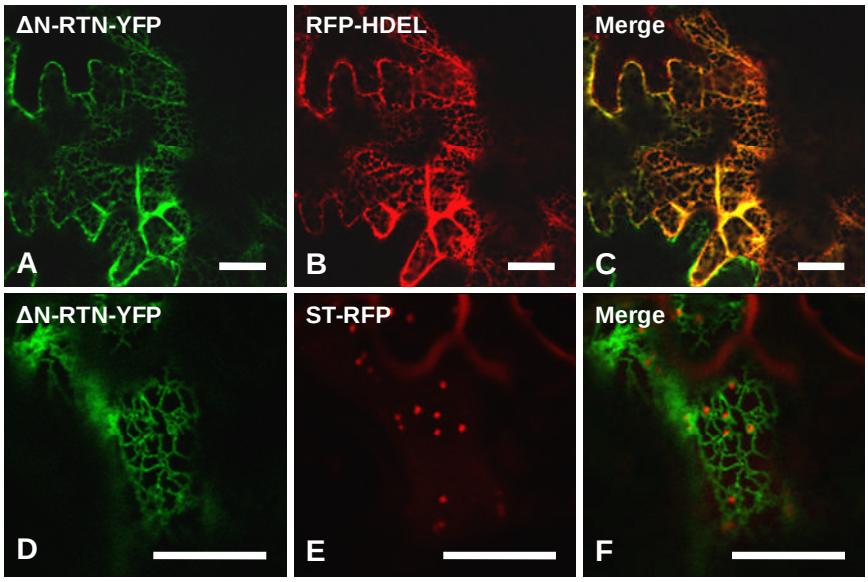

Figure 5.4 Removal of the N-terminus of RTN13 results in reduced expression and loss of constriction of the ER lumen. Confocal images of *Agrobacterium*-infiltrated tobacco leaf epidermal cells transiently expressing (A) ΔN-RTN13-YFP (green), (B) RFP-HDEL (red) and (C) merged image; (D) ΔN-RTN13-YFP, (E) ST-RFP and (F) merged image of (D) and (E). Scale bar = 20 μm.

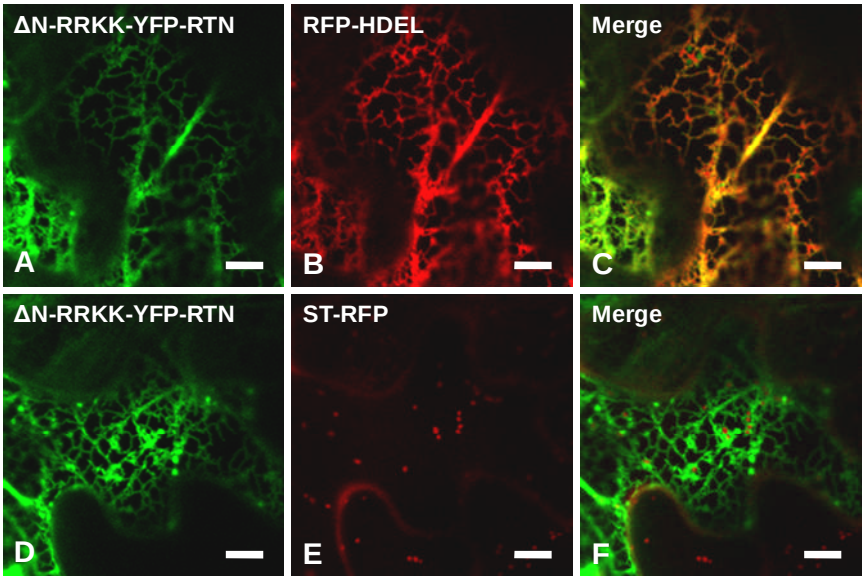

Figure 5.5 Retention of possible stop-transfer signal improves expression of RTN13 compared with ΔN-RTN13, but makes it incapable of inducing luminal constrictions. Confocal images of *Agrobacterium*-infiltrated tobacco leaf epidermal cells transiently expressing (A) ΔN-RRKK-RTN13-YFP (green), (B) RFP-HDEL (red) and (C) merged image; (D) ΔN-RRKK-RTN13-YFP, (E) ST-RFP and (F) merged image of (D) and (E). Scale bar = 5 μm.

with ΔN-RTN13-YFP, indicating that previous mutations may have inhibited correct insertion into the ER membrane (Figure 5.5 A-C). However, as it still lacked the majority of the N-terminal region, this mutant did not express as well as wild-type RTN13. Again, although ΔN-RRKK-RTN13-YFP localised to the ER, constrictions were not seen, and there was no co-localisation with ST-RFP (Figure 5.5 D-F). In light of these results, a double mutant lacking both the N- and C-terminus was not tested as this would most likely result in low expression levels akin to the N- and C-terminal mutants.

5.5 Transmembrane topology prediction and western blot analysis of RTN13 mutants reveal potential expression problems

5.5.1 Topology prediction

Small changes in the amino acid sequence of RTN13 may give rise to incorrect membrane insertion and protein degradation. Using TOPCONS (Bernsel *et al*., 2009), the prediction of transmembrane domains and protein topology alters when the above described mutations are made (Figure 5.6). Truncation of the ER retrieval motif does not affect topology or the number of predicted TM domains. Removal of the N- or C-terminus results in disruption to the C-terminal region of the protein, although the addition of the stop-transfer signal – RRKK - restores the number of transmembrane domains and topology of RTN13.

5.5.2 Western blot

Expression levels and the presence of full-length protein needed to be established to reinforce the results obtained by confocal microscopy. Western blot analysis of full-length and mutant forms of RTN13 firstly indicated that YFP-tagging results in a molecular weight shift when run on SDS-PAGE (Figure 5.7). These run in an opposite fashion to myc-tagged RTN13 whereby N-terminal fusions run slightly faster than C-terminal fusions. The nature of this size-shift is yet to be determined, although in all cases, there is evidence of a cleavage product which could potentially represent YFP and a portion of RTN13, which run at approximately 27 kDa. Tagging

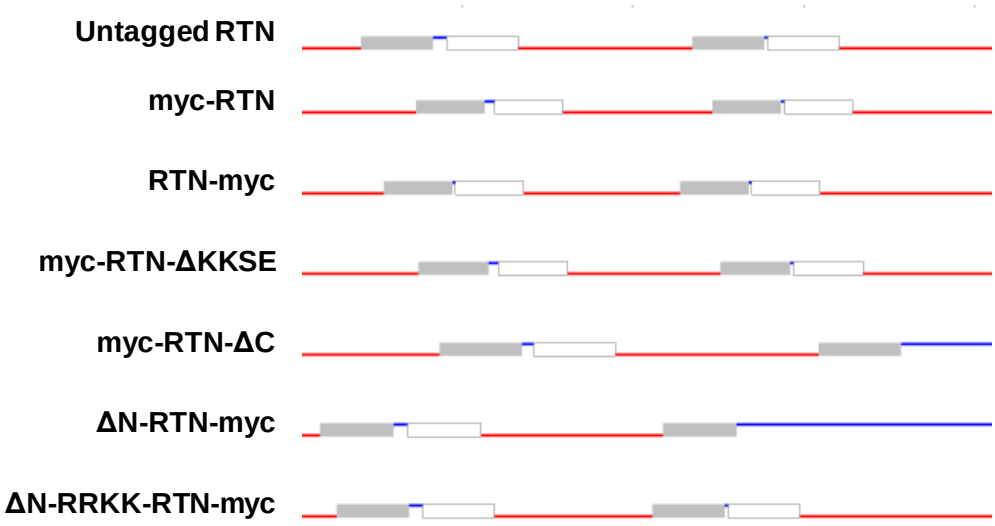

Figure 5.6 TOPCONS topology predictions of RTN13 truncation mutants. Untagged and myc-tagged variants of RTN13 mutants indicating orientation (red represents cytosolic, blue represents luminal) and number of transmembrane domains.

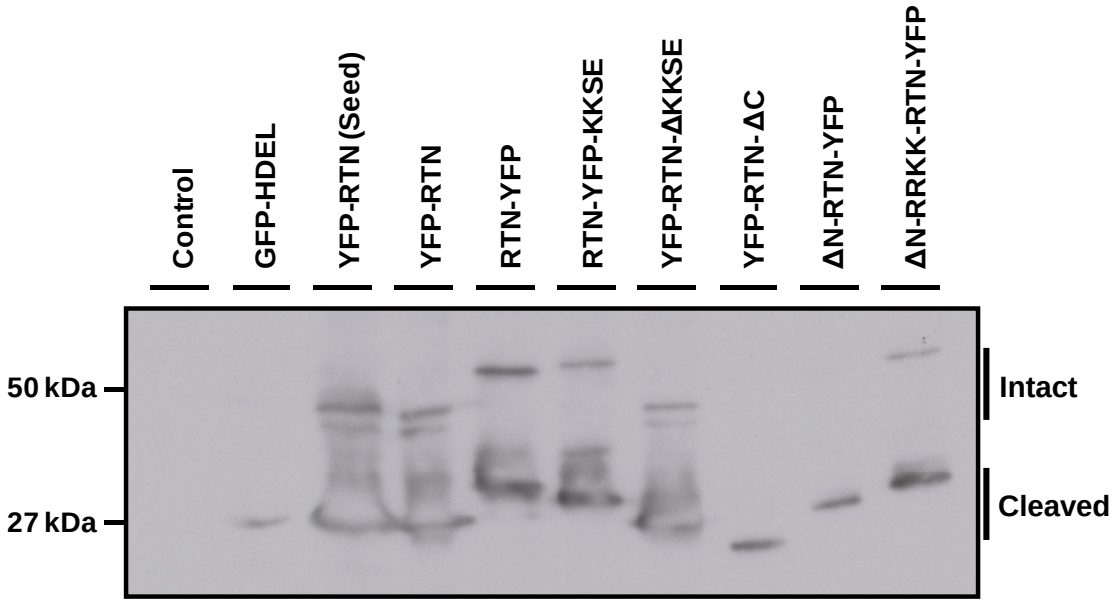

Figure 5.7 Western blot analysis of RTN13 mutants. Western blot of agro-infiltrated tobacco leaf sectors using anti-GFP antibody following resolution of YFP-tagged RTN13 mutants by SDS-PAGE. Protein bands are detected at approximately 50 kDa with breakdown products at 27 kDa. Un-infiltrated tobacco leaf, GFP-HDEL and transgenic YFP-RTN13 *Arabidopsis* seeds were used as controls.

with different epitopes at either terminus of RTN13 may result in differential trimming of the protein.

Both wild type YFP-RTN13 and YFP-RTN13-ΔKKSE were expressed at equal levels, whereas YFP-RTN13-ΔC or any associated degradation product was not detected. Full length ΔN-RTN13-YFP was also not detected, although small amounts of degradation product were seen at a similar size to GFP-HDEL. Full length ΔN-RRKK-RTN13-YFP was detected at low levels, which is concurrent with topology prediction similar to that of wild-type RTN13. In this instance, a more stable protein conformation may allow this mutant to insert correctly into the ER membrane and minimise degradation.

5.6 Removal of the loop region results in reduced expression levels of RTN13

The orientation and function of the hydrophilic loop flanked by the two hydrophobic regions of the RHD has been shown to face the cytosol (Figure 4.4). Whether reticulons adopted a 'v' or 'w' structure in the membrane was based on whether the loop region faced the cytosol or the ER lumen. In order to determine its function, the loop region of RTN13 was replaced with two myc-tags in an attempt to mimic the size of the loop, but remove any functionality of the loop domain. When expressed transiently, YFP-RTN13-ΔLoop localised to the ER and co-localised with RFP-HDEL (Figure 5.8 A-C), albeit with reduced expression levels, indicating that the loop region may also be necessary for correct folding and expression. However, constrictions cannot be seen within the ER lumen and therefore the loop region, or at least the overall structure of RTN13, may need to be intact in order to shape the ER membrane.

5.7 Pulse-chase analysis of RTN13 mutants reveals differential levels of turnover

In order to confirm that low expression of these truncation mutants was due to degradation, the stability of myc-tagged mutants was assessed over 5 hours in a pulse-chase experiment using transfected protoplasts (Figure 5.9). Full-length myc-RTN13 and myc-RTN13-ΔKKSE were stable over the 5 hour chase, whereas myc-RTN13-ΔC showed little sign of being produced, although this is in agreement with

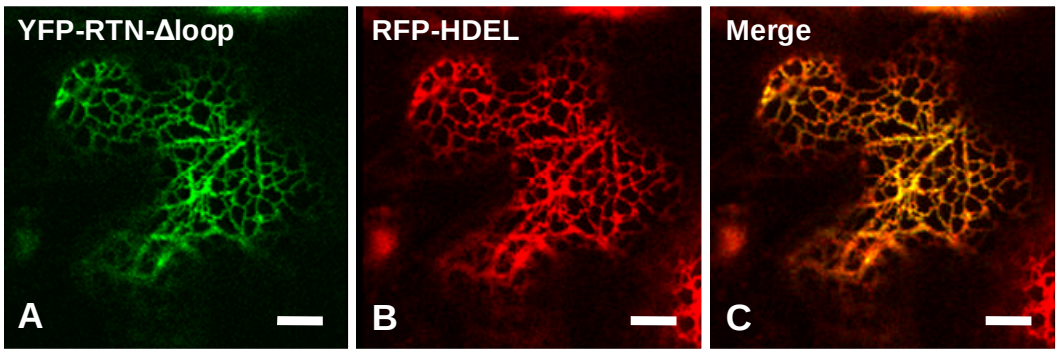

Figure 5.8 Removal of the hydrophilic loop results in a loss of both expression and constriction of the ER lumen. Confocal images of *Agrobacterium*-infiltrated tobacco leaf epidermal cells transiently expressing (A) YFP-RTN-ΔLoop (green), (B) RFP-HDEL (red) and (C) the merged image of (A) and (B). Scale bar = 10 µm.

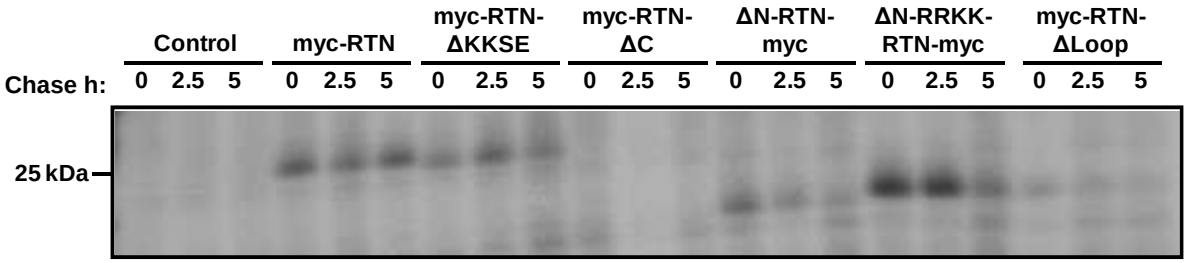

Figure 5.9 RTN13 truncation mutants show varying levels of stability. Pulse-chase of transfected tobacco protoplasts expressing RTN13 mutants immunoprecipitated with anti-myc antibody. The fate of myc-tagged proteins were followed over 5 hours. Protein products were detected at approximately 25 kDa.

the low expression of the YFP-tagged form. The ΔN-RTN13-myc construct was expressed at the zero hour time point, but was quickly turned over. Retention of the residues – RRKK - increased the stability of the protein over 2.5 hours, although protein turnover was evident after 5 hours. The myc-RTN13-ΔLoop construct was expressed at low levels at the zero hour time point, but was then quickly turned over in a similar fashion to ΔN-RTN13-myc. This confirms that major deletions made to RTN13 result in unstable proteins and no distinction can be made between the deletion of important functional domains and domains required merely to achieve correct protein folding.

5.8 Analysis of hydrophobic regions of the RHD

The number of transmembrane domains in reticulon proteins would dictate its orientation and structure in the membrane. It is widely accepted that there are two hydrophobic regions within the RHD, but it has been questioned as to whether they are further subdivided into four transmembrane domains. Topological analysis revealed that RTN13 forms a 'w' structure in the ER membrane, and therefore the four membrane-spanning regions of YFP-RTN13 (as predicted by TOPCONS) were sequentially and cumulatively shortened from 22-24 to 17 residues to determine whether the unusual length of the transmembrane domains was responsible for the formation and maintenance of ER tubules (Figures 5.10, 5.11 and Appendix Figure A13). The transmembrane length and structure of reticulons may also be responsible for their localisation, since the removal of the ER retrieval motif has no effect. Hence, four mutant constructs were co-expressed in tobacco using agro-infiltration with the luminal marker RFP-HDEL, with the premise that if the transmembrane domains are reduced to a 'normal' ER length, they will no longer be able to over-induce curvature upon the ER membrane - therefore alleviating the luminal constrictions.

5.8.1 Cumulative shortening of the RTN13 TM domains reduces the ER membrane constriction phenotype

In comparison to wild type YFP-RTN13 (Figure 5.12 A-D), shortening the first transmembrane domain (ΔTM1) in RTN13 resulted in a reduction in the constriction

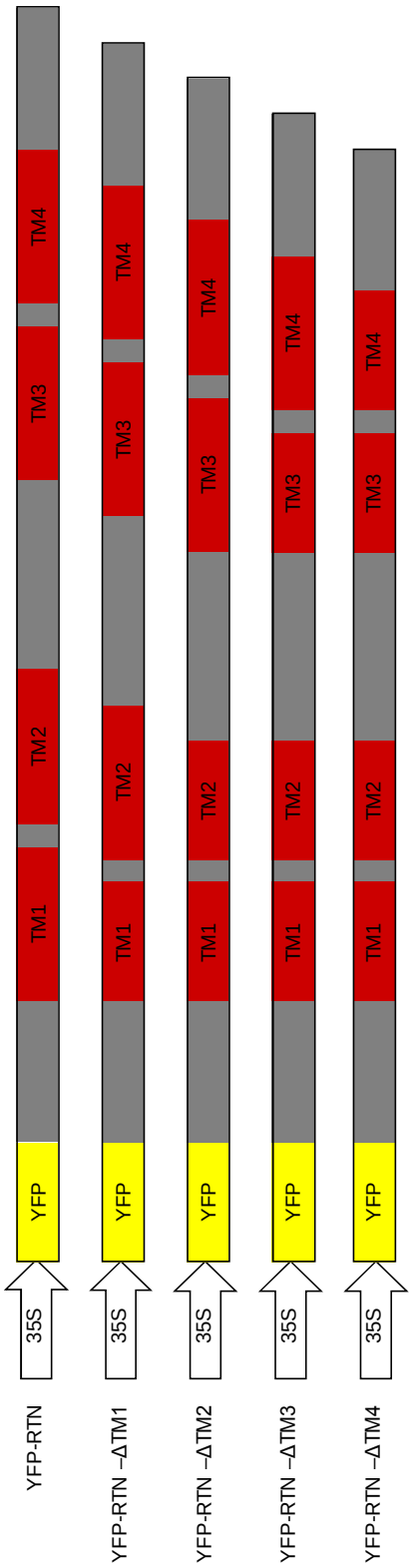

Figure 5.10 Constructs used in the over-expression of RTN13 ΔTM mutants in Tobacco. 35S driven RTN13 constructs tagged with YFP. Tags are positioned at the N-terminus. Sequential and cumulative deletions have been made to the TM domains.

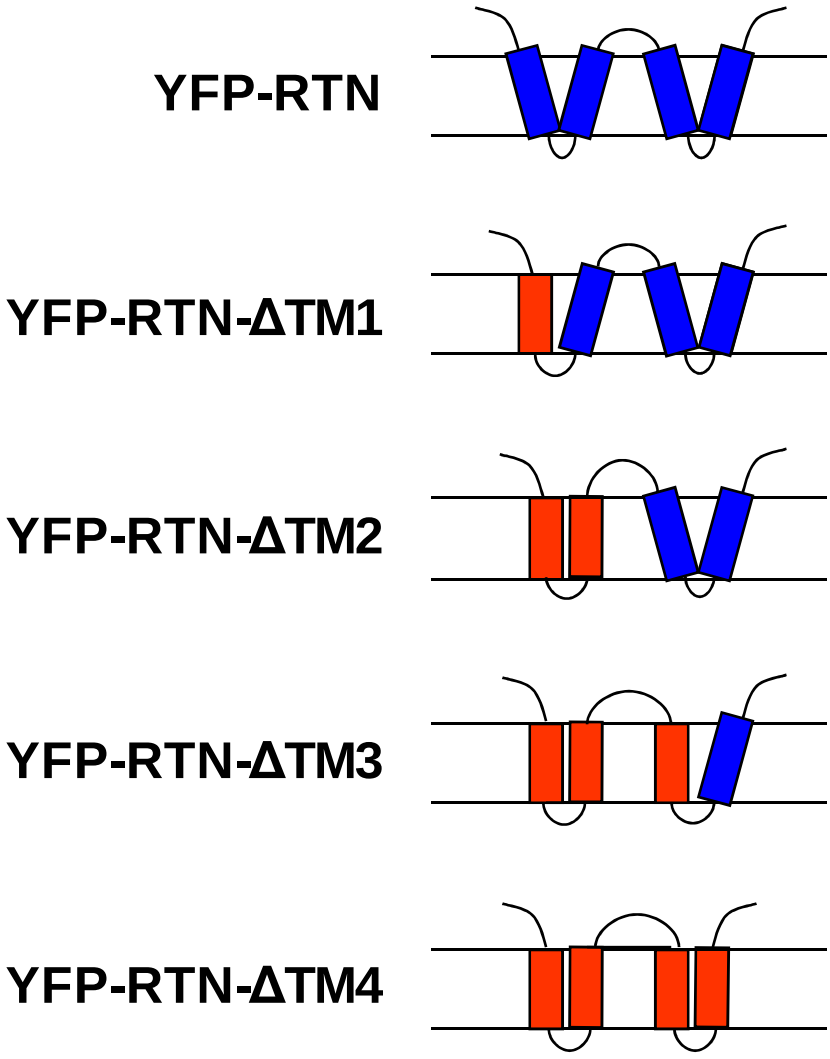

Figure 5.11 Schematic of orientation and insertion of TM domains in the ER membrane. The TM domains of the ΔTM mutants are predicted to insert in a more relaxed orientation in the ER membrane when each TM domain has been shortened. Truncation mutations were made in a sequential and cumulative manner.

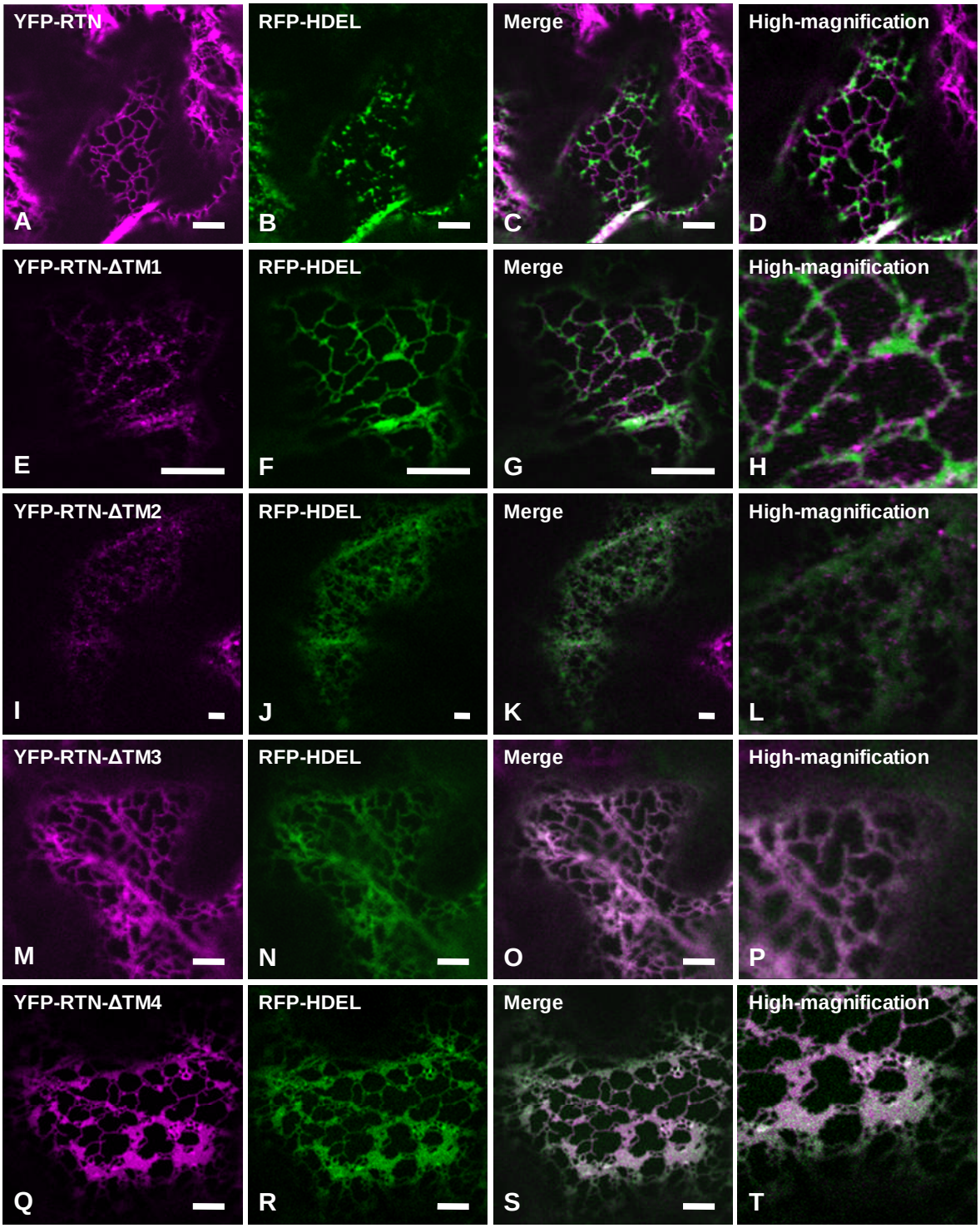

Figure 5.12 Progressive shortening of RTN13 TM domains results in loss of constriction and eventual formation of sheets in the ER. Confocal images of *Agrobacterium*-infiltrated tobacco leaf epidermal cells transiently expressing (A) YFP-RTN13, (E) YFP-RTN13-ΔTM1, (I) YFP-RTN13-ΔTM2, (M) YFP-RTN13-ΔTM3 and (Q) YFP-RTN13-ΔTM4 (magenta) all co-expressed with RFP-HDEL (green). (C), (G), (K), (O) and (S) are merged images of their respective YFP and RFP channels and (D), (H), (L), (P) and (T) are high-magnification sections of the respective merged images. Scale bars = 10 µm.

phenotype seen with RFP-HDEL, and YFP-RTN13-ΔTM1 itself now formed a punctate pattern loosely following the structure of the ER (Figure 5.12 E-H). When YFP-RTN13-ΔTM2 was co-expressed with RFP-HDEL, both proteins had a punctate pattern, but an ER network could still be visualised (Figure 5.12 I-L). In this mutant, two of the transmembrane domains have been shortened and two are still full-length which may therefore be the most disruptive of all the ΔTM mutants in terms of membrane insertion because two of the transmembrane domains would be 'inducing curvature' and two would be in a 'relaxed' state. When YFP-RTN13-ΔTM3 was co-expressed with RFP-HDEL, both proteins co-localised and highlighted a normal ER pattern (Figure 5.12 M-P). In some instances, small regions of sheets began to appear containing both RTN13 and RFP-HDEL. By co-expressing a RTN13 mutant with RFP-HDEL where all four TM domains had been shortened, termed YFP-RTN13-ΔTM4, an extensive production of sheets was seen containing both RTN13 and RFP-HDEL (Figure 5.12 Q-T). Where RTN13 was previously thought to impose curvature on ER tubules and was only found on curved membranes, over-expression of this 'shortened' mutant now caused sheets to form, akin to what was observed upon over-expression of the membrane protein GFP-calnexin (Runions *et al*., 2006; Figure 3.6.1). Moreover, RTN13 now inhabits the sheets.

5.8.2 Trans-membrane topology prediction and western-blot analysis of RTN13-ΔTM mutants

5.8.2.1 Topology prediction

The altered phenotypes seen when expressing RTN-ΔTM2-3 may be due to the defective insertion of the transmembrane domains into the ER membrane and their subsequent recognition and turn-over as substrates for degradation. Topology prediction of these mutants suggests that any shortening of at least two of the transmembrane domains reduces the number of overall transmembrane domains from four to two, with only RTN13-ΔTM1 predicted to retain the four original transmembrane domains. However in ΔTM1, the N-terminus of the protein (encoding YFP) now faces the lumen of the ER, which may explain its punctate pattern – whereby RTN13 over-expression may be constricting the movement of its

own N-terminus (Figure 5.13). This may give an indication as to why the phenotypes seen with ΔTM1-3 are unlike that of wild type RTN13 and ΔTM4.

5.8.2.2 Western blot

Interesting phenotypes were observed when YFP-tagged forms of the ΔTM mutants were examined by confocal microscopy. To investigate the expression of the ΔTM mutants, infiltrated tobacco leaves were subjected to western blot analysis (Figure 5.14). SDS-PAGE resolution of total extracts of RTN13-ΔTM2 and ΔTM3 revealed that protein levels were reduced in comparison the full-length RTN13, ΔTM1 and ΔTM4. Microsomes were fractionated (with starting material four times greater than that of the 'total' extracts) in order to assess whether the – albeit small amount of protein – had in fact inserted into the membrane. Accordingly, all mutants, including ΔTM2 and ΔTM3, were present in the microsomal fraction. However, it was undetermined as to whether these reduced protein levels reflected a reduction in protein expression, or the degradation of fully synthesised protein.

5.9 Factors influencing the localisation of RTN13

RTN13 remains localised to the ER upon the removal of the ER-retrieval motif (KKSE) and shortening of the transmembrane domains. Not present in all reticulon isoforms, the ER retrieval motif may represent an evolutionary relic - now redundant, suggesting that other mechanisms now retain reticulons in the ER. However, when combining the mutants ΔTM4 and ΔKKSE, RTN13 redistributed to punctate structures and only faintly highlighted the ER (Figure 5.15 A-C). The double mutant YFP-RTN13-ΔTM4-ΔKKSE co-localises with the Golgi marker ST-RFP indicating that the length of the transmembrane domains primarily controls ER localisation and the ER-retrieval motif acts as a 'fail-safe' mechanism to ensure ER retention. Further structures containing YFP-RTN13-ΔTM4-ΔKKSE were observed which could potentially represent organelles further along the secretory pathway such as the trans-Golgi network, although co-expression with the relevant reporter proteins has not yet been tested.

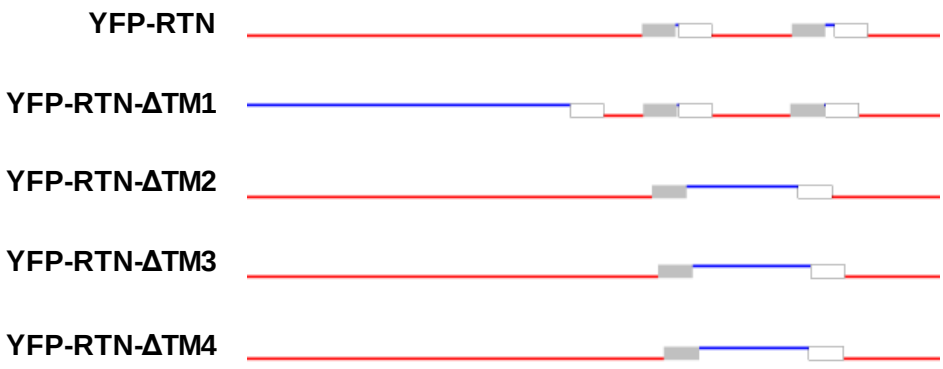

Figure 5.13 TOPCONS topology predictions of RTN13 ΔTM mutants. YFP-tagged variants of RTN13 ΔTM mutants indicating orientation (red represents cytosolic, blue represents luminal) and number of TM domains.

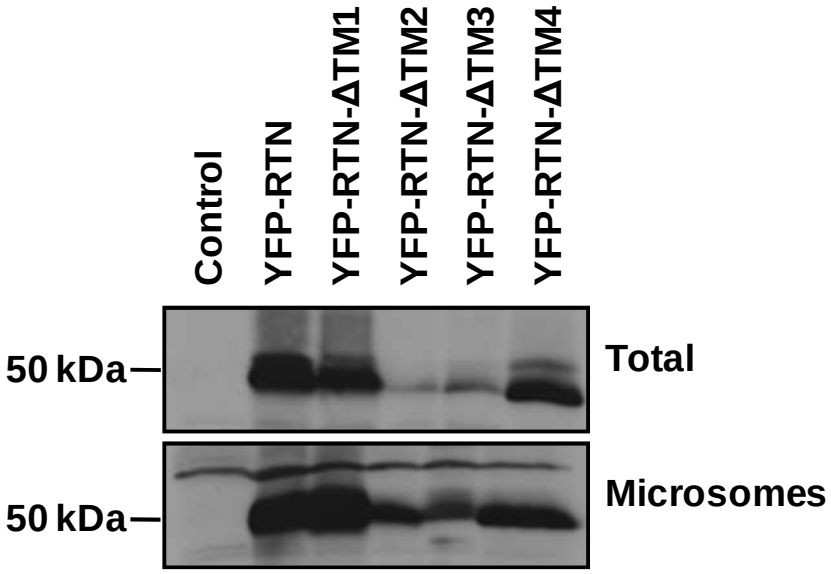

Figure 5.14 Western blot analysis of RTN13 ΔTM mutants. Western blot of agro-infiltrated tobacco leaf sectors using anti-GFP antibody following resolution of YFP-tagged RTN13 ΔTM mutants by SDS-PAGE. Protein bands detected at approximately 50 kDa. Un-infiltrated tobacco leaves were used as controls. Total and microsomal fractions were prepared for each sample.

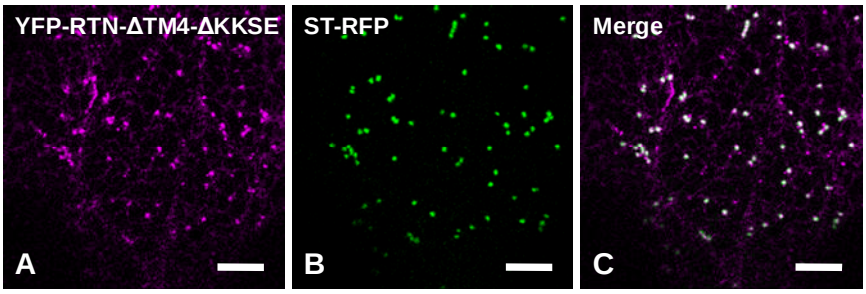

Figure 5.15 Determining the minimal requirements for ER localisation of RTN13. Confocal images of *Agrobacterium*-infiltrated tobacco leaf epidermal cells transiently expressing (A) YFP-RTN-ΔTM4-ΔKKSE (magenta), (B) ST-RFP (green) and (C) the merged image of (A) and (B). Scale bar = 10 µm.

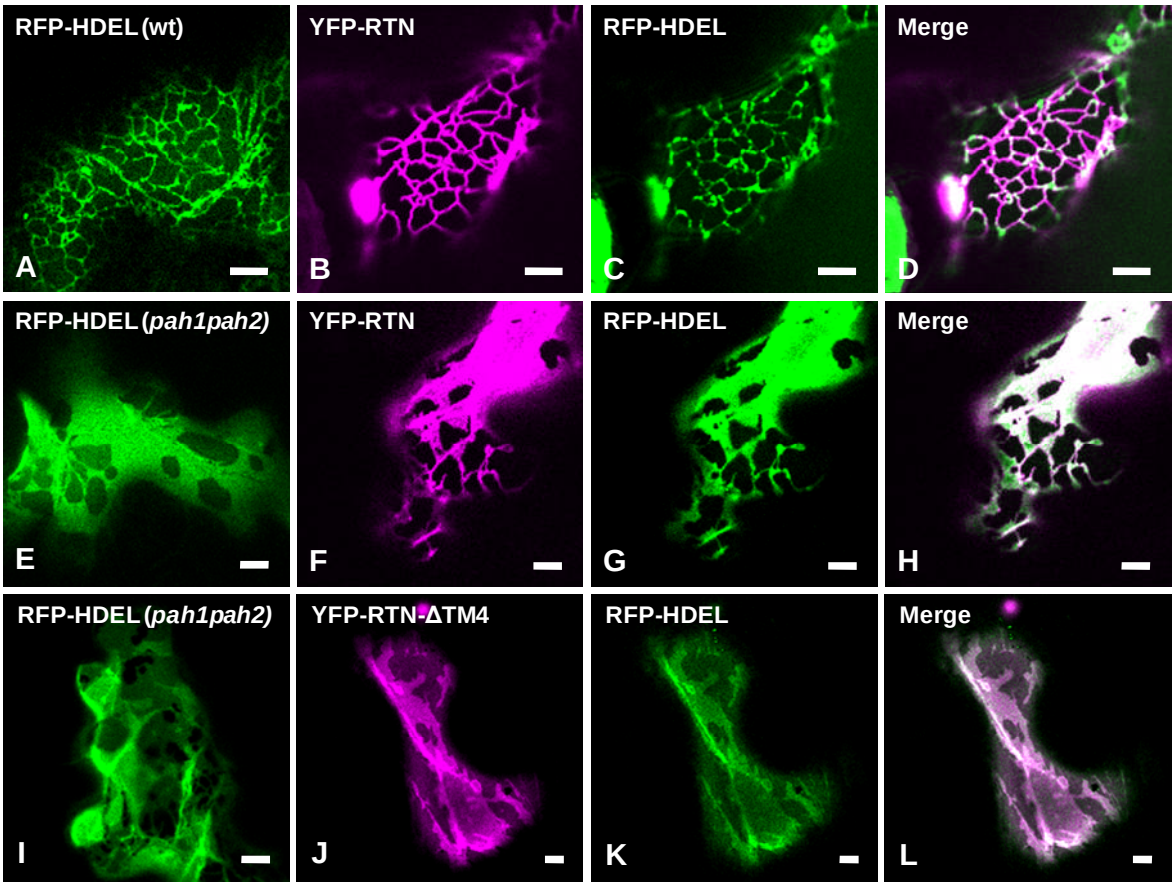

Figure 5.16 Biolistic transformation of *pah1pah2* double mutant in *Arabidopsis*. Confocal images of biolistically transformed wild-type and *pah1pah2* mutant *Arabidopsis* expressing (A), (E) and (I) RFP-HDEL (green) and co-expressing (B) and (F) YFP-RTN, (J) YFP-RTN-ΔTM4 (magenta) with (C), (G) and (K) RFP-HDEL. Merged images of respective YFP and RFP channels are shown in (D), (H) and (L). *Arabidopsis* backgrounds indicated in the first column of images. Scale bar = 10 µm.

5.10 RTN13 induces curvature of flattened membranous sheets to form tubules

5.10.1 *pah1pah2* mutant

In the double mutant *pah1pah2* in *Arabidopsis,* a defect in lipid metabolism causes the accumulation of lipids in the ER resulting in the formation of massive sheets, leaving very few tubules (Figure 5.16 E, I). By transforming *Arabidopsis* leaf cells using biolistic gene delivery with RTN13 and an ER marker, the ability of RTN13 to form tubules could be tested. DNA constructs of YFP-RTN13 and RFP-HDEL were delivered biolistically into both wild-type and mutant backgrounds and visualised after 2 days using confocal microscopy. In wild-type cells, RTN13 could be seen to form constrictions within the lumen of the ER, as highlighted by RFP-HDEL, consistent with the phenotype seen in tobacco (Figure 5.16 A-D). However, in the mutant background, the expression of RTN13 disrupted the extensive sheets in the ER, forming an intermediate phenotype between sheets and tubules (Figure 5.16 F-H). YFP-RTN13 was found within the ER sheets, but to a lesser extent than RFP-HDEL, and was more prominent in the tubules, similar to the induction of sheets with BFA (Figure 3.8). This indicates that RTN13 can induce the formation of tubules in the ER *in vivo* and the level of tubulation may be dependent on its level of expression.

5.10.2 Shortening of RTN13 TM domains reduces tubule formation

Having shown that full-length RTN13 can induce tubulation, the next logical step was to test whether the length of the transmembrane domains is responsible for this ability. Therefore, the ΔTM mutant YFP-RTN13-ΔTM4 was introduced into the *pah1pah2* mutant background in order to determine whether it had the ability to form tubules. In tobacco, the over-expression of YFP-RTN13-ΔTM4 caused sheets to form in the ER. In *Arabidopsis,* when co-expressed with RFP-HDEL, YFP-RTN13-ΔTM4 localised to the ER sheets and the formation of tubules was not apparent (Figure 5.16 J-L). This indicates that the unusual length of the transmembrane domains is responsible for the curvature-forming ability of RTN13 *in vivo*.

5.11 Discussion

The main focus of this chapter was to dissect the function of the individual domains of RTN13. The following paragraphs summarise the resulting observations.

A deletion mutant of the C-terminal ER-retrieval motif of RTN13 remains localised in the ER and does not affect the capacity of RTN13 to induce ER tubule constrictions. Truncation of the N- and C-termini and the loop region results in loss of expression and reduced protein stability, although ER localisation is still evident. Retention of four residues upstream of the first transmembrane domain improves stability and is thought to act as a stop-transfer signal, enabling the correct insertion into the ER membrane during protein synthesis.

Sequential shortening of the predicted transmembrane domains results in RTN13 being no longer capable to produce ER constrictions. Accordingly, expression of RTN13 in the *Arabidopsis* mutant *pah1pah2*, where the ER forms mostly cisternal sheets, results in the induction of tubules within the ER sheets. The shortened transmembrane RTN13 mutants are however unable to form tubules in the *pah1pah2* mutant.

A double mutant combining shortened transmembrane domains and lacking an ER-retrieval motif results in exit of RTN13 from the ER and its mistargeting to the Golgi.

The analysis of the individual domains of RTN13 shown in this chapter reveals that, although the N- and C-termini and the loop region are required for overall protein stability and insertion into the membrane, they are not necessary for ER localisation. In contrast, the length of the transmembrane domains, as part of the RHD, is an important factor in ER localisation, making the ER-retrieval motif redundant. The transmembrane domains are also important in conveying membrane curvature to the ER tubules, and when shortened, they no longer possess the ability form or maintain tubules.

YFP-tagged mutants lacking either the ER-retrieval motif, N- or C-terminus, or a potential stop-transfer motif of RTN13, were transiently expressed in tobacco leaves with the ER marker RFP-HDEL, or the Golgi marker ST-RFP in order to determine the localisation of mutants and whether they constrict the ER lumen. This revealed that the ER-retrieval motif (KKSE) was unnecessary for ER localisation and when absent, did not affect the ability of RTN13 to form constrictions in ER tubules. However, when truncating either the N- or C-terminus, expression levels were reduced compared to full length RTN13 and, although ER localisation was still apparent, these mutants no longer constricted the ER lumen. In comparison, expression was improved when four residues upstream of the first transmembrane domain were retained (RRKK), which may act as a stop-transfer motif and help RTN13 insert correctly into the membrane (Cocquerel *et al*., 2000). Disruption of the first hydrophobic domain of RTN3 in mammals results in misfolding and incorrect insertion in to the ER membrane (He *et al*., 2007), which is likely to disrupt such a motif. The reduced expression levels of these mutants were confirmed by western blot and pulse-chase analysis. A further mutant was tested, whereby the loop region of RTN13 (33 residues) was replaced by two myc-tags (20 residues) in order to determine the role of the loop. Again, this mutant displayed reduced expression levels compared to full length RTN13, although it still co-localised with RFP-HDEL. None of the mutants tested were ever observed to label the Golgi.

Therefore, it seems neither the ER-retrieval motif, N- and C-termini nor the loop region are responsible for ER localisation of RTN13. Presumably, the reduced expression levels reflect an unstable protein conformation, and the mutants are promptly degraded. Therefore, other than the loop region, it would appear that ER localisation is achieved by the retention of the RHD, which is consistent with the literature (van de Velde *et al*., 1994). It has been shown in tobacco cells that mutants lacking either the first or second hydrophobic regions of the RHD of the *Arabidopsis* reticulons 1-4 are capable of localising to the ER, although constrictions in the ER tubules are no longer formed (Sparkes *et al*., 2010).

To investigate the role of the transmembrane domains, which in themselves are unusually long for ER resident proteins (Moreau *et al*., 2007), four RTN13 mutants were constructed which sequentially and cumulatively shortened the length of the

four predicted transmembrane domains from 22-24 residues to 17. Tagged with YFP, these mutants were expressed in tobacco leaves with the ER marker RFP-HDEL. The shortening of the first transmembrane domain (ΔTM1) results in a punctate distribution of RTN13, and a non-constricted phenotype in the ER lumen - visualised with RFP-HDEL. Expression of ΔTM2 and ΔTM3 results in reduced expression (determined by western blot analysis), and although ΔTM2 expression remained punctate, ΔTM3 now highlighted a normal reticular ER pattern, comparable with that of RFP-HDEL. Neither ΔTM2 nor ΔTM3 are able to constrict the ER lumen. Interestingly, ΔTM4 was expressed to levels comparable to full length RTN13, but rather than constricting the ER lumen, it formed sheets within the ER containing both RTN13 and RFP-HDEL. It was previously shown that RTN13 preferentially inserts into curved membranes and is excluded from sheets (Figure 3.8). This was thought to be due to the length of the transmembrane domains, and is consistent with the finding that a mutant of RTN13 with shortened transmembrane domains, similar to that of a normal ER-resident protein, can insert into and is the likely cause of the formation of sheets within the ER (akin to the over-expression of calnexin (Runions *et al*., 2006; Figure 3.6.1)).

Although these data indicate a functional role of the transmembrane domain length of RTN13, the mechanism behind ER localisation remains elusive. In separate mutations, neither the removal of the ER-retrieval motif, nor the shortening of the transmembrane domains resulted in mislocalisation of RTN13 from the ER. However, when a double mutant (ΔTM4-ΔKKSE) was expressed in tobacco leaves, only a small proportion of RTN13 was observed in the ER. In contrast, the majority of YFP-RTN13-ΔTM4-ΔKKSE highlighted punctate structures which were confirmed as Golgi using the marker ST-RFP. The fluorescence observed in the ER is likely to represent newly synthesised, trafficking RTN13, which is no longer being retained. Therefore, RTN13 possesses a dual ER-retention mechanism, whereby transmembrane length and an ER-retrieval motif contribute towards ER localisation, although the presence of both is unnecessary.

A third ER-retrieval signal is present in the first transmembrane domain of RTN13. Sato *et al*., (1999) suggested that some ER resident membrane proteins such as Sec12p are retrieved from the Golgi by means of detection by the Golgi resident

Rer1 protein family. These proteins recognise and retrieve mislocalised ER membrane proteins by the detection of a motif found in the transmembrane domains; a leucine residue separated from tyrosine by a stretch of 11 amino acids. Such a motif is present in the first predicted transmembrane domain of RTN13, although it was not tested whether this motif contributes to ER localisation. Further studies have refined this motif in yeast, which have yet to be tested experimentally in plants (Sato *et al*., 2003).

Having attributed ER localisation of RTN13 to the transmembrane domains, the ability of RTN13 to induce curvature on ER tubules was investigated, utilising a double mutant transgenic *Arabidopsis* line, denoted *pah1pah2*. Owing to a defect in lipid metabolism, the ER is devoid of tubules and exists almost entirely of cisternal sheets. Using biolistic gene delivery, wild type and mutant *Arabidopsis* plants were transfected with YFP-tagged RTN13 and RFP-HDEL. In wild type cells, RTN13 was able to constrict ER tubules, comparable to that of tobacco. In the *pah1pah2* mutant background, the expression of RTN13 induced the formation of tubules within the sheets of the ER and, although not to the extent of wild type ER tubules, there was marked disruption of the ER sheets forming an intermediate sheet-tubule phenotype.

This tubule-inducing phenotype was further used to investigate the ability of the RTN13 shortened transmembrane domain mutants described previously. When the RTN13 mutant with all four predicted transmembrane domains shortened (ΔTM4) was transfected into the *pah1pah2* mutant plant, its expression did not induce tubule formation in the ER sheets and instead was found present within the sheets, similar to the phenotype seen in tobacco (Figure 5.12).

These results indicate that the unusual conformation of transmembrane domains within the RHD of RTN13 contributes to the formation of ER tubules and, upon over-expression, can induce tubules in cisternal sheets. However, it is unlikely that reticulons alone are responsible for the morphogenesis of tubular structures within ER membranes. In order to disrupt the morphology of the ER in mammalian and yeast cells, down-regulation of genes other than reticulon is required, including the reticulon-related proteins DP1 and Yop1p (Voeltz *et al*., 2006) and the newly identified atlastin and Sey1p proteins. Atlastins and Sey1p have been identified as

components necessary to generate branched ER membrane structures and their GTPase activity catalyses homotypic fusion between ER tubules (Hu *et al*., 2009; Orso *et al*., 2009).

Homologues of these components have been identified in *Arabidopsis*. HVA22 is thought to be a homologue of the reticulon-like DP1/Yop1p proteins (Nziengui Schoefs, 2008) and RHD3 (root hair defective) is thought to be a homologue of atlastin/Sey1p (Hu *et al*., 2009). However, information on these *Arabidopsis* counterparts is limited, although a knockout of one of the three RHD3 isoforms produces ER tubules with an altered morphology (Zheng *et al*., 2004).

These results prove the hypothesis that the transmembrane domains of RTN13 are important for inducing membrane curvature and stabilising the protein within the membrane, although the precise structure of RTN13 remains unknown. The results presented in the preceding chapters have been based on the over-expression of RTN13 in tobacco leaves using agro-infiltration. Although these experiments have addressed the localisation, topology and curvature-inducing elements of RTN13, the function of RTN13 in its native organism, *Arabidopsis thaliana*, are still to be explored. This is the subject of the next and final chapter of this thesis.

Chapter 6: Functional characterisation of RTN13 in *Arabidopsis*

6.1 Introduction

6.1.1 Functions of reticulons

Reticulons have been found to interact with several proteins involved in a range of cellular functions (Yang & Strittmatter, 2007). Some of these functions also apply, in most cases, to reticulons in plant cells. However, many developments in reticulon research, in particular mammalian studies, cannot always be applied to plant biology. The most notable case is the expression of Rtn4a which inhibits the regeneration of axons in mammals (GrandPre *et al*., 2000). Reticulons have been implicated in vesicle-mediated transport between the ER and Golgi (Steiner *et al*., 2004; Wakana *et al*., 2005), re-assembly of the nuclear envelope following cell division (Kiseleva *et al*., 2007) and apoptosis (Tagami *et al*., 2000). Reticulon research has been carried out in mammals, yeast, *Caenorhabditis elegans*, *Xenopus laevis* and zebrafish and can be divided into two streams, one of which mainly focuses on the medical relevance of reticulon proteins, and the other, which broaches the subject of how reticulons curve membranes.

In contrast, research into plant reticulons is in its early stages. Although the presence of reticulon genes in plants had been acknowledged (Oertle *et al*., 2003b), only in recent years has interest in their function arisen.

6.1.2 Reticulons in *Arabidopsis*

There are 21 isoforms of reticulon in *Arabidopsis*, five of which (RTN17-21) are thought to be enzyme-linked at their N-termini (see reviews Nziengui & Schoefs, 2008; Sparkes *et al*., 2009a). These genes display ubiquitous and tissue-specific expression profiles, where at least one isoform is enriched in each different tissue of the plant (see Appendix Figure A8). Using TOPCONS, the predicted structure and topology of all *Arabidopsis* RTNs is a ‘w’ conformation with both the N- and C-termini facing the cytosol (see Appendix Figure A8). The first 15 reticulons were designated as reticulon-like, non-chordate taxa - class B (RTNLB) by Oertle *et al*., (2003b), and new members of the family have extended their number to 21, based on the presence of RHD sequences (Nziengui *et* al., 2007). These proteins share their

RHDs with their mammalian and yeast counterparts, of which there are only four and two reticulon genes, respectively. Many other plant species contain reticulon genes. For example, rice (*Oryza sativa*) has 17 reticulon genes and grape vine (*Vitis vinifera*) has 6 (Nziengui & Schoefs, 2008). This increase in the number of genes in higher plants may represent redundancy within the genome, or it may represent complex regulatory expression of tissue-specific reticulon proteins.

6.1.3 Reticulon expression in seeds

The focus of this study is the seed-specific expression of reticulons in *Arabidopsis*. Although RTN13 is the only reticulon to be expressed exclusively in seeds, it is not the only reticulon protein present in the seed. RTN1 is ubiquitously expressed in the plant, including high levels of expression (relative to overall expression of this particular isoform) in the maturing seed (eFP Browser, Winter *et al*., 2007). RTN2 is another reticulon which is expressed ubiquitously at low levels and expressed most highly in the dry seed. RTN1 and RTN2 have been shown to interact with each other by yeast two-hybrid analysis (Hwang & Gelvin, 2004). Therefore, these seed-resident reticulons may interact with each other and even form hetero-oligomeric complexes, as mammalian and yeast reticulons have been shown to homo-oligomerise (Shibata *et al*., 2008).

6.2 Aims and experimental approach

Previous work in this study has been based on 35S-driven over-expression of RTN13 cDNA in tobacco leaves. In order to establish how RTN13 behaves in its native organism, *Arabidopsis*, and whether its phenotype is comparable with that of tobacco, the previously described 35S:YFP-RTN13 was stably transformed into wild type *Arabidopsis*, and also a transgenic *Arabidopsis* line expressing the ER marker GFP-HDEL. Using confocal microscopy, YFP-RTN13 was analysed using GFP-HDEL, auto-fluorescence and organellar dyes in order to compare expression of RTN13 with the ER, protein storage vacuoles and lipid bodies, respectively. Expression of RTN13 was investigated in tissues including embryos, roots and leaves.

A second transgenic *Arabidopsis* line was created expressing a YFP-tagged genomic sequence of RTN13 expressed under its native promoter. The spatial and temporal expression of RTN13 was then confirmed in its native tissue - the late maturing embryo.

In order to determine any function of RTN13, a T-DNA insertional knockout line was acquired (termed *rtn13*) and diminished RTN13 transcript levels were confirmed using RT-PCR. It was then investigated whether two of the major processes in the maturing seed - protein deposition in the storage vacuoles and the formation of lipid bodies, were affected in any way in the *rtn13* knockout.

6.3 Cloning and construct design

When over-expressing RTN13 in *Arabidopsis*, 35S:YFP-RTN13 in the plant binary vector pVKH18-En6 shown in previous chapters was used (Figure 3.1). The native promoter and genomic sequence (including introns) of RTN13 were amplified whole from genomic DNA and cloned into the plant binary vector pGreenII-0029 in frame with YFP at the C-terminus (Figure 6.3). Positive plants were selected by kanamycin screening and fluorescence either in the dry seed (35S:YFP-RTN13) or in ageing siliques of the plant (native-RTN13-YFP).

6.4 Over-expression and localisation of RTN13 in *Arabidopsis*

Various tissues of transgenic *Arabidopsis* expressing YFP-RTN13 were examined. Expression was examined in embryonic, leaf and roots cells, which all displayed a reticular ER distribution (Figure 6.1). Utilising the auto-fluorescence of the protein storage vacuoles, it was determined whether the over-expression of RTN13 had any effect on the deposition within, or morphology of the vacuoles (Figure 6.1 A-C). RTN13 was found to surround the vacuoles, and vacuolar morphology and distribution were comparable with that of wild type cells (see Figure 6.7-6.8). In a similar experiment, expression of YFP-RTN13 was compared with that of the lipid bodies, as highlighted by the lipophilic dye LD540 (Figure 6.1 G-I, Spandl *et al*., 2009). This dye is compatible with the emission spectra of YFP, unlike Nile Red (see section 6.6.3.3).

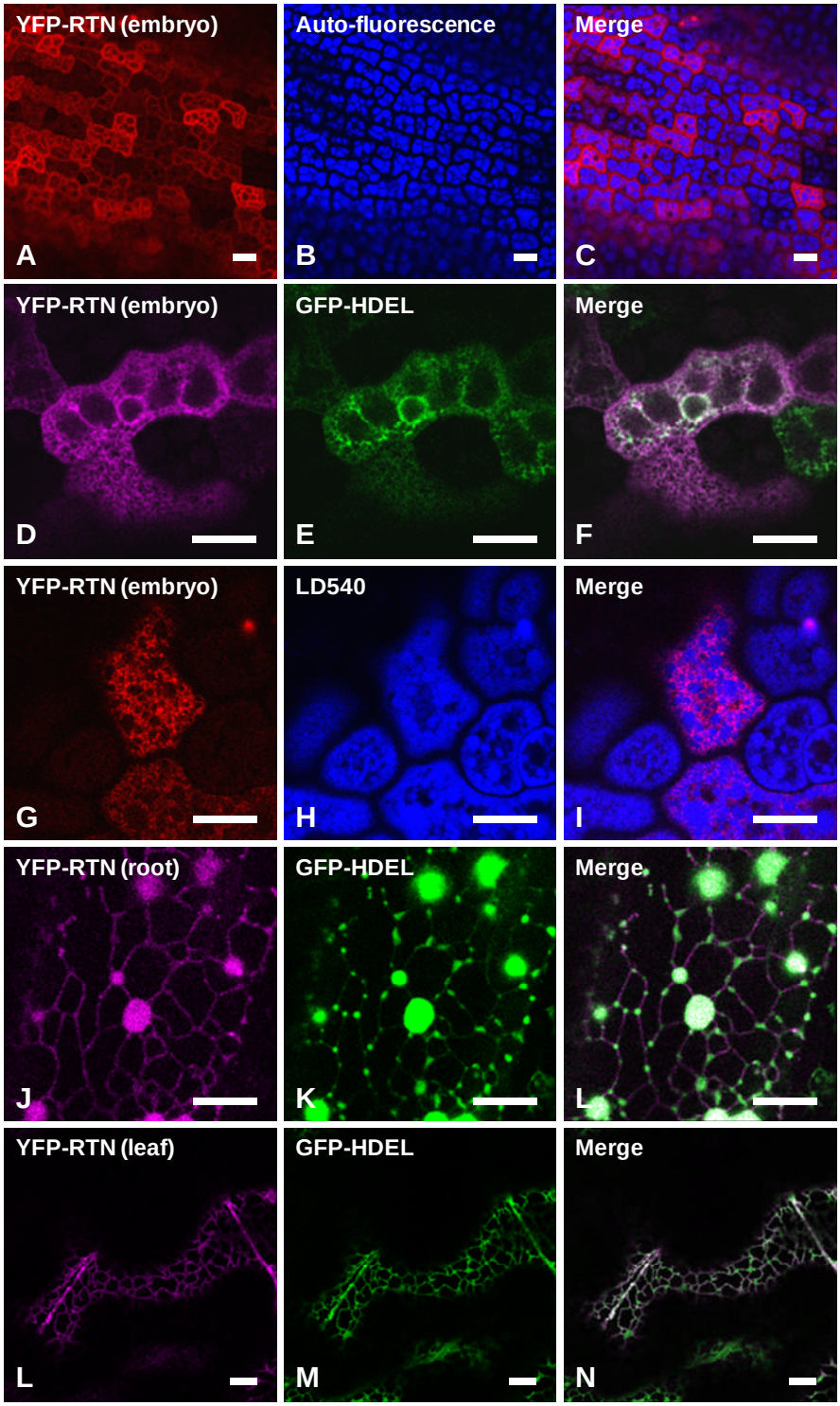

Figure 6.1 Localisation of YFP-RTN13 under a 35S promoter in *Arabidopsis*. Stably transformed *Arabidopsis* embryos expressing (A) YFP-RTN13 (red), (B) auto-fluorescence of the storage vacuoles (blue) and (C) merged images of (A) and (B). Embryonic expression of (D) YFP-RTN13 (magenta), (E) GFP-HDEL (green) and (F) merged images of (D) and (E). Embryonic expression of (G) YFP-RTN13 (red), (H) the lipid dye LD540 (blue) and (I) merged images of (G) and (H). Root cells expressing (J) YFP-RTN13 (magenta), (K) GFP-HDEL and (L) merged images of (J) and (K). Leaf cells expressing (L) YFP-RTN13, (M) GFP-HDEL and (N) merged images of (L) and (M). Scale bars = 10 µm.

Similarly, YFP-RTN13 surrounded the lipid bodies, with no difference seen to that of a wild type cell (see Figure 6.8). YFP-RTN13 plants were crossed with a stable *Arabidopsis* line expressing the ER marker GFP-HDEL. The expression of the 35S driven RTN13 in the embryo appeared patchy, with a further complication that GFP-HDEL did not seem to express in seeds (data not shown), therefore, 24 h imbibed seeds were used for co-localisation of YFP-RTN13 with GFP-HDEL, where the expression of GFP-HDEL defined the ER as expected (Figure 6.1 D-F). A similar phenotype to that seen in tobacco, with constrictions present in the lumen of the ER, was observed between GFP-HDEL and YFP-RTN13 in root (Figure 6.1 J-L) and epidermal leaf cells (Figure 6.1 L-N). This confirms that constriction of the ER lumen is not a tobacco-specific phenomenon and that the RTN13 over-expression phenotype is reproducible in its native species.

6.5 Analysis of RTN13 at native expression levels

Work presented so far in this study has been based on the over-expression of RTN13. However, in *Arabidopsis*, RTN13 is expressed in the later stages of seed maturation, and is not expressed in any other tissue in the plant (Figure 6.2, Winter *et al*., 2007). In order to validate the expression pattern of RTN13, its genomic sequence under the expression of its native promoter was cloned into a plant binary vector in frame with YFP at the C-terminus (Figure 6.3). This construct was then transformed into *Agrobacterium* and used to generate transgenic *Arabidopsis*. Following selection of a heterozygous line, siliques in the later stages of development were selected and the embryos of the developing seeds within were dissected. Expression of RTN13 is initiated at the early curled-cotyledon stage of embryonic development (Figure 6.4 A-B, for embryonic development stages see Appendix Figure A9), and expression increases through the late curled/early green-cotyledon stage (Figure 6.4 C-D) and peaks at the late green-cotyledon stage (Figure 6.4 E-F). At all developmental stages, YFP-tagged RTN13 was observed in a reticular pattern similar to that seen with the 35S-driven construct (Figure 6.1 A) - surrounding the nuclear envelope (data not shown). However, due to the resolution of the embryonic images, it remains unclear as to whether RTN13 is present in the nuclear envelope, or merely in tubular ER in close proximity to the nucleus. Although mRNA transcripts are detected in the

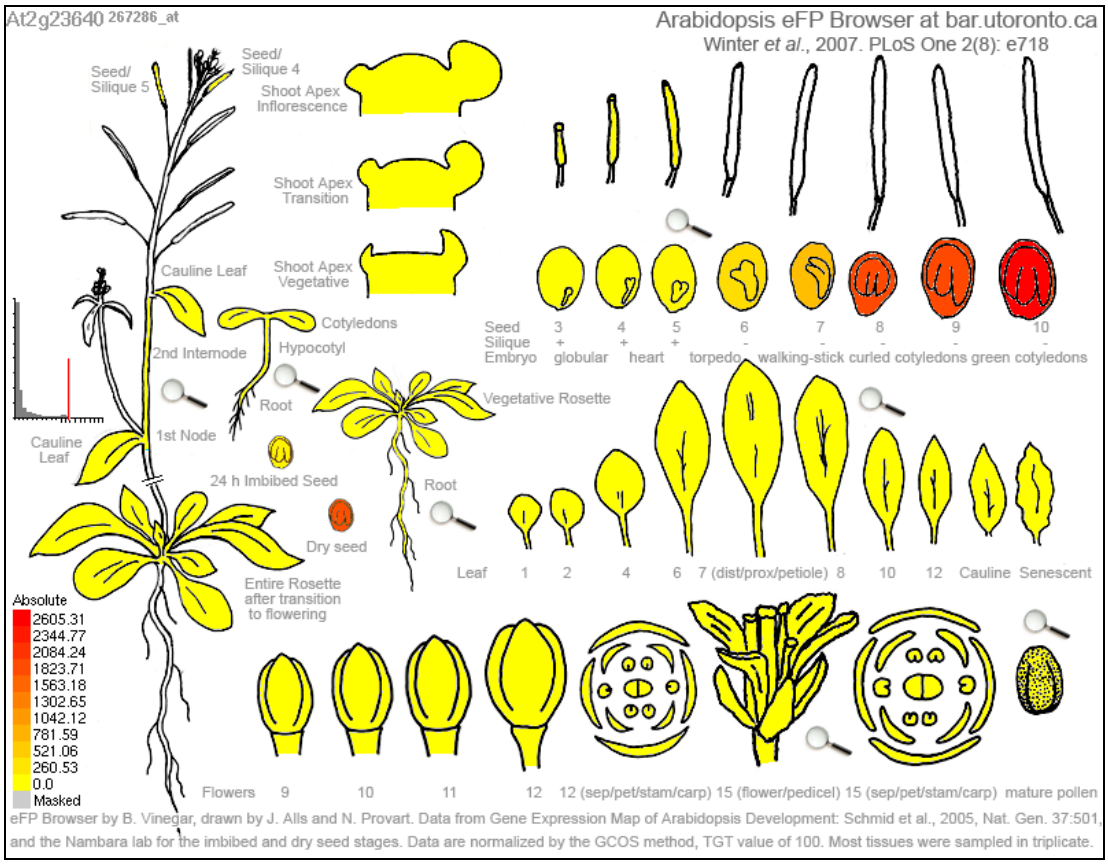

Figure 6.2 Transcriptional tissue-specificity of RTN13. mRNA transcript expression data as presented in eFP browser for *Arabidopsis* gene At2g23640 (RTN13). Increased expression levels are shown in red, whereas no expression is shown in yellow. Expression data are shown in all major anatomical tissues and organs.

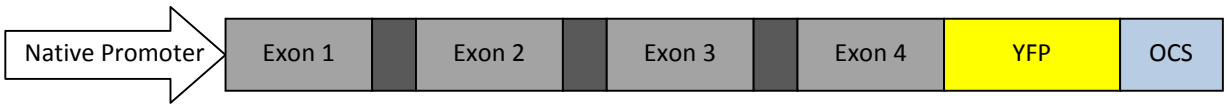

Figure 6.3 Construct design of genomic RTN13-YFP with its native promoter. The native promoter and full genomic sequence of RTN13 were amplified directly from *Arabidopsis* genomic DNA using PCR. The sequence was then cloned in frame with YFP and an OCS terminator in the plant binary vector pGreen-0029.

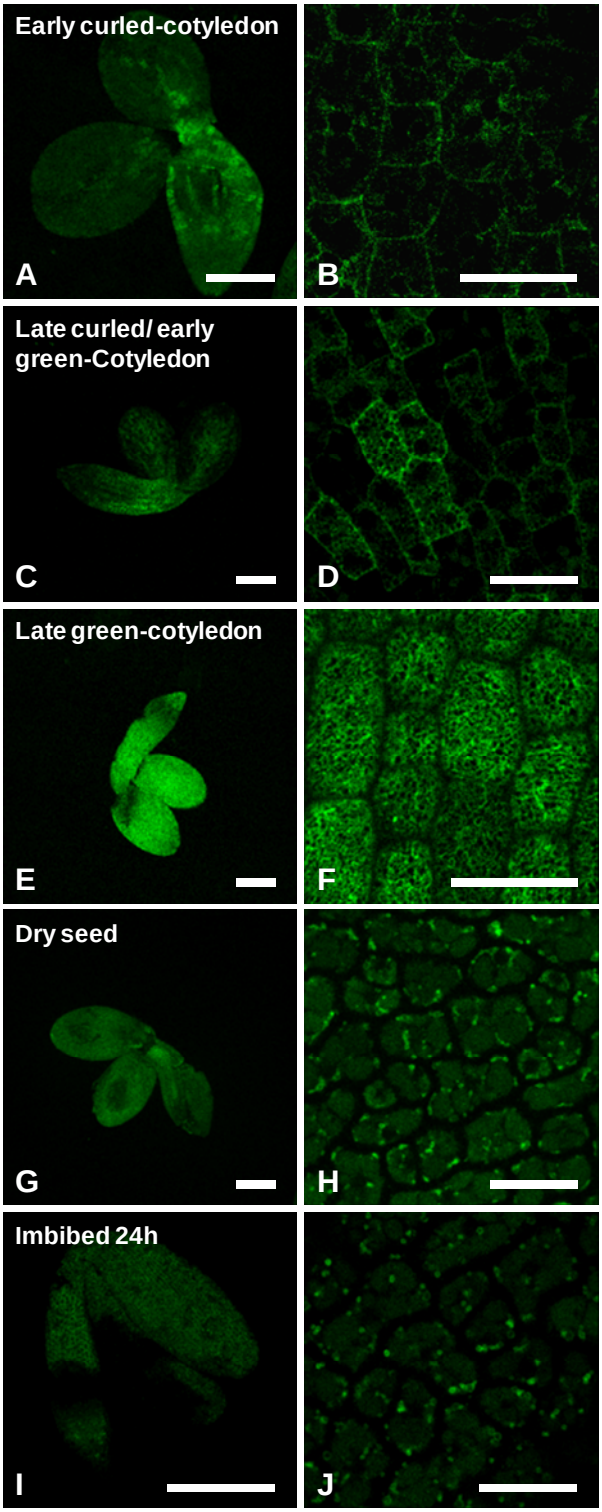

Figure 6.4 Analysis of native-RTN13-YFP expression in the later stages of seed maturation. Expression is initiated in the early curled-cotyledon (A)-(B). Mid-levels of expression observed at late curled/early green-cotyledon stage (C)-(D). Highest expression levels observed at late green-cotyledon stage (E)-(F). Expression ceases in mature embryo (derived from dry seed) (G)-(H). Similarly reduced expression levels in a 24h imbibed seed (I)-(J). Scale bars in left column = 200 µm, right column = 20 µm.

mature embryo from dry seed (Winter *et al*., 2007), fluorescence of native-RTN13-YFP was seen to localise to small punctate structures (Figure 6.4 G-H). Similarly, in the 24 h imbibed embryo, very little fluorescence was detected (Figure 6.4 I-J). These results indicate that RTN13 expression is specific to maturating embryos and localises to the ER.

6.6 Functional analysis of RTN13

6.6.1 RTN13 in the context of seed maturation

The sheer number of reticulons present in *Arabidopsis* may indicate that each tissue has its own reticulon protein which can be individually regulated, in addition to ubiquitously expressed reticulons such at RTN1. Table 6.1 lists the genes which are expressed with the same spatial and temporal pattern as RTN13 using the software 'Expression Angler' (Toufighi *et al*., 2005). Genes of note are HVA22B, Oleosins 1 and 2, and the Tonoplast Intrinsic Protein (TIP) 3;1. These genes are involved in some of the major processes during seed maturation including dehydration of the seed, morphology of the protein storage vacuoles and the formation of lipid bodies.

HVA22B is thought to be a homologue of the mammalian DP1 and yeast Yop1p, (Nziengui & Schoefs, 2008). It shares approximately 30% homology with these proteins, which themselves share 30% homology with the mammalian and yeast reticulons (Voeltz *et al*., 2006).

Oleosins are structural proteins which span the lipid monolayer surrounding lipid bodies – storage compartments containing triacylglycerol (TAG) stores required for seed germination. Containing two transmembrane domains, the N- and C-termini face the cytosol with a hydrophobic loop region containing a proline-knot (Tzen *et al*., 1992) embedded in the TAG core of the lipid bodies (Napier *et al*., 1996). Oleosins 1 and 2, respectively, are the most abundant oleosin proteins expressed in *Arabidopsis*, and knockout lines show unregulated lipid body size (Shimada *et al*., 2008). Oleosins are targeted to lipid bodies via the ER and their specific topology is a necessary requirement for correct localisation (Abell *et al*., 2004).

Table 6.1 Analysis of genes with similar expression pattern to RTN13

Gene	Correlation coefficient	Description	Function
At2g23640	1.000	reticulon family protein (RTNLB13)	Bait gene
At1g70840	0.887	MLP31 (MLP-LIKE PROTEIN 31)	Defence
At3g50980	0.885	XERO1 (DEHYDRIN XERO 1)	Water regulation
At5g62490	0.879	ATHVA22B	Unknown
At5g40420	0.878	OLE2__OLEO2 (OLEOSIN 2)	Lipid body synthesis
At4g10020	0.878	AtHSD5 (hydroxysteroid dehydrogenase)	Oxidoreductase activity
At4g24150	0.871	AtGRF8 (GROWTH-REGULATING FACTOR 8);	Transcription activator
At5g45690	0.867	unknown protein	Unknown
At2g33070	0.862	NSP2 (NITRILE SPECIFIER PROTEIN 2)	Glucosinolate catabolism, nitrile biosynthesis
At3g56350	0.860	superoxide dismutase, putative / manganese superoxide dismutase, putative	Antioxidant
At4g25140	0.859	OLE1__OLEO1 (OLEOSIN 1)	Lipid body synthesis
At2g41260	0.857	ATM17__M17	Embryonic development
At1g72100	0.857	late embryogenesis abundant domain-containing protein / LEA domain-containing protein	Embryonic development
At1g73190	0.857	ALPHA-TIP__TIP3;1; water channel	Tonoplast intrinsic protein
At1g02700	0.855	unknown protein	Unknown
At3g15670	0.854	late embryogenesis abundant protein, putative / LEA protein, putative	Embryonic development
At3g53040	0.854	late embryogenesis abundant protein, putative / LEA protein, putative	Embryonic development
At1g14950	0.852	major latex protein-related / MLP-related	Defence
At1g48130	0.850	ATPER1; antioxidant/ thioredoxin peroxidase	Antioxidant
At3g58450	0.849	universal stress protein (USP) family protein	Stress response
At2g21490	0.846	LEA (DEHYDRIN LEA)	Embryonic development
At2g23240	0.838	plant EC metallothionein-like family 15 protein	
At5g50600	0.838	AtHSD1 (hydroxysteroid dehydrogenase)	Oxidoreductase activity
At1g77950	0.838	AGL67 (AGAMOUS-LIKE 67)	Transcription factor
At2g28420	0.837	lactoylglutathione lyase family protein / glyoxalase I family protein	Carbohydrate metabolism
At1g05510	0.837	Protein is tyrosine-phosphorylated and its phosphorylation state is modulated in response to ABA in Arabidopsis thaliana seeds	Unknown

The tonoplast intrinsic proteins are one of four classes of plant aquaporins which facilitate the passive transport of water and other small polar molecules across lipid bilayers. TIPs are abundant during seed maturation, and are suggested to have a role in seed desiccation, as well as a role in seed rehydration upon imbibition (Maurel *et al*., 1997).

Limited information regarding the structure of the endoplasmic reticulum in the developing embryo is available. The ER is the organelle responsible for storage protein and lipid biosynthesis, whereby synthesis of these storage compounds is at its highest in the developing seed (Maltman *et al*., 2007). However, it has been postulated that the ER may have up to 16 morphologically distinct subdomains (Staehelin, 1997), and could be involved in many more processes linked to seed development and maturation.

Electron micrographs of developing seeds of broad bean (*Vicia faba*) by Harris, (1979), described an extensive interconnecting network of cisternal and tubular ER found throughout the stage of storage protein deposition. At the beginning of this stage, approximately 60% of the total volume of ER is cisternal, and tubular ER (also described as smooth ER) is thought to act as a transitional form of membrane which converts to cisternal ER at a time of storage protein synthesis. The reverse transition appears to occur during desiccation and maturation of the seed, which is consistent with the late expression of RTN13 in the developing embryo of *Arabidopsis*.

6.6.2 T-DNA knockout

In order to study the function of RTN13, a homozygous T-DNA knockout line was obtained (from the Nottingham *Arabidopsis* Stock Centre, NASC) and its homozygosity, insertion into the RTN13 gene and reduced transcript levels were verified using PCR and RT-PCR. PCR was used to confirm whether the *rtn13* knockout line obtained was a segregating line or truly homozygous, then to confirm the presence of the T-DNA insertion and finally, its orientation (Figure 6.5 A-C). The precise insertion of the T-DNA sequence within the genomic sequence of RTN13 was then determined by sequencing genomic DNA using an oligonucleotide

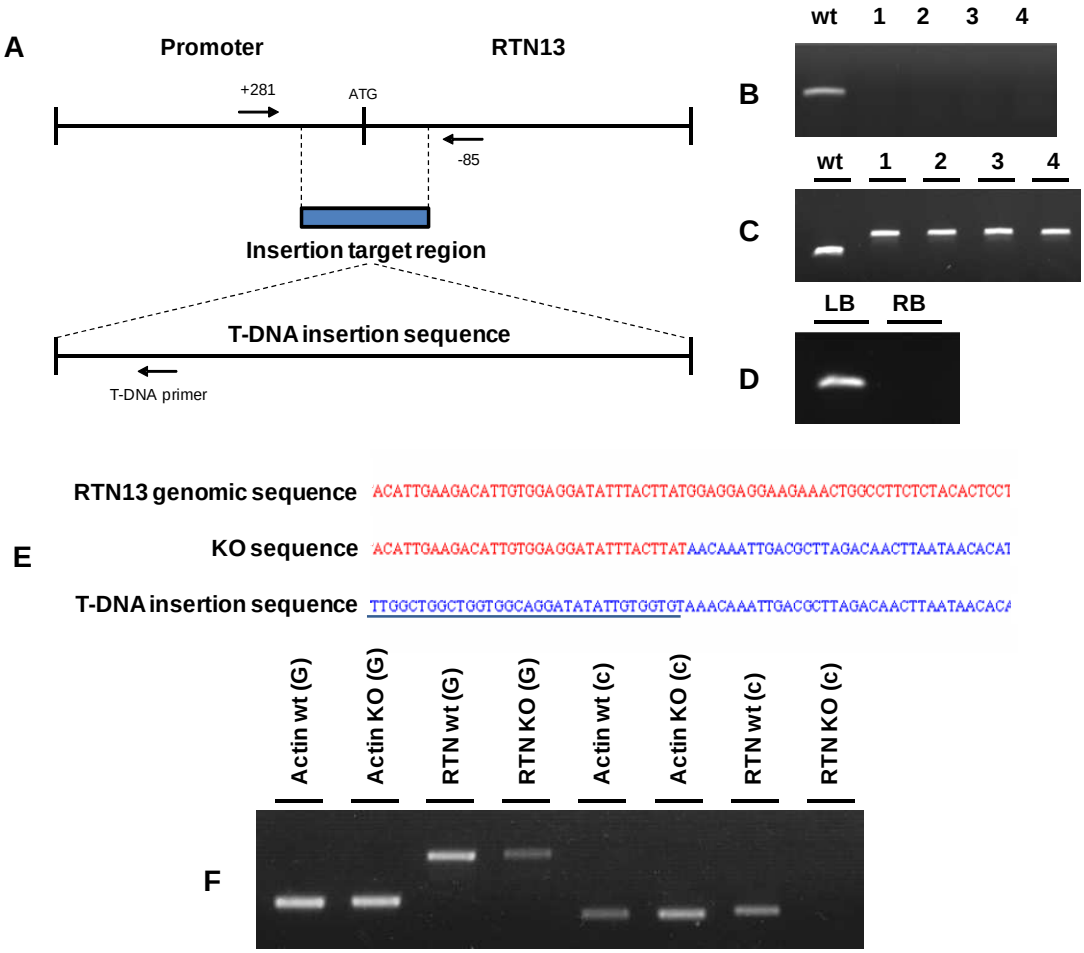

Figure 6.5 Confirmation of T-DNA knockout of RTN13 transcript levels. (A) Schematic of RTN13, T-DNA and primers used. (B) Initially using genomic DNA extracts from potential knockout plants, primers outside the T-DNA insertion region were used to establish the presence of an insertion. (C) The same primers again were combined with a primer within the T-DNA to ensure presence of T-DNA insertion and (D) orientation of insertion confirmed by using T-DNA primer and alternate flanking RTN13 primers. (E) T-DNA specific primer used to sequence knock out genomic DNA which indicates where RTN13 genomic sequence ends and T-DNA insertion begins. RTN13 genomic sequence (red) downstream of ATG. Knockout sequence (red/blue) shows region where T-DNA (blue) has inserted. A small region of the 5' T-DNA sequence (blue) has been lost during the recombination event (underlined). (F) Genomic (g) and cDNA (c) prepared from wild type and knock out plants screening for the presence of actin (control) and RTN13. mRNA (and therefore cDNA) levels are diminished in the RTN13 knock out sample. 30 PCR cycles were used to ensure saturation (if any) of product. All samples run on 0.8% agarose DNA gels stained with ethidium bromide.

primer extending from the T-DNA insertion itself. The T-DNA sequence was found to be inserted in the first exon of RTN13 (Figure 6.5 D, E). RNA from wild type and knockout seeds was then reverse-transcribed to yield cDNA relative to expression levels of genes in the seed. Using actin as a control, the knockout line was verified by the absence of a band relating to RTN13 cDNA, in comparison with wild type (Figure 6.5 F).

6.6.3 Preliminary analysis of RTN13 knockout

A germination assay was performed comparing wild type, *rtn13* knockout and YFP-RTN13 over-expressing seeds to determine any defects during germination and early growth stages. Scoring of the seedlings' progression through the growth stages was performed as described in Boyes *et al*., (2001). However, no differences between the 50 seedlings per sample group were observed during the first 12 days of germination (data not shown).

6.6.3.1 Deposition of storage proteins

Storage proteins, such as 2S albumin and 12S cruciferin, which are destined for the protein storage vacuoles (PSVs) are first synthesised in the ER. Initiation of expression of such storage proteins begins earlier in seed development than RTN13, but continues to be expressed through to the mature seed (eFP Browser, Winter *et al*., 2007). On the premise that reticulons help maintain ER shape and may be involved in membrane trafficking (Wakana *et al*., 2005), the correct processing and deposition of proteins destined for PSVs was investigated in the *rtn13* knockout line. The wild type, knockout and over-expressing lines were resolved by SDS-PAGE using a storage protein-specific acrylamide gel composition (Shimada *et al*., 2003), and subjected to Coomassie blue staining (Figure 6.6). Both the knockout and over-expressing lines were comparable with wild type, with no accumulation of unprocessed storage protein precursors (Figure 6.6, indicated with arrows), which is normally indicative of reduced trafficking to the storage vacuoles. The morphology of the PSVs in wild type and *rtn13* knockout embryos were also visualised using auto-fluorescence (Figure 6.8 B, E). However, no difference could be discerned between the two.

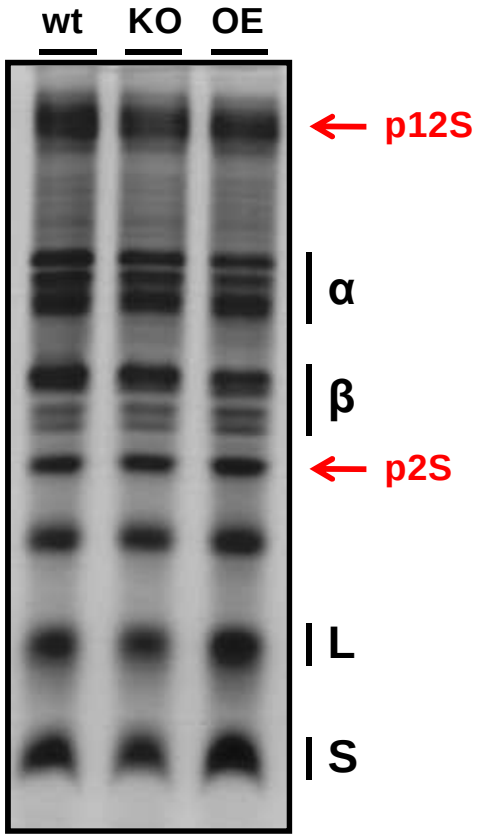

Figure 6.6 Analysis of storage protein processing in *Arabidopsis* seeds. Coomassie staining of 40% acrylamide high-bis SDS-PAGE comparing wild type, *rtn13* knockout (KO) and YFP-RTN13 over-expressing (OE) seeds. Proteins from 10 *Arabidopsis* seeds loaded in each lane. α and β processed subunits of 12S precursors and large (L) and small (S) subunits of the 2S precursors shown. Protein precursors indicated in with red arrowheads.

6.6.3.2 Structure of the ER

During the course of this study, when visualising the ER in plant cells, the soluble, luminal marker GFP-HDEL (and its derivatives) has proven an invaluable tool. However, the 35S-driven ER marker does not appear to label the ER in seeds. 35S expression of YFP-RTN13 has already been shown to be varied between cells (Figure 6.1 A). This posed a potential problem when attempting to visualise the ER in *rtn13* knockout seeds. Preliminary work cloning a new ER marker Sec61α-GFP (akin to Greenfield & High, 1999) proved potentially lethal as no transgenic progeny could be obtained from repeated transformation attempts, although expression in tobacco leaves was established (see Appendix Figure A10). The organellar dye $DiOC_6$ which, at higher concentrations and longer incubations times, is reported to highlight the ER (Quader & Schnepf, 1986), was therefore used, but no obvious difference was observed when wild type and knockout embryos were incubated with $DiOC_6$ and visualised using confocal microscopy (Figure 6.7).

6.6.3.3 Lipid body formation

Due to the similar expression patterns between RTN13 and oleosins 1 and 2, the morphology of the lipid bodies was investigated in wild type and *rtn13* knockout embryos using the lipophilic dye Nile Red. The most advantageous region of the cell to image was the periphery of the cell, where the morphology of the lipid bodies is not restricted by the PSVs. No difference could be seen between the wild type and knockout lines (Figure 6.8 A-C). Size of the lipid bodies did not exceed the expected diameter (0.2-2 μm) reported in the literature (Napier *et al*., 1996; data not shown). Therefore, the knocking out of the RTN13 gene does not appear to affect the morphology of lipid bodies.

6.6.3.4 Lipid analysis

To investigate whether the *rtn13* knockout line had a more subtle effect on the storage of lipids within the seed, *Arabidopsis* seeds were subjected to gas chromatography-based lipid analysis, whereby the total fatty acids and their composition were compared between different sets of seeds. A preliminary analysis

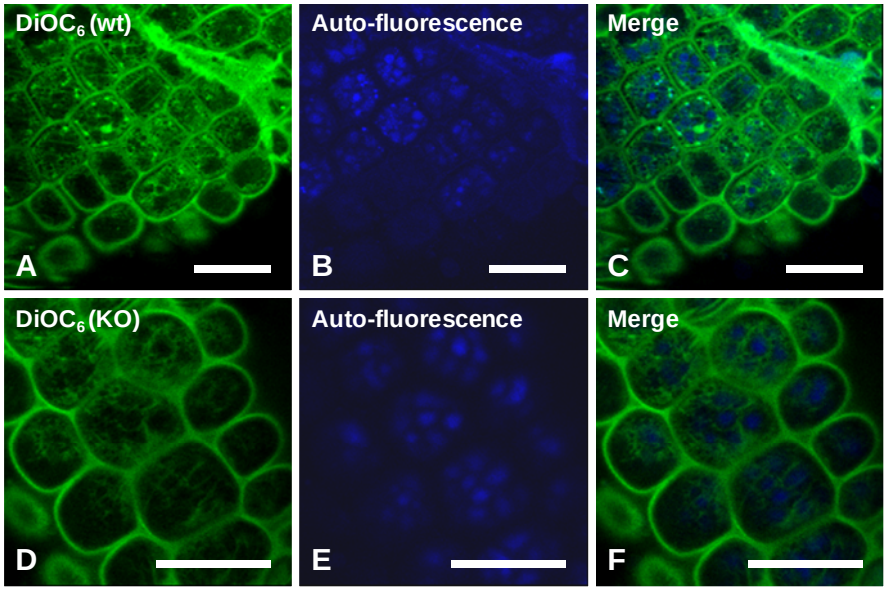

Figure 6.7 Comparison between wild type and *rtn13* knockout seeds using ER stain $DiOC_6$. Wild type (A)-(C) and *rtn13* knockout (D)-(F) seed embryos stained with $DiOC_6$ to highlight the ER (green). Auto-fluorescence of the protein storage vacuoles is shown in blue. Merged images shown in (C) and (F), respectively. Scale bars = 20 µm.

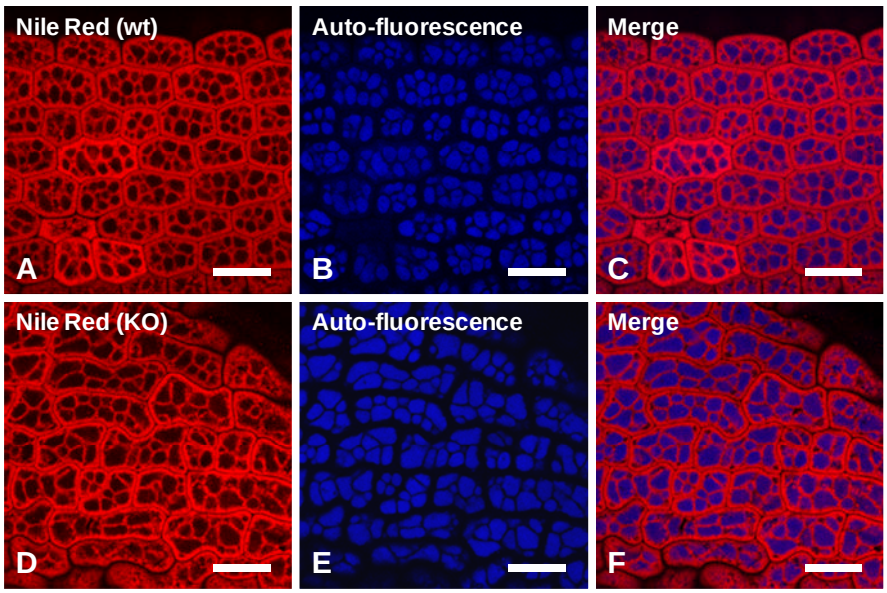

Figure 6.8 Comparison between wild type and *rtn13* knockout seeds using lipid body dye Nile Red. Wild type (A)-(C) and *rtn13* knockout (D)-(F) seed embryos stained with Nile Red to highlight lipid bodies (red). Auto-fluorescence of the protein storage vacuoles is shown in blue. Merged images shown in (C) and (F), respectively. Scale bars = 20 µm.

led to further investigation of the lipid content in *rtn13* knockout seeds. Firstly, although the composition of fatty acids in wild type and knockout seeds was comparable, the total amount of lipid appeared to be significantly higher in the knockout seed (data not shown). This potentially interesting result led to a more rigorous analysis, including the over-expressing YFP-RTN13 line. 10 plants of the wild type, knockout and over-expressing lines were grown simultaneously in two geographical locations (Biological Sciences department and Warwick HRI, Wellesbourne). Therefore, the environment in which they grow (for example, in a greenhouse) is similar, but comparable trends observed in plants growing in different locations makes the results more reproducible. The seeds were harvested and 100 seeds of each plant were analysed (Figure 6.9). Upon this more thorough analysis, lipid content in the seeds was comparable and deemed not significant when comparing wild type to knockout and over-expressing seeds. The total lipid levels in the over-expressing line in location 2 were significantly higher than the wild type, but this was not true for location 1. Therefore, these results are not sufficiently conclusive to indicate a positive effect of RTN13 over-expression on total lipid levels.

In light of this data, the morphology and lipid content of lipid bodies in the *rtn13* knockout and over-expressing line are not affected when transcript levels of RTN13 are either increased or abolished.

6.6.3.5 Proteomic analysis of RTN13 knockout

To investigate any subtle (or un-tested) changes within *Arabidopsis* seeds which lack the expression of RTN13, total protein extracts were prepared from wild type and *rtn13* knockout seeds and subjected to 2-dimentional SDS-PAGE and Difference In-Gel Electrophoresis (DIGE). However, preliminary analysis of the protein indicated that there was no difference between the two samples (data not shown). However, it has been reported that after protein extraction and resolution, not all desired proteins can be visualised, and methods of extraction vary depending on whether membrane or soluble proteins are to be analysed (Isaacson *et al*., 2006).

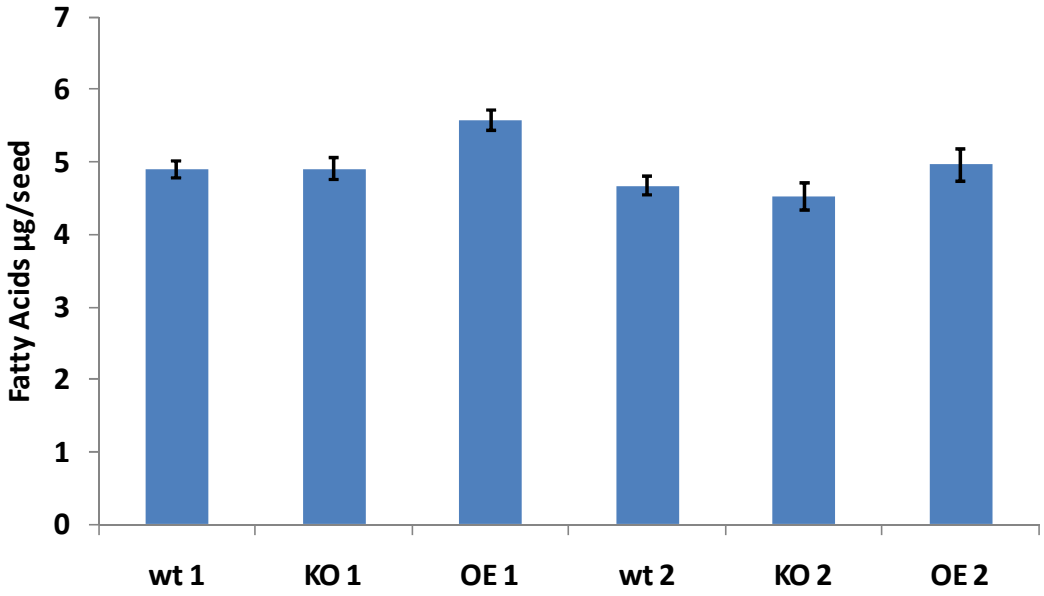

n	10	10	10	10	9	10
t-test		0.9323	0.0014		0.4763	0.2630
Significant		No	Yes		No	No
Change (µg)		+0.016	+0.684		-0.160	+0.290

Figure 6.9 Lipid analysis of wild type, *rtn13* knockout and YFP-RTN13 over-expressing *Arabidopsis* seeds. Total fatty acid content of *Arabidopsis* seeds were analysed using gas chromatography. *rtn13* knockout and YFP-RTN13 over-expressing seeds were compared with wild type seeds in two geographical locations (1-2). T-tests showing statistical significance against wild type seeds are shown.

6.7 Discussion

The previously described 35S-driven YFP-RTN13 localises to the ER in *Arabidopsis* embryos, roots and leaves. In roots and leaves, constriction of the tubular ER was observed when RTN13 was expressed in an *Arabidopsis* line transformed with GFP-HDEL. In embryos, RTN13 localises to the ER, is excluded from the protein storage vacuoles and co-localises with GFP-HDEL in imbibed seeds.

Wild type and GFP-HDEL *Arabidopsis* lines were transformed with 35S:YFP-RTN13 in order to determine the localisation of RTN13 within its native organism and compare any phenotype observed with expression in tobacco. Embryonic, root and leaf cells were examined. YFP-RTN13 localised to the ER, similar to that in tobacco and in root and leaf cells, RTN13 over-expression induced the formation of constrictions in tubular ER. This had already been observed when YFP-RTN13 was biolistically delivered into *Arabidopsis* (Figure 4.16) and shows that the formation of constrictions is not a species-specific phenomenon. YFP-RTN13 localised to the ER in the embryo and co-localised with GFP-HDEL in imbibed seeds, although constrictions were not observed at this stage of development.

RTN13 under control of its native promoter is expressed in the late stages of embryo maturation and localises to the ER. Expression ceases in the mature embryo and imbibed seed, which is consistent with the expression levels based on transcript levels using eFP Browser (Winter *et al*., 2007).

In order to determine the tissue-specific expression pattern of RTN13, the genomic sequence of RTN13 was expressed under its native promoter with YFP fused at the C-terminus. A heterozygous transgenic line was created and the expression of RTN13 examined. mRNA transcript levels illustrated in eFP Browser indicated that expression of RTN13 occurs in the early curled-cotyledon, and peaking in the late green-cotyledon stages. High transcript levels are also detected in the dry seed and are reduced in the 24 h imbibed seed. There is no expression of RTN13 in any other tissue of the plant. The expression of native RTN13 in *Arabidopsis* was intended to validate these mRNA expression levels, and determine the localisation of RTN13 at native expression levels. Ageing siliques from three different stages of development

were selected and expression levels compared with dry and imbibed seeds. Embryos were dissected and subjected to confocal imaging to establish the expression of RTN13. Low levels of expression were observed at the early curled-cotyledon stage; mid-levels of expression were evident at the late curled/early green-cotyledon stage and the highest expression was observed at the late green-cotyledon stage (Figure 6.4). RTN13 labelled the ER in the embryo at all stages. However, when examining either dry or imbibed seeds, although mRNA transcripts were detected at these stages (eFP Browser), fluorescence had diminished in the embryo, whereby small punctae and the PSVs were now weakly fluorescent. This may indicate that the protein is turned over upon seed dehydration.

These data indicate that both the over-expression and native expression of RTN13 result in localisation to the ER, and under the control of its native promoter, RTN13 is specifically expressed during the late stages of embryo maturation, and ceases in the fully mature, dry seed. Although RTN13 is the only reticulon to be expressed exclusively in seeds, RTN1 and RTN2 are also expressed in the seed (see Appendix Figure A8). Presumably, the formation and maintenance of ER tubules may be upheld by the expression of all three isoforms, as they display similar properties. However, the N-termini, thought to carry out the functional, rather than structural, role of reticulons (Iwahashi *et al*., 2007), vary between these isoforms. Therefore, the N-terminus of RTN13, although one of the shortest of all *Arabidopsis* reticulons, may possess a functional role within cells of the developing embryo. To elucidate this functional role, an *Arabidopsis* T-DNA insertional *rtn13* knockout line was obtained and characterised.

The effects of knocking out RTN13 were investigated using a homozygous T-DNA insertion line which was confirmed by RT-PCR. Seed germination, protein trafficking to the vacuole and ER, vacuole and lipid body morphology and lipid levels in the seed were analysed. However, no obvious phenotypic differences were detected between wild type and knockout plants.

A homozygous T-DNA insertional knockout of RTN13 was obtained (from NASC) and the position of insertion was confirmed in the first exon of RTN13. Diminished expression levels were then established by RT-PCR. Expression Angler software (Toufighi *et al*., 2005) generated a list of candidate genes expressed with a similar

pattern to RTN13. Of the 25 genes suggested, the most notable were HVA22 (a homologue of the reticulon-like DP1 and Yop1p genes); oleosin 1 and 2; and αTIP, a tonoplast intrinsic protein functioning as a water uptake channel in the vacuolar membrane. Based on these related genes and potential interacting partners, several characteristics of seeds were compared between wild type, knockout and the over-expressing RTN13 lines.

The rate of germination and the processing of storage protein precursors were investigated, although no difference was observed between the three lines. The morphology of the ER, storage vacuoles and lipid bodies were examined using $DiOC_6$, auto-fluorescence and Nile Red, respectively. Similarly, no difference was observed between the morphology of these organelles. Owing to the timely expression pattern of RTN13 and oleosins, which are incorporated into the lipid monolayer of the lipid bodies in the ER, the three lines were subjected to gas chromatography-based lipid analysis from two sets of samples grown independently. However, no significant difference was evident between the samples. Total proteins extracted from wild type and knockout seeds were subjected to 2D-gel DIGE analysis, though preliminary results suggested no difference between the two samples.

The fact that no phenotype was observed in the *rtn13* knockout may indicate that other reticulon isoforms present in the seed can compensate for its loss. Owing to its short N- and C-termini, RTN13 may act solely as a structural protein helping shape ER tubules; a role which can be compensated for by RTN1 and RTN2. Accordingly, RTN1, 2 and 4 have been shown to interact with each other through yeast two hybrid (Hwang & Gelvin, 2004) and recently, it has been shown that RTN13 can homo- and hetero-dimerise with RTN3 and RTN4 (Sparkes *et al*., 2010) The expression patterns of many of the *Arabidopsis* reticulons overlap throughout the tissues of the plant and may indicate a relatively high degree of redundancy within the reticulon gene family.

As suggested previously, however, the tubular morphology of the ER is unlikely to be dependent on one protein alone, and therefore other proteins such as HVA22 and RHD3 may be involved in generating ER tubules. Seed-specific isoforms of these genes are present in *Arabidopsis*, of which HVA22B is displays a similar expression

pattern to RTN13. Through the regulation of tubules and sheets within the ER at various developmental stages, cellular processes such as the deposition of storage proteins or the formation of lipid bodies can be achieved with the most efficient distribution of ER. Reticulons, in part, may help regulate the balance between sheets and tubules within the cell, whilst also being involved in other cellular processes via interactions with their N-terminal regions; processes which take place near the ER membrane.

Cisternal ER is suggested to be the site of protein synthesis and is often visualised as being studded with ribosomes. In contrast, tubular ER is often described as smooth ER, and is implicated in lipid metabolism and protein export. The extending reach of cortical ER tubules and increased surface area (in relation to sheets) may facilitate the transfer of lipids from the ER to surrounding organelles, and increase the efficiency of protein export from the ER and its subsequent delivery to downstream organelles in the secretory pathway.

As reticulons have been shown to insert preferentially into curved membranes, this mechanism of segregation may be a feature common to many proteins, or at least reticulons may sequester proteins to regions of tubular ER – where they can carry out specific functions. As the reticulon homology domain is seemingly the ‘core’ of the protein – present in all reticulons, then it is plausible that the down-regulation of one isoform may be compensated by others. RTN13 is similar to the mammalian Rtn4c in that they both comprise little more than the RHD. However, in order to induce a morphological change in the ER, proteins other than Rtn4c are required to be down-regulated, namely DP1. In yeast, a deletion of Rtn1p, Rtn2p and Yop1p results in only a moderate growth defect (Voeltz *et al*., 2006), and as was shown here - knocking out RTN13 has no effect in *Arabidopsis*, questioning the functional role of individual reticulon proteins.

Chapter 7: Concluding summary and perspectives

7.1 Summary

Characterisation of reticulons in plants is still in its early stages. While the work presented in this thesis draws parallels with reticulon research in mammals and yeast, novel characteristics of reticulons in plants have been discovered. In this study, the constricted phenotype seen in ER tubules when RTN13 is over-expressed, the unique topology and transmembrane domain conformation of RTN13 and the factors influencing localisation of RTN13 to the ER membrane have been elucidated.

General characterisation of RTN13 over-expression reveals that, in tobacco leaves, RTN13 localises to the endoplasmic reticulum and induces the formation of constrictions in the lumen of ER tubules. The level of expression seems to correlate to the severity of constriction within the ER lumen. RTN13 localises to tubular regions of the ER and is excluded from flattened sheets. The constricted phenotype can only be visualised using markers with fluorescent proteins facing the lumen of the ER, for example, GFP-HDEL and GFP-calnexin. Cytosolically tagged proteins, such as αTIP-GFP and YFP-RTN13 itself, show no constriction. It can be speculated that over-expression of RTN13 affects only the membrane of the ER, but this effect only becomes visible as luminal constrictions. This is somewhat supported by FRAP experiments which indicate that the dynamics of both GFP-HDEL and GFP-calnexin are perturbed when RTN13 is over-expressed. However, seeing as RTN13 induces such severe morphological changes in the ER, it is surprising that anterograde transport of a variety of molecules tested is relatively unaffected, with only protein trafficking to the tonoplast membrane being perturbed.

Protease protection and bimolecular fluorescence complementation indicate that the long hydrophobic regions within the RHD of RTN13 contain four transmembrane domains which sit as a ‘w’ in the lipid bilayer of the ER, with the N- and C-termini and loop regions facing the cytosol. This topology is shared with at least four other *Arabidopsis* isoforms and is likely to extend to all *Arabidopsis* reticulon family members.

A more in depth analysis of the individual domains of RTN13 reveals that the full length protein is required for stable expression and correct insertion into the ER

membrane. Localisation of RTN13 to the ER is determined by both the presence of a full-length RHD and the specific length of the transmembrane domains within. Shortening of the transmembrane domains in addition to removal of the C-terminal ER-retrieval motif results is mislocalisation of RTN13 to the Golgi. The length of the transmembrane domains is also responsible for RTN13's ability to curve membranes and induce tubulation in sheets. The RHD, therefore, is the key structural feature of reticulons, which explains its high degree of conservation.

When expressed in *Arabidopsis*, RTN13 localises to the ER and is able to constrict the lumen of ER tubules, similar to what is seen in tobacco. Under the expression of its native promoter, RTN13 localises to the ER and is expressed in the late maturing embryo. A T-DNA insertional knockout of RTN13 yielded no observable phenotype, indicating the possibility of other reticulons to compensate for its loss. This degree of redundancy may be a recurring theme for plant reticulons. In mammals and yeast, multiple reticulon genes need to be knocked out to obtain an observable phenotype, indicating that a similar strategy may be necessary to observe a phenotype in plants. Plants also possess a large number of reticulon family members (21) compared with mammals (4) and yeast (2) and therefore, although N-terminal sequences may differ, with regards to the structure of the ER, the loss of one reticulon isoform may well be compensated for.

7.2 Outlook

The logical progression of this project would be to extend the study of the structural properties of RTN13, and to dissect the mechanisms involved in plant ER tubule formation. Expression of members of the HVA22 family (DP1/Yop1p) and RHD3 (Atlastin/Sey1p) may provide an insight into the dynamics of ER tubule formation, fusion and maintenance. A knockout of RHD3 in *Arabidopsis* has already been shown to form long, cable-like ER strands (Zheng *et al*., 2004).

The extent of RTN13 oligomerisation can be determined in order to model how reticulons may induce curvature as higher oligomeric complexes and the precise nature of RTN13 homotypic interactions can be established and interaction partners ascertained. Techniques such as sucrose gradients may indicate the number of

reticulon proteins in a single complex or ‘arc’, and studies using the BiFC system and FRET-FLIM (fluorescence energy transfer/fluorescence life-time imaging) can be used to identify the nature of homo-and hetero-interactions. Also, FRAP can be used to study the mobility of reticulon ‘complexes’ and any of the mutants described in this study can be investigated using similar techniques in order to identify regions of reticulons essential to their function.

The techniques listed here and described throughout this thesis can be applied to other members of the *Arabidopsis* reticulon family. Preliminary investigation of some of these members has already been initiated (Hwang & Gelvin, 2004; Nziengui *et al*., 2007; Sparkes *et al*., 2010).

In order to better understand the pattern of reticulon expression in *Arabidopsis*, expression profiling of the non-enzyme linked reticulons has begun at Warwick. The expression of RTN1-18, under their native promoters and fluorescently tagged with YFP, will help localise these proteins, not only to subcellular organelles, but to specific tissues and developmental stages of plant growth. Expression of reticulons has been detected in roots, leaves, meristems, flowers, pollen and seeds. Reticulon localisation will indicate expression in specific cell types, more in depth than that of whole-tissue based mRNA transcript levels and provide the foundation for targeted reverse genetics studies.

Continuing the theme of reticulons expressed in the seed, through the use of T-DNA knockouts and RNAi, the remaining reticulon isoforms in the *rtn13* knockout seed (RTN1 and RTN2), can be down-regulated in order to investigate the functional relevance of an intact tubular ER in seeds. These, in combination with the functional analysis of HVA22 and RHD3, can help link ER shape with protein and lipid secretion and storage in seeds and provide insights into yield improvement for biotechnological applications.

Characteristics common to reticulons in mammals, yeast, plants and several other eukaryotic organisms are being unravelled. Although progress has been made through the course of this study, many questions remain in the reticulon field. How are reticulons proteins structured, both individually and as a scaffold? How are these

scaffolds regulated in such dynamic domains of the ER such as constantly remodelling tubules? Does the formation and segregation of reticulons into tubular ER affect the localisation of other proteins? Finally, is the current model of the ER as simple as rough and smooth, cisternal and tubular? Or are there more functionally distinct domains of the ER which, at present, are indistinguishable? The answers to these questions will increase our understanding of the complex structure of the endoplasmic reticulum.

Chapter 8: References

Abell, B. M., Hahn, M., Holbrook, L. A. and Moloney, M. M. (2004) Membrane topology and sequence requirements for oil body targeting of oleosin. *Plant J* **37**(4):461-70.

Abell, B. M., Rabu, C., Leznicki, P., Young, J. C. and High, S. (2007) Post-translational integration of tail-anchored proteins is facilitated by defined molecular chaperones. *J Cell Sci* **120**(10):1743-51.

Alder, N. N., Shen, Y., Brodsky, J. L., Hendershot, L. M. and Johnson A. E. (2005) The molecular mechanism underlying BiP-mediated gating of the Sec61 translocon of the endoplasmic reticulum. *J Cell Biol* **168**:389-399.

Anderson, D. and Hetzer, M. (2008) Reshaping of the endoplasmic reticulum limits the rate for nuclear envelope formation. *J Cell Biol* **182**:911-924.

Anelli, T. and Sitia, R. (2008) Protein quality control in the early secretory pathway. *EMBO J* **27**:315-327.

Argon, Y. and Simen, B. B. (1999) GRP94, an ER chaperone with protein and peptide binding properties. *Semin Cell Dev Biol* **10**(5):495-505.

Audhya, A., Desai, A. and Oegema, K. (2007) A role for Rab5 in structuring the endoplasmic reticulum. *J Cell Biol* **178**(1):43-56.

Batoko, H., Zheng, H.Q., Hawes, C. and Moore, I. (2000) A rab1 GTPase is required for transport between the endoplasmic reticulum and golgi apparatus and for normal golgi movement in plants. *Plant Cell* **12**(11):2201-2218.

Bauer, M. and Pelkmans, L. (2006) A new paradigm for membrane-organizing and -shaping scaffolds. *FEBS Lett* **580**:5559-5564.

Becker, T., Bhushan, S., Jarasch, A., Armache, J. P., Funes, S., Jossinet, F., Gumbart, J., Mielke, T., Berninghausen, O., Schulten, K., Westhof, E., Gilmore, R., Mandon, E. C. and Beckmann, R. (2009) Structure of monomeric yeast and mammalian Sec61 complexes interacting with the translating ribosome. *Science* **326**(5958):1369-73.

Benghezal, M., Wasteneys, G. O. and Jones, D. A. (2000) The C-terminal di-lysine motif confers endoplasmic reticulum localization to type I membrane proteins in plants. *Plant Cell* **12**(7):1179-201.

Benyamini, P., Webster, P. and Meyer, D. I. (2009) Knockdown of p180 eliminates the terminal differentiation of a secretory cell line. *Mol Biol Cell* **20**(2):732-44.

Bernsel, A., Viklund, H., Hennerdal, A. and Elofsson, A. (2009) TOPCONS: consensus prediction of membrane protein topology. *Nucleic Acids Res.* **37**:W465-8.

Birtić, S. & Kranner, I. (2006) Isolation of high-quality RNA from polyphenol-, polysaccharide- and lipid-rich seeds. *Phytochem Anal* **17**(3):144-148.

Blobel, G. and Sabatini, D. D. (1971) Ribosome-membrane interaction in eukaryotic cells. *Biomembranes* **2**:193-195

Boevink, P., Santa Cruz, S., Hawes, C., Harris, N. and Oparka, K. J. (1996) Virus-mediated delivery of the green fluorescent protein to the endoplasmic reticulum of plant cells. *Plant J* **10**:935-941.

Boevink, P., Oparka, K., Santa Cruz, S., Martin, B., Batteridge, A. and Hawes, C. (1998) Stacks on tracks: the plant Golgi apparatus traffics on an actin/ER network. *Plant J* **15**:441-447.

Boevink, P., Martin, B., Oparka, K., Santa Cruz, S. and Hawes, C. (1999) Transport of virally expressed green fluorescent protein through the secretory pathway in tobacco leaves is inhibited by cold shock and brefeldin A. *Planta* **208**: 392-400.

Bokman, S. H. and Ward, W. W. (1981) Renaturation of green-fluorescent protein. *Biochem Biophys Res Comm* **101**(4):1372-1380.

Bouchekhima, A. N., Frigerio, L. and Kirkilionis, M. (2009) Geometric quantification of the plant endoplasmic reticulum. *J Microsc* **234**(2):158-72.

Boulaflous, A., Saint-Jore-Dupas, C., Herranz-Gordo, M. C., Pagny-Salehabadi, S., Plasson, C., Garidou, F., Kiefer-Meyer, M. C., Ritzenthaler, C., Faye, L. and Gomord, V. (2009) Cytosolic N-terminal arginine-based signals together with a luminal signal target a type II membrane protein to the plant ER. *BMC Plant Biol* **9**:144.

Boyes, D. C., Zayed, A. M., Ascenzi, R., McCaskill, A. J., Hoffman, N. E., Davis, K. R. and Görlach, J. (2001) Growth stage-based phenotypic analysis of *Arabidopsis*: a model for high throughput functional genomics in plants. *Plant Cell* **13**(7):1499-510.

Brach, T., Soyk, S., Müller, C., Hinz, G., Hell, R., Brandizzi, F. and Meyer, A. J. (2009) Non-invasive topology analysis of membrane proteins in the secretory pathway. *Plant J* **57**(3):534-41.

Brambillasca, S., Yabal, M., Makarow, M. and Borgese, N. (2006) Unassisted translocation of large polypeptide domains across phospholipid bilayers. *J Cell Biol* **175**:767-777.

Brandizzi, F., Frangne, N., Marc-Martin, S., Hawes, C., Neuhaus, J. M. and Paris, N. (2002) The destination for single-pass membrane proteins is influenced markedly by the length of the hydrophobic domain. *Plant Cell* **14**(5):1077-92.

Brodsky, J. L. and Schekman, R. (1993) A Sec63p-BiP complex from yeast is required for protein translocation in a reconstituted proteoliposome. *J Cell Biol* **123**(6):1355-63.

Chen, M. S., Huber, A. B., van der Haar, M. E., Frank, M., Schnell, L., Spillmann, A. A., Christ, F. and Schwab, M. E. (2000) Nogo-A is a myelin-associated neurite outgrowth inhibitor and an antigen for monoclonal antibody IN-1. *Nature* **403**:434-439.

Chernomordik, L. V. and Kozlov, M. M. (2003) Protein–lipid interplay in fusion and fission of biological membranes. *Annu Rev Biochem* **72**:175-207.

Chiang, C. F., Okou, D. T., Griffin, T. B., Verret, C. R. and Williams, N. M. V. (2001) Green Fluorescent Protein Rendered Susceptible to Proteolysis: Positions for Protease-Sensitive Insertions. *Arch Biochem Biophys* **394**(2):229-35.

Claude, A. (1943) The constitution of protoplasm. *Science* **97**:451-456.

Clough, S.J. & Bent, A.F. (1998) Floral dip: a simplified method for *Agrobacterium*-mediated transformation of *Arabidopsis thaliana*. *Plant J* **16**(6):735-743.

Cocquerel, L., Wychowski, C., Minner, F., Penin, F. and Dubuisson, J. (2000) Charged residues in the transmembrane domains of hepatitis C virus glycoproteins play a major role in the processing, subcellular localization, and assembly of these envelope proteins. *J Virol* **74**(8):3623-33.

D'Arrigo, A., Manera, E., Longhi, R. and Borgese, N. (1993) The specific subcellular localization of two isoforms of cytochrome b5 suggests novel targeting pathways. *J Biol Chem* **268**:2802-2808.

DaSilva, L. L., Snapp, E. L., Denecke, J., Lippincott-Schwartz, J., Hawes, C. and Brandizzi, F. (2004) Endoplasmic reticulum export sites and Golgi bodies behave as single mobile secretory units in plant cells. *Plant Cell* **16**:1753-1771.

Di Cola, A., Frigerio, L., Lord, J. M., Ceriotti, A. and Roberts, L. M. (2001) Ricin A chain without its partner B chain is degraded after retrotranslocation from the endoplasmic reticulum to the cytosol in plant cells. *Proc Natl Acad Sci U S A* **25**:14726-31.

Di Scala, F., Dupuis, L., Gaiddon, C., De Tapia, M., Jokic, N., Gonzalez de Aguilar, J. L., Raul, J. S., Ludes, B. and Loeffler, J. P. (2005) Tissue specificity and regulation of the N-terminal diversity of reticulon 3. *Biochem J* **385**(1):125-34.

Diekmann, H., Klinger, M., Oertle, T., Heinz, D., Pogoda, H. M., Schwab, M. E. and Stuermer, C. A. (2005) Analysis of the reticulon gene family demonstrates the absence of the neurite growth inhibitor Nogo-A in fish. *Mol Biol Evol* **22**(8):1635-48.

Dodd, D. A., Niederoest, B., Bloechlinger, S., Dupuis, L., Loeffler, J. P. and Schwab, M. E. (2005) Nogo-A, -B, and -C are found on the cell surface and interact together in many different cell types. *J Biol Chem* **280**(13):12494-502.

Dreier, L. and Rapoport, T. A. (2000) In vitro formation of the endoplasmic reticulum occurs independently of microtubules by a controlled fusion reaction. *J Cell Biol* **148**(5):883-98.

Dunkley, T. P., Hester, S., Shadforth, I. P., Runions, J., Weimar, T., Hanton, S. L., Griffin, J. L., Bessant, C., Brandizzi, F., Hawes, C., Watson, R. B., Dupree, P. and Lilley, K. S. (2006) Mapping the *Arabidopsis* organelle proteome. *Proc Natl Acad Sci U S A* **103**:6518-6523.

English, A. R., Zurek, N. and Voeltz, G. K. (2009) Peripheral ER structure and function. *Curr Opin Cell Biol* **21**(4):596-602.

Evans, E. A., Gilmore, R. and Blobel, G. (1986) Purification of microsomal signal peptidase as a complex. *Proc Natl Acad Sci U S A* **83**(3):581-5.

Farsad, K. and De Camilli, P. (2003) Mechanisms of membrane deformation. *Curr Opin Cell Biol* **15**:372-381.

Frigerio, L., de Virgilio, M., Prada, A., Faoro, F. and Vitale, A. (1998) Sorting of phaseolin to the vacuole is saturable and requires a short C-terminal peptide. *Plant Cell* **10**:1031–1042.

Fournier, A. E., GrandPré, T., Gould, G., Wang, X. and Strittmatter, S. M. (2002) Nogo and the Nogo-66 receptor. *Prog Brain Res* **137**:361-9.

Galili, G., Sengupta-Gopalan, C. and Ceriotti, A. (1998) The endoplasmic reticulum of plant cells and its role in protein maturation and biogenesis of oil bodies. *Plant Mol Biol* **38**(1-2):1-29.

Gething, M. J. (1999) Role and regulation of the ER chaperone BiP. *Semin Cell Dev Biol* **10**:465-472.

Goetz, J. G., Genty, H., St-Pierre, P., Dang, T., Joshi, B., Sauvé, R., Vogl, W. and Nabi, I. R. (2007) Reversible interactions between smooth domains of the endoplasmic reticulum and mitochondria are regulated by physiological cytosolic Ca2+ levels. *J Cell Sci* **120**(20):3553-64.

Gomord, V., Wee, E. and Faye, L. (1999) Protein retention and localization in the endoplasmic reticulum and the golgi apparatus. *Biochimie* **81**(6):607-18.

GrandPré, T., Nakamura, F., Vartanian, T. and Strittmatter, S. M. (2000) Identification of the Nogo inhibitor of axon regeneration as a Reticulon protein. *Nature* **403**(6768):439-44.

Greenfield, J. J. and High, S. (1999) The Sec61 complex is located in both the ER and the ER-Golgi intermediate compartment. *J Cell Sci* **112**(10):1477-86.

Grudnik, P., Bange, G. and Sinning, I. (2009) Protein targeting by the signal recognition particle. *Biol Chem* **390**:775-782.

Haas, A. K., Yoshimura, S., Stephens, D. J., Preisinger, C., Fuchs, E. and Barr, F. A. (2007) Analysis of GTPase-activating proteins: Rab1 and Rab43 are key Rabs required to maintain a functional Golgi complex in human cells. *J Cell Sci* **120**(17):2997-3010.

Halic, M., Becker, T., Pool, M. R., Spahn, C. M., Grassucci, R. A., Frank, J. and Beckmann, R. (2004). Structure of the signal recognition particle interacting with the elongation-arrested ribosome. *Nature* **427**:808-814.

Hamman, B. D., Chen, J. C., Johnson, E. E. and Johnson, A. E. (1997) The aqueous pore through the translocon has a diameter of 40–60Å during co-translational protein translocation at the ER membrane. *Cell* **89**:535-544.

Hamman, B. D., Hendershot, L. M. and Johnson, A. E. (1998) BiP maintains the permeability barrier of the ER membrane by sealing the lumenal end of the translocon pore before and early in translocation. *Cell* **92**:747-758.

Hanton, S. L., Bortolotti, L. E., Renna, L., Stefano, G. and Brandizzi, F. (2005) Crossing the divide--transport between the endoplasmic reticulum and Golgi apparatus in plants. *Traffic* **6**(4):267-77.

Hanton, S. L., Chatre, L., Matheson, L. A., Rossi, M., Held, M. A. and Brandizzi, F. (2008) Plant Sar1 isoforms with near-identical protein sequences exhibit different localisations and effects on secretion. *Plant Mol Biol* **67**:283-294.

Hara-Nishimura, I., Shimada, T., Hatano, K., Takeuchi, Y. and Nishimura, M. (1998) Transport of storage proteins to protein storage vacuoles is mediated by large precursor-accumulating vesicles. *Plant Cell* **10**:825-836.

Harris, N. (1979) Endoplasmic Reticulum in Developing Seeds of *Vicia faba*. *Planta* **146**:63-69.

Hartl, F.U. and Hayer-Hartl, M. (2002). Molecular chaperones in the cytosol: From nascent chain to folded protein. *Science* **295**:1852-1858.

Hartmann, E., Sommer, T., Prehn, S., Görlich, D., Jentsch, S. and Rapoport, T. A. (1994) Evolutionary conservation of components of the protein translocation complex. *Nature* **367**(6464):654-7.

Haseloff, J., Siemering, K. R., Prasher, D. C. and Hodge, S. (1997) Removal of a cryptic intron and subcellular localization of green fluorescent protein are required to mark transgenic *Arabidopsis* plants brightly. *Proc Natl Acad Sci U S A* **94**(6):2122-7.

Hausmann, L. & Töpfer, R. (1999) Entwicklung von Plasmid-Vektoren. P*flanzenzücht* **45**:155–172.

Hawes, C. & Satiat-Jeunemaitre, B. (2001) Plant Cell Biology: A Practical Approach. Oxford University Press, USA

Hawes, C., Osterrieder, A., Hummel, E. and Sparkes, I. (2008) The plant ER–Golgi interface. *Traffic* **9**:1571-1580.

He, W., Hu, X., Shi, Q., Zhou, X., Lu, Y., Fisher, C. and Yan, R. (2006) Mapping of interaction domains mediating binding between BACE1 and RTN/Nogo proteins. *J Mol Biol* **363**(3):625-34.

He, W., Shi, Q., Hu, X. and Yan, R. (2007) The membrane topology of RTN3 and its effect on binding of RTN3 to BACE1. *J Biol Chem* **282**(40):29144-51.

Helenius, A. and Aebi, M. (2001) Intracellular functions of N-linked glycans. *Science* **291**(5512):2364-9.

Hellens, R., Mullineaux, P. and Klee, H. (2000) A guide to *Agrobacterium* binary Ti vectors. *Trends in Plant Science* **5**(10):446-451.

Hepler, P. K. (1981) The structure of the endoplasmic reticulum revealed by osmium tetroxide-potassium ferricyanide staining. *Eur J Cell Biol* **26**:102-110.

Herman, E. and Schmidt, M. (2004) Endoplasmic reticulum to vacuole trafficking of endoplasmic reticulum bodies provides an alternate pathway for protein transfer to the vacuole. *Plant Physiol* **136**(3):3440-6.

Herman, E. M. (2008) Endoplasmic reticulum bodies: solving the insoluble. *Curr Opin Plant Biol* **11**(6):672-9.

High, S. and Abell, B. M. (2004) Tail-anchored protein biosynthesis at the endoplasmic reticulum: the same but different. *Biochem Soc Trans* **32**(5):659-62.

Hu, C. D., Chinenov, Y. and Kerppola ,T. K. (2002) Visualization of interactions among bZIP and Rel family proteins in living cells using bimolecular fluorescence complementation. *Mol Cell* **9**(4):789-98.

Hu, J., Shibata, Y., Voss, C., Shemesh, T., Li, Z., Coughlin, M., Kozlov, M. M., Rapoport, T. A. and Prinz, W. A. (2008) Membrane proteins of the endoplasmic reticulum induce high-curvature tubules. *Science* **319**(5867):1247-50.

Hu, J., Shibata, Y., Zhu, P. P., Voss, C., Rismanchi, N., Prinz, W. A., Rapoport, T. A. and Blackstone, C. (2009) A class of dynamin-like GTPases involved in the generation of the tubular ER network. *Cell* **138**(3):549-61.

Hunter, P. R., Craddock, C. P., Di Benedetto, S., Roberts, L.M. and Frigerio, L. (2007) Fluorescent reporter proteins for the tonoplast and the vacuolar lumen identify a single vacuolar compartment in *Arabidopsis* cells. *Plant Physiol* **145**(4):1371-82.

Hwang, H. H. & Gelvin, S. B. (2004) Plant proteins that interact with VirB2, the Agrobacterium tumefaciens pilin protein, mediate plant transformation. *Plant Cell* **16**(11):3148-67.

Irons, S.L., Evans, D. E., Brandizzi F. (2003) The first 238 amino acids of the human lamin B receptor are targeted to the nuclear envelope in plants. *J Exp Bot* **54**:943–950.

Isaacson. T., Damasceno. C. M., Saravanan, R. S., He, Y., Catalá, C., Saladié, M. and Rose, J. K. (2006) Sample extraction techniques for enhanced proteomic analysis of plant tissues. *Nat Protoc* **1**(2):769-74.

Iwahashi, J., Kawasaki, I., Kohara, Y., Gengyo-Ando, K., Mitani, S., Ohshima, Y., Hamada, N., Hara, K., Kashiwagi, T. and Toyoda, T. (2002) *Caenorhabditis elegans* reticulon interacts with RME-1 during embryogenesis. *Biochem Biophys Res Commun* **293**(2):698-704.

Iwahashi, J., Hamada, N. and Watanabe, H. (2007) Two hydrophobic segments of the RTN1 family determine the ER localization and retention. *Biochem Biophys Res Commun* **355**(2):508-12.

Jackson, M. R., Nilsson, T. and Peterson, P. A. (1990) Identification of a consensus motif for retention of transmembrane proteins in the endoplasmic reticulum. *EMBO J* **9**(10):3153-62.

Jolliffe, N. A., Brown, J. C., Neumann, U., Vicré, M., Bachi, A., Hawes, C., Ceriotti, A., Roberts, L. M. and Frigerio, L. (2004) Transport of ricin and 2S albumin precursors to the storage vacuoles of *Ricinus communis* endosperm involves the Golgi and VSR-like receptors. *Plant J* **39**(6):821-33.

Jouhet, J., Maréchal, E. and Block, M. A. (2007) Glycerolipid transfer for the building of membranes in plant cells. *Prog Lipid Res* **46**(1):37-55.

Kiseleva, E., Morozova, K. N., Voeltz, G. K., Allen, T. D. and Goldberg, M. W. (2007) Reticulon 4a/NogoA locates to regions of high membrane curvature and may have a role in nuclear envelope growth. *J Struct Biol* **160**(2):224-35.

Klein, E. M., Mascheroni, L., Pompa, A., Ragni, L., Weimar, T., Lilley, K. S., Dupree, P. and Vitale, A. (2006) Plant endoplasmin supports the protein secretory pathway and has a role in proliferating tissues. *Plant J* **48**(5):657-73.

Koizumi, N., Martinez, I. M., Kimata, Y., Kohno, K., Sano, H. and Chrispeels, M. J. (2001) Molecular characterization of two *Arabidopsis* Ire1 homologs, endoplasmic reticulum-located transmembrane protein kinases. *Plant Physiol* **127**:949-962.

Korkhov, V. M. and Zuber, B. (2009) Direct observation of molecular arrays in the organized smooth endoplasmic reticulum. *BMC Cell Biol* **10**:59.

Lang, D., Zimmer, A. D., Rensing, S. A. and Reski, R. (2008) Exploring plant biodiversity: the *Physcomitrella* genome and beyond. *Trends Plant Sci* **13**(10):542-9.

Lauring, B., Kreibich, G. and Weidmann, M. (1995) The intrinsic ability of ribosomes to bind to endoplasmic reticulum membranes is regulated by signal recognition particle and nascent-polypeptide-associated complex. *Proc Natl Acad Sci U S A*. **92**(21):9435-9.

Lee, H. I., Gal, S., Newman, T. C. and Raikhel, N. V. (1993) The *Arabidopsis* endoplasmic reticulum retention receptor functions in yeast. *Proc Natl Acad Sci USA* **90**:11433-11437.

Lee, M. C., Miller, E. A., Goldberg, J., Orci, L. and Schekman, R. (2004) Bi-directional protein transport between the ER and Golgi. *Annu Rev Cell Dev Biol* **20**:87-123.

Liu, Y., Vidensky, S., Ruggiero, A. M., Maier, S., Sitte, H. H. and Rothstein, J. D. (2008) Reticulon RTN2B regulates trafficking and function of neuronal glutamate transporter EAAC1. *J Biol Chem* **283**(10):6561-71.

Luedeke, C., Frei, S. B., Sbalzarini, I., Schwarz, H., Spang, A. and Barral, Y. (2005) Septin-dependent compartmentalization of the endoplasmic reticulum during yeast polarized growth. *J Cell Biol* **169**:897-908.

Ma, B., Cui, M. L., Sun, H. J., Takada, K., Mori, H., Kamada, H. and Ezura, H. (2006) Subcellular localization and membrane topology of the melon ethylene receptor CmERS1. *Plant Physiol* **141**(2):587-97.

Malhotra, J. D. and Kaufman, R. J. (2007) The endoplasmic reticulum and the unfolded protein response. *Semin Cell Dev Biol* **18**:716-731.

Maliga, P., Sz-Breznovits, A. and Marton, L. (1973). Streptomycin-resistant plants from callus culture of haploid tobacco. *Nat New Biol* 244:29–30.

Maltman, D. J., Gadd, S. M., Simon, W. J. and Slabas, A. R. (2007) Differential proteomic analysis of the endoplasmic reticulum from developing and germinating seeds of castor (*Ricinus communis*) identifies seed protein precursors as significant components of the endoplasmic reticulum. *Proteomics* **7**(9):1513-28.

Marmagne, A., Rouet, M. A., Ferro, M., Rolland, N., Alcon, C., Joyard, J., Garin, J., Barbier-Brygoo, H. and Ephritikhine, G. (2004) Identification of new intrinsic proteins in *Arabidopsis* plasma membrane proteome. *Mol Cell Proteomics* **3**(7):675-91.

Marshall, R. S., Jolliffe, N. A., Ceriotti, A., Snowden, C. J., Lord, J. M., Frigerio, L., and Roberts, L. M. (2008) The role of CDC48 in the retro-translocation of non-ubiquitinated toxin substrates in plant cells. *J Biol Chem* **283**(23):15869-77.

Martin, H. G., Henley, J. M. and Meyer, G. (2006) Novel putative targets of N-ethylmaleimide sensitive fusion protein (NSF) and alpha/beta soluble NSF attachment proteins (SNAPs) include the Pak-binding nucleotide exchange factor betaPIX. *J Cell Biochem* **99**(4):1203-15.

Martinez, M. and Chrispeels, M. J. (2003) Genomic analysis of the unfolded protein response in *Arabidopsis* shows its connection to important cellular processes. *Plant Cell* **15**:561-576.

Matlack, K. E., Misselwitz, B., Plath, K. and Rapoport, T. A. (1999) BiP acts as a molecular ratchet during posttranslational transport of prepro-alpha factor across the ER membrane. *Cell* **97**(5):553-64.

Mattaj, I. W. (2004) Sorting out the nuclear envelope from the endoplasmic reticulum. *Nature Rev Mol Cell Biol* **5**:65-69.

Maurel, C. (1997) Aquaporins and water permeability of plant membranes. *Annu Rev Plant Physiol Plant Mol Biol* **48**:399-429.

McMahon, H. T. and Mills, I. G. (2004) COP and clathrin-coated vesicle budding: different pathways, common approaches. *Curr Opin Cell Biol* **16**(4):379-91.

Michelsen, K., Yuan, H. and Schwappach, B. (2005) Hide and run. Arginine-based endoplasmic-reticulum-sorting motifs in the assembly of heteromultimeric membrane proteins. *EMBO Rep* **6**:717-722.

Moore, I., Galweiler, L., Grosskopf, D., Schell, J. and Palme, K. (1998) A transcription activation system for regulated gene expression in transgenic plants. *Proc Natl Acad Sci USA* **95**(1):376-381.

Moreau, P., Bessoule, J. J., Mongrand, S., Testet, E., Vincent, P. and Cassagne, C. (1998) Lipid trafficking in plant cells. *Prog Lipid Res* **37**(6):371-91.

Moreau, P., Brandizzi, F., Hanton, S., Chatre, L., Melser, S., Hawes, C. and Satiat-Jeunemaitre, B. (2007) The plant ER-Golgi interface: a highly structured and dynamic membrane complex. *J Exp Bot* **58**:49-64.

Morris, N. J., Ross, S. A., Neveu, J. M., Lane, W. S. and Lienhard, G. E. (1999) Cloning and characterization of a 22 kDa protein from rat adipocytes: a new member of the reticulon family. *Biochim Biophys Acta* **1450**(1):68-76.

Mothes, W., Prehn, S. and Rapoport, T. A. (1994) Systematic probing of the environment of a translocating secretory protein during translocation through the ER membrane. *EMBO J* **13**:3937-3982.

Munro, S. and Pelham, H. R. (1987) A C-terminal signal prevents secretion of luminal ER proteins. *Cell* **48**(5):899-907.

Munro, S. (1995) An investigation of the role of transmembrane domains in Golgi protein retention. *EMBO J* **14**(19):4695-704.

Murashige, R. & Skoog, F. (1962). A revised medium for rapid growth and bioassays with tobacco tissue cultures. *Physiol Plant* **15**:473–497.

Muriel, M. P., Dauphin, A., Namekawa, M., Gervais, A., Brice, A. and Ruberg, M. (2009) Atlastin-1, the dynamin-like GTPase responsible for spastic paraplegia SPG3A, remodels lipid membranes and may form tubules and vesicles in the endoplasmic reticulum. *J Neurochem* **110**(5):1607-16.

Murphy, D. J. (1993) Structure, Function and biogenesis of storage lipid bodies and oleosins in plants. *Prog Lipid Res* **32**:247–280.

Nakamura, Y., Koizumi, R., Shui, G., Shimojima, M., Wenk, M. R., Ito, T. and Ohta, H. (2009) *Arabidopsis* lipins mediate eukaryotic pathway of lipid metabolism and cope critically with phosphate starvation. *Proc Natl Acad Sci U S A* **106**(49):20978-83.

Napier, J. A., Stobart, A. K. and Shewry, P. R. (1996) The structure and biogenesis of plant oil bodies: the role of the ER membrane and the oleosin class of proteins. *Plant Mol Biol* **31**(5):945-56.

Nikonov, A. V., Snapp, E., Lippincott-Schwartz, J. and Kreibich, G. (2002) Active translocon complexes labeled with GFP-Dad1 diffuse slowly as large polysome arrays in the endoplasmic reticulum. *J Cell Biol* **158**(3):497-506.

Noiva, R., Freedman, R. B. and Lennarz, W. J. (1993) Peptide binding to protein disulfide isomerase occurs at a site distinct from the active sites. *J Biol Chem* **268**:19210-19217.

Novak, G., Kim, D., Seeman, P. and Tallerico, T. (2002) Schizophrenia and Nogo: elevated mRNA in cortex, and high prevalence of a homozygous CAA insert. *Brain Res Mol Brain Res* **107**(2):183-9.

Nziengui, H., Bouhidel, K., Pillon, D., Der, C., Marty, F. and Schoefs, B. (2007) Reticulon-like proteins in *Arabidopsis thaliana*: structural organization and ER localization. *FEBS Lett* **581**(18):3356-62.

Nziengui, H. and Schoefs, B. (2008) Functions of reticulons in plants: What we can learn from animals and yeasts. *Cell Mol Life Sci* **66**(4):584-95.

Oertle, T., Huber, C., van der Putten, H. and Schwab, M. E. (2003a) Genomic structure and functional characterisation of the promoters of human and mouse nogo/rtn4. *J Mol Biol* **325**(2):299-323.

Oertle ,T., Klinger, M., Stuermer, C. A. and Schwab, M. E. (2003b) A reticular rhapsody: phylogenic evolution and nomenclature of the RTN/Nogo gene family. *FASEB J* **17**(10):1238-47.

Oertle, T. and Schwab, M. E. (2003) Nogo and its paRTNers. *Trends Cell Biol* **13**(4):187-94.

Ohno, H., Stewart, J., Fournier, M. C., Bosshart, H., Rhee, I., Miyatake, S., Saito T., Gallusser, A., Kirchhausen, T. and Bonifacino, J. S. (1995) Interaction of tyrosine-based sorting signals with clathrin-associated proteins. *Science* **269**:1872-1875.

Okamoto, T., Nakayama, H., Seta, K., Isobe, T. and Minamikawa, T. (1994) Posttranslational processing of a carboxy-terminal propeptide containing a KDEL sequence of plant vacuolar cysteine endopeptidase. *FEBS Lett* **351**:31-34.

Okamoto, T., Shimada, T., Hara-Nishimura, I., Nishimura, M. and Minamikawa, T. (2003) C-terminal KDEL sequence of a KDEL-tailed cysteine proteinase (sulfhydryl-endopeptidase) is involved in formation of KDEL vesicle and in efficient vacuolar transport of sulfhydryl-endopeptidase. *Plant Physiol* **132**(4):1892-900.

Oparka, K. J. (2005) Plasmodesmata. *Ann Plant Rev* **18**:331.

Orso, G., Pendin, D., Liu, S., Tosetto, J., Moss, T. J., Faust, J. E., Micaroni, M., Egorova, A., Martinuzzi, A., McNew, J. A. and Daga, A. (2009) Homotypic fusion of ER membranes requires the dynamin-like GTPase atlastin. *Nature* **460**(7258):978-83.

Ostlund, C., Folker, E. S., Choi, J. C., Gomes, E. R., Gundersen, G. G. and Worman, H. J. (2009) Dynamics and molecular interactions of linker of nucleoskeleton and cytoskeleton (LINC) complex proteins. *J Cell Sci* **122**(22):4099-108.

Oufattole, M., Park, J. H., Poxleitner, M., Jiang, L. and Rogers, J.C. (2005) Selective membrane protein internalization accompanies movement from the endoplasmic reticulum to the protein storage vacuole pathway in *Arabidopsis*. *Plant Cell* **17**(11):3066-80.

Palade, G. (1975) Intracellular aspects of the process of protein synthesis. *Science* **189**:347-358 .

Park, E.C., Shim, S. and Han, J. K. (2005) Identification and expression of XRTN2 and XRTN3 during *Xenopus* development. *Dev Dyn* **233**(1):240-7.

Park, E. C., Shim, S. and Han, J. K. (2007) Identification and expression of XRTN1-A and XRTN1-C in *Xenopus laevis*. *Dev Dyn* **236**(12):3545-53.

Pattison, R. J. and Amtmann, A. (2009) N-glycan production in the endoplasmic reticulum of plants. *Trends Plant Sci* **14**(2):92-9.

Pedrazzini, E., Giovinazzo, G., Bielli, A., de Virgilio, M., Frigerio, L., Pesca, M., Faoro, F., Bollini, R., Ceriotti, A. and Vitale, A. (1997) Protein quality control along the route to the plant vacuole. *Plant Cell* **9**:1869-1880.

Pedrazzini, E. (2009) Tail-Anchored Proteins in Plants. *J Plant Biol* **52**:88-101.

Phillipson, B. A., Pimpl, P., da Silva, L. L. P., Crofts, A. J., Taylor, J. P., Movafeghi, A., Robinson, D. G. and Denecke, J. (2001) Secretory bulk flow of soluble proteins is efficient and COPII dependent. *Plant Cell* **13**:2005–2020.

Pokrywka, N. J., Payne-Tobin, A., Raley-Susman, K. M. and Swartzman, S. (2009) Microtubules, the ER and Exu: new associations revealed by analysis of mini spindles mutations. *Mech Dev* **126**(5-6):289-300.

Pomorski, T., Holthuis, J. C., Herrmann, A. and van Meer, G. (2004) Tracking down lipid flippases and their biological functions. *J Cell Sci* **117**(6):805-13.

Porter, K. R., Claude, A., and Fullham, E.F. (1945) A study of tissue culture cells by electron microscopy: methods and preliminary observations. *J Exp Med* **81**:233-246.

Poulsen, L. R., López-Marqués, R. L. and Palmgren, M. G. (2008) Flippases: still more questions than answers. *Cell Mol Life Sci* **65**(20):3119-25.

Praefcke, G. J. and McMahon, H. T. (2004) The dynamin superfamily: universal membrane tubulation and fission molecules? *Nat Rev Mol Cell Biol* **5**(2):133-47.

Puhka, M., Vihinen, H., Joensuu, M. and Jokitalo, E. (2007) Endoplasmic reticulum remains continuous and undergoes sheet-to-tubule transformation during cell division in mammalian cells. *J Cell Biol* **179**(5):895-909.

Quader, H. & Schnepf, E. (1986) Endoplasmic reticulum and cytoplasmic streaming: fluorescence microscopical observations in adaxial epidermis cells of onion bulb scales. *Protoplasma* **131**:250-252.

Quader, H., Hofmann, A. and Schnepf, E. (1989) Reorganisation of the endoplasmic reticulum in epidermal cells of onion bulb scales after cold stress: involvement of cytoskeletal elements. *Planta* **177**:273-280.

Rahier, A., Darnet, S., Bouvier, F., Camara, B. and Bard, M. (2006) Molecular and enzymatic characterizations of novel bifunctional 3*β*-hydroxysteroid dehydrogenases/C-4 decarboxylases from *Arabidopsis thaliana*. *J Biol Chem* **281**: 27264-27277.

Rapoport, T. A. (2007) Protein translocation across the eukaryotic endoplasmic reticulum and bacterial plasma membranes. *Nature* **450**:663-669

Ridge, R. W., Uozumi, Y., Plazinski, J., Hurley, U. A. and Williamson, R. E. (1999) Developmental transitions and dynamics of the cortical ER of *Arabidopsis* cells seen with green fluorescent protein. *Plant Cell Physiol* **40**:1253-126.

Riemer, J., Bulleid, N. and Herrmann, J. M. (2009) Disulfide formation in the ER and mitochondria: two solutions to a common process. *Science* **324**(5932):1284-7.

Rismanchi, N., Soderblom, C., Stadler, J., Zhu, P. P. and Blackstone, C. (2008) Atlastin GTPases are required for Golgi apparatus and ER morphogenesis. *Hum Mol Genet* **17**(11):1591-604.

Rodriguez-Feo, J. A., Hellings, W. E., Verhoeven, B. A., Moll, F. L., de Kleijn, D. P., Prendergast, J., Gao, Y., van der Graaf, Y., Tellides, G., Sessa, W. C. and Pasterkamp, G. (2007) Low levels of Nogo-B in human carotid atherosclerotic plaques are associated with an atheromatous phenotype, restenosis, and stenosis severity. *Arterioscler Thromb Vasc Biol* **27**(6):1354-60.

Römer, W., Berland, L., Chambon, V., Gaus, K., Windschiegl, B., Tenza, D., Aly, M. R., Fraisier, V., Florent, J. C., Perrais, D., Lamaze, C., Raposo, G., Steinem, C., Sens, P., Bassereau, P. and Johannes, L. (2007) Shiga toxin induces tubular membrane invaginations for its uptake into cells. *Nature* **450**(7170):670-5.

Romisch, K. (2005) Endoplasmic reticulum-associated degradation. *Annu Rev Cell Dev Biol* **21**:435-56.

Ronchi, P., Colombo, S., Francolini, M. and Borgese, N. (2008) Transmembrane domain-dependent partitioning of membrane proteins within the endoplasmic reticulum. *J Cell Biol* **181**(1):105-18.

Runions, J., Brach, T., Kuhner, S., and Hawes, C. (2006) Photoactivation of GFP reveals protein dynamics within the endoplasmic reticulum membrane. *J Exp Bot* **57**:43-50.

Saint-Jore, C.M., Evins, J., Batoko, H., Brandizzi, F., Moore, I. and Hawes, C. (2002) Redistribution of membrane proteins between the Golgi apparatus and endoplasmic reticulum in plants is reversible and not dependent on cytoskeletal networks. *Plant J* **29**(5):661-678.

Salinas, S., Proukakis, C., Crosby, A. and Warner, T. T. (2008) Hereditary spastic paraplegia: clinical features and pathogenetic mechanisms. *Lancet Neurol* **7**:1127-1138.

Sato, K., Nishikawa, S. and Nakano, A. (1996) Membrane protein retrieval from the Golgi apparatus to the endoplasmic reticulum (ER): characterization of the RER1 gene product as a component involved in ER localization of Sec12p. *Mol Biol Cell* **6**(11):1459-77.

Sato, K., Ueda, T. and Nakano, A. (1999) The *Arabidopsis thaliana* RER1 gene family: its potential role in the endoplasmic reticulum localization of membrane proteins. *Plant Mol Biol* **41**(6):815-24.

Sato, K., Sato, M. and Nakano, A. (2003) Rer1p, a retrieval receptor for ER membrane proteins, recognizes transmembrane domains in multiple modes. *Mol Biol Cell* **14**(9):3605-16.

Schatz, G. and Dobberstein, B. (1996) Common principles of protein translocation across membranes. *Science* **271**(5255):1519-26.

Schiefelbein, J. W. and Somerville, C. (1990) Genetic Control of Root Hair Development in *Arabidopsis thaliana*. *Plant Cell* **2**(3):235-243.

Schuldiner, M., Metz, J., Schmid, V., Denic, V., Rakwalska, M., Schmitt, H. D., Schwappach, B. and Weissman, J. S. (2008) The GET complex mediates insertion of tail-anchored proteins into the ER membrane. *Cell* **134**(4):634-45.

Senden, N. H., Timmer, E. D., Boers, J. E., van de Velde ,H. J., Roebroek, A. J., Van de Ven, W. J., Broers, J. L. and Ramaekers, F. C. (1996) Neuroendocrine-specific protein C (NSP-C): subcellular localization and differential expression in relation to NSP-A. *Eur J Cell Biol* **69**(3):197-213.

Sheetz, M. P. and Singer, S. J. (1974) Biological membranes as bilayer couples. A molecular mechanism of drug–erythrocyte interactions. *Proc Natl Acad Sci USA* **71**:4457-4461.

Shibata, Y., Voeltz, G. K. and Rapoport, T. A. (2006) Rough sheets and smooth tubules. *Cell* **126**(3):435-9.

Shibata, Y., Voss, C., Rist, J. M., Hu, J., Rapoport, T. A., Prinz, W. A. and Voeltz, G. K. (2008) The reticulon and DP1/Yop1p proteins form immobile oligomers in the tubular endoplasmic reticulum. *J Biol Chem* **283**(27):18892-904.

Shibata, Y., Hu, J., Kozlov, M. M. and Rapoport, T. A. (2009) Mechanisms shaping the membranes of cellular organelles. *Annu Rev Cell Dev Biol* **25**:329-54.

Shimada, T., Fuji, K., Tamura, K., Kondo, M., Nishimura, M. and Hara-Nishimura, I. (2003) Vacuolar sorting receptor for seed storage proteins in *Arabidopsis thaliana*. *Proc Natl Acad Sci U S A* **100**(26):16095-100.

Shimada, T. L., Shimada, T., Takahashi, H., Fukao, Y. and Hara-Nishimura, I. (2008) A novel role for oleosins in freezing tolerance of oilseeds in *Arabidopsis thaliana*. *Plant J* **55**(5):798-809.

Shnyrova, A., Frolov, V. A. and Zimmerberg, J. (2008) ER biogenesis: self-assembly of tubular topology by protein hairpins. *Curr Biol* **18**(11):474-6.

Sironen, R. K., Karjalainen, H. M., Törrönen, K. J., Elo, M. A., Hyttinen, M. M., Helminen, H. J. and Lammi, M. J. (2004) Reticulon 4 in chondrocytic cells: barosensitivity and intracellular localization. *Int J Biochem Cell Biol* **36**(8):1521-31.

Snapp, E. L., Hegde, R. S., Francolini, M., Lombardo, F., Colombo, S., Pedrazzini, E., Borgese, N. and Lippincott-Schwartz, J. (2003) Formation of stacked ER cisternae by low affinity protein interactions. *J Cell Biol* **163**(2):257-69.

Spandl, J., White, D. J., Peychl, J. and Thiele, C. (2009) Live cell multicolor imaging of lipid droplets with a new dye, LD540. *Traffic* **10**(11):1579-84.

Sparkes, I. A., Frigerio, L., Tolley, N. and Hawes, C. (2009a) The plant endoplasmic reticulum: a cell-wide web. *Biochem J* **423**(2):145-55.

Sparkes, I. A., Ketelaar, T., De Ruijter, N. C. A. and Hawes, C. (2009b) Grab a Golgi: laser trapping of Golgi bodies reveals in vivo interactions with the endoplasmic reticulum. *Traffic* **10**:567-571.

Sparkes, I., Runions, J., Hawes, C. and Griffing L. (2009c) Movement and remodeling of the endoplasmic reticulum in nondividing cells of tobacco leaves. *Plant Cell* **21**(12):3937-49.

Sparkes, I., Tolley, N., Aller, I., Svozil, J., Osterrieder, A., Botchway, S. , Mueller, C., Frigerio, L. and Hawes, C. (2010) Five plant reticulon isoforms share ER localisation, topology, ER membrane shaping properties and the ability to form both homo- and heterotypic interactions. *Plant Cell* **In press**.

Spiess, M. (1995) Heads or tails: what determines the orientation of proteins in the membrane. *FEBS Lett* **369**:76-79.

Staehelin, L., A. (1997) The plant ER: a dynamic organelle composed of a large number of discrete functional domains. *Plant J* **11**(6):1151-65.

Steiner, P., Kulangara, K., Sarria, J. C., Glauser, L., Regazzi, R. and Hirling, H. (2004) Reticulon 1-C/neuroendocrine-specific protein-C interacts with SNARE proteins. *J Neurochem* **89**(3):569-80.

Tagami, S., Eguchi, Y., Kinoshita, M., Takeda, M. and Tsujimoto ,Y. (2000) A novel protein, RTN-XS, interacts with both Bcl-XL and Bcl-2 on endoplasmic reticulum and reduces their anti-apoptotic activity. *Oncogene* **19**(50):5736-46.

Teasdale, R. D. and Jackson, M. R. (1996) Signal-mediated sorting of membrane proteins between the endoplasmic reticulum and the golgi apparatus. *Annu Rev Cell Dev Biol* **12**:27-54.

Teng, F. Y. and Tang, B. L. (2008a) Cell autonomous function of Nogo and reticulons: The emerging story at the endoplasmic reticulum. *J Cell Physiol* **216**(2):303-8.

Teng, F. Y. and Tang, B. L. (2008b) Nogo-A and Nogo-66 receptor in amyotrophic lateral sclerosis. *J Cell Mol Med* **12**(4):1199-204.

Toufighi, K., Brady, S. M., Austin, R., Ly, E. and Provart, N. J. (2005) The Botany Array Resource: e-Northerns, Expression Angling, and promoter analyses. *Plant J* **43**(1):153-63.

Toyooka, K., Okamoto, T. and Minamikawa, T. (2000) Mass transport of proform of a KDEL- tailed cysteine protease (SH-EP) to protein storage vacuoles by endoplasmic reticulum-derived vesicle is involved in protein mobilization in germinating seeds. *J Cell Biol* **148**:453-463.

Tuteja, R. (2005) Type I signal peptidase: An overview. *Arch Biochem Biophys* **441**:107-111.

Tzen, J. T., Lie, G. C. and Huang, A. H. (1992) Characterization of the charged components and their topology on the surface of plant seed oil bodies. *J Biol Chem* **267**(22):15626-34.

van de Velde, H. J., Roebroek, A. J., Senden, N. H., Ramaekers, F. C. and Van de Ven, W. J. (1994) NSP-encoded reticulons, neuroendocrine proteins of a novel gene family associated with membranes of the endoplasmic reticulum. *J Cell Sci* **107**(9):2403-16.

van Meer, G., Voelker, D. R. and Feigenson, G. W. (2008) Membrane lipids: where they are and how they behave. *Nat Rev Mol Cell Biol* **9**:112-24.

Vitale, A., Bielli, A. and Ceriotti, A. (1995) The binding protein associates with monomeric phaseolin. *Plant Physiol* **107**:1411-1418.

Vitale, A. and Denecke, J. (1999) The endoplasmic reticulum-gateway of the secretory pathway. *Plant Cell* **11**(4):615-28.

Voeltz ,G. K., Rolls, M. M. and Rapoport, T. A. (2002) Structural organization of the endoplasmic reticulum. *EMBO Rep* **3**(10):944-50.

Voeltz, G. K., Prinz, W. A., Shibata, Y., Rist, J. M. and Rapoport, T. A. (2006) A class of membrane proteins shaping the tubular endoplasmic reticulum. *Cell* **124**(3):573-86.

Voeltz, G. K. and Prinz, W. A. (2007) Sheets, ribbons and tubules - how organelles get their shape. *Nat Rev Mol Cell Biol* **8**(3):258-64.

Wakana, Y., Koyama, S., Nakajima, K., Hatsuzawa, K., Nagahama, M., Tani, K., Hauri, H. P., Melançon, P. and Tagaya, M. (2005) Reticulon 3 is involved in membrane trafficking between the endoplasmic reticulum and Golgi. *Biochem Biophys Res Commun* **334**(4):1198-205.

Wakefield, S. & Tear, G. (2006) The Drosophila reticulon, Rtnl-1, has multiple differentially expressed isoforms that are associated with a sub-compartment of the endoplasmic reticulum. *Cell Mol Life Sci* **63**(17):2027-38.

Walter, M., Chaban, C., Schütze, K., Batistic, O., Weckermann, K., Näke, C., Blazevic, D., Grefen, C., Schumacher, K., Oecking, C., Harter, K. and Kudla, J. (2004) Visualization of protein interactions in living plant cells using bimolecular fluorescence complementation. *Plant J* **40**(3):428-38.

Wang, H., Lockwood, S. K., Hoeltzel, M. F. and Schiefelbein, J. W. (1997) The ROOT HAIR DEFECTIVE 3 gene encodes an evolutionarily conserved protein with GTP-binding motifs and is required for regulated cell enlargement in *Arabidopsis*. *Genes Dev* **11**(6):799-811.

Wang, H., Lee, M. M. and Schiefelbein, J. W. (2002) Regulation of the cell expansion gene RHD3 during *Arabidopsis* development. *Plant Physiol* **129**(2):638-49.

Watari, A. & Yutsudo, M. (2003) Multi-functional gene ASY/Nogo/RTN-X/RTN4: apoptosis, tumor suppression, and inhibition of neuronal regeneration. *Apoptosis* **8**(1):5-9.

Wessels, H. P. and Spiess, M. (1988) Insertion of a multispanning membrane protein occurs sequentially and requires only one signal sequence. *Cell* **55**:61-70.

Wildasin, K. (2004) Role of reticulon proteins in Alzheimer's disease. *Lancet Neurol* **3**(10):576.

Winter, D., Vinegar, B., Nahal, H., Ammar, R., Wilson, G. V. and Provart, N. J. (2007) An "electronic Fluorescent Pictograph" browser for exploring and analyzing large-scale biological data sets. *PLoS One* **2**(1):e718.

Worman, H. J. and Gundersen, G. G. (2006) Here come the SUNs: a nucleocytoskeletal missing link. *Trends Cell Biol* **16**(2):67-9.

Woźniak, M. J., Bola, B., Brownhill, K., Yang, Y. C., Levakova, V. and Allan, V. J. (2009) Role of kinesin-1 and cytoplasmic dynein in endoplasmic reticulum movement in VERO cells. *J Cell Sci* **122**(12):1979-89.

Wright, G. D., Arlt, J., Poon, W. C. K. and Read, N. D. (2007) Optical tweezers micromanipulation of filamentous fungi. *Fungal Genet Biol* **44**:1-13.

Yan, R., Shi, Q., Hu, X. and Zhou, X. (2006) Reticulon proteins: emerging players in neurodegenerative diseases. *Cell Mol Life Sci* **63**(7-8):877-89.

Yang, Y. S. & Strittmatter, S. M. (2007) The reticulons: a family of proteins with diverse functions. *Genome Biol* **8**(12):234.

Yang, Y. S., Harel, N. Y. and Strittmatter, S. M. (2009) Reticulon-4A (Nogo-A) redistributes protein disulfide isomerase to protect mice from SOD1-dependent amyotrophic lateral sclerosis. *J Neurosci* **29**(44):13850-9.

Young, B. P., Craven, R. A., Reid, P. J., Willer, M. and Stirling, C. J. (2001) Sec63p and Kar2p are required for the translocation of SRP-dependent precursors into the yeast endoplasmic reticulum in vivo. *EMBO J* **20**:262-271.

Zamyatnin, A. A., Solovyex, A. G., Bozhkov, P. V., Valkonen, J. P., Morozov, S. Y. and Savenkov, E. I. (2006) Assessment of the integral membrane protein topology in living cells. *Plant J* **46**(1):145-154.

Zheng, H., Kunst, L., Hawes, C. and Moore, I. (2004) A GFP-based assay reveals a role for RHD3 in transport between the endoplasmic reticulum and Golgi apparatus. *Plant J* **37**(3):398-414.

Zimmerberg, J. and Kozlov, M. M. (2006) How proteins produce cellular membrane curvature. *Nat Rev Mol Cell Biol* **7**(1):9-19.

Appendix

Table A1 Oligonucleotide primers used to generate constructs

Construct	**Primer**	**Sequence 5' – 3'**
Sequencing primers	pBluescript fwd	CGCCATTCGCCATTCAGG
	pBluescript rev	GCGAGTCAGTGAGCGAGG
	35S-CaMV fwd	CCTTCGCAAGACCCTTCCTC
	35S-CaMV rev	CCCTTATCTGGGAACTACTC
	pVKH18-En6 fwd	CCTTCGCAAGACCCTTCCTC
	pVKH18-En6 rev	CATGCAAGACCGGCAACAG
	pGreenII-0179 fwd	GTCGGTGCTGAGAGTGAATGG
	pGreenII-0179 rev	GTAGTTGTACTCCAGCTTGTG
RTN untagged	*XbaI* fwd	ATCGCGCTTCTAGAATGGCCAACGAC
	SacI rev	GCGCGCGCGTCGACCTCTGATTTTTTCACTTTCT CT
RTN-myc	*XbaI* fwd	ATCGCGCTTCTAGAATGGCCAACGAC
	SacI rev	CGCGCGCGGAGCTCTTACAGATCCTCTTCAGAG ATGAGTTTCTGCTCCTCTGATTTTTTC
myc-RTN	*XbaI* fwd	GACGACGCTCTAGAATGGAGCAGAAACTCATC TCTGAAGAGGATCTGGCCAACGACGTGACCAA AGATC
	SacI rev	GCGCGCGCGTCGACCTCTGATTTTTTCACTTTCT CT
RTN-myc-KKSE	*XbaI* fwd	ATCGCGCTTCTAGAATGGCCAACGAC
	SacI rev	GACGACGC GAGCTC CTA CTCTGATTTTTT CAGATCCTCTTCAGAGATGAGTTTCTGCTC CACTTTCTCTTCTGTACCATGGTGT
YFP-RTN	*XbaI* fwd	GCAGCAGCTCTAGAATGGGCAGCAAGGG
	Fusion fwd	CTGTACAAGGTGATCGCCAACGACGTGACC
	Fusion rev	GGTCACGTCGTTGGCGATCACCTTGTACAG
	SacI rev	GCAGCAGCGAGCTCCTACTCTGATTTTTTCACT TTC
RTN-YFP	*XbaI* fwd	ACTGCGCTTCTAGAATGGCCAACGAC
	Fusion fwd	GTGAAAAAATCAGAGGGCAGCAAGGGCGAG
	Fusion rev	CTCGCCCTTGCTGCCCTCTGATTTTTTCAC
	SacI rev	GCAGCAGCGAGCTCCTAGATCACCTTGTACAGC TCGTC

Table A1 (continued)

RTN-YFP-KKSE	*XbaI* fwd	ACTGCGCTTCTAGAATGGCCAACGAC
	Fusion fwd	ACAGAAGAGAAAGTGGGCAGCAAGGGCGAG
	Fusion rev	CTCGCCCTTGCTGCCCACTTTCTCTTCTGT
	SacI rev	GACGACGCGAGCTCCTACTCTGATTTTTTGATA CCTTGTACAGCTCGTCCATG
myc-RTN-ΔKKSE	*XbaI* fwd	GACGACGCTCTAGAATGGAGCAGAAACTCATC TCTGAAGAGGATCTGGCCAACGACGTGACCAA AGATC
	SacI rev	GCAGCAGCGAGCTCCTACACTTTCTCTTCTGTA CCATGGTG
myc-RTN-ΔC	*XbaI* fwd	GACGACGCTCTAGAATGGAGCAGAAACTCATC TCTGAAGAGGATCTGGCCAACGACGTGACCAA AGATC
	SacI rev	GCAGCAGCGAGCTCCTACAGATCCTCTTCAGAG ATGAGTTTCTGCTCCTCTTCCCACAACTTTGGA ACCGTC
ΔN-RTN-myc	*XbaI* fwd	GCAGCAGCTCTAGAATGGAGCAGAAACTCATC TCTGAAGAGGATCTGCTGGCCTTCTCTACACTC CTGGTCTC
	SacI rev	CGCGCGCGGAGCTCTTACAGATCCTCTTCAGAG ATGAGTTTCTGCTCCTCTGATTTTTTC
ΔN-RRKK-RTN-myc	*XbaI* fwd	GCAGCAGCTCTAGAATGGAGCAGAAACTCATC TCTGAAGAGGATCTGAGGAGGAAGAAACTGGC CTTCTCTAC
	SacI rev	CGCGCGCGGAGCTCTTACAGATCCTCTTCAGAG ATGAGTTTCTGCTCCTCTGATTTTTTC
YFP-RTN-ΔKKSE	*XbaI* fwd	GCAGCAGCTCTAGAATGGGCAGCAAGGG
	SacI rev	GCAGCAGCGAGCTCCTACACTTTCTCTTCTGTA CCATGGTG
YFP-RTN-ΔC	*XbaI* fwd	GCAGCAGCTCTAGAATGGGCAGCAAGGG
	SacI rev	GCAGCAGCGAGCTCCTACAGATCCTCTTCAGAG ATGAGTTTCTGCTCCTCTTCCCACAACTTTGGA ACCGTC

Table A1 (continued)

ΔN-RTN-YFP	*XbaI* fwd	GCAGCAGCTCTAGAATGGAGCAGAAACTCATC TCTGAAGAGGATCTGCTGGCCTTCTCTACACTC CTGGTCTC
	SacI rev	GCAGCAGCGAGCTCCTAGATCACCTTGTACAGC TCGTC
ΔN-RRKK-RTN-YFP	*XbaI* fwd	GCAGCAGCTCTAGAATGGAGCAGAAACTCATC TCTGAAGAGGATCTGAGGAGGAAGAAACTGGC CTTCTCTAC
	SacI rev	GCAGCAGCGAGCTCCTAGATCACCTTGTACAGC TCGTC
myc-RTN–ΔLoop	*XbaI* fwd	GACGACGCTCTAGAATGGAGCAGAAACTCATC TCTGAAGAGGATCTGGCCAACGACGTGACCAA AGATC
	Fusion fwd	GAGCAGAAACTCATCTCTGAAGAGGATCTGGA GCAGAAACTCATCTCTGAAGAGGATCTGTGGA TGTTTCGAGTCGGTGCT
	Fusion rev	CAGATCCTCTTCAGAGATGAGTTTCTGCTCCAG ATCCTCTTCAGAGATGAGTTTCTGCTCGAGAAG GCGAAGTAAACTCCC
	SacI rev	GCGCGCGCGTCGACCTCTGATTTTTTCACTTTCT CT
YFP-RTN –ΔLoop	*XbaI* fwd	GCAGCAGCTCTAGAATGGGCAGCAAGGG
	Fusion fwd	GAGCAGAAACTCATCTCTGAAGAGGATCTGGA GCAGAAACTCATCTCTGAAGAGGATCTGTGGA TGTTTCGAGTCGGTGCT
	Fusion rev	CAGATCCTCTTCAGAGATGAGTTTCTGCTCCAG ATCCTCTTCAGAGATGAGTTTCTGCTCGAGAAG GCGAAGTAAACTCCC
	SacI rev	GCGCGCGCGTCGACCTCTGATTTTTTCACTTTCT CT
YFP-RTN –ΔTM1	*XbaI* fwd	GCAGCAGCTCTAGAATGGGCAGCAAGGG
	Fusion fwd	ACCATAACCATTGTATCTTGGATCG
	Fusion rev	GCTAAGTAAAATCCATGTCGATGTT
	SacI rev	GCAGCAGCGAGCTCCTACTCTGATTTTTTCACT TTC

Table A1 (continued)

YFP-RTN –ΔTM2	*XbaI* fwd	GCAGCAGCTCTAGAATGGGCAGCAAGGG
	Fusion fwd	ATCGCAGTCGTCTCTATGATTTTCC
	Fusion rev	GGTTATGGTGCTAAGTAAAATCCAT
	SacI rev	GCAGCAGCGAGCTCCTACTCTGATTTTTTCACT TTC
YFP-RTN –ΔTM3	*XbaI* fwd	GCAGCAGCTCTAGAATGGGCAGCAAGGG
	Fusion fwd	TTGTCAAGAAATGGGAACCTTCTCG
	Fusion rev	GGTTCTCGCGAAAACAAACCATTCA
	SacI rev	GCAGCAGCGAGCTCCTACTCTGATTTTTTCACT TTC
YFP-RTN –ΔTM4	*XbaI* fwd	GCAGCAGCTCTAGAATGGGCAGCAAGGG
	Fusion fwd	TTCCATACTTGTCTCTTCATCGGTT
	Fusion rev	TCTTGACAAGGTTCTCGCGAAAACA
	SacI rev	GCAGCAGCGAGCTCCTACTCTGATTTTTTCACT TTC
Native-RTN-YFP	*KpnI* fwd	CACATAGGTACCCTCGACAAGATAATTACCTTT CCTGG
	XhoI rev	CACATACTCGAGCTCTGATTTTTTCACTTTCTCT TCTGTACC
YN-RTN	*XhoI* fwd	GGGCTCGAGATGGTGAGCAAGGGCGAGGAG
	Fusion fwd	AACGTCTATATCATGGCCAACGACGTGACC
	Fusion rev	GGTCACGTCGTTGGCCATGATATAGACGTT
	XbaI rev	CCCTCTAGACTACTCTGATTTTTTCACTTTC
YC-RTN	*XhoI* fwd	CCCCTCGAGATGGCCGACAAGCAGAAGAACGG C
	Fusion fwd	GACGAGCTGTACAAGGCCAACGACGTGACC
	Fusion rev	GGTCACGTCGTTGGCCTTGTACAGCTCGTC
	XbaI rev	CCCTCTAGACTACTCTGATTTTTTCACTTTC
RTN-YN	*XhoI* fwd	GGGCTCGAGATGGCCAACGACGTGACCAA
	Fusion fwd	GTGAAAAAATCAGAGGTGAGCAAGGGCGAG
	Fusion rev	CTCGCCCTTGCTCACCTCTGATTTTTTCAC
	XbaI rev	CCCTCTAGATTACATGATATAGACGTTGTGGC
RTN-YC	*XhoI* fwd	GGGCTCGAGATGGCCAACGACGTGACCAA
	Fusion fwd	GTGAAAAAATCAGAGGCCGACAAGCAGAAG
	Fusion rev	CTTCTGCTTGTCGGCCTCTGATTTTTTCAC
	XbaI rev	CCCTCTAGATTACTTGTACAGCTCGTCCATG

Table A1 (continued)

RTN –YC–RTN	*XhoI* fwd	GGGCTCGAGATGGCCAACGACGTGACCAA
	Fusion 1	TCGGAGGAGTTTGTAGCCGACAAGCAGAAG
	Fusion 2	CTTCTGCTTGTCGGCTACAAACTCCTCCGA
	Fusion 3	GACGAGCTGTACAAGGTGGAGACAGTGAGG
	Fusion 4	CCTCACTGTCTCCACCTTGTACAGCTCGTC
	XbaI rev	CCCTCTAGACTACTCTGATTTTTTCACTTTC
RT-PCR	RTN fwd	GGTCGAACCGGAACTATCAG
	RTN rev	GTAACACATATATTTTACAGTAAAAGACAA
	Actin fwd	CACCATCATCACAAGCATCC
	Actin rev	TGCTGACCGTATGAGCAAAG
KO Screening	RTN (+281) fwd	CACAACCTTACCACGACGTGTTAC
	RTN (-85) rev	AGCCCAGTTTCTTCCTCCTC
	T-DNA LBb1.3	ATTTTGCCGATTTCGGAAC

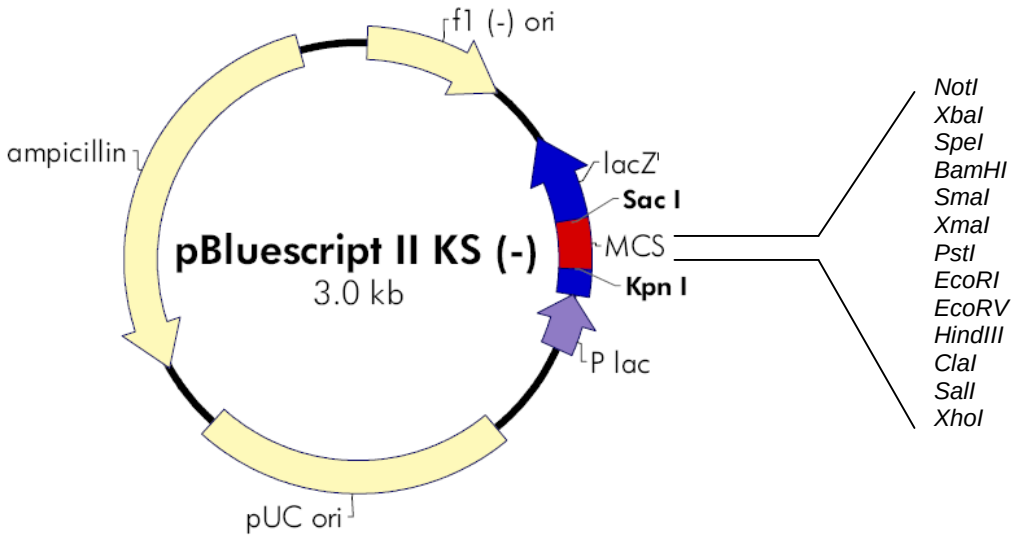

Figure A1 Vector map of pBluescript sub-cloning vector. pBluescript (Stratagene) is a small (3kb) sub-cloning vector conferring ampicillin resistance (100µg/ml) in bacteria. It has a wide range of cloning sites which interrupt the *lacZ* gene for blue/white colony screening.

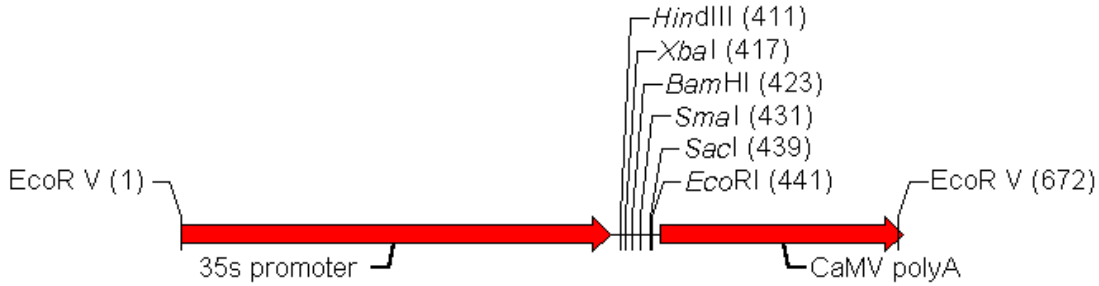

Figure A2 Vector map of 35S-CaMV PEG-mediated transfection vector. 35S-CaMV (Hellens *et al.*, 2000) is a small (3kb) vector conferring ampicillin resistance (100µg/ml) in bacteria. It has a limited number of cloning sites which are positioned between a 35S promoter and terminator. This vector can be used for sub-cloning and PEG-mediated transfections.

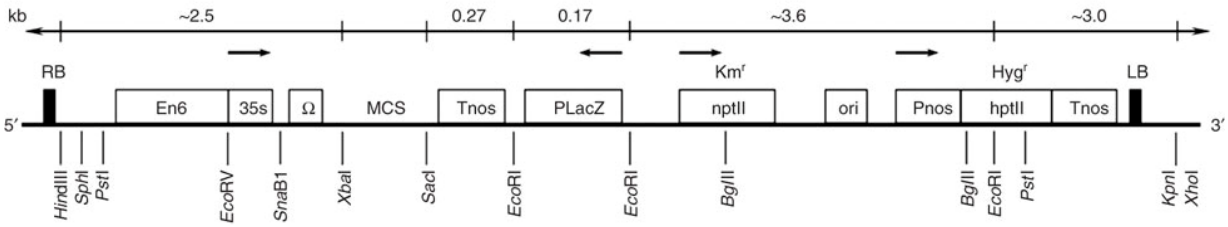

Figure A3 Vector map of pVKH18-En6 plant transformation vector. pVKH18-En6 (Moore *et al*., 1998) is a 14kb plant binary vector including a 9kb T-DNA region containing a 6x enhanced 35S CaMV promoter and a nos terminator between the left and right borders. It confers kanamycin (50µg/ml) resistance in bacteria and hygromycin (20µg/ml) resistance in plants, and contains only two restriction sites; *XbaI* and *SacI*.

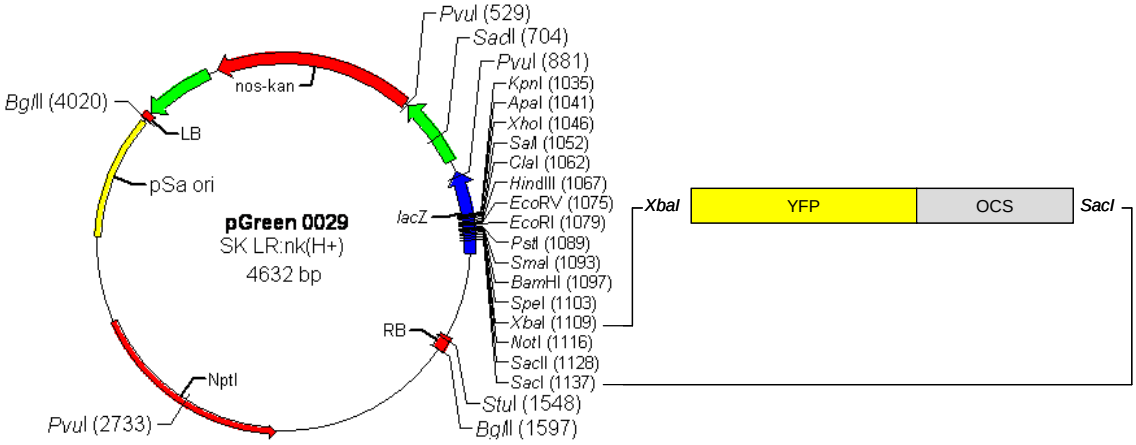

Figure A4 Vector map of pGreenII-0029 YFP-OCS plant transformation vector. pGreenII-0029 (Hellens *et al*., 2000) is a 4.6kb plant binary vector containing YFP and an octane synthase (OCS) terminator. It confers kanamycin (50µg/ml) resistance in bacteria and plants. It has a wide range of cloning sites which interrupt the *lacZ* gene for blue/white colony screening.

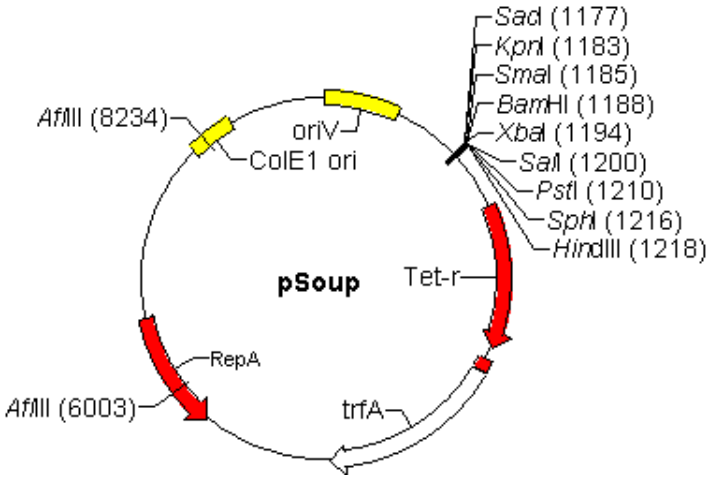

Figure A5 Vector map of pSoup plant transformation helper plasmid. pSoup (Hellens *et al*., 2000) is a plant binary helper vector conferring tetracycline (4µg/ml) resistance in bacteria and is pre-transformed in the *Agrobacterium tumefaciens* strain C58.

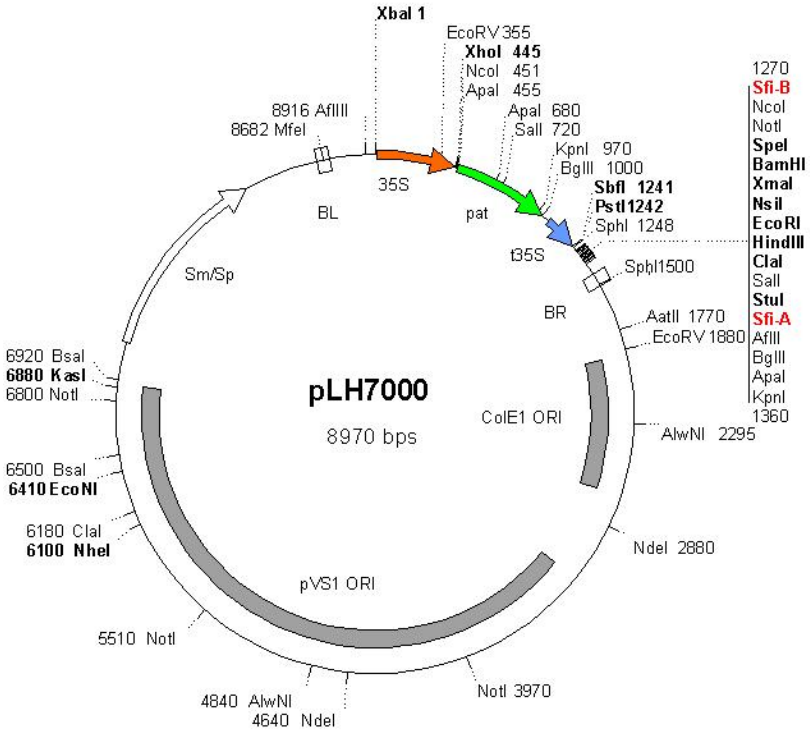

Figure A6 Vector map of pLH7000 plant transformation vector. pLH7000 (Hausmann & Töpfer, 1999) is a 9kb plant binary vector used for Bi-molecular Fluorescence Complementation (BiFC). It confers streptomycin (100µg/ml) and Spectinomycin (100µg/ml) resistance in bacteria and contains a 35S CaMV promoter and terminator.

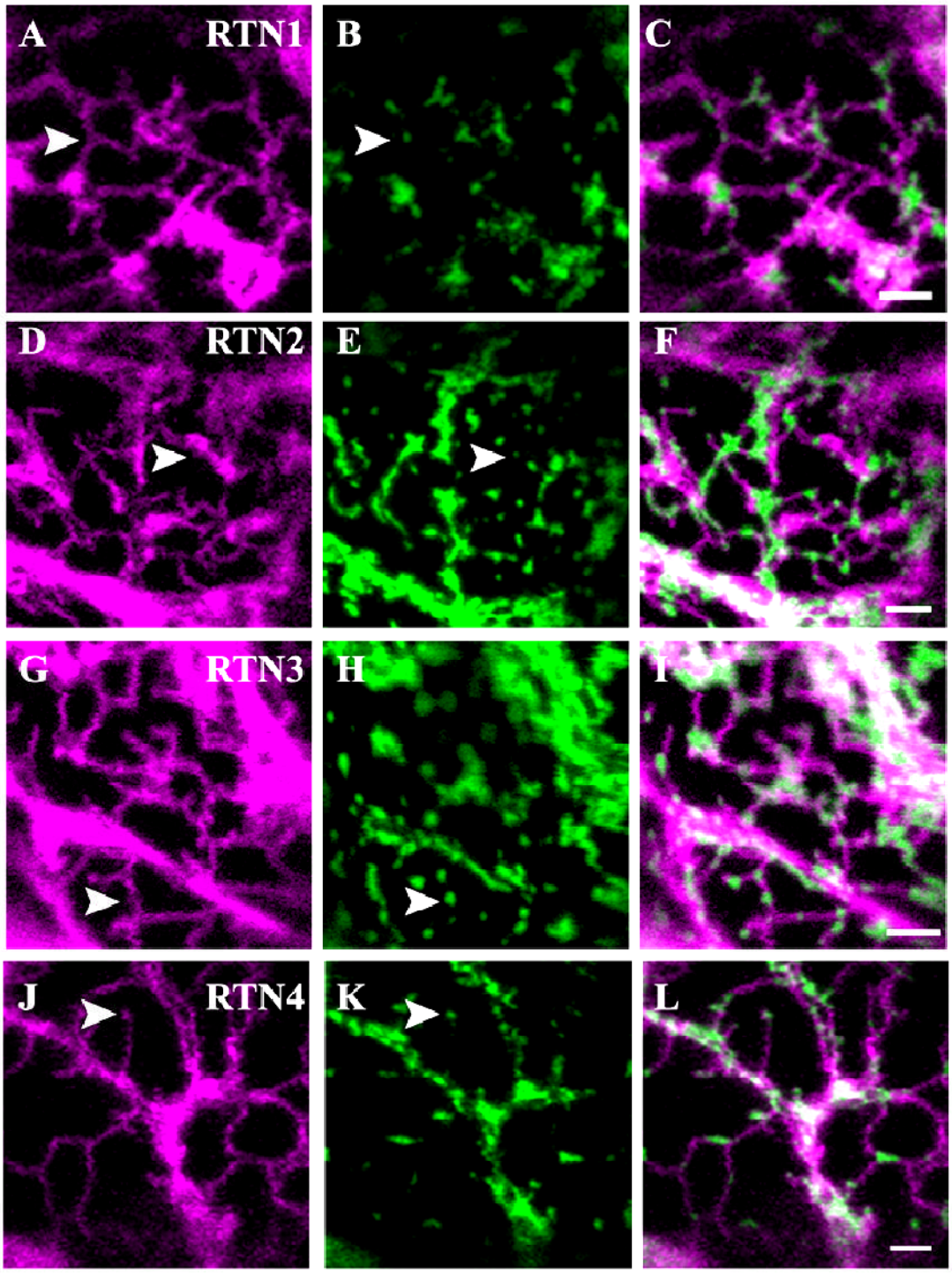

Figure A7 Transient co-expression of *Arabidopsis* YFP-RTN1-4 with GFP-HDEL in tobacco leaf epidermal cells. YFP-tagged RTN1-4 (magenta) co-expressed with ER marker GFP-HDEL (green). Merged images shown in right-hand column. Image modified from Sparkes *et al.*, (2010). Arrowheads represent constriction points. Scale bars = 2 µm.

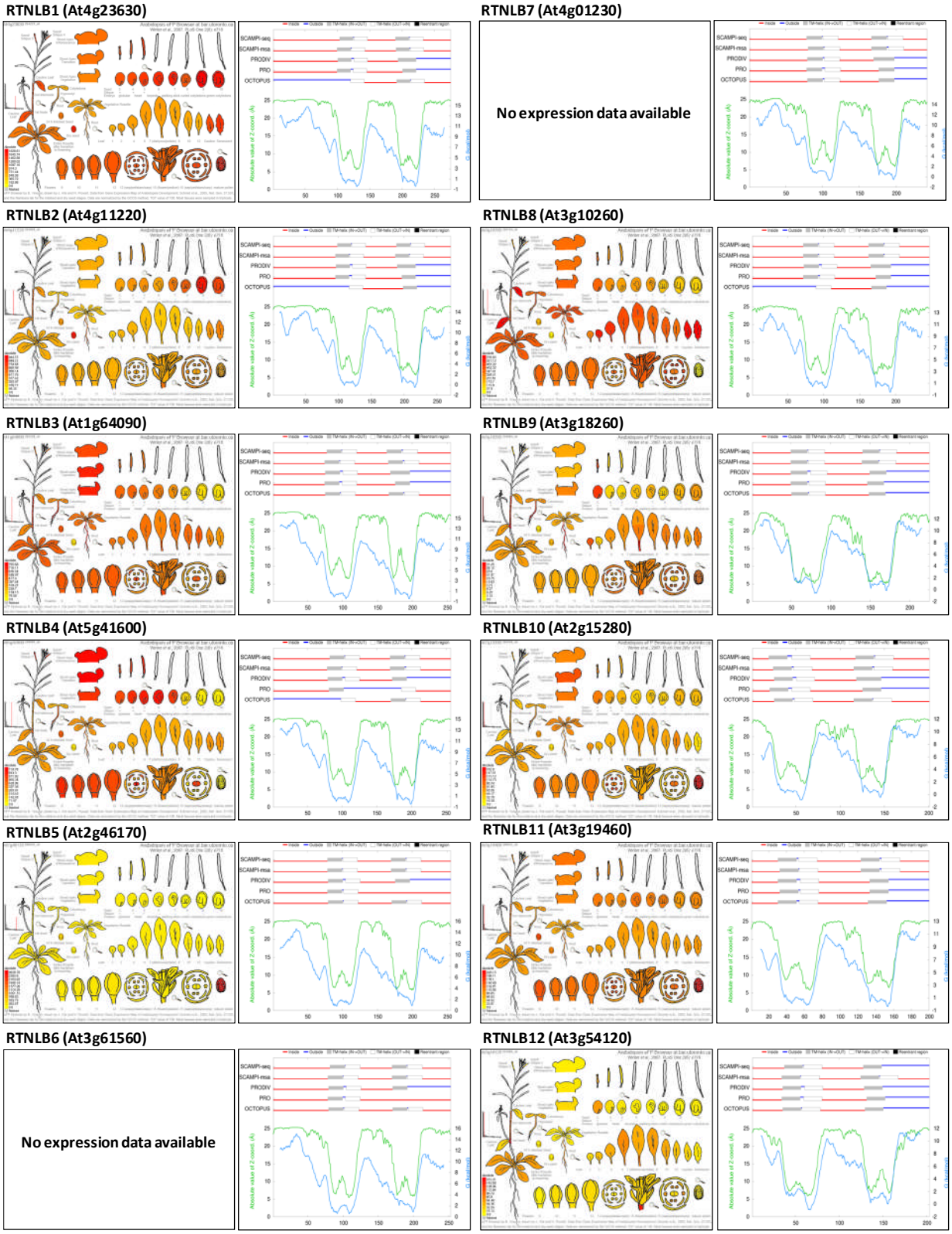

Figure A8 Expression profiles and topology analysis of the 21 *Arabidopsis* RTN genes using eFP Browser (Winter *et al*., 2007) and TOPCONS (Bernsel *et al*., 2009), respectively.

RTNLB13 (At2g23640)

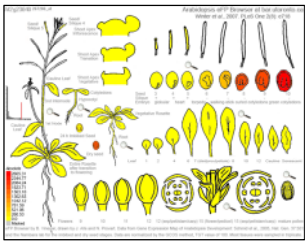

RTNLB19 (At2g26260)*

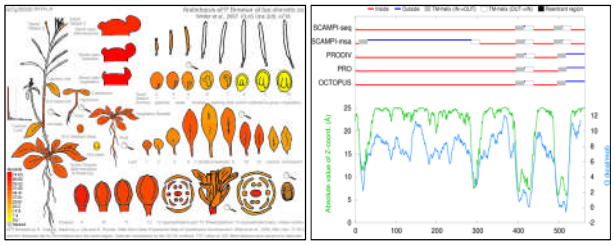

RTNLB14 (At1g68230)

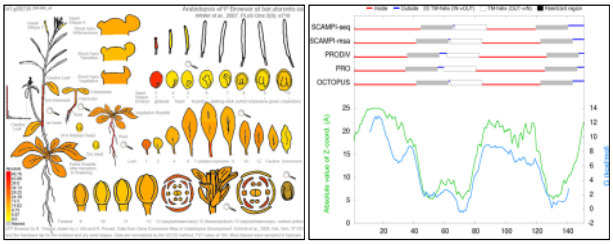

RTNLB20 (At2g43420)*

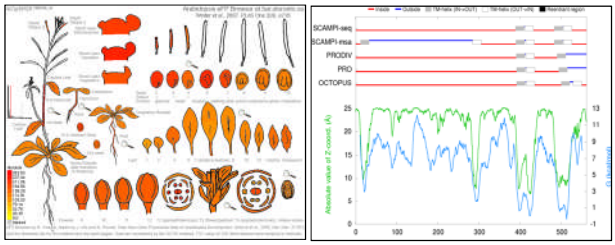

RTNLB15 (At2g01240)

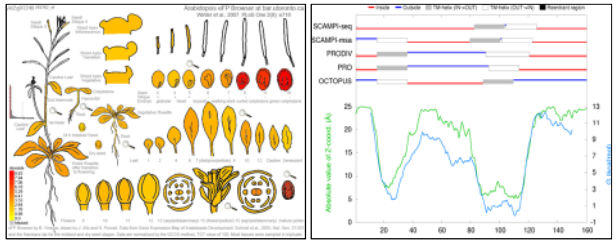

RTNLB21 (At5g58000)*

No expression data available

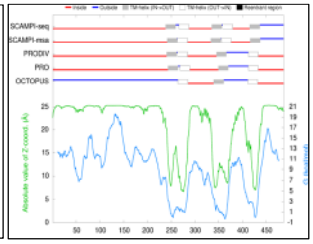

RTNLB16 (At3g10915)

No expression data available

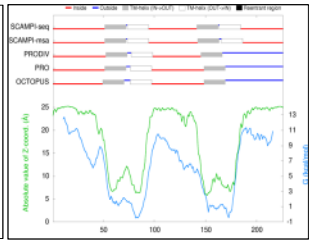

RTNLB17 (At2g20590)*

No expression data available

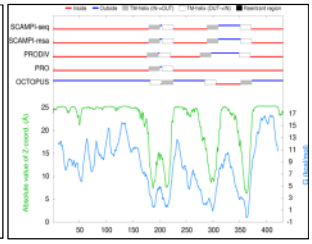

RTNLB18 (At4g28430)*

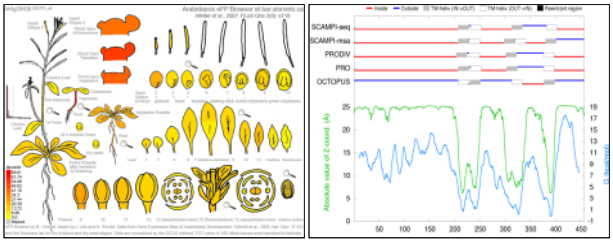

Figure A8 (continued) * = Proposed enzyme-linked RTNs

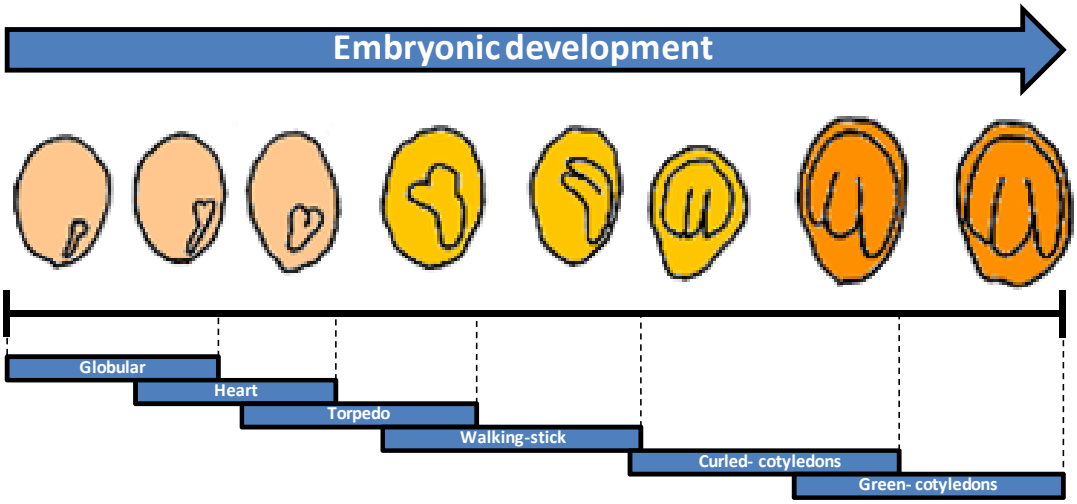

Figure A9 Stages of development during embryonic maturation. Image modified from eFP Browser (Winter *et al*., 2007).

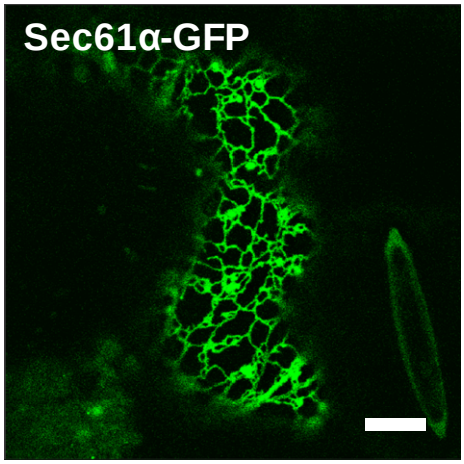

Figure A10 Transient expression of Sec61α-GFP in tobacco leaf epidermal cells. Sec61α-GFP was cloned into the plant binary vector pGreenII-0029 and expressed in tobacco cells using *Agrobacterium*-mediated infiltration. Scale bar = 20 µm.

MANDVTKDPTPKSDIVEDIYLWRRKKLAFSTLLVSTSTWILLS**FYGFT**

TIT**IVSWIG**IAVVSMIFLWGSLLRLLSKVEPELSGLEVSEEFVVETVR

SCRMLMEEMVR**WMFRVGAESEWFVFART**VLGFWILSR**IGNLLD**FHTCL

FIGLVMGLTVPKLWEEYGDQIQKHLGSLKDKSKGAYNTTHEKILEMKN

KLHHGTEEKVKKSE

Stop-transfer signal, Transmembrane domain, **ΔTM mutants**, ER-retrieval motif

Total length= 206 residues, N-terminus=22, TM1=22, TM2=23, Loop=33, TM3=23, TM4=23, C-=49, MW=~25 kDa

Figure A11 Amino acid sequence of RTN13

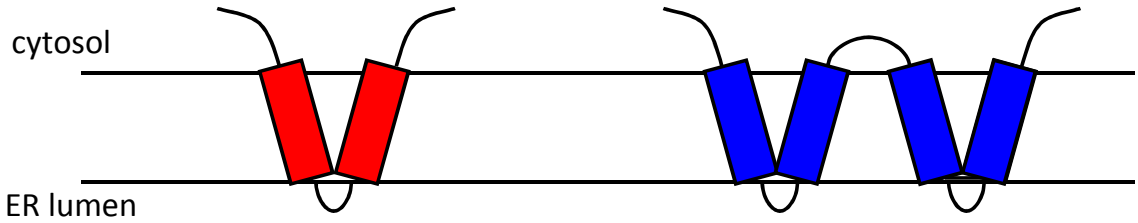

Figure A12 Proposed structures of reticulons

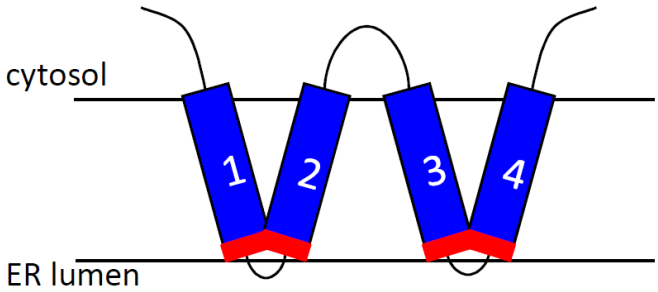

Figure A13 Representation of ΔTM shortenings

Publications

Traffic 2008; **9:** 94–102
Blackwell Munksgaard

doi: 10.1111/j.1600-0854.2007.00670.x

Overexpression of a Plant Reticulon Remodels the Lumen of the Cortical Endoplasmic Reticulum but Does not Perturb Protein Transport

Nicholas Tolley[1,†], Imogen A. Sparkes[2,†], Paul R. Hunter[1], Christian P. Craddock[1], James Nuttall[1], Lynne M. Roberts[1], Chris Hawes[2], Emanuela Pedrazzini[3] and Lorenzo Frigerio[1,*]

[1]Department of Biological Sciences, University of Warwick, Coventry CV4 7AL, UK
[2]School of Life Sciences, Oxford Brookes University, Gipsy Lane, Oxford OX3 0BP, UK
[3]Istituto di Biologia e Biotecnologia Agraria-Consiglio Nazionale delle Ricerche, via Bassini 15, 20133 Milano, Italy
**Corresponding author: Lorenzo Frigerio, l.frigerio@warwick.ac.uk*
†*These authors contributed equally to this work.*

We have cloned a member of the reticulon (RTN) family of *Arabidopsis thaliana* (RTNLB13). When fused to yellow fluorescent protein (YFP) and expressed in tobacco leaf epidermal cells, RTNLB13 is localized in the endoplasmic reticulum (ER). Coexpression of a soluble ER luminal marker reveals that YFP-tagged, myc-tagged or untagged RTNLB13 induces severe morphological changes to the lumen of the ER. We show, using fluorescence recovery after photobleaching (FRAP) analysis, that RTNLB13 overexpression greatly reduces diffusion of soluble proteins within the ER lumen, possibly by introducing constrictions into the membrane. In spite of this severe phenotype, Golgi shape, number and dynamics appear unperturbed and secretion of a reporter protein remains unaffected.

Key words: *Arabidopsis thaliana*, endoplasmic reticulum, FRAP, Golgi, organelle shape, plant, protein transport, reticulon, secretory pathway

Received 5 June 2007, revised and accepted for publication 29 October 2007, uncorrected manuscript published online 2 November 2007

The endoplasmic reticulum (ER) is the port of entry of the secretory pathway. In plant cells, the ER is both pleomorphic (1,2) and extremely dynamic (3,4). In most mature plant cells, the ER is connected to the nuclear envelope and basically comprises cisternae and tubules in transvacuolar strands and an extensive cortical network of tubules, predominantly connected by three-way junctions (1,5). While the ER of animal cells is tightly linked to microtubules, the plant ER is associated with, and grows along, the actin cytoskeleton (3). Actin depolymerization inhibits both ER remodelling and movement, but it does not disrupt the basic polygonal architecture of the cortical tubular network (3,4). Likewise, the animal ER network formation is independent of microtubules (6). This suggests that factors other than the cytoskeleton must be involved in maintaining the shape and geometry of this organelle. Recently, a family of membrane proteins called reticulons (RTNs) have been shown to affect mammalian and yeast ER tubule formation and cortical network maintenance (7–9). Reticulons are ubiquitous in eukaryotes and share a carboxy-terminal reticulon homology domain (RHD), which contains two large hydrophobic regions (10). It has recently been proposed that both these regions function as transmembrane domains that form a hairpin within the ER membrane bilayer, with the connecting loop being exposed to the cytosol (7) and determining both ER localization and retention (11). The resulting wedge-like topology (akin to a 'W' in the membrane) would then be asymmetrically distributed within the bilayer, thereby imposing curvature on the membrane (7,9). Accordingly, both overexpression and downregulation of the two yeast RTNs lead to morphological alterations of the tubular ER (7,8,12,13).

Very little is known about the function of RTN proteins in plants. The *Arabidopsis thaliana* genome contains at least 19 closely related RTN-like proteins, 15 of which have been annotated [(10); Figure 1A]. To date, three members of the *Arabidopsis* RTN family have been identified in a screen for binding partners of the *Agrobacterium tumefaciens* pilin protein and named VirB2-interacting protein (BTI) (14) (Figure 1A, italicized). BTI-green fluorescent protein (GFP) fusions were visualized in root cells at low resolution and showed a distribution not incompatible with ER (14). One of these proteins and two further isoforms (Figure 1A, underlined) were also identified in a large-scale screen of the *Arabidopsis* organelle proteome (15) and assigned an ER localization. Very recently, two other isoforms, RTNLB2 and RTNLB4, have been localized to the ER in *A. thaliana* (16). However, no functional information has been reported so far. Reticulons show great variability in their N-terminal domains, which are involved in a wide variety of interactions (10,17). As there is virtually no functional information available about the role of RTNs in plant cells, we resolved to study one of the isoforms with the shortest N-terminal domain. We selected RTNLB13 (Figure 1A, boxed) on the grounds of its small size, which comprises an intact RHD flanked by very short N- and C-terminal regions (Figure S1). We reasoned that this 'minimal' RTN would be a good starting point to analyze the putative structural role of this protein family. If the RHD does have a role in conferring the shape of the cortical ER, RTNLB13 should be capable of affecting this process.

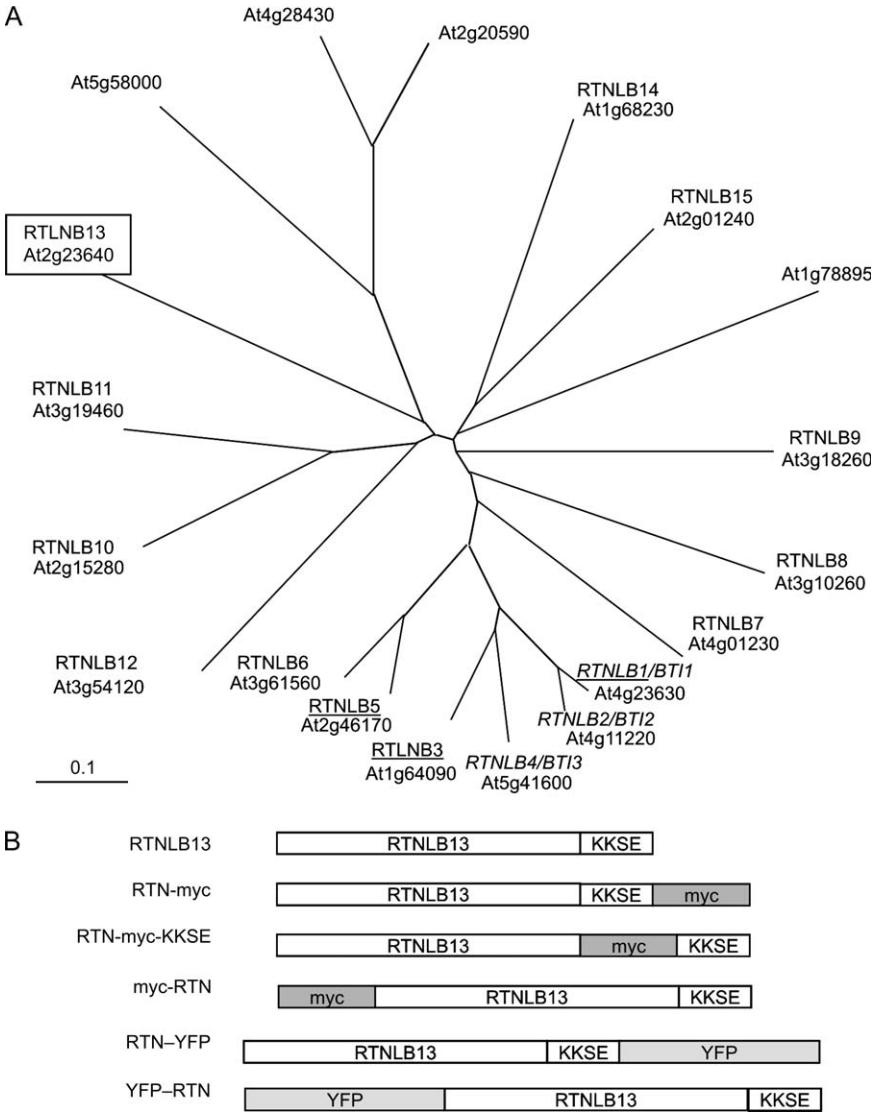

Figure 1: Phylogenetic tree of plant RTN and constructs used in this study. A) Unrooted phylogenetic tree of the annotated RTN isoforms in *Arabidopsis thaliana*. The RHDs of 19 *Arabidopsis* RTN isoforms – as identified with ARAMEMNON (30) – were aligned using CLUSTALW (31). The tree was drawn with TREEVIEW (32). The scale represents the evolutionary distance expressed as the number of substitutions per amino acid. The 15 annotated isoforms are named RTNLB (10). RTNLB13 (boxed) was chosen for this study. The isoforms in italics represent the three RTNs identified as *Agrobacterium* pilin protein-binding partners (14). The underlined isoforms have been identified as ER residents in an *Arabidopsis* organelle proteome analysis (15). B) Diagrams of the chimeric sequences expressed in this study. Each sequence was placed downstream of the CaMV35S promoter in vector pVKH18-EN6. The components of each chimeric construct, including the C-terminal KKSE motif encoded in RTNLB13, are not drawn to scale.

In this work, we tested two hypotheses (i) that RTNLB13 is localized in the ER and (ii) that it is involved in the maintenance of cortical ER morphology. We show that RTNLB13 is indeed localized in the cortical ER in tobacco epidermal cells and that its overexpression causes constriction of the lumen of ER tubules. However, this loss in structure does not affect downstream organelles such as the Golgi complex and it does not inhibit anterograde protein transport out of the ER.

Results and Discussion

The coding sequence of RTNLB13 [Figure 1A; (10)] was cloned by reverse transcriptase-polymerase chain reaction (RT-PCR) from *Arabidopsis* total seed RNA. We generated a number of constructs in the binary expression vector pVKH18-EN6 (18) (Figure 1B), including untagged RTNLB13 and RTNLB13 with a C- or N-terminal myc tag or fused to yellow fluorescent protein (YFP). As *Arabidopsis* RTNLB13 contains a canonical dilysine ER retention motif at its C-terminus (KKSE), it is likely that this is exposed to the cytosol as predicted (7). The C-terminal myc fusion masks the KKSE motif. However, it is not clear whether this is necessary for ER retention as several members of the mammalian RTN family lack a similar motif (10) but have nevertheless been localized to the ER membrane (7,11). In order to assess whether a fully exposed KKSE retrieval sequence was necessary for the correct localization/function of RTNLB13, we also generated constructs in which the last four codons (for KKSE) were appended to the 3′ side of the myc tag (Figure 1B).

We expressed untagged or myc-tagged RTNLB13 in tobacco leaf epidermal cells by *Agrobacterium* infiltration (18) together with signal sequence-GFP-HDEL (GFP-HDEL) as

a soluble marker for the ER lumen (19) (Figure 2). When coexpressed with an empty (negative-control) vector, GFP-HDEL revealed the typical morphology of plant ER, labelling the nuclear envelope, and transvacuolar strands (Figure 2A) plus the extensive cortical network of tubules (Figure 2B,C). When untagged (Figure 2D–F) or N-terminally myc-tagged RTNLB13 (Figure 2G–I) was coexpressed with GFP-HDEL, the appearance of the cortical ER was dramatically altered: the ER tubules were no longer detectable and were replaced by clusters of large vesicle-like structures (Figure 2, panels E and F, H and I). Thus, coexpression of RTNLB13 led to an apparent loss of the cortical ER architecture. Remarkably, RTNLB13 expression did not seem to affect the nuclear envelope (Figure 2, compare panel A with panels D and G). This is consistent with what has been observed in mammalian and yeast cells, where RTNs have been shown to insert preferentially into ER tubules rather than in ER sheets such as the nuclear envelope (7–9). The presence of the myc tag did not appear to influence RTNLB13, and expression of RTN-myc or RTN-myc-KKSE produced similar phenotypes to the untagged protein (Figure S2). Expression of the myc-tagged RTNLB13 constructs was also confirmed by immunoblot of proteins from the infiltrated leaf sectors with anti-myc antibody (Figure S2).

In order to verify if the effect on ER morphology results from RTNLB13 overexpression, we performed a time–course experiment. Leaves were infiltrated with GFP-HDEL-containing agrobacteria, and 24 h later, the same

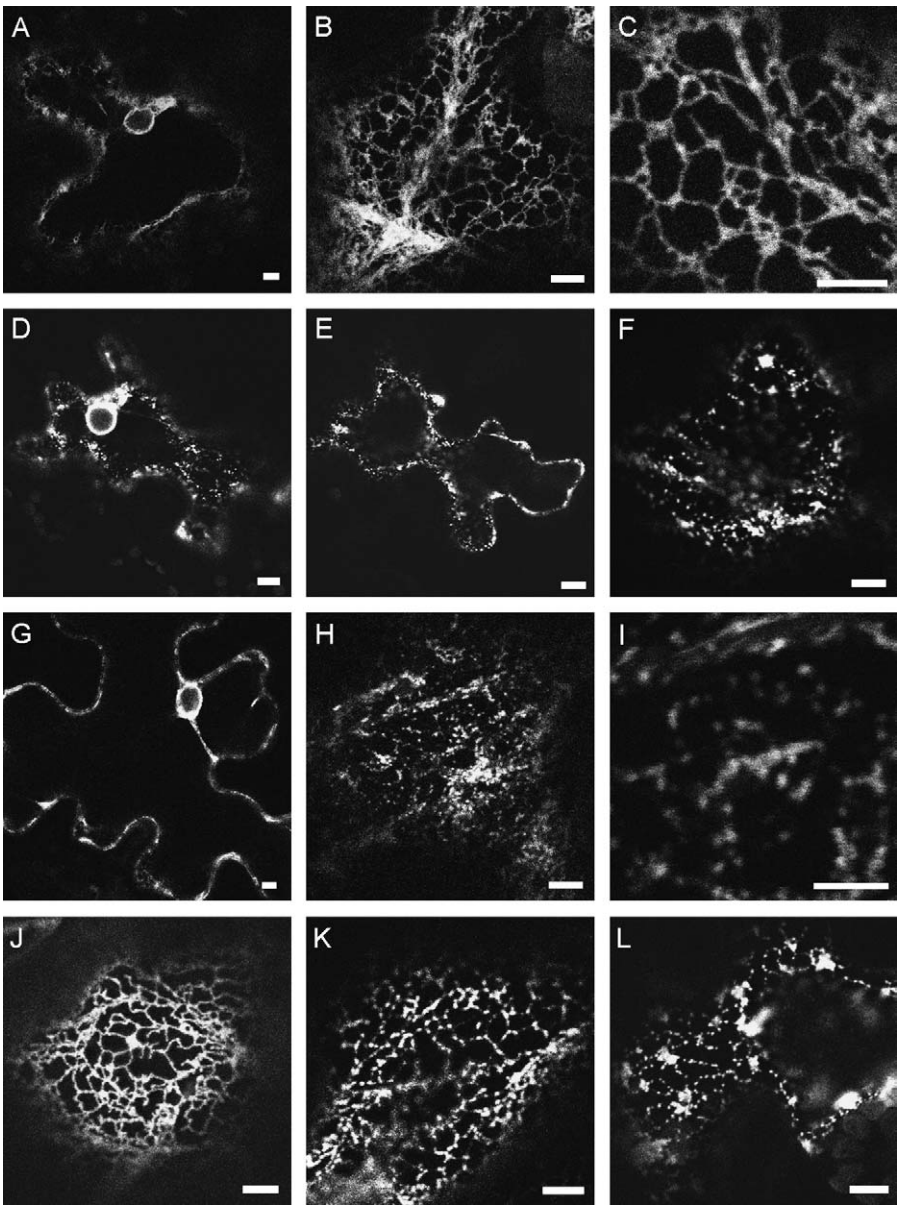

Figure 2: Expression of RTNLB13 causes apparent disruption of ER tubules. Tobacco leaf epidermal cells were infiltrated with agrobacteria containing the expression plasmid for GFP-HDEL together with the constructs indicated below. Leaf sectors were visualized by confocal laser scanning microscopy. A–C) Empty plasmid. D–F) Untagged RTNLB13. G–I) myc-RTN. J–L) Time–course. Leaves were infiltrated with GFP-HDEL-containing agrobacteria, and 24 h later, the same sectors were reinfiltrated with RTNLB13-containing agrobacteria. J, 48 h from first transfection; K, 72 h; and L, 96 h. Bars: 5 μm.

sectors were reinfiltrated with RTNLB13-containing agrobacteria. The ER appeared normal 48 h after the first infiltration (Figure 2J). However, after a further 24 h, progressive fragmentation of the cortical ER was observed (Figure 2K), culminating in the severe phenotype after 96 h (Figure 2L). This result confirms that the presence of, and/or build-up of, RTNLB13 protein in the infiltrated sectors was responsible for the apparent disruption of tubules in the cortical ER.

The effect of RTNLB13 on the ER structure hinted at its probable location in the ER itself. To test this, we coexpressed RTNLB13–YFP or YFP–RTNLB13 fusions with GFP-HDEL in tobacco leaf epidermal cells. For both constructs (Figure 1B), because of the topology of the protein, YFP is predicted to be exposed to the cytosol. Both proteins clearly localized to the ER (Figure 3, panels A and G, D and J, respectively; see also Figure 5, panels E and H). Remarkably, ER tubule morphology based on YFP fluorescence appeared normal. In the case of the coexpressed GFP-HDEL, however, we observed a similar vesiculated phenotype as caused by expression of the untagged or myc-tagged RTNLB13 (Figure 3, panels B and E). Merging the images clearly shows that only the luminal GFP reporter reveals the vesiculation/fragmentation phenotype, whereas YFP, which is exposed to the cytosolic face of the ER membrane, seems to highlight normal tubules (arrowheads in Figure 3, panels A–C and D–F). To ascertain whether RTN expression leads to alterations to the lumen of ER tubules, we coexpressed YFP-tagged RTNLB13 with the ER membrane marker GFP–calnexin (4,20). This reporter is inserted in the ER membrane but,

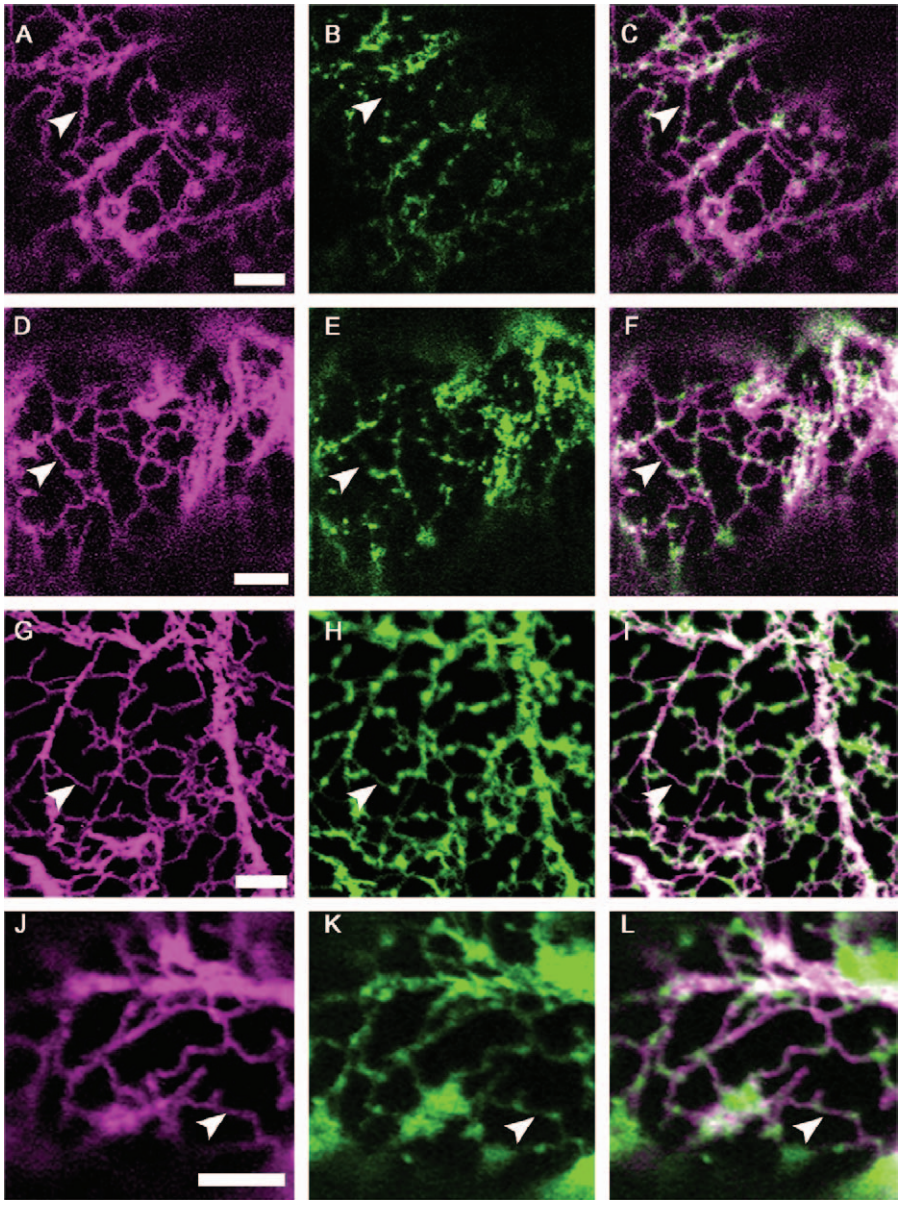

Figure 3: RTNLB13 fusions to YFP are localized in the cortical ER and cause constriction of the ER lumen. Tobacco leaf epidermal cells were infiltrated with agrobacteria containing the expression constructs indicated below. Leaf sectors were visualized by confocal laser scanning microscopy. A) YFP–RTN. B) GFP-HDEL. C) Merged images. D) RTN–YFP. E) GFP-HDEL. F) Merged images. G) YFP–RTN. H) GFP–calnexin. I) Merged images. J) RTN–YFP. K) GFP–calnexin. L) Merged images. Constriction of the ER lumen results in the absence of the luminal marker (GFP-HDEL) from the ER tubules (see arrowheads B and E), while the ER membrane marker GFP–calnexin is present in both open and constricted tubules (see arrowheads in all panels). Bars: 5 μm.

unlike RTN–YFP or YFP–RTN, has the GFP moiety, which replaces luminal domain of calnexin, exposed to the ER lumen. Figure 3 (panels H and K) shows that GFP–calnexin has a fragmented phenotype similar to that of GFP–HDEL, while YFP–RTN once again highlights intact ER tubules (panels G and J). At high magnification and detector gain, it is however possible to discern fine links between the vesiculated areas (arrowheads in Figure 3, panels G–I and J–L). In general, the 'vesiculation' was always milder when YFP-tagged RTN was expressed compared with untagged or myc-tagged constructs. It is possible that the presence of the soluble, tightly folded YFP, which is an even larger protein than RTNLB13 itself, may affect RTN function and mitigates the overexpression phenotype by affecting RTN folding, the way it inserts in the membrane or its interaction with potential partners (7).

We hypothesize that overexpression of RTNLB13, while not physically disrupting cortical ER tubules, strongly affects the distribution of markers within the ER lumen, possibly by causing severe remodelling of the membrane of the tubules, which in turn restricts the flow of luminal content. If this is the case, we would expect diffusion of proteins within the ER lumen to be inhibited. To test this, we performed fluorescence recovery after photobleaching (FRAP) experiments. YFP–RTN was expressed in leaf epidermal cells of a tobacco plant stably expressing GFP-HDEL and the infiltrated sectors treated with latrunculin B to disrupt the actin cytoskeleton. This treatment inhibits movement of the ER network but does not affect protein transport processes in the plant endomembrane system (4,21). This way, recovery of GFP-HDEL fluorescence after photobleaching of regions of the cortical ER can only be ascribed to diffusion of the protein within the ER lumen rather than movement of the whole ER assembly (4). Regions of the ER in cells coexpressing GFP-HDEL and YFP–RTN and cells solely expressing GFP-HDEL as a control were selectively bleached (Figure 4). Recovery of fluorescence in the ER lumen was very rapid in cells not expressing RTN, with maximum fluorescence recovery after 20 seconds (Figure S4, panel A). In contrast, fluorescence recovery in YFP–RTN-expressing cells showing the

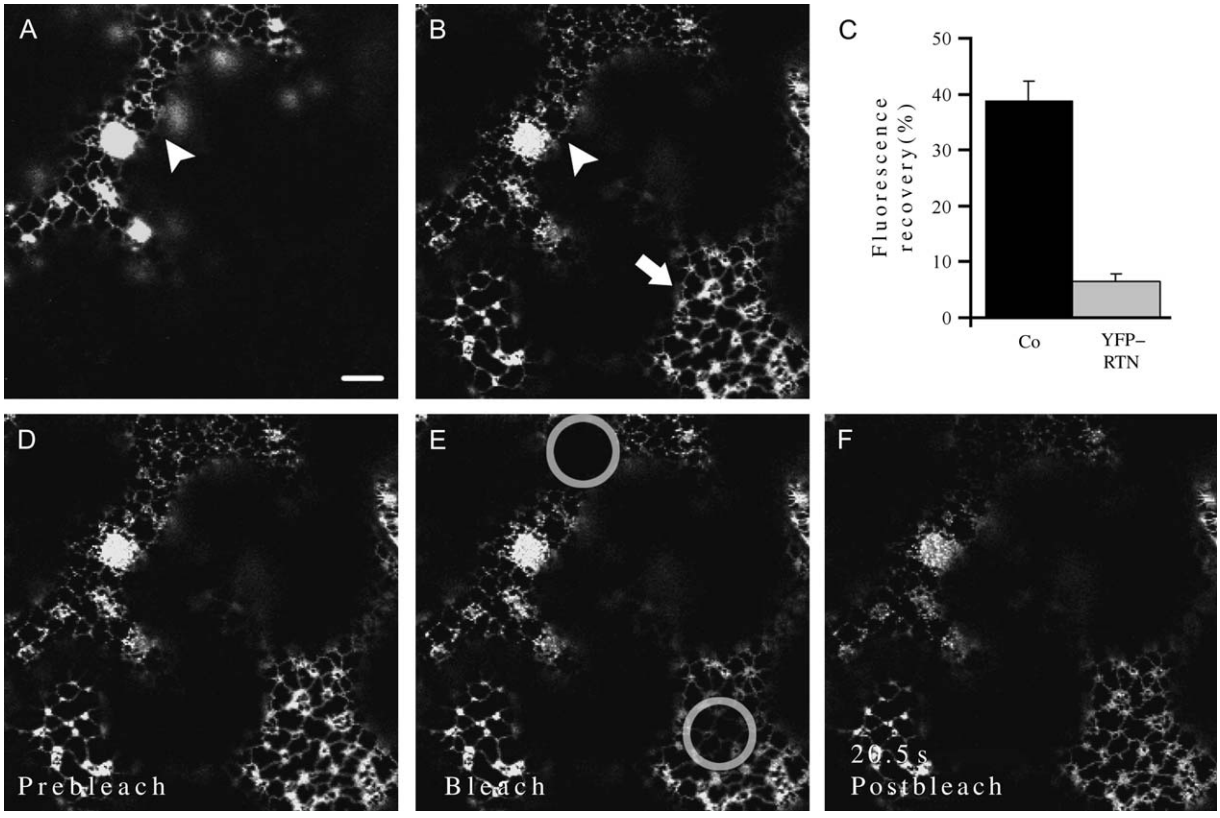

Figure 4: Diffusion of an ER luminal marker is inhibited by YFP–RTNLB13. Tobacco leaf epidermal cells from a stable line expressing GFP-HDEL were infiltrated with agrobacteria containing YFP–RTNLB13 (YFP–RTN). YFP–RTN fluorescence is shown in A, while GFP-HDEL is in B. Two 190-μm^2 regions of cells either coexpressing both GFP-HDEL and YFP–RTNLB13 (A and B, arrowhead) or just GFP-HDEL (B, arrow) were bleached (E, circle) and recovery was monitored over time. C) Graphical representation of the percentage of GFP-HDEL fluorescence recovered 20 seconds postbleach is shown, $n = 5$. Co, control cell expressing GFP-HDEL. YFP–RTN, cells coexpressing GFP-HDEL and YFP–RTNLB13. Representative images from prebleach (D), bleach (E) and 20.5 seconds postbleach (F) samples are shown. Note the lack of fluorescence recovery in the cell expressing both constructs. Bar: 10 μm.

typical vesiculate phenotype was about sixfold slower at the same time-point (Figure 4), without having reached its maximum after 40 seconds (Figure S4, panel A). This result confirms that the overexpression of RTNLB13 must induce physical changes to the ER membrane, possibly resulting in constrictions that inhibit diffusion of luminal proteins.

As a control, the diffusion of GFP–calnexin in the presence of RTN was also studied by FRAP (Figures S3 and S4, panel B). The coexpression of YFP–RTN inhibited recovery of the membrane marker to a lesser extent than that of the luminal marker, as may be expected because of the observation that GFP–calnexin, unlike GFP-HDEL, is detected over the whole ER network (Figure 3).

Albeit a milder effect than the complete breakdown of ER tubules, we suspected initially, the severe alteration of the ER membrane upon RTNLB13 overexpression raises the question as to whether this remodelling of the tubular ER inhibits secretory protein exit and transport from the ER. Indeed, low-magnification immunofluorescence data in HeLa cells showed that overexpression of full-length RTN3 may affect distribution of two Golgi markers (22). To test this, we coexpressed untagged RTNLB13 with GFP-HDEL and the Golgi marker sialyltransferase (ST)–YFP (21). Comparison of cells expressing all three constructs (Figure 5, panels A–C, cell at left-hand side) or just ST–YFP (data not shown) showed that the morphology and distribution of the Golgi complexes does not appear to be affected in cells where RTNLB13 expression alters the morphology of the ER (Figure 5, panels A–C). We also coexpressed ST–cyan fluorescent protein (CFP) (17) with YFP-tagged RTNLB13. When compared with control cells, cells expressing YFP–RTN or RTN–YFP present a comparable distribution of Golgi bodies (Figure 5, panels D–F and G–I, respectively). These appear to be of similar size to the control cells (compare two cells in Figure 5D), further indicating that Golgi morphology appears unaffected at the resolution of the microscope.

To assess whether the effect on tubular morphology resulted in inhibition of anterograde transport through the secretory pathway, we coexpressed myc-tagged reticulon (myc-RTN) with both GFP-HDEL and a secreted variant of phaseolin [Δ418 (23)] in tobacco protoplasts. In protoplasts, we could monitor similar ER lumen vesiculation to that observed in epidermal leaf cells (Figure S5). We subjected protoplasts to pulse–chase analysis and analyzed secretion of Δ418 by immunoprecipitation from both cell homogenates and incubation media. Figure 6A,C shows that the coexpression of RTNLB13 did not affect secretion of Δ418 into the medium. In comparison,

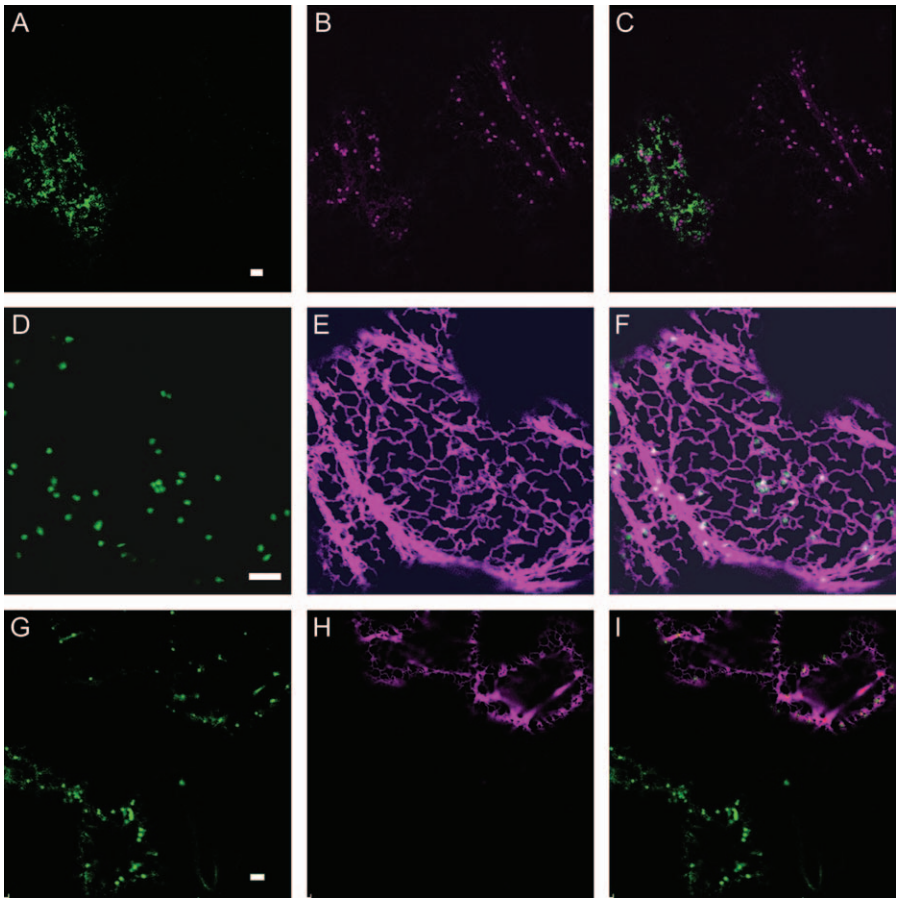

Figure 5: RTNLB13 does not affect Golgi number or morphology. Tobacco leaf epidermal cells were infiltrated with agrobacteria containing the expression constructs indicated below. Leaf sectors were visualized by confocal laser scanning microscopy. A) Untagged RTN with GFP-HDEL. B) Untagged RTN with ST–YFP. C) Merged images. D) ST–CFP. E) YFP–RTN. F) Merged images. G) ST–CFP. H) RTN–YFP. I) merged images. Bars: 10 μm.

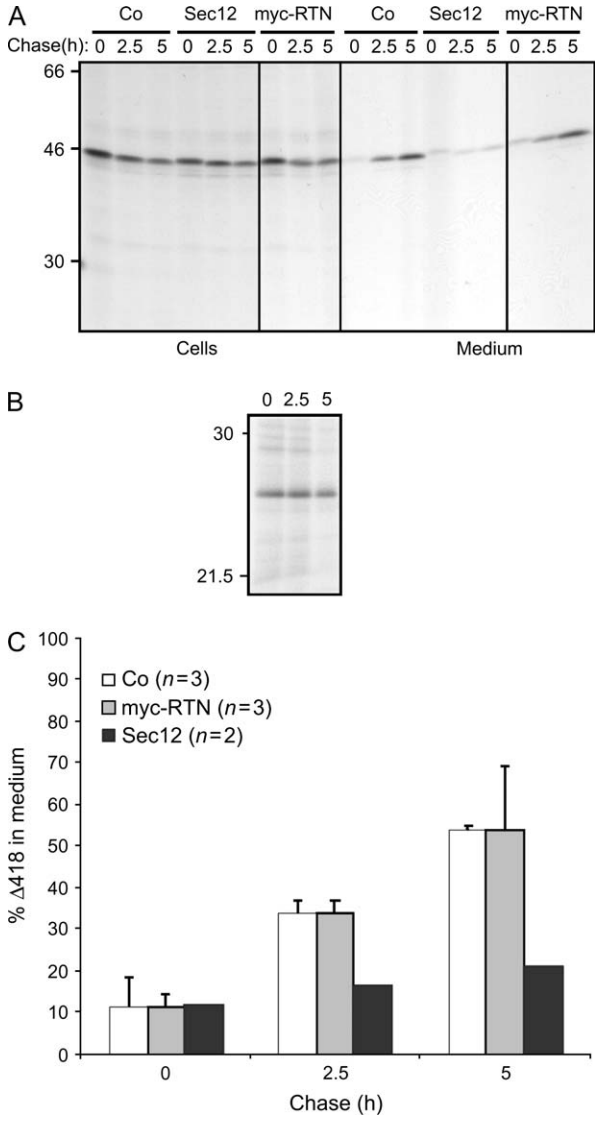

Figure 6: RTNLB13 does not affect anterograde transport of a secreted reporter protein. A) Tobacco mesophyll protoplasts were transfected with plasmids encoding phaseolin Δ418 and Sec12, myc-RTN or empty vector as a control (Co). Protoplasts were pulse labelled for 1 h with ^{35}S methionine and cysteine and then chased for the indicated times. Cell homogenates and protoplast incubation media were subjected to immunoprecipitation with anti-phaseolin antiserum. Immunoselected polypeptides were resolved by 15% SDS–PAGE and revealed by autoradiography. Numbers to the left of the blot indicate molecular weight markers (kDa). A representative result is shown. B) Homogenates from protoplasts coexpressing phaseolin Δ418 and myc-RTN treated as in A were subjected to a further round of immunoprecipitation with anti-myc monoclonal antibody. C) Quantification of experiments performed as in A. The intensity of the polypeptides immunoselected from the incubation media was quantified by densitometry using TotalLab. Care was taken to analyze films within the linear dynamic range of exposure. Histograms indicate average values. Bars indicate standard deviation.

coexpression of Sec12, which has been shown to interfere with COPII formation and ER exit (24), had a strong inhibitory effect on secretion (Figure 6C). To confirm that myc-RTN was being expressed, we also performed immunoprecipitation with anti-myc antibodies from the same samples (Figure 6B). This yielded a polypeptide of the size predicted for RTNLB13 (about 25 kDa). The protein was remarkably stable over the course of the 5 h chase. In accordance with the observed ER localization of YFP-tagged RTN, the myc-RTN protein was exclusively immunoprecipitated from microsomal membranes (Figure S6). Thus, we conclude that the RTN-induced ER morphology alteration has no major effect on the anterograde secretory pathway. This is similar to what was observed when the loop joining the RHD transmembrane regions of Rtn1 was overexpressed in yeast (8).

Our results are compatible with the hypothesis that RTN proteins are involved in conferring shape to the ER tubules. We do not yet know, however, if different, longer plant RTN isoforms are also capable of producing the effect observed with RTNLB13. Intuitively, it makes sense to imagine that an excess of RTN in the membrane will force the curvature of the tubules, eventually introducing constrictions that lead to reduced diffusion of luminal material. This would in turn accumulate in vesicle-like luminal pockets. It was surprising, however, to discover that such a marked phenotype – which in functional terms is almost equivalent to the physical disaggregation of the ER tubules, as far as their lumen is concerned – was not mirrored by an inhibition of protein transport. This raises the question of whether the tubular network architecture of the cortical ER is essential for the proper function of this organelle.

As the number of *Arabidopsis* RTN isoforms is relatively high, and GeneVestigator analysis (25) indicates that they are ubiquitously expressed (data not shown), it will be quite difficult to perform reverse genetics by studying insertional knockout mutants. It will also be difficult to achieve a comprehensive downregulation of all isoforms by RNA interference because of differences in sequence. Although beyond the scope of the present study, a more useful avenue may be to restrict any knockdown to the most abundant RTNs as a high concentration of these proteins is important for large-scale tubulation in yeast (7,8). At present, the interacting partners of the cytosolic variable domains of plant RTNs remain unknown, but their identification may provide pointers to any alternative roles, beyond the shaping of ER tubules, that specific RTNs possess.

Materials and Methods

Recombinant DNA

The coding sequence for RTNLB13 (At2g23640) was amplified from total *A. thaliana* seed RNA by RT-PCR using the following primers: forward 5′ ACTGCGCTTCTAGAATGGCCAACGAC 3′ and reverse 5′ GCAGCAGCGAGCTCCTACTCTGATTTTTTCACTTTC 3′.

The myc tag was added to the N-terminus of RTNLB13 using primer fwd 5′ GACGACGCTCTAGAATGGAGCAGAAACTCATCTCTGAAGAGGATCTG GCCAACGACGTGACCAAAGATC 3′ (XbaI) and to the C-terminus using primer rev 5′ CGCGCGCGGAGCTCTTACAGATCCTCTTCAGAGATGAGTTTCTGCTC-CTCTGATTTTTTC 3′ (*Sac*I). For the addition of KKSE to the RTN-myc, the following primer was used: rev 5′ GACGACGCGAGCTCCTACTCTGATT-TTTTCAGATCCTCTTCAGAGATGAGTTTCTGCTCCACTTTCTCTTCTGTACCA-TGGTGT 3′ (*Sac*I).

YFP fusions were generated by fusion PCR. For YFP–RTN, YFP was amplified using the following primers: fwd 5′ GCAGCAGCTCTAGAATGGG-CAGCAAGGG 3′ (*Xba*I) and rev 5′ GGTCACGTCGTTGGCGATCACCTTGTACAG 3′ and RTN with the following primers: fwd 5′ CTGTACAAGGTGATCGC-CAACGACGTGACC 3′ and rev 5′ GCAGCAGCGAGCTCCTACTCTGATTTT-TTCACTTTC 3′ (*Sac*I). For RTN-YFP, the following primers were used: for RTN, fwd 5′ ACTGCGCTTCTAGAATGGCCAACGAC 3′ (*Xba*I) and rev 5′ CTCGCCCTTGCTGCCCTCTGATTTTTTCAC 3′; for YFP, fwd 5′ GTGAAA-AAATCAGAGGGCAGCAAGGGCGAG 3′ and rev 5′ GCAGCAGCGAGCTCC-TAGATCACCTTGTACAGCTCGTC 3′ (*Sac*I).

All constructs were cloned into the *Xba*I and *Sac*I sites of expression vector pVKH18-EN6 (18) and inserted into *A. tumefaciens* strain EHA105. For transient expression in tobacco protoplasts, myc-RTN and RTN-myc were cloned into the *Xba*I and *Sac*I sites of expression vector pDHA (26).

The construction of Syalyl transferase-monomeric red fluorescent protein (ST-mRFP) and ST–CFP was described previously (4,27).

Confocal microscopy

Nicotiana tabacum cv. Petit Havana SR1 leaves were infiltrated with *Agrobacterium* containing the indicated expression constructs as described previously (18,28). Constructs were infiltrated at the following optical density unless stated otherwise: ST–CFP/YFP/mRFP 0.04, GFP-HDEL 0.04, RTN fusions 0.05. Leaf sections were observed after 48–72 h with a Leica TCS SP2 confocal microscope equipped with a ×63 (1.3 NA) oil immersion objective or with a Zeiss LSM510 Meta equipped with a ×63 (1.4 NA) oil immersion objective using appropriate filters or spectral selection. The confocal microscope settings were kept constant throughout experiments. Fluorescence recovery after photobleaching studies were performed on leaf segments treated with latrunculin B (0.01 M, 30 min) using Zeiss LSM510 Meta 514 nm/458 nm excitation and beam splitters for detection of YFP and GFP, respectively. GFP was bleached within a defined region of interest with 10 iterations of 100% 405 nm laser power and subsequent recovery monitored. The bleach area was constant in all experiments (190 μm^2). Relative levels of fluorescence were normalized to 100% prior to bleach and subsequent recovery plotted as a percentage of prebleaching fluorescence intensity. Images were assembled in Adobe Photoshop CS.

Protoplast transfection and pulse–chase analysis

Protoplasts were transfected exactly as described previously (29). Pulse–chase analysis and immunoprecipitation were performed as described (23) with polyclonal anti-phaseolin antiserum or monoclonal 9E10 anti-myc antibody (a gift from John M. Jarvis, MRC LMB, Cambridge).

Acknowledgment

N. T. is indebted to a BBSRC studentship. I. A. S. was funded by Oxford Brookes University.

Supplementary Materials

Figure S1: Multiple alignment of protein sequences of 19 *Arabidopsis* RTN isoforms. Alignment was performed with ClustalW (31) and visualized with Jalview (33). RTNLB13 is highlighted in yellow. Blue boxes highlight conserved residues.

Figure S2: C-terminally myc-tagged RTNLB13 affects the morphology of the ER. Tobacco leaf epidermal cells were infiltrated with agrobacteria containing expression plasmid for GFP-HDEL and the constructs indicated below. Leaf sectors were visualized by CLSM (A–F). A–C) RTN-myc. D–F) RTN-myc-KKSE. Bars: 5 μm. G) Total protein homogenates from tobacco leaf sectors infiltrated with the indicated constructs were resolved on SDS–PAGE and subjected to immunoblot with anti-myc antibody. Because of the nature of leaf sector sampling, the relative levels of the detected polypeptides are not comparable. Numbers at the left indicate molecular weight markers (kDa). The difference in electrophoretic mobility between the myc-RTN (black arrowhead) and RTN-myc (white arrowhead) polypeptides has not yet been investigated, but it could result from differential migration properties of the highly unstructured N- and C-terminal domains of the RTN protein (34) in the presence or absence of the myc tag. Alternatively, it could indicate proteolytic trimming of the unprotected N-terminus of RTN-myc.

Figure S3: Diffusion of an ER membrane marker is inhibited by YFP–RTNLB13. Tobacco epidermal cells transiently expressing either the ER membrane marker GFP–Calnexin (A–C) or coexpressing GFP–Calnexin and YFP–RTNLB13 (D–H) were bleached (B and G, circle), and recovery was monitored over time. Graphical representation of the percentage of GFP–calnexin recovery 60 sec postbleach is shown, $n = 13$. Co, control cells expressing GFP–calnexin; RTN, cells coexpressing YFP–RTNLB13 and GFP–calnexin. Representative images from prebleach (A, D–F), bleach (B and G) and recovery (C and H) are shown. Scale bar: 5 μm.

Figure S4: Effect of YFP–RTN expression on FRAP of an ER luminal (GFP-HDEL) and membrane marker (GFP–calnexin) in tobacco epidermal cells. Representative graphs of the percentage FRAP of GFP-HDEL (A, light blue plot) and GFP–calnexin (B, light blue plot) expressed in tobacco epidermal cells was monitored over time. Cells coexpressing these fluorescent markers with YFP–RTN were also photobleached (dark blue plots), and fluorescence recovery over time was monitored. The recovery rates were normalized as described previously (4).

Figure S5: Overexpression of myc-RTN leads to morphological alterations of the cortical ER in tobacco protoplasts. Protoplasts were transfected with GFP-HDEL and empty vector as a control (Co) or untagged RTNLB13 (RTN). Protoplasts were visualized by CLSM. Single optical slices of the cortical ER are shown. Green, GFP; magenta, chlorophyll autofluorescence. Note the loss of the reticular ER network architecture in the presence of RTNLB13, as shown in Figure 2 for intact leaves. Scale bars: 5 μm.

Figure S6: myc-RTN and RTN-myc are stable over a 6-h chase and are associated with microsomes. A) Protoplasts were transfected with the indicated constructs, pulse labelled for 1 h with ^{35}S methionine and cysteine and then chased for the indicated times. Cell homogenates were subjected to immunoprecipitation with anti-myc antibody. Immunoselected polypeptides were resolved by 15% SDS–PAGE and revealed by autoradiography. Numbers at the left indicate molecular weight markers (kDa). The difference in electrophoretic mobility between the myc-RTN and RTN-myc polypeptides has not yet been investigated. B) Protoplasts transfected as in A were homogenized in 12% (w/w) sucrose and microsomal membranes separated by ultracentrifugation. Total cell homogenates (T), membranes (M) and supernatants (S) were immunoprecipitated with anti-myc antibody. Immunoselected polypeptides were resolved by 15% SDS–PAGE and revealed by autoradiography. Numbers at the left indicate molecular weight markers (kDa).

Supplemental materials are available as part of the online article at http://www.blackwell-synergy.com

References

1. Boevink P, SantaCruz S, Hawes C, Harris N, Oparka KJ. Virus-mediated delivery of the green fluorescent protein to the endoplasmic reticulum of plant cells. Plant J 1996;10:935–941.
2. Staehelin LA. The plant ER: a dynamic organelle composed of a large number of discrete functional domains. Plant J 1997;11: 1151–1165.
3. Boevink P, Oparka K, Santa Cruz S, Martin B, Batteridge A, Hawes C. Stacks on tracks: the plant Golgi apparatus traffics on an actin/ER network. Plant J 1998;15:441–447.
4. Runions J, Brach T, Kuhner S, Hawes C. Photoactivation of GFP reveals protein dynamics within the endoplasmic reticulum membrane. J Exp Bot 2006;57:43–50.
5. Lichtscheidl I, Hepler P. Endoplasmic reticulum in the context of plant cells. In: Smallwood M, Knox J, Bowles D, editors. Membranes: Specialized Functions in Plants. Oxford: BIOS Scientific Publishers; 1996, pp. 383–402.
6. Dreier L, Rapoport TA. In vitro formation of the endoplasmic reticulum occurs independently of microtubules by a controlled fusion reaction. J Cell Biol 2000;148:883–898.
7. Voeltz GK, Prinz WA, Shibata Y, Rist JM, Rapoport TA. A class of membrane proteins shaping the tubular endoplasmic reticulum. Cell 2006;124:573–586.
8. De Craene JO, Coleman J, Estrada de Martin P, Pypaert M, Anderson S, Yates JR III, Ferro-Novick S, Novick P. Rtn1p is involved in structuring the cortical endoplasmic reticulum. Mol Biol Cell 2006; 17:3009–3020.
9. Voeltz GK, Prinz WA. Sheets, ribbons and tubules – how organelles get their shape. Nat Rev Mol Cell Biol 2007;8:258–264.
10. Oertle T, Klinger M, Stuermer CAO, Schwab ME. A reticular rhapsody: phylogenic evolution and nomenclature of the RTN/Nogo gene family. FASEB J 2003;17:1238–1247.
11. Iwahashi J, Hamada N, Watanabe H. Two hydrophobic segments of the RTN1 family determine the ER localization and retention. Biochem Biophys Res Commun 2007;355:508–512.
12. Borgese N, Francolini M, Snapp E. Endoplasmic reticulum architecture: structures in flux. Curr Opin Cell Biol 2006;18:358–364.
13. Shibata Y, Voeltz GK, Rapoport TA. Rough sheets and smooth tubules. Cell 2006;126:435–439.
14. Hwang H-H, Gelvin SB. Plant proteins that interact with VirB2, the Agrobacterium tumefaciens pilin protein, mediate plant transformation. Plant Cell 2004;16:3148–3167.
15. Dunkley TP, Hester S, Shadforth IP, Runions J, Weimar T, Hanton SL, Griffin JL, Bessant C, Brandizzi F, Hawes C, Watson RB, Dupree P, Lilley KS. Mapping the Arabidopsis organelle proteome. Proc Natl Acad Sci U S A 2006;103:6518–6523.
16. Nziengui H, Bouhidel K, Pillon D, Der C, Marty F, Schoefs B. Reticulon-like proteins in Arabidopsis thaliana: structural organization and ER localization. FEBS Lett 2007;581:3356–3362.
17. Yan R, Shi Q, Hu X, Zhou X. Reticulon proteins: emerging players in neurodegenerative diseases. Cell Mol Life Sci 2006;63: 877–889.
18. Batoko H, Zheng H-Q, Hawes C, Moore I. A Rab1 GTPase is required for transport between the endoplasmic reticulum and Golgi apparatus for normal Golgi movement in plants. Plant Cell 2000;12: 2201–2217.
19. Boevink P, Martin B, Oparka K, Santa Cruz S, Hawes C. Transport of virally expressed green fluorescent protein through the secretory pathway in tobacco leaves is inhibited by cold shock and brefeldin A. Planta 1999;208:392–400.
20. Irons SL, Evans DE, Brandizzi F. The first 238 amino acids of the human lamin B receptor are targeted to the nuclear envelope in plants. J Exp Bot 2003;54:943–950.
21. Brandizzi F, Snapp EL, Roberts AG, Lippincott-Schwartz J, Hawes C. Membrane protein transport between the endoplasmic reticulum and the Golgi in tobacco leaves is energy dependent but cytoskeleton independent: evidence from selective photobleaching. Plant Cell 2002; 14:1293–1309.
22. Wakana Y, Koyama S, Nakajima K, Hatsuzawa K, Nagahama M, Tani K, Hauri HP, Melancon P, Tagaya M. Reticulon 3 is involved in membrane trafficking between the endoplasmic reticulum and Golgi. Biochem Biophys Res Commun 2005;334:1198–1205.
23. Frigerio L, de Virgilio M, Prada A, Faoro F, Vitale A. Sorting of phaseolin to the vacuole is saturable and requires a short C-terminal peptide. Plant Cell 1998;10:1031–1042.
24. Phillipson BA, Pimpl P, daSilva LL, Crofts AJ, Taylor JP, Movafeghi A, Robinson DG, Denecke J. Secretory bulk flow of soluble proteins is efficient and COPII dependent. Plant Cell 2001;13:2005–2020.
25. Zimmermann P, Hirsch-Hoffmann M, Hennig L, Gruissem W. GENEVESTIGATOR. Arabidopsis microarray database and analysis toolbox. Plant Physiol 2004;136:2621–2632.
26. Tabe LM, Wardley-Richardson T, Ceriotti A, Aryan A, McNabb W, Moore A, Higgins TJV. A biotechnological approach to improving the nutritive value of alfalfa. J Ani Sci 1995;73:2752–2759.
27. Brandizzi F, Frangne N, Marc-Martin S, Hawes C, Neuhaus JM, Paris N. The destination for single-pass membrane proteins is influenced markedly by the length of the hydrophobic domain. Plant Cell 2002; 14:1077–1092.
28. Sparkes IA, Runions J, Kearns A, Hawes C. Rapid, transient expression of fluorescent fusion proteins in tobacco plants and generation of stably transformed plants. Nat Protoc 2006;1:2019–2025.
29. Pedrazzini E, Giovinazzo G, Bielli A, de Virgilio M, Frigerio L, Pesca M, Faoro F, Bollini R, Ceriotti A, Vitale A. Protein quality control along the route to the plant vacuole. Plant Cell 1997;9:1869–1880.
30. Schwacke R, Schneider A, van der Graaff E, Fischer K, Catoni E, Desimone M, Frommer WB, Flugge U-I, Kunze R. ARAMEMNON, a novel database for Arabidopsis integral membrane proteins. Plant Physiol 2003;131:16–26.
31. Thompson JD, Higgins DG, Gibson TJ. CLUSTAL W: improving the sensitivity of progressive multiple sequence alignment through sequence weighting, position-specific gap penalties and weight matrix choice. Nucleic Acids Res 1994;22:4673–4680.
32. Page RD. TreeView: an application to display phylogenetic trees on personal computers. Comput Appl Biosci 1996;12:357–358.
33. Clamp M, Cuff J, Searle SM, Barton GJ. The Jalview Java alignment editor. Bioinformatics 2004;20:426–427.
34. Li M, Song J. The N-and C-termini of the human Nogo molecules are intrinsically unstructured: bioinformatics, CD, NMR characterization, and functional implications. Proteins 2007;68:100–108.

BJ www.biochemj.org

Biochem. J. (2009) **423**, 145–155 (Printed in Great Britain) doi:10.1042/BJ20091113

REVIEW ARTICLE

The plant endoplasmic reticulum: a cell-wide web

Imogen A. SPARKES*, Lorenzo FRIGERIO†, Nicholas TOLLEY† and Chris HAWES*[1]

*School of Life Sciences, Oxford Brookes University, Oxford OX3 0BP, U.K., and †Department of Biological Sciences, University of Warwick, Coventry CV4 7AL, U.K.

The ER (endoplasmic reticulum) in higher plants forms a pleomorphic web of membrane tubules and small cisternae that pervade the cytoplasm, but in particular form a polygonal network at the cortex of the cell which may be anchored to the plasma membrane. The network is associated with the actin cytoskeleton and demonstrates extensive mobility, which is most likely to be dependent on myosin motors. The ER is characterized by a number of domains which may be associated with specific functions such as protein storage, or with direct interaction with other organelles such as the Golgi apparatus, peroxisomes and plastids. In the present review we discuss the nature of the network, the role of shape-forming molecules such as the recently described reticulon family of proteins and the function of some of the major domains within the ER network.

Key words: endoplasmic reticulum, exit site, Golgi apparatus, peroxisome, plastid, reticulon.

INTRODUCTION

The ER (endoplasmic reticulum) was first described by electron microscopists in the 1960s [1]. Subsequently, the development of vital stains, improved tissue preservation techniques and video imaging technology [2], culminating in the exploitation of fluorescent protein technology [3], has allowed the documentation of the extremely dynamic and pleomorphic nature of the ER [Figure 1 and Supplementary Movie S1 (at http://www.BiochemJ.org/bj/423/bj4230145add.htm)] ([3,4] and references therein). Traditionally the ER has been classified into two forms, rough and smooth, depending on the presence or absence of membrane-bound ribosomes [5]. However, the highly dynamic nature of the organelle is exemplified by the rapid changes that can be made between cisternal and tubular forms in response to developmental [6,7], physiological [8] or environmental cues. It is these two morphological forms that are now more commonly used to describe the organelle, even though their importance was apparent from earlier work using selective membrane staining and thick-section electron microscopy [9–11]. For instance, in developing *Arabidopsis* roots, cisternal ER is more common in meristematic and elongating cells, whereas tubular forms predominate in the more vacuolate and mature elongated cells [6]. Positionally, the ER can be described in terms of two populations, the cortical network and cytoplasmic ER which may also extend across *trans*-vacuolar strands [8]. Both forms of ER exhibit motility, although cytoplasmic ER may also get caught in cytoplasmic streams and thus show much more rapid unidirectional movement.

The ER effectively compartmentalizes the cytoplasm into two fractions, a reducing cytosol and an oxidizing ER lumen, bounded by the ER membrane. The outer nuclear envelope can also be considered to be a distinct domain of the ER being connected to the tubular network and, in some algae such as the yellow-green xanthophyte *Tribonema,* can function as the ER, transporting cargo directly to the *cis*-Golgi [12]. The ER has numerous and diverse functions from the generic biosynthesis of phospholipids, the synthesis, glycosylation, folding and quality control of secretory proteins [13–15], the maintenance of the calcium homoeostasis of the cell [16], through to the more specialized formation of storage material such as protein and oil bodies [17–19]. Clear links between these multiple biological functions and the unique morphology and dynamics of the ER, however, have not yet been established.

In the present review we will focus on recent data that have revealed the true dynamic nature of the ER network in plant cells and the functional significance of some of the more important ER domains.

THE ER AS A DYNAMIC MEMBRANE NETWORK

As previously mentioned, a typical ER network is composed of several structurally distinct domains: tubules, cisternae and the nuclear envelope. In any given static 'snapshot' of the cortical ER, the vast majority of tubules form a polygonal network underlying the plasma membrane and are interconnected by three-way junctions, with a small subset of 'open-ended' tubules undergoing growth/retraction (Figure 1 and Supplementary Movie S1). The continual extension/retraction of tubules appears to be random, although outgrowth has been observed to follow the track of Golgi bodies in tobacco epidermal cells [20]. Static nodules of ER within the dynamic network have been reported in onion bulb cells, and are also apparent in tobacco and *Arabidopsis* epidermal cells [21]. Recent micromanipulation studies in *Arabidopsis* leaf epidermal cells have indicated that these static 'islands' of ER appear to act as anchor points, presumably connected through to the plasma membrane, around which the ER remodels [22]. Drastic rearrangements of the entire network also appear to be random, apart from regions of 'fast-flowing' movement which coincide with cytoplasmic streaming. Therefore, based on these

Abbreviations used: BFA, brefeldin A; DAG, diacylglycerol; ER, endoplasmic reticulum; ERES, ER exit site(s); GFP, green fluorescent protein; PAC, precursor accumulating; PAGFP, photoactivatable GFP; PMP, peroxisome membrane protein; RFP, red fluorescent protein; RHD, reticulon homology domain; RTNLB, reticulon-like gene in plants, i.e. non-metazoan group B; SNARE, soluble *N*-ethylmaleimide-sensitive fusion protein-attachment protein receptor; TAG, triacylglycerol; TGD4, trigalactosyldiacylglycerol 4; YFP, yellow fluorescent protein.

All authors contributed equally to this review.

[1]To whom correspondence should be addressed (email c.hawes@brookes.ac.uk).

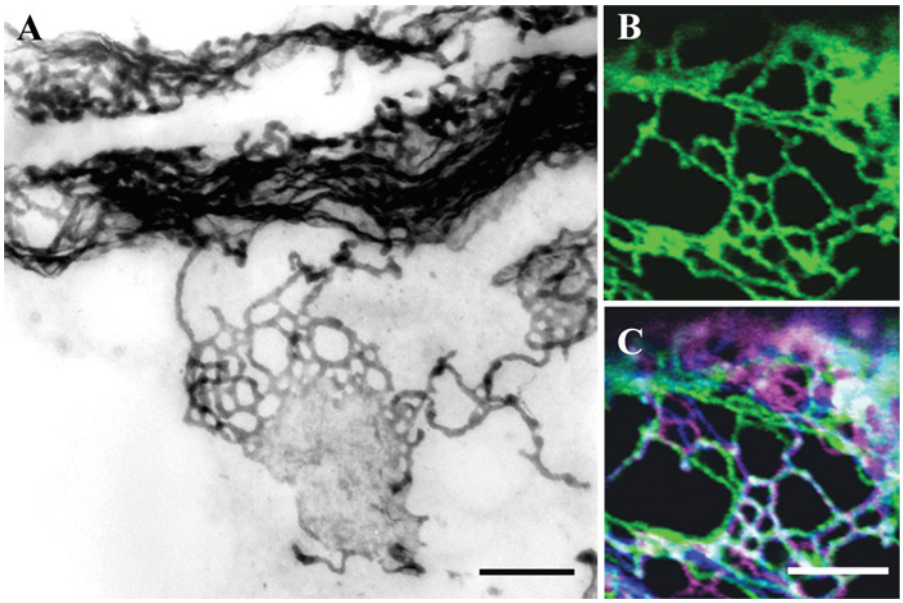

Figure 1 Morphology and dynamics of higher plant ER

Electron micrograph of an osmium-impregnated maize root tip meristem cell (**A**) and confocal image of tobacco epidermal leaf cells expressing an ER lumenal marker (GFP–HDEL) (**B**) clearly showing the two structural domains, tubules and cisternal elements. Consecutive images were taken of GFP–HDEL in tobacco leaf epidermal cells, false coloured and overlaid to generate a single plane image. The dynamic nature of cortical ER remodelling is apparent as the three images were taken 6.5 s apart, where white indicates GFP–HDEL fluorescence at all three time points (**C**). Scale bar = 500 nm (for **A**) and 5 μm (for **B** and **C**).

morphological observations, ER network remodelling requires factors that regulate tubule extension, network stabilization, three-way junction and anchor-point formation, and modulation of ER shape through tubulation compared with cisternalization (Figure 2). Given the complexity of these factors and the highly dynamic nature of the ER network, efforts to model ER movement have been limited to date in any system, with static models of ER geometry [23–25] providing the foundation for future studies.

Unlike animal cells, the cortical ER network in higher plants overlies the actin cytoskeleton rather than microtubules [26–28]. Despite this fundamental difference, depolymerization of the actin or microtubules in higher plants [21] and mammals respectively does not result in a concomitant destruction of the ER network, but does perturb tubule extension and remodelling [29]. While microtubule depolymerization appears to have no effect on ER dynamics in mature, non-growing cells [20], it does affect the cortical network in elongating characean internodal cells [30]. ER in characean internodal cells can be split into two types; a fast cytoplasmic streaming region in the endoplasm, and the more 'sedate' cortical network above. Drug inhibition studies have shown that, whereas the streaming ER is dependent on actin, cortical network remodelling is dependent on the microtubules during the early stages of cell elongation. It has also been reported that oryzalin has an effect on ER dynamics in tobacco leaf epidermal cells, *Arabidopsis* roots and BY-2 cells, but the effects were specific to the drug rather than microtubule depolymerization *per se* [31]. Furthermore, in mammals, long-term depolymerization of microtubules (2 h as opposed to 15 min) and overexpression of full length and truncations of several microtubule-interacting proteins [CLIMP-63 (63 kDa cytoskeleton-linking membrane protein), tau and kinesin] results in ER network shrinkage [29] (and see [27] and references therein). Therefore the cytoskeleton plays an important role in tubule extension and, in mammals, network stabilization. Interestingly, *in vitro* reconstitution studies on *Xenopus* ER microsomes have indicated that ER network formation can occur in the absence of microtubules and thus the formation of a polygonal network may be an intrinsic property of the ER membrane [32].

Myosins and ER movement

It is well documented that organelle movement in higher plant cells is actin-dependent [26,33–39], and thus it has been assumed that myosin motors are generating the motive forces. The role of myosins has received much attention of late, and the genetic dissection of the 17 *Arabidopsis* myosin genes has been carried out through overexpression of truncated variants lacking the myosin head domain [40–43]. RNAi (RNA interference) down-regulation and T-DNA (transferred DNA) insertional mutagenesis have verified the role of some myosin isoforms in organelle movement [42–44]. The 17 myosins are split into two classes: VIII contains four members and XI contains 13. Class XI has been implicated in organelle movement [40–43]. Tracking algorithms can quantify the movement of discrete organelles such as Golgi bodies, peroxisomes and, to some extent, mitochondria. The movement characteristics of the ER network are more complicated, and algorithms to relatively easily monitor ER characteristics such as tubule growth, network remodelling and surface area compared with volume are currently underway and still in their infancy [25]. Once these have been developed, a comprehensive study of any drastic or subtle effects of these myosins on ER remodelling can be undertaken. Location studies have indicated that of the 17 *Arabidopsis* myosins, the class VIII myosin ATM1 (*Arabidopsis thaliana* myosin 1) is present in small puncta which were proposed to overlie the ER, although its effects on ER dynamics were not documented [45]. Biochemical co-fractionation and immunocytochemistry studies have indicated that a 175 kDa heavy-chain myosin is associated with the ER in tobacco BY-2 cells and therefore may be responsible for network dynamics [46]. Overexpression of two myosin tail domains (XIK and XI2) in tobacco were reported to have no effect on ER

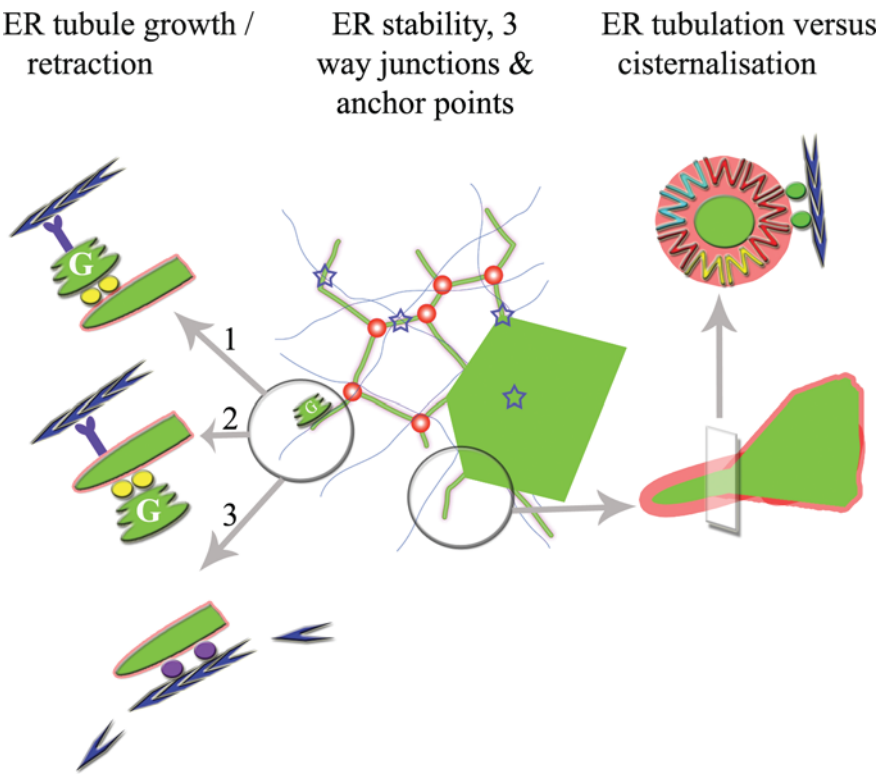

Figure 2 Schematic representation of higher plant ER dynamics

ER tubule growth/retraction may be (in)dependent of Golgi body (G) movement. (1) Golgi body movement, via myosins (blue) processing along actin (blue arrowheads) remodels the attached/tethered ER (yellow spheres), or (2) Golgi body movement is a direct result of association with the ER. Actin polymerization may also remodel the ER through interaction with actin-associated factors (3, purple circles). Potential factors involved in three way junction (red sphere) and anchor point (blue star) formation are unknown. ER tubulation appears to be due to reticulons (W), and their speculated hetero/homoligomerization. Factors required for reticulon association/movement within the ER membrane are unknown (green circle). An animation related to this Figure is available at http://www.Biochemj.org/bj/423/0145/bj4230145add.htm.

structure, although studies on ER dynamics were not presented [42].

Tubule formation, cisternae and anchoring

While the cytoskeleton provides the tracks along which ER tubule extension occurs, the 'extended' membrane is presumably composed of either 'stretched' ER membrane growing and flexing in new directions, or of *de novo* synthesized ER membrane. Such growing tubules can fuse laterally with other tubules forming the new polygons. Thus multiple homotypic membrane fusions can be generated along one ER tubule. In mammals several genes have been shown to have an essential role in homotypic membrane fusion (see [27] and references therein). To date there are no candidate plant proteins mediating such fusion events, other than potential ER SNAREs (soluble *N*-ethylmaleimide-sensitive fusion protein-attachment protein receptors) [47].

Factors regulating three-way junction and anchor-point formation are unknown (Figure 2). An intriguing possibility is that anchor points attach the ER to the plasma membrane thus 'anchoring' it in place in the cell as suggested from the video-enhanced microscopy studies of onion epidermal cells [2]. There is, however, no evidence to suggest that anchor points necessarily correspond with the position of tripartite junctions. Thus three-way junction formation could simply be a thermodynamically favourable configuration of stretched, interconnected membrane tubules.

The biological significance of ER shape in terms of tubulation compared with cisternalization is an interesting topic which is gaining renewed interest. A shift to cisternal over tubular ER was proposed to occur due to an increased secretory load in differentiating maize root cap cells [10] and during mobilization of seed storage protein in germinating mung bean cotyledons [9]. Similar conclusions were drawn from several studies in mammals; Rajasekaran et al. [48] showed that upon inducing secretion in rat pancreatic acinar carcinoma cells, the rough ER undergoes a structural change from tubular to cisternal form. However, this structural change was not concomitant with an overall increase in surface area, leading the authors to postulate that cisternal ER is more biosynthetically efficient. Additionally, overexpression of certain membrane proteins induces a shift to a more cisternal form of ER over tubular [49], as does a block in ER–Golgi trafficking through BFA (brefeldin A) treatment and expression of dominant-negative mutants involved at the ER–Golgi interface [50]. Intriguingly, ER remodelling is drastically affected during oomycete infection of leaves and can be mimicked by mechanical stimuli [51,52]. In both cases ER cisternae form around the infection/wound site, and are hypothesized to reflect increased protein and/or lipid production for the delivery of defence-related compounds to the site of action [51]. However, it is unclear whether this is a direct or indirect effect of the remodelling of the underlying cytoskeleton. Internal/external scaffold proteins, or regulation of internal volume by ion pumps and water flow restriction [53] have been suggested to control ER tubulation. However, the latter two models may be difficult to reconcile with the dynamic nature and permeability of the ER membrane.

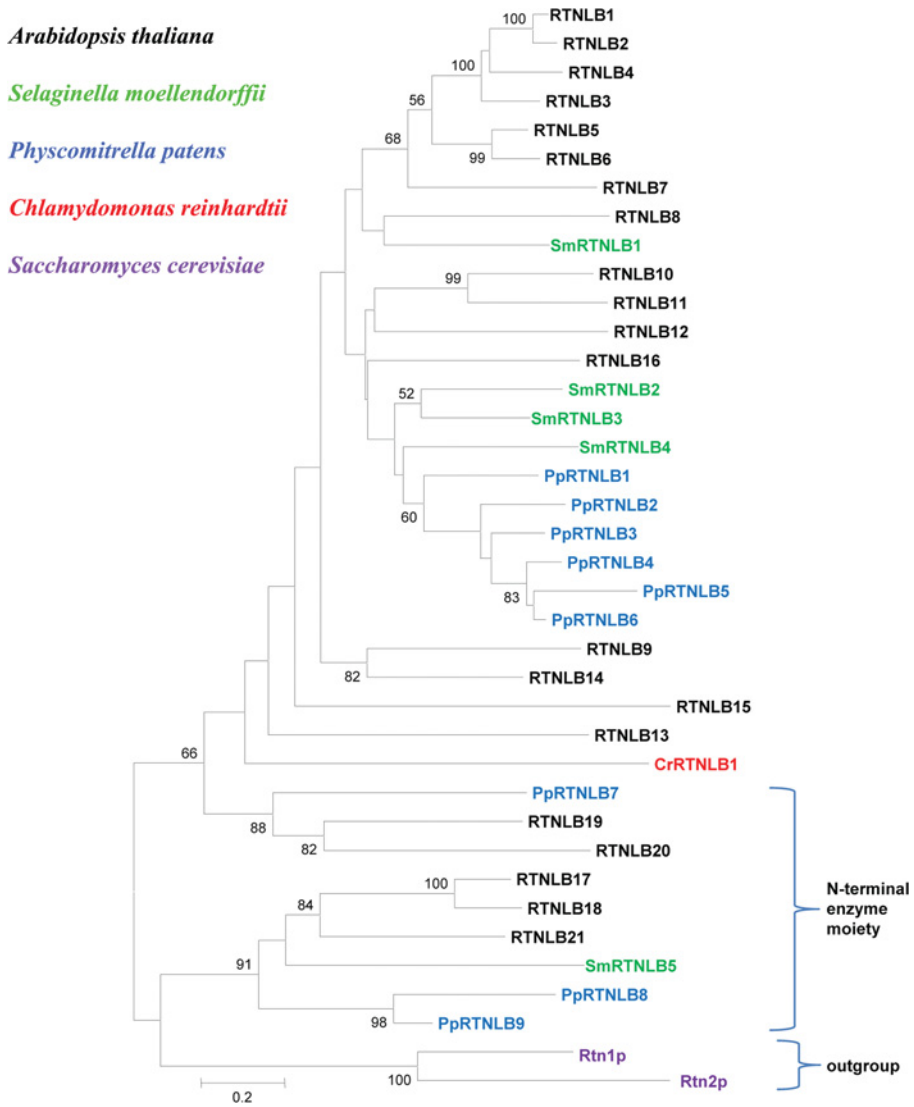

Figure 3 Evolutionary relationships of plant RHDs

The RHD sequences from the indicated reticulon proteins were aligned with ClustalW. The tree was produced with MEGA4.1 using the minimum evolution method with 1000 bootstrap repetitions. Yeast Rtn1p and Rtn2p were used as the outgroup. Bootstrap test results are shown where higher than 50. *P. patens*, *S. moellendorffii* and *C. reinhardtii* reticulons are here defined as PpRTNLB, SmRTNLB and CrRTNLB respectively. For the full accession numbers refer to Supplementary Figure S1 (at http://www.BiochemJ.org/bj/423/bj4230145add.htm).

Reticulons

As mentioned previously, the shape of the tubular ER does not depend on its attachment to the cytoskeleton [32], indicating the requirement for factors present within the ER membrane itself. It has previously been found that a family of membrane proteins called reticulons are enriched in tubular ER and can lead to ER tubule formation in an *in vitro* assay [54]. Reticulons are ubiquitous in higher eukaryotes. They contain a signature RHD (reticulon homology domain) which comprises two large hydrophobic regions, possibly further subdivided into four membrane-spanning segments [55]. Each RHD transmembrane segment is longer than the typical transmembrane helices of ER-localized membrane proteins [56], and therefore is likely to be inserted into the ER membrane at an angle [57,58]. This wedge-shaped conformation is postulated to confer curvature to the ER membrane [59,60] (Figure 2). The topology of plant reticulons has not yet been determined experimentally. Bioinformatic topology prediction for the *Arabidopsis* reticulon gene family using TOPCONS indicates that all members have a predicted 'W' topology, with N- and C-termini, plus the short loop between the large hydrophobic regions, exposed to the cytosol [61]. The same topology was described experimentally for mammalian Rtn4c [54]. A direct link between reticulon topology, transmembrane domain length and curvature has however not yet been established.

In the first systematic classification of reticulons [55], plant reticulon genes were denominated RTNLB (reticulon-like gene in plants, i.e. non-metazoan group B). Reticulon genes are very abundant in higher plants [55]. While only a single reticulon-like sequence was found in a search of the genome of the green alga *Chlamydomonas reinhardtii*, the moss *Physcomitrella patens* has at least nine isoforms, and at least five reticulon-like proteins are encoded by the spikemoss *Selaginella moellendorffii* genome (Figure 3). The *Arabidopsis* genome contains 21 isoforms (reported in [62]). Only four reticulon genes have been described in the human genome so far, but alternative splicing may account

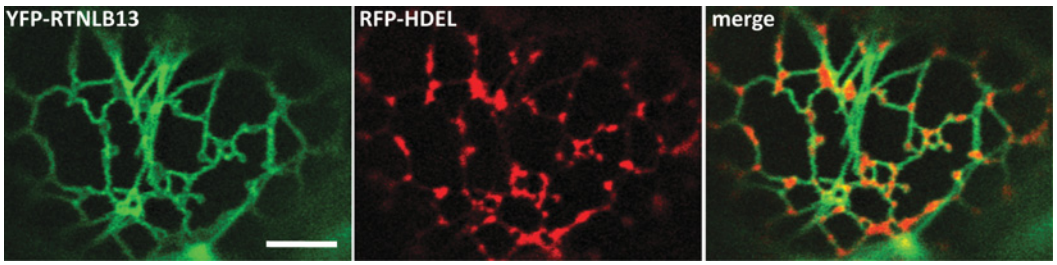

Figure 4 Overexpression of AtRTNLB13 induces constrictions in the tubular ER

Tobacco epidermal cells were agroinfiltrated with constructs encoding YFP–RTNLB13 (green) and the luminal ER marker RFP–HDEL (red). Note that while RTNLB13 labels the tubular ER, the luminal marker is constricted into discrete sections of the network. Scale bar = 5 μm.

for more numerous protein products [55]. The explosion of plant RTN gene diversity is very likely to reflect the increasing complexity and multifunctional role of the ER during higher plant evolution. It is tempting to speculate that different reticulons may underpin the variety of plant ER subdomains [63] and specialized ER functions such as the biosynthesis of oil bodies [64]. While the RHDs are highly conserved and the C-termini of reticulons are in general rather short, the N-terminal regions of reticulons are highly variable both in length and in sequence. This suggests that the N-terminus may be the key region for the intrinsic reticulon biological activity and protein–protein interactions. The *Arabidopsis* sequences of RTNLB17 to RTNLB21 stand out for a particularly long N-terminus that probably carries enzymatic activity [62]. Indeed, RTNLB19 was first identified for its activity as a 3-β-hydroxysteroid dehydrogenase/C-4 decarboxylase [65]. RTNLB20 is also annotated as a sterol dehydrogenase [66]. The *Arabidopsis* genome, however, encodes several sterol dehydrogenase isoforms that do not contain an RHD [65]. This, together with the fact that the long N-terminal regions of RTNLB17, RTNLB18 and RTNLB21 share similarity with a protein of so far unknown biological function, suggests that, beside its intrinsic structural role, the RHD may have been employed as an ER membrane-tethering domain. As enzyme-linked reticulons also exist in *P. patens* and *S. moellendorffii* (Figure 3), it is possible that the differentiation between reticulon-like tethers and 'structural' reticulons occurred early during plant evolution.

Plant reticulons have so far attracted limited attention, with only three functional works published in the literature [62,67,68]. Three reticulons (RTNLB1, RTNLB2 and RTNLB4) were found to interact with a pilin protein of *Agrobacterium tumefaciens* in a yeast two-hybrid screen [67]. Down-regulation of RTNLB1 by antisense resulted in lower rates of *Agrobacterium*-mediated transformation. GFP (green fluorescent protein) fusions to the coding sequences of these reticulons appeared to localize in structures reminiscent of the cortical ER in *Arabidopsis* roots [67]. It will be interesting to understand how these ER membrane proteins interact *in vivo* with the pilus proteins of *Agrobacterium*.

More recently, in an independent study, RTNLB2 and RTNLB4 were again fused to GFP and confirmed that these proteins localize to the ER, but also in punctate structures, in transgenic *Arabidopsis* or in transiently transfected protoplasts. No functional roles were established [62]. ER residence of RTNLB1 and RTNLB3 was also confirmed by proteome localization data [69].

Our laboratories have cloned one of the smallest reticulon isoforms, RTNLB13, which comprises an intact RHD flanked by very short N- and C-terminal regions. Upon overexpression of untagged RTNLB13 in tobacco epidermal cells, the cortical ER lost its normal reticular shape and became strikingly fragmented. However, when YFP–RTNLB13 (where YFP is yellow fluorescent protein) was co-expressed with the luminal marker RFP–HDEL (where RFP is red fluorescent protein), it was apparent that ER tubules remained intact (Figure 4). Thus the observed fragmentation results from a remodelling of the luminal space. FRAP (fluorescence recovery after photobleaching) analysis confirmed that overexpression of RTNLB13 results in the severely restricted diffusion of luminal ER proteins [68]. Preliminary analysis of anterograde transport by monitoring the secretory kinetics of a reporter protein under RTNLB13 overexpression indicated that, despite this severe morphological phenotype at the level of the ER, anterograde protein transport is unaffected [68]. This seems to indicate that a fully connected tubular ER network may not be necessary for a functional secretory pathway. Intriguingly, overexpression of RTNLB13 results in nodes of seemingly unrestricted ER lumen even though RTNLB13 surrounds these areas (Figure 4). Based on the earlier discussion of ER dynamics, it is possible that lack of restriction is due to steric hindrance from large protein complexes/scaffolds at immotile anchor points and/or potential interactions with factors required for ER network stability, perhaps with actin (Figure 2).

In total, 16 out of the 21 *Arabidopsis* reticulons contain the canonic dilysine ER membrane retrieval motif KKXX [70,71]. The addition of fluorescent proteins to the C-terminus of RTNLB2 and RTNLB4 however did not prevent the proteins from localizing to the ER [62]. Similarly, C-terminal tagging of RTNLB13 with YFP did not affect ER localization and stability [68]. It is possible that ER residence is afforded by the transmembrane topology of RTN and, more importantly, by their ability to interact with other ER-resident proteins or to homo-oligomerize [72]. The di-lysine motif could then have persisted either as an evolutionary relic or a safety valve mechanism.

Some of the interactions that guarantee ER residence are likely to be homotypic, as described for mammalian reticulons [72]. Indeed, RTNLB1–RTNLB3 were found to interact with each other, as well as with AtRabE1a, in a yeast two-hybrid assay [67]. No other interactions have so far been described for plant reticulons.

Dynamics of the ER surface

ER dynamics can be split into two types: network remodelling, as described above, and movement of the ER membrane surface itself. Previously Runions et al. [49], using a PAGFP (photoactivatable GFP) fusion to the transmembrane domain of calnexin (an ER-resident chaperone), demonstrated that, upon photoactivation, the fluorescent pool of protein displayed varying velocities and migrated in a radial or vectorial manner. Upon depolymerization of the actin cytoskeleton, only radial diffusive movement of the

photoactivated pool was observed, indicating an actin-dependent vectorial movement. Such studies demonstrated that, in tobacco leaf epidermal cells, if activation of the PAGFP construct on the ER membrane is continuous, the whole of the ER network can become fluorescent in 11 min, indicating that the whole pool of ER-targeted protein must pass through the activation spot in that time (J. Runions, personal communication). Such data indicate that the ER may present a mobile surface permitting movement of proteins within the cell. Certainly the ER has been implicated in the transport of viral movement proteins from the sites of synthesis in TMV (tobacco mosaic virus)-infected tobacco cells to the plasmodesmata during the infection process [73,74], and more recently in the movement of viral RNA granules [74,75]. Further studies are required to quantify the types and the physiological significance of membrane surface movement.

FUNCTIONAL DOMAINS OF THE ER

It has been suggested that there are numerous functional domains within the ER network of a plant cell, ranging from areas which accumulate specific products to connections with individual organelles [63]. For instance it has been hypothesized that the junction between the outer nuclear envelope and the ER forms a gated domain which controls the exchange of protein between the two organelles [63]. However, photobleaching experiments using GFP-tagged constructs of ER-resident proteins have shown that there can be free diffusion of protein between the lumen of the nuclear envelope and ER [20], although some degree of control here could be expected as these connections would be the site of entry of membrane-bound proteins specific to the inner and outer nuclear envelopes [76]. Another major domain would be at the plasma membrane where the desmotubules of plasmodesmata are most likely formed from compression of cortical ER passing between neighbouring cells [77]. This extensive topic is however, outside the scope of the present review.

ERES (ER exit sites)

Perhaps the most dynamic and controversial domain of the ER is that which represents sites of export to the Golgi apparatus, the so called ERES. This critical junction in the secretory pathway mediates the transport of both soluble and membrane cargo (proteins and lipids), and somehow involves the COPII coat protein machinery [78]. Transport between the two organelles can be bidirectional and it is thought that retrograde transport from the Golgi to the ER is mediated by COPI vesicles, as blockage of the COPI machinery either by BFA [79] or by expression of non-functional ARF1 (ADP-ribosylation factor 1) results in the redistribution of Golgi membrane markers into the ER [80]. All of the molecular components of ERES identified in yeast and mammalian cells exist in plants [78,81] and most of the components, with the exception of the exit site scaffold protein Sec16 [82], have been co-located to the Golgi using fluorescent protein constructs.

In leaves, live-cell imaging of epidermal cells expressing a range of exit site markers such as the small GTPase Sar1p [50], COPII coat components Sec23p/Sec24p, Sec13 [80,83], and ER and *cis*-Golgi SNAREs [84] in combination with Golgi membrane markers [26], resulted in the development of the 'motile export site' hypothesis. This proposes that Golgi bodies and the ERES exist as a tight unit embedded into the ER membrane and are motile over or with the ER membrane [49,50,78]. Such a concept has been challenged in BY-2 cells where Yang et al. [85] suggested that there was only transient association of Golgi stacks with ERES. However, more recently it has been confirmed that in *Arabidopsis* leaves, tobacco leaves and BY-2 cells, COPII exit site proteins Sec24 and Sec13 maintain a constant association with Golgi stacks [83]. Thus unless new Golgi stacks are being formed, exit sites and Golgi bodies are never found separate from each other. It has however been shown that the ER has the capacity to form new exit sites, and thus new Golgi, in response to the expression of membrane cargo such as the ERD2 (ER retention defective 2) protein, but not in response to overexpression of soluble secretory cargo such as secreted GFP [86]. Also the ER has the capacity to produce new Golgi stacks after the dissolution of the Golgi with BFA [79]. A study on tobacco BY-2 cells showed that the first reformation event was the appearance at the ER surface of buds and clusters of vesicles which appeared to fuse together to form mini-stacks that subsequently differentiated into large Golgi stacks prior to fission into two stacks [87]. To date there is no evidence that this process requires the formation of free COPII vesicles at the ERES.

The exact physical nature of ERES is a matter of controversy. In leaves, hypocotyls and suspension culture cells (i.e. vacuolate cells) it is clear that Golgi bodies are intimately associated with the ER [26,78,88]. However, the structure of the ER–Golgi interface is still a matter of speculation. We have proposed that due to the closeness of the two organelles, cargo transfer could easily be mediated by direct membrane connections or tubules [89]. This would require the COPII scaffold to form in order to initiate membrane curvature and maybe concentrate putative cargo receptors, but would not require the formation of independent COPII vesicles. Thus the Golgi itself could be considered to be a specialized domain of the ER with ERES initiating the biogenesis of a new Golgi stack depending on the physiological requirements of the cell. Direct connections between the plant Golgi and the ER have long been reported in the ultrastructural literature using conventional fixation and selective staining techniques [20,90–93]. In contrast, there have been no ultrastructural reports of COPII vesicles between the ER and Golgi in the majority of plant tissues studied by live-cell imaging of the ER and Golgi. In rapidly frozen freeze-substituted root and suspension culture material, however, tomographic analysis reveals vesicles which were assumed to be COPII [94,95]. These data were used to support the 'stop-and-go' hypothesis of Golgi function, whereby rapidly moving free Golgi are captured by tethering proteins such as P115 (see below) at the ERES, where cargo exchange takes place via COPII vesicles. When replete, Golgi bodies would be released back into the cytosol. However, until the necessary live-cell imaging experiments can be successfully carried out on such cytoplasmically dense cells, there will be no firm evidence for one population of Golgi stacks that exist free of the ER and another population that is permanently attached to ERES, but can occasionally break free from their tethers [89]. However, it is clear that, in meristems, Golgi movement appears restricted compared with that in more vacuolate cells and as such it is possible that there may be populations of Golgi stacks with different ER associations [78].

The functional connection between the ER and Golgi body is mirrored by the close association of the two compartments; live-cell imaging has indicated that Golgi body movement appears to mirror the underlying ER (Supplementary Movie S2 at http://www.BiochemJ.org/bj/423/bj4230145add.htm), and on occasion ER tubule formation appears to follow the path of Golgi bodies [20,26,49]. Therefore, based on these observations, the question as to whether the movement of these compartments are (in)dependent of one another was posed [89]. Recently, using laser-trapping technology we have shown that it is possible to capture and manipulate individual Golgi bodies in *Arabidopsis* leaf epidermal cells co-expressing fluorescent ER and Golgi

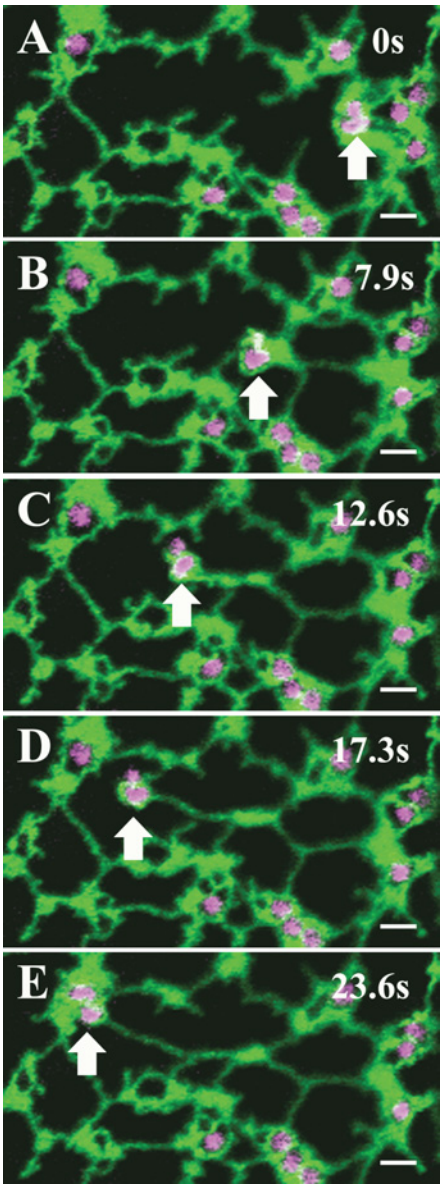

Figure 5 Golgi micromanipulation affects ER remodelling

A Golgi body (magenta, white arrow), in an *Arabidopsis thaliana* leaf epidermal cell treated with latrunculin b, was trapped and subsequent movement resulted in the remodelling of the associated ER (green). Sequential images from a movie sequence are shown and times are indicated. Scale bar = 2 μm.

markers [22]. If the actin cytoskeleton was depolymerized to inhibit Golgi movement, Golgi bodies associated with the cortical ER could be captured in the focused laser beam and any lateral movement of the beam resulted not only in lateral displacement of the Golgi stack, but also in the extension or growth of the associated ER tubule (Figure 5 and Supplementary Movie S3 at http://www.BiochemJ.org/bj/423/bj4230145add.htm). Thus Golgi bodies do appear to have an attachment to the ER. On occasions when Golgi bodies could be pulled free from ER tubules it was possible to recapture the ER simply by docking a Golgi body on to the tip of the tubule, which resulted in attachment being re-established. This supports the contention that there must be a system of tethering factors or peripheral matrix proteins that can freely attach to the ER maintaining the cohesiveness of the export site/Golgi complex [94]. These results do not formally prove that in an unperturbed system Golgi body movement induces ER remodelling directly. Therefore the question remains as to whether Golgi body movement and ER remodelling are interdependent processes which utilize the same set of molecular motors/tethering factors, or whether actin polymerization directly affects ER tubule growth through tethering factors (Figure 2).

Although there is an extensive literature on ER–Golgi tethering factors in mammalian and yeast cells (see [96,97]), only more recently have peripheral membrane proteins been identified in plant Golgi which may have a tethering role [98,99]. Some of these, the homologues of P115, CASP and Golgin 84 appear to be located towards the *cis*-face of the Golgi and could be candidates for ER-tethering factors [94,98]. Sinka et al. [100] have recently proposed a model for the Golgi whereby the organelle is surrounded by a mass of tentacular molecules of tethering protein that, via Rab-binding sites, capture Rab-containing membranes such as ER-to-Golgi carriers. Some plant *trans*-Golgi-associated proteins have also been shown to bind small ATPases such as ARL1 [101–103] and AtRabH1$^{b/c}$ [102]. As yet, Rab binding has not been reported on *cis*-Golgi proteins, but such a model could explain the ability of individual laser-trapped Golgi to re-capture ER membranes.

PAC (precursor accumulating) vesicles and ER-to-vacuole transport

Several proteins can be targeted to the vacuole directly from the ER, in a route that does not involve the Golgi apparatus. Hara-Nishimura et al. [104] have reported that pumpkin storage protein precursors exit the ER in large PAC vesicles which eventually fuse with protein storage vacuoles. The PAC vesicles seem to acquire proteins carrying Golgi-modified N-glycans, which are seen by electron microscopy at the periphery of the ER-derived protein core [104]. In addition to storage proteins, a class of cysteine proteases which carry the ER retention signal H/KDEL, have also been observed to travel to the vacuole, where the ER retention signal is removed [105]. A small proportion of some recombinant proteins bearing H/KDEL have also been shown to reach the vacuole, in a route that may [106], or may not [107], require transport through the Golgi apparatus. The molecular details of these ER-to-vacuole transport routes are at present unclear.

The ER as a storage compartment: oil bodies, grass storage proteins and fusiform bodies

Whether or not they can be classified as specific domains, the ER in many tissue types has the capacity to store material in so called 'ER bodies' [19]. Such material can either remain in the ER or be exported from the ER and exist as discrete organelles such as oil bodies or protein bodies [19,63].

Oil bodies are essential storage organelles in seeds and are formed from the ER by insertion of TAGs (triacylglycerols) within the lipid bilayer of the ER (see [108] for a review). TAGs are synthesized by DAGTs [DAG (diacylglycerol) transferases] which are located to distinct subdomains of the ER [109]. Being hydrophobic, TAGs accumulate between the lipid bilayer and form a bud that enlarges into an oil body, which can eventually break free from the ER. The lipid monolayer of the oil body is characterized by small proteins of the oleosin family which cover the surface of the oil bodies. These proteins are synthesized on the ER membrane and are transported on the ER to sites of synthesis of oil bodies [110]. This again demonstrates the capacity of the ER surface to act as a dynamic surface for transport of macromolecules (see above).

In dicotyledonous plants, most of the protein that is destined for storage in specialized vacuoles during seed maturation is passed

through the Golgi apparatus and deposited in a storage vacuole [111,112]. However, in many grasses and cereals storage proteins such as the prolamins are sequestered in the ER as an insoluble matrix and form distinct protein bodies that may remain in the ER or be delivered directly to the vacuole for storage [15,17,19,113].

Perhaps one of the most striking examples of 'ER bodies' are the fusiform bodies commonly found in the lumen of the ER of *Arabidopsis* and highlighted by many GFP fusions [18,114,115]. These can be large, 1 μm in diameter and up to 10 μm long and predominantly contain a β-glucosidase (PYK10) with the C-terminal ER retrieval KDEL motif. Similar bodies containing an inducible β-glucosidase (BGL1) have been identified in wounded cotyledons and rosette leaves [18]. Remarkably, these fusiform bodies move at considerable speed in the cytosol and, as it is assumed that the ER has no luminal cytoskeleton, the motive force must come from movement of the whole of the ER, thus reflecting the motile nature of this organelle, as revealed by the photoactivation experiments described previously [49].

Peroxisome biogenesis and the role of the ER

Until recently, the potential role of the ER in peroxisome biogenesis has been hotly debated. The cortical ER is far-reaching throughout the cell, and observations indicating an intimate association between the ER and other classes of organelle can be frequently found. This is compounded by the variable morphology of peroxisomes, which in some cases are spherical but can even have long tail-like protrusions called peroxules [37,116], which apparently co-align with the ER [117]. Such observations and the occasional apparent direct membrane continuities between peroxisomes and the ER seemed to indicate that peroxisomes arose from the ER [118]. However, the development of molecular and genetic tools proved that peroxisome matrix proteins were synthesized on free polyribosomes and inserted directly into peroxisomes via interaction with cytosolic receptors (PEX5 and PEX7). The 'multiplication-by-division' model whereby peroxisomes arise from the growth and division of pre-existing peroxisomes was thus proposed [119]. However, this model could not reconcile how peroxisomes were able to be synthesized *de novo* in certain yeast and mammalian cell line mutants, and how PMPs (peroxisome membrane proteins) and lipids could be synthesized and transported to the organelle.

Several targeting studies and chemical (BFA) perturbation at the ER–Golgi interface have indicated that certain plant PMPs (APX, PEX10 and PEX16) are located to the ER [120–126]. However, transient expression studies in tobacco leaf epidermal cells indicated that both PEX2 and PEX10 do not localize to the ER upon BFA treatment or through genetic perturbation (Sar1–GTP locked mutant) at the ER–Golgi interface [127]. Studies of the TBSV (tomato bushy stunt virus) replication protein, p33, have shown that it targets to the peroxisomes and traffics to the ER in vesicular carriers containing PMPs, but it is unclear whether this retrograde pathway occurs in uninfected cells [128]. Similar studies of PMPs in yeast and mammalian cell cultures have been performed, and are detailed in several reviews [129,130]. The development of new fluorescent protein tools allowing the visualization of pools of protein through photoactivation have shown that Pex16p, a PMP in mammals, is present in the ER and subsequently traffics to the peroxisomes [131].

The current model for peroxisome biogenesis therefore appears to be an interplay between the autonomous 'multiplication-by-division' and the ER vesiculation model, whereby peroxisome precursors containing early PMPs bud from the ER into which additional matrix and late PMPs are post-translationally inserted to allow for growth and division.

ER–plastid interactions

For many years there have been regular reports of connections between ER and plastid envelopes (see [63,132] for reviews) which have mainly derived from ultrastructural studies [133]. This has led to much speculation as to the function of such connections and whether they also facilitate direct transfer of macromolecules between the two organelles.

It is well established that chloroplast development requires lipid precursors, such as DAGs, that are synthesized in the ER membrane [132,134]. Therefore there has been much speculation on the possible routes of transfer of lipid precursors from the ER to the plastid membrane, including protein-mediated transfer, vesicle trafficking or direct transfer via contact sites between the two organelles [132]. The validity of these contact sites has been tested in protoplasts expressing GFP targeted to the lumen of the ER. On rupturing protoplasts, ER fragments remained attached to chloroplasts [134] and optical trapping and displacement of such chloroplasts resulted in stretching out of the ER fragments [135]. This does not however preclude the possibility that the ER in such a disrupted system is 'sticky' and experiments need to be performed *in vivo* to confirm these results. Recently an *Arabidopsis* gene, *TGD4* (trigalactosyldiacylglycerol 4), has been described which encodes an ER membrane protein which is proposed to be a component of the machinery mediating lipid transfer to the chloroplast membrane, as a mutant prevents the availability of ER DAG for chloroplast galactoglycerolipid synthesis [134]. The authors proposed one model where TGD4 could be active in mediating lipid transfer at ER chloroplast contact sites. However, it has also been reported that there may be a trafficking pathway from the ER to plastids via the Golgi apparatus. Several chloroplast proteins including a carbonic anhydrase [136] and a nucleotide pyrophosphatase/phosphodiesterase [137] have been shown to be N-glycosylated and their transport is BFA-sensitive indicating passage through the Golgi. If it is assumed that the transport vector from the Golgi to the chloroplast is membrane bounded then this could also be a pathway for the trafficking of plastid lipids or lipid precursors.

Although it is not impossible that such ER plastid membrane contact sites are involved in lipid transfer between the organelles, it must be appreciated that in many cells there is limited free cytosolic space. This may be restricted by large central vacuoles or even by the sheer number of chloroplasts themselves. Therefore in the context of the presence of a highly mobile ER phase within the cell, it is hardly surprising that it frequently makes and breaks contact with the surface of other organelles.

Another possible function of the cortical ER network is a role in graviperception of statocytes. A number of years ago it was suggested that graviperception may be sensed by the sedimentation of amyloplasts (statoliths) on to cortical ER in root cap statocytes which would generate a signal to the root growth zone [138]. This model however was subsequently dismissed [139], but has recently been revisited [140]. In *Arabidopsis* root cells it was shown that sedimenting statoliths can cause deformation of cortical ER, as they are induced to sediment by reorientation of the root. It was proposed that this interaction is a mode of mechanosensing that could induce the gravity-perceiving response.

OUTSTANDING QUESTIONS

Although the ER is one of the major organelles in the cell occupying a major portion of the cytosol, and much is known about its functions in terms of protein synthesis, folding, glycosylation and quality control, there are still many questions to be answered regarding its structure and relationships to other organelles.

For instance, why does the ER maintain such an energetically unfavourable shape in being tubular with some cisternae, while alterations to its shape do not seem to severely affect anterograde secretory traffic? Is there a function for the movement of the ER network in terms of moving proteins and even other organelles around the cytoplasm? Is there direct exchange of lipids and protein between the ER and other organelles such as mitochondria and plastids and, most intriguingly, what proteins are involved in anchoring the cortical ER network to the plasma membrane? Is there direct molecular exchange with the plasma membrane and is the cortical microtubule network interacting in any way with the ER? Such questions will undoubtedly be addressed in the near future.

ACKNOWLEDGEMENTS

We thank Stefano Gattolin and Eleanor Pinnock for help with the phylogenetic analysis of plant reticulons.

FUNDING

The work in the C. H. and L. F. Laboratories has been supported by the Leverhulme Trust; the Biotechnology and Biological Sciences Research Council; and the EU PharmaPlanta consortium.

REFERENCES

1 Porter, K. R. and Machado, R. D. (1960) Studies on the endoplasmic reticulum. IV. Its form and distribution during mitosis in cells of onion root tip. J. Biophys. Biochem. Cytol. **7**, 167–180
2 Lichtscheidl, I. K. and Url, W. G. (1990) Organisation and dynamics of cortical endoplasmic reticulum in inner epidermal cells of onion bulb scales. Protoplasma **157**, 203–215
3 Boevink, P., Santa Cruz, S., Hawes, C., Harris, N. and Oparka, K. J. (1996) Virus-mediated delivery of the green fluorescent protein to the endoplasmic reticulum of plant cells. Plant J. **10**, 935–941
4 Hepler, P. K., Palevitz, B. A., Lancelle, S. A. and McCauley, M. (1990) Cortical endoplasmic reticulum in plants. J. Cell Sci. **96**, 335–373
5 Gunning, B. E. and Steer, M. W. (1969) Plant Cell Biology, Structure and Function, Jones and Bartlett Publishers, Sudbury, U.S.A.
6 Ridge, R. W., Uozumi, Y., Plazinski, J., Hurley, U. A. and Williamson, R. E. (1999) Developmental transitions and dynamics of the cortical ER of *Arabidopsis* cells seen with green fluorescent protein. Plant Cell Physiol. **40**, 1253–1261
7 Gupton, S. L., Collings, D. A. and Allen, N. S. (2006) Endoplasmic reticulum targeted GFP reveals ER organization in tobacco NT-1 cells during cell division. Plant Physiol. Biochem **44**, 95–105
8 Quader, H., Hofmann, A. and Schnepf, E. (1989) Reorganisation of the endoplasmic reticulum in epidermal cells of onion bulb scales after cold stress: involvement of cytoskeletal elements. Planta **177**, 273–280
9 Harris, N. and Chrispeels, M. J. (1980) The endoplasmic reticulum of mung-bean cotyledons quantitative morphology of cisternal and tubular ER during seedling growth. Planta **148**, 293–303
10 Stephenson, J. L. M. and Hawes, C. R. (1986) Stereology and stereometry of endoplasmic reticulum during differentiation in the maize root cap. Protoplasma **131**, 32–46
11 Hawes, C. R., Juniper, B. E. and Horn, J. C. (1981) Low and high voltage electron microscopy of mitosis and cytokinesis in maize. Planta **152**, 397–407
12 Massalski, A. and Leedale, G. F. (1969) Cytology and ultrastructure of the Xanthophyceae. I. Comparative morphology of the zoospores of *Bumilleria sicula Borzi* and *Tribonema vulgare Pascher*. Brit. Phycol. J. **4**, 159–180
13 Pattison, R. J. and Amtmann, A. (2009) N-glycan production in the endoplasmic reticulum of plants. Trends Plant Sci. **14**, 92–99
14 Vitale, A. and Denecke, J. (1999) The endoplasmic reticulum: gateway of the secretory pathway. Plant Cell **11**, 615–628
15 Vitale, A. and Boston, R. S. (2008) Endoplasmic reticulum quality control and the unfolded protein response: insights from plants. Traffic **9**, 1581–1588
16 Hong, B., Ichida, A., Wang, Y., Gens, J. S., Pickard, B. G. and Harper, J. F. (1999) Identification of a calmodulin-regulated Ca^{2+}-ATPase in the endoplasmic reticulum. Plant Physiol. **119**, 1165–1175
17 Vitale, A. and Ceriotti, A. (2004) Protein quality control mechanisms and protein storage in the endoplasmic reticulum. A conflict of interests? Plant Physiol. **136**, 3420–3426
18 Hara-Nishimura, I., Matsushima, R., Shimada, T. and Nishimura, M. (2004) Diversity and formation of endoplasmic reticulum-derived compartments in plants. Are these compartments specific to plant cells? Plant Physiol. **136**, 3435–3439
19 Herman, E. M. (2008) Endoplasmic reticulum bodies: solving the insoluble. Curr. Opin. Plant Biol. **11**, 672–679
20 Brandizzi, F., Snapp, E. L., Roberts, A. G., Lippincott-Schwartz, J. and Hawes, C. (2002) Membrane protein transport between the endoplasmic reticulum and the Golgi in tobacco leaves is energy dependent but cytoskeleton independent: evidence from selective photobleaching. Plant Cell **14**, 1293–1309
21 Knebel, W., Quader, H. and Schnepf, E. (1990) Mobile and immobile endoplasmic reticulum in onion bulb epidermis cells: short- and long-term observations with a confocal laser scanning microscope. Eur. J. Cell Biol. **52**, 328–340
22 Sparkes, I. A., Ketelaar, T., De Ruijter, N. C. A. and Hawes, C. (2009) Grab a Golgi: laser trapping of Golgi bodies reveals *in vivo* interactions with the endoplasmic reticulum. Traffic **10**, 567–571
23 Sbalzarini, I. F., Mezzacasa, A., Helenius, A. and Koumoutsakos, P. (2005) Effects of organelle shape on fluorescence recovery after photobleaching. Biophys. J. **89**, 1482–1492
24 Radochova, B., Janacek, J., Schwarzerova, K., Demjenova, E., Tomori, Z., Karen, P. and Kubinova, L. (2005) Analysis of endoplasmic reticulum of tobacco cells using confocal microscopy. Image Anal. Stereol. **24**, 181–185
25 Bouchekhima, A. N., Frigerio, L. and Kirkilionis, M. (2009) Geometric quantification of the plant endoplasmic reticulum. J. Microsc. **234**, 158–172
26 Boevink, P., Oparka, K., Santa Cruz, S., Martin, B., Betteridge, A. and Hawes, C. (1998) Stacks on tracks: the plant Golgi apparatus traffics on an actin/ER network. Plant J. **15**, 441–447
27 Vedrenne, C. and Hauri, H. P. (2006) Morphogenesis of the endoplasmic reticulum: beyond active membrane expansion. Traffic **7**, 639–646
28 Reuzeau, C., McNally, J. G. and Pickard, B. G. (1997) The endomembrane sheath: a key structure for understanding the plant cell? Protoplasma **200**, 1–9
29 Terasaki, M., Chen, L. B. and Fujiwara, K. (1986) Microtubules and the endoplasmic reticulum are highly interdependent structures. J. Cell Biol. **103**, 1557–1568
30 Foissner, I., Menzel, D. and Wasteneys, G. O. (2009) Microtubule-dependent motility and orientation of the cortical endoplasmic reticulum in elongating Characean internodal cells. Cell Motil. Cytoskel. **66**, 142–155
31 Langhans, M., Niemes, S., Pimpl, P. and Robinson, D. G. (2009) Oryzalin bodies: in addition to its anti-microtubule properties, the dinitroaniline herbicide oryzalin causes nodulation of the endoplasmic reticulum. Protoplasma **236**, 73–84
32 Dreier, L. and Rapoport, T. A. (2000) *In vitro* formation of the endoplasmic reticulum occurs independently of microtubules by a controlled fusion reaction. J. Cell Biol. **148**, 883–898
33 Liebe, S. and Menzel, D. (1995) Actomyosin-based motility of endoplasmic reticulum and chloroplasts in Vallisneria mesophyll cells. Biol. Cell **85**, 207–222
34 Nebenfuhr, A., Gallagher, L. A., Dunahay, T. G., Frohlick, J. A., Mazurkiewicz, A. M., Meehl, J. B. and Staehelin, L. A. (1999) Stop-and-go movements of plant Golgi stacks are mediated by the acto-myosin system. Plant Physiol. **121**, 1127–1141
35 Van Gestel, K., Kohler, R. H. and Verbelen, J. P. (2002) Plant mitochondria move on F-actin, but their positioning in the cortical cytoplasm depends on both F-actin and microtubules. J. Exp. Bot. **53**, 659–667
36 Mathur, J., Mathur, N. and Hulskamp, M. (2002) Simultaneous visualisation of peroxisomes and cytoskeletal elements reveals actin and not microtubule-based peroxisome motility in plants. Plant Physiol. **128**, 1031–1045
37 Mano, S., Nakamori, C., Hayashi, M., Kato, A., Kondo, M. and Nishimura, M. (2002) Distribution and characterization of peroxisomes in Arabidopsis by visualization with GFP: dynamic morphology and actin-dependent movement. Plant Cell Physiol. **43**, 331–341
38 Collings, D. A., Harper, J. D. I. and Vaughn, K. C. (2003) The association of peroxisomes with the developing cell plate in dividing onion root cells depends on actin microfilaments and myosin. Planta **218**, 204–216
39 Jedd, G. and Chua, N. H. (2002) Visualization of peroxisomes in living plant cells reveals acto-myosin-dependent cytoplasmic streaming and peroxisome budding. Plant Cell Physiol. **43**, 384–392
40 Sparkes, I. A., Teanby, N. A. and Hawes, C. (2008) Truncated myosin XI tail fusions inhibit peroxisome, Golgi, and mitochondrial movement in tobacco leaf epidermal cells: a genetic tool for the next generation. J. Exp. Bot. **59**, 2499–2512
41 Avisar, D., Abu-Abied, M., Belausov, E., Sadot, E., Hawes, C. and Sparkes, I. A. (2009) A comparative study of the involvement of 17 *Arabidopsis* myosin family members on the motility of Golgi and other organelles. Plant Physiol. **150**, 700–709

42 Avisar, D., Prokhnevsky, A. I., Makarova, K. S., Koonin, E. V. and Dolja, V. V. (2008) Myosin XI-K is required for rapid trafficking of Golgi stacks, peroxisomes and mitochondria in leaf cells of *Nicotiana benthamiana*. Plant Physiol. **146**, 1098–1108

43 Peremyslov, V. V., Prokhnevsky, A. I., Avisar, D. and Dolja, V. V. (2008) Two class XI myosins function in organelle trafficking and root hair development in *Arabidopsis thaliana*. Plant Physiol. **146**, 1109–1116

44 Prokhnevsky, A. I., Peremyslov, V. V. and Dolja, V. V. (2008) Overlapping functions of the four class XI myosins in *Arabidopsis* growth, root hair elongation and organelle motility. Proc. Natl. Acad. Sci. U.S.A. **105**, 19744–19749

45 Golomb, L., Abu-Abied, M., Belausov, E. and Sadot, E. (2008) Different subcellular localizations and functions of *Arabidopsis* myosin VIII. BMC Plant Biol. **8**, 3

46 Yokota, E., Ueda, S., Tamura, K., Orii, H., Uchi, S., Sonobe, S., Hara-Nishimura, I. and Shimmen, T. (2008) An isoform of myosin XI responsible for the translocation of endoplasmic reticulum in tobacco cultured BY-2 cells. J. Exp. Bot. **60**, 197–212

47 Uemura, T., Ueda, T., Ohniwa, R. L., Nakano, A., Takeyasu, K. and Sato, M. H. (2004) Systematic analysis of SNARE molecules in *Arabidopsis*: dissection of the post-Golgi network in plant cells. Cell Struct. Funct. **29**, 49–65

48 Rajasekaran, A. K., Morimoto, T., Hanzel, D. K., Rodriguez-Boulan, E. and Kreibich, G. (1993) Structural reorganization of the rough endoplasmic reticulum without size expansion accounts for dexamethasone-induced secretory activity in AR42J cells. J. Cell Sci. **105**, 333–345

49 Runions, J., Brach, T., Kuhner, S. and Hawes, C. (2006) Photoactivation of GFP reveals protein dynamics within the endoplasmic reticulum membrane. J. Exp. Bot. **57**, 43–50

50 DaSilva, L. L., Snapp, E. L., Denecke, J., Lippincott-Schwartz, J., Hawes, C. and Brandizzi, F. (2004) Endoplasmic reticulum export sites and Golgi bodies behave as single mobile secretory units in plant cells. Plant Cell **16**, 1753–1771

51 Takemoto, D., Jones, D. A. and Hardham, A. R. (2003) GFP-tagging of cell components reveals the dynamics of subcellular re-organization in response to infection of *Arabidopsis* by oomycete pathogens. Plant J. **33**, 775–792

52 Hardham, A. R., Takemoto, D. and White, R. G. (2008) Rapid and dynamic subcellular reorganization following mechanical stimulation of *Arabidopsis* epidermal cells mimics responses to fungal and oomycete attack. BMC Plant Biol. **8**, 63

53 Voeltz, G. K., Rolls, M. M. and Rapoport, T. A. (2002) Structural organization of the endoplasmic reticulum. EMBO Rep. **3**, 944–950

54 Voeltz, G. K., Prinz, W. A., Shibata, Y., Rist, J. M. and Rapoport, T. A. (2006) A class of membrane proteins shaping the tubular endoplasmic reticulum. Cell **124**, 573–586

55 Oertle, T., Klinger, M., Stuermer, C. A. O. and Schwab, M. E. (2003) A reticular rhapsody: phylogenic evolution and nomenclature of the RTN/Nogo gene family. FASEB J. **17**, 1238–1247

56 Brandizzi, F., Frangne, N., Marc-Martin, S., Hawes, C., Neuhaus, J. M. and Paris, N. (2002) The destination for single-pass membrane proteins is influenced markedly by the length of the hydrophobic domain. Plant Cell **14**, 1077–1092

57 Shibata, Y., Voeltz, G. K. and Rapoport, T. A. (2006) Rough sheets and smooth tubules. Cell **126**, 435–439

58 Voeltz, G. K. and Prinz, W. A. (2007) Sheets, ribbons and tubules: how organelles get their shape. Nat. Rev. Mol. Cell Biol. **8**, 258–264

59 Zimmerberg, J. and Kozlov, M. M. (2006) How proteins produce cellular membrane curvature. Nat. Rev. Mol. Cell Biol. **7**, 9–19

60 Hu, J., Shibata, Y., Voss, C., Shemesh, T., Li, Z., Coughlin, M., Kozlov, M. M., Rapoport, T. A. and Prinz, W. A. (2008) Membrane proteins of the endoplasmic reticulum induce high-curvature tubules. Science **319**, 1247–1250

61 Bernsel, A., Viklund, H., Falk, J., Lindahl, E., von Heijne, G. and Elofsson, A. (2008) Prediction of membrane-protein topology from first principles. Proc. Natl. Acad. Sci. U.S.A. **105**, 7177–7181

62 Nziengui, H., Bouhidel, K., Pillon, D., Der, C., Marty, F. and Schoefs, B. (2007) Reticulon-like proteins in *Arabidopsis thaliana*: structural organization and ER localization. FEBS Lett. **581**, 3356–3362

63 Staehelin, L. A. (1997) The plant ER: a dynamic organelle composed of a large number of discrete functional domains. Plant J. **11**, 1151–1165

64 Murphy, D. J. and Vance, J. (1999) Mechanisms of lipid-body formation. Trends Biochem. Sci. **24**, 109–115

65 Rahier, A., Darnet, S., Bouvier, F., Camara, B. and Bard, M. (2006) Molecular and enzymatic characterizations of novel bifunctional 3β-hydroxysteroid dehydrogenases/C-4 decarboxylases from *Arabidopsis thaliana*. J. Biol. Chem. **281**, 27264–27277

66 Schwacke, R., Schneider, A., van der Graaff, E., Fischer, K., Catoni, E., Desimone, M., Frommer, W. B., Flugge, U.-I. and Kunze, R. (2003) ARAMEMNON, a novel database for *Arabidopsis* integral membrane proteins. Plant Physiol. **131**, 16–26

67 Hwang, H.-H. and Gelvin, S. B. (2004) Plant proteins that interact with VirB2, the *Agrobacterium tumefaciens* pilin protein, mediate plant transformation. Plant Cell **16**, 3148–3167

68 Tolley, N., Sparkes, I. A., Hunter, P. R., Craddock, C. P., Nuttall, J., Roberts, L. M., Hawes, C., Pedrazzini, E. and Frigerio, L. (2008) Overexpression of a plant reticulon remodels the lumen of the cortical endoplasmic reticulum but does not perturb protein transport. Traffic **9**, 94–102

69 Dunkley, T. P., Hester, S., Shadforth, I. P., Runions, J., Weimar, T., Hanton, S. L., Griffin, J. L., Bessant, C., Brandizzi, F., Hawes, C. et al. (2006) Mapping the *Arabidopsis* organelle proteome. Proc. Natl. Acad. Sci. U.S.A. **103**, 6518–6523

70 Contreras, I., Ortiz-Zapater, E. and Aniento, F. (2004) Sorting signals in the cytosolic tail of membrane proteins involved in the interaction with plant ARF1 and coatomer. Plant J. **38**, 685–698

71 Nilsson, T., Jackson, M. and Peterson, P. A. (1989) Short cytoplasmic sequences serve as retention signals for transmembrane proteins in the endoplasmic reticulum. Cell **58**, 707–718

72 Shibata, Y., Voss, C., Rist, J. M., Hu, J., Rapoport, T. A., Prinz, W. A. and Voeltz, G. K. (2008) The reticulon and DP1/Yop1p proteins form immobile oligomers in the tubular endoplasmic reticulum. J. Biol. Chem. **283**, 18892–18904

73 Heinlein, M., Padgett, H. S., Gens, J. S., Pickard, B. G., Casper, S. J., Epel, B. L. and Beachy, R. N. (1998) Changing patterns of localization of the tobacco mosaic virus movement protein and replicase to the endoplasmic reticulum and microtubules during infection. Plant Cell **10**, 1107–1120

74 Wright, K. M., Wood, N. T., Roberts, A. G., Chapman, S., Boevink, P., Mackenzie, K. M. and Oparka, K. J. (2007) Targeting of TMV movement protein to plasmodesmata requires the actin/ER network: evidence from FRAP. Traffic **8**, 21–31

75 Christensen, N. M., Faulkner, C. and Oparka, K. (2009) Evidence for unidirectional flow through plasmodesmata. Plant Physiol. **150**, 96–104

76 Evans, D. E., Irons, S. L., Graumann, K. and Runions, J. (2009) The plant nuclear envelope. In Functional Organization of the Plant Nucleus. (Meier, I., ed.), pp. 9–28, Springer-Verlag Berlin, Heidelberg

77 Oparka, K. J. (2005) Plasmodesmata. Ann. Plant. Rev. **18**, 331

78 Hawes, C., Osterrieder, A., Hummel, E. and Sparkes, I. (2008) The plant ER–Golgi interface. Traffic **9**, 1571–1580

79 Saint-Jore, C. M., Evins, J., Batoko, H., Brandizzi, F., Moore, I. and Hawes, C. (2002) Redistribution of membrane proteins between the Golgi apparatus and endoplasmic reticulum in plants is reversible and not dependent on cytoskeletal networks. Plant J. **29**, 661–678

80 Stefano, G., Renna, L., Chatre, L., Hanton, S. L., Moreau, P., Hawes, C. and Brandizzi, F. (2006) In tobacco leaf epidermal cells, the integrity of protein export from the endoplasmic reticulum and of ER export sites depends on active COPI machinery. Plant J. **46**, 95–110

81 Robinson, D. G., Herranz, M.-C., Bubeck, J., Pepperkok, R. and Ritzenthaler, C. (2007) Membrane dynamics in the early secretory pathway. Crit. Rev. Plant Sci. **26**, 199–225

82 Watson, P., Townley, A. K., Koka, P., Palmer, K. J. and Stephens, D. J. (2006) Sec16 defines endoplasmic reticulum exit sites and is required for secretory cargo export in mammalian cells. Traffic **7**, 1678–1687

83 Hanton, S. L., Chatre, L., Matheson, L. A., Rossi, M., Held, M. A. and Brandizzi, F. (2008) Plant Sar1 isoforms with near-identical protein sequences exhibit different localisations and effects on secretion. Plant Mol. Biol. **67**, 283–294

84 Chatre, L., Brandizzi, F., Hocquellet, A., Hawes, C. and Moreau, P. (2005) Sec22 and Memb11 are v-SNAREs of the anterograde endoplasmic reticulum-Golgi pathway in tobacco leaf epidermal cells. Plant Physiol. **139**, 1244–1254

85 Yang, Y. D., Elamawi, R., Bubeck, J., Pepperkok, R., Ritzenthaler, C. and Robinson, D. G. (2005) Dynamics of COPII vesicles and the Golgi apparatus in cultured *Nicotiana tabacum* BY-2 cells provides evidence for transient association of Golgi stacks with endoplasmic reticulum exit sites. Plant Cell **17**, 1513–1531

86 Hanton, S. L., Chatre, L., Renna, L., Matheson, L. A. and Brandizzi, F. (2007) *De novo* formation of plant endoplasmic reticulum export sites is membrane cargo induced and signal mediated. Plant Physiol. **143**, 1640–1650

87 Langhans, M., Hawes, C., Hillmer, S., Hummel, E. and Robinson, D. G. (2007) Golgi regeneration after brefeldin A treatment in BY-2 cells entails stack enlargement and cisternal growth followed by division. Plant Physiol. **145**, 527–538

88 Robinson, D. G., Langhans, M., Saint-Jore-Dupas, C. and Hawes, C. (2008) BFA effects are tissue and not just plant specific. Trends Plant Sci. **13**, 405–408

89 Hawes, C. and Satiat-Jeunemaitre, B. (2005) The plant Golgi apparatus: going with the flow. Biochim. Biophys. Acta **1744**, 466–480

90 Mollenhauer, H. H., Morre, D. J. and Vanderwoude, W. J. (1975) Endoplasmic reticulum–Golgi apparatus associations in maize root tips. Mikroskopie **31**, 257–272

91 Mollenhauer, H. H. and Morre, D. J. (1976) Transition elements between endoplasmic reticulum and Golgi apparatus in plant cells. Cytobiologie **13**, 297–306

92 Harris, N. and Oparka, K. J. (1983) Connections between dictyosomes, ER and GERL in cotyledons of mung bean (*Vigna radiata* L.). Protoplasma **114**, 93–102

93 Juniper, B., Hawes, C. R. and Horne, J. C. (1982) The relationship between dictyosomes and the forms of endoplasmic reticulum in plant cells with different export programs. Bot. Gaz. **143**, 135–145
94 Kang, B. H. and Staehelin, L. A. (2008) ER-to-Golgi transport by COPII vesicles in *Arabidopsis* involves a ribosome-excluding scaffold that is transferred with the vesicles to the Golgi matrix. Protoplasma **234**, 51–64
95 Staehelin, L. A. and Kang, B. H. (2008) Nanoscale architecture of endoplasmic reticulum export sites and of Golgi membranes as determined by electron tomography. Plant Physiol. **147**, 1454–1468
96 Barr, F. A. and Short, B. (2003) Golgins in the structure and dynamics of the Golgi apparatus. Curr. Opin. Cell Biol. **15**, 405–413
97 Sztul, E. and Lupashin, V. (2006) Role of tethering factors in secretory membrane traffic. Am. J. Physiol. Cell Physiol. **290**, C11–C26
98 Latijnhouwers, M., Gillespie, T., Boevink, P., Kriechbaumer, V., Hawes, C. and Carvalho, C. M. (2007) Localization and domain characterization of *Arabidopsis* golgin candidates. J. Exp. Bot. **58**, 4373–4386
99 Renna, L., Hanton, S. L., Stefano, G., Bortolotti, L., Misra, V. and Brandizzi, F. (2005) Identification and characterization of AtCASP, a plant transmembrane Golgi matrix protein. Plant Mol. Biol. **58**, 109–122
100 Sinka, R., Gillingham, A. K., Kondylis, V. and Munro, S. (2008) Golgi coiled-coil proteins contain multiple binding sites for Rab family G proteins. J. Cell Biol. **183**, 607–615
101 Latijnhouwers, M., Hawes, C. and Carvalho, C. (2005) Holding it all together? Candidate proteins for the plant Golgi matrix. Curr. Opin. Plant Biol. **8**, 632–639
102 Osterrieder, A., Carvalho, C. M., Latijnhouwers, M., Johansen, J. N., Stubbs, C., Botchway, S. and Hawes, C. (2009) Fluorescence lifetime imaging of interactions between Golgi tethering factors and small GTPases in plants. Traffic **10**, 1034–1046
103 Stefano, G., Renna, L., Hanton, S. L., Chatre, L., Haas, T. A. and Brandizzi, F. (2006) ARL1 plays a role in the binding of the GRIP domain of a peripheral matrix protein to the Golgi apparatus in plant cells. Plant Mol. Biol. **61**, 431–449
104 Hara-Nishimura, I., Shimada, T., Hatano, K., Takeuchi, Y. and Nishimura, M. (1998) Transport of storage proteins to protein storage vacuoles is mediated by large precursor-accumulating vesicles. Plant Cell **10**, 825–836
105 Toyooka, K., Okamoto, T. and Minamikawa, T. (2000) Mass transport of proform of a KDEL- tailed cysteine protease (SH-EP) to protein storage vacuoles by endoplasmic reticulum-derived vesicle is involved in protein mobilization in germinating seeds. J. Cell Biol. **148**, 453–463
106 Petruccelli, S., Otegui, M. S., Lareu, F., Tran Dinh, O., Fitchette, A. C., Circosta, A., Rumbo, M., Bardor, M., Carcamo, R., Gomord, V. and Beachy, R. N. (2006) A KDEL-tagged monoclonal antibody is efficiently retained in the endoplasmic reticulum in leaves, but is both partially secreted and sorted to protein storage vacuoles in seeds. Plant Biotechnol. J. **4**, 511–527
107 Frigerio, L., Pastres, A., Prada, A. and Vitale, A. (2001) Influence of KDEL on the fate of trimeric or assembly-defective phaseolin: selective use of an alternative route to vacuoles. Plant Cell **13**, 1109–1126
108 Huang, A. H. (1996) Oleosins and oil bodies in seeds and other organs. Plant Physiol. **110**, 1055–1061
109 Shockey, J. M., Gidda, S. K., Chapital, D. C., Kuan, J. C., Dhanoa, P. K., Bland, J. M., Rothstein, S. J., Mullen, R. T. and Dyer, J. M. (2006) Tung tree DGAT1 and DGAT2 have non redundant functions in triacylglycerol biosynthesis and are localized to different subdomains of the endoplasmic reticulum. Plant Cell **18**, 2294–2313
110 Wahlroos, T., Soukka, J., Denesyuk, A., Wahlroos, R., Korpela, T. and Kilby, N. J. (2003) Oleosin expression and trafficking during oil body biogenesis in tobacco leaf cells. Genesis **35**, 125–132
111 Jolliffe, N. A., Craddock, C. P. and Frigerio, L. (2005) Pathways for protein transport to seed storage vacuoles. Biochem. Soc. Trans. **33**, 1016–1018
112 Robinson, D. G., Oliviusson, P. and Hinz, G. (2005) Protein sorting to the storage vacuoles of plants: a critical appraisal. Traffic **6**, 615–625
113 Lending, C. R. and Larkins, B. A. (1989) Changes in the zein composition of protein bodies during maize endosperm development. Plant Cell **1**, 1011–1023
114 Hawes, C., Saint-Jore, C. M., Brandizzi, F., Zheng, H., Andreeva, A. V. and Boevink, P. (2001) Cytoplasmic illuminations: in planta targeting of fluorescent proteins to cellular organelles. Protoplasma **215**, 77–88
115 Matsushima, R., Kondo, M., Nishimura, M. and Hara-Nishimura, I. (2003) A novel ER-derived compartment, the ER body, selectively accumulates a β-glucosidase with an ER-retention signal in *Arabidopsis*. Plant J. **33**, 493–502
116 Scott, I., Sparkes, I. A. and Logan, D. C. (2007) The missing link:inter-organellar connections in mitochondria and peroxisomes? Trends Plant Sci. **12**, 380–381
117 Sinclair, A. M., Trobacher, C. P., Mathur, N., Greenwood, J. S. and Mathur, J. (2009) Peroxule extension over ER-defined paths constitutes a rapid subcellular response to hydroxyl stress. Plant J. **59**, 231–242
118 Novikoff, P. M. and Novikoff, A. B. (1972) Peroxisomes in absorptive cells of mammalian small intestine. J. Cell Biol. **53**, 532–560
119 Lazarow, P. B. and Fujiki, Y. (1985) Biogenesis of peroxisomes. Annu. Rev. Cell Biol. **1**, 489–530
120 Flynn, C. R., Heinze, M., Schumann, U., Gietl, C. and Trelease, R. N. (2005) Compartmentalization of the plant peroxin, AtPex10p, within subdomain(s) of ER. Plant Sci. **168**, 635–652
121 Mullen, R. T., Lisenbee, C. S., Flynn, C. R. and Trelease, R. N. (2001) Stable and transient expression of chimeric peroxisomal membrane proteins induces an independent 'zippering' of peroxisomes and an endoplasmic reticulum subdomain. Planta **213**, 849–863
122 Mullen, R. T., Lisenbee, C. S., Miernyk, J. A. and Trelease, R. N. (1999) Peroxisomal membrane ascorbate peroxidase is sorted to a membranous network that resembles a subdomain of the endoplasmic reticulum. Plant Cell **11**, 2167–2185
123 Lisenbee, C. S., Heinze, M. and Trelease, R. N. (2003) Peroxisomal ascorbate peroxidase resides within a subdomain of rough endoplasmic reticulum in wild-type *Arabidopsis* cells. Plant Physiol. **132**, 870–882
124 Lisenbee, C. S., Karnik, S. K. and Trelease, R. N. (2003) Overexpression and mislocalization of a tail-anchored GFP redefines the identity of peroxisomal ER. Traffic **4**, 491–501
125 Karnik, S. K. and Trelease, R. N. (2005) *Arabidopsis* peroxin 16 coexists at steady state in peroxisomes and endoplasmic reticulum. Plant Physiol. **138**, 1967–1981
126 Karnik, S. K. and Trelease, R. N. (2007) *Arabidopsis* peroxin16 trafficks through the ER and an intermediate compartment to pre-existing peroxisomes via overlapping molecular targeting signals. J. Exp. Bot. **58**, 1677–1693
127 Sparkes, I. A., Hawes, C. and Baker, A. (2005) AtPEX2 and AtPEX10 are targeted to peroxisomes independently of known endoplasmic reticulum trafficking routes. Plant Physiol. **139**, 690–700
128 McCartney, A. W., Greenwood, J. S., Fabian, M. R., White, K. A. and Mullen, R. T. (2005) Localisation of the tomato bushy stunt virus replication protein p33 reveals a peroxisome-to-endoplasmic reticulum sorting pathway. Plant Cell **17**, 3513–3531
129 Tabak, H. F., van der Zand, A. and Braakman, I. (2008) Peroxisomes: minted by the ER. Curr. Opin. Cell Biol. **20**, 393–400
130 Titorenko, V. I. and Mullen, R. T. (2006) Peroxisome biogenesis: the peroxisomal endomembrane system and the role of the ER. J. Cell Biol. **174**, 11–17
131 Kim, P. K., Mullen, R. T. and Lippincott-Schwartz, J. (2004) Evidence for endoplasmic reticulum origins of peroxisomes. Mol. Biol. Cell **15**, 621
132 Andersson, M. and Dormann, P. (2009) Chloroplast membrane lipid biosynthesis and transport. In The Chloroplast: Interactions with the Environment (Sandelius, A. and Aronsson, H., eds), pp. 125–128, Springer-Verlag, Berlin-Heidelberg
133 McLean, B., Whatley, J. M. and Juniper, B. E. (1988) Continuity of chloroplasts and endoplasmic reticulum membranes in Chara and Equisetum. New Phytol. **109**, 59–65
134 Xu, C., Fan, J., Cornish, A. J. and Benning, C. (2008) Lipid trafficking between the endoplasmic reticulum and the plastid in *Arabidopsis* requires the extraplastidic TGD4 protein. Plant Cell **20**, 2190–2204
135 Andersson, M. X., Goksor, M. and Sandelius, A. S. (2007) Optical manipulation reveals strong attracting forces at membrane contact sites between endoplasmic reticulum and chloroplasts. J. Biol. Chem. **282**, 1170–1174
136 Villarejo, A., Buren, S., Larsson, S., Dejardin, A., Monne, M., Rudhe, C., Karlsson, J., Jansson, S., Lerouge, P., Rolland, N. et al. (2005) Evidence for a protein transported through the secretory pathway en route to the higher plant chloroplast. Nat. Cell Biol. **7**, 1224–1231
137 Nanjo, Y., Oka, H., Ikarashi, N., Kaneko, K., Kitajima, A., Mitsui, T., Munoz, F. J., Rodriguez-Lopez, M., Baroja-Fernandez, E. and Pozueta-Romero, J. (2006) Rice plastidial N-glycosylated nucleotide pyrophosphatase/phosphodiesterase is transported from the ER-Golgi to the chloroplast through the secretory pathway. Plant Cell **18**, 2582–2592
138 Sievers, A. and Volkmann, D. (1972) Verursacht differentieller Druck der Amyloplasten auf ein komplexes Endomembranesystem die Geoperzeption in Wurzeln. Planta **102**, 160–172
139 Juniper, B. and French, A. (1973) The distribution and redistribution of endoplasmic reticulum (ER) in geoperceptive cells. Planta **109**, 211–224
140 Leitz, G., Kang, B. H., Schoenwaelder, M. E. and Staehelin, L. A. (2009) Statolith sedimentation kinetics and force transduction to the cortical endoplasmic reticulum in gravity-sensing *Arabidopsis* columella cells. Plant Cell **21**, 843–860

Received 21 July 2009; accepted 4 August 2009
Published on the Internet 25 September 2009, doi:10.1042/BJ20091113

Biochem. J. (2009) **423**, 145–155 (Printed in Great Britain) doi:10.1042/BJ20091113

online data

SUPPLEMENTARY ONLINE DATA
The plant endoplasmic reticulum: a cell-wide web

Imogen A. SPARKES*, Lorenzo FRIGERIO†, Nicholas TOLLEY† and Chris HAWES*[1]

*School of Life Sciences, Oxford Brookes University, Oxford OX3 0BP, U.K., and †Department of Biological Sciences, University of Warwick, Coventry CV4 7AL, U.K.

Arabidopsis thaliana

>AtRTNLB1 At4g23630
GGVLGGATAAWVVFELMEYHLLTLLCHVMIVVLAVLFLWSNATMFINKSPPKIPEVH
IPEEPILQLASGLRIEINRGFSSLREIASGRDLKKFLIAIAGLWVLSILGGCFNFLT
LAYIAL
>AtRTNLB2 At4g11220
MSGGVFGGATVAWVLFELMEYHLLTLLCHVMIVALAVLFLWSNATMFIHKSPPKIPE
VHIPEEPLLQLASGLRIEINRGISSLREIASGRDIKKFLSAIAGLWVLSILGGCYSF
LTLAYIALVL
>AtRTNLB3 At1g64090
SGGVLGAATVSWILFELLEYNLLTLFGHISILALAVLFLWSSASTFIHKSPLHIPEV
HIPEDVVLQLASGLRIEINRGFTVLRDIASGRDLKKFLLVIAGLWVLSKVGSSCNFL
TLIYIA
>AtRTNLB4 At5g41600
VSGGVLGAVTASWVLFELFEYHLLAFLCHFAIFALAALFLWSNACTFIHKSTPHIPE
VHIPEDPILQLVSGLRIEINRGLTLLRNIASGKDVKKFILVIAGLWVLSIIGSCYNF
LTLFYTA
>AtRTNLB5 At2g46170
LSGAVLGVATAIWVLFELVEYHLLSLLCHISILALGGLFLWSNAHTLINKTSPQIPE
IHVPEEAFLVVASSLRNELNQAFVILRSIALGRDLKKFLMVVVGLWIISVVGNWFNF
LTLVYI
>AtRTNLB6 At3g61560
LSASVLGVATAIWVLFELVEYHFLSLVCHILIFALAALFLLSNAHAFMNKTPPKIPE
IHIKEEHFLMIVSALRNELNQAFVILRSIALGRDLKKFLMVVFGLWIISVVGNWFNF
LTLVYI
>AtRTNLB7 At4g01230
VTLGLLSAVTVIWLLFGFGGRRLLTSLCRGSILFLLLSFLWSNALNKSPENMMDIYI
PEKPLLQAASAMTFELNCAFATLRSIALERDIKNFVMAVIGLWLVSVIGNWFSFLSL
LYIC
>AtRTNLB8 At3g10260
KISASVLMGATAIWVLFEWINFHFLSLVCYALLLGMIAQFVWSNASGFLNRSQSRVP
RLVLPKDFFAEVGVAVGKEVNRGLLFLQDLACKGNLKQFLMAVIGLWVAAMVGSCCN
FLTVLY
>AtRTNLB9 At3g18260
AATLVIGVSILWFLMEVVEYNFITLICHASMTSMLFFFIWSTASDFLNWERPLIPEV
VLDESSFKQLARSFHVRFNQILTKLLDVACGRDPPLFFLTTISLYIVSIIGTYFNFV
NLLFIG
>AtRTNLB10 At2g15280
GGFLLLGSTTLLWFLFEKCGYSFFPFVVNTQLLSVVILFLWAKSAILFNRPMPQLPN
LEITEEFVFMVADAIRVWINTVLAVAREIYVGRNAKQLFRVSVVLWTVSFVGNFLNF
LTILYLG
>AtRTNLB11 At3g19460
RTGAVILLISSTGFWFLFERAGYNLLSFVSNVLLLLVAIFFLWAKSATVLNRPLPPV
PNMEIPEEFANKAADDLRVWINYVLSIASDITIARNPIRLLQVSLVLWAISYVGTLI
NSLTLVYIG
>AtRTNLB12 At3g54120
NVSVGIVTVTIASWMVFEAFAYTIFTLISSVLLLLLSILFLWSKSASILNRPSPPLP
EFQISEAMAEEASIWLRIHVNKLLQVSHDIAMARDSELYTKVAVSLFLLSLIGSLMD
FQTLCHTS
>AtRTNLB13 At2g23640
KLAFSTLLVSTSTWILLSFYGFTTITIVSWIGIAVVSMIFLWGSLLRLLSKVEPELS
GLEVSEEFVVETVRSCRMLMEEMVRWMFRVGAESEWFVFARTVLGFWILSRIGNLLD
FHTCLFIG
>AtRTNLB14 At1g68230
KKESGTILGVFTLIWFLFEVVEYPFITFLCQILLLFIFIFLICKPPSINDLRISESN
WRFLFNKINWFIIKLYDISSGKDFRLLFLAVVSLWILSVVGNYFSSLTLLYIGES
>AtRTNLB15 At2g01240
KLRDNTCNGHTLLVPLGVHGSSISSASLLNLVTPHAHSLPLGQLNQPDSPLKALFSM
MEGHLLMLYEIAYGKDNKTFLKTILYVAIIYNIGSYISLLTILYIC
>AtRTNLB16 At3g10915
HLSLGVIIISTVAWLIFEFSGLPFLSVSSDVLLIVIMISFVHARVSAFRNRQLHSLP
ELVLSEEMVNSAAASFRIKLNHLLVMAHDVTVGNDFRLFFKVVICLWLLSAIGSYIS
LCTLLYIG
>AtRTNLB17 At2g20590
KSTLWFGFGCLSFLSSCFAKGVNFSVFSAVSNLGLVLLCGSFLSNTLCQRKNEDTKR
AFHVSEDDVLRSARRVLPATNFFISKTSELFSGEPSMTLKVTPFLLLGAEYGHLITL
WRLSAFG
>AtRTNLB18 At4g28430
KSTLWFGFGCICFLSTCFAAKGFNFSVFSAISYLGLLFLGVSFLSNTLRQRVTEEAR
RELKLSEDDVLRIARRMLPITNLAISKTSELFSGEPAMTLKVAPFVLMGAEYGYLIT
LWRLCAFG
>AtRTNLB19 At2g26260
LKQTLIAIFILISIYYNFVATGSTVVTALSKALLVASVFLFLHGILPEKIFGYTVEK
IPASQFHLSKDSSHDLSLSVISSWNTTVKALRSLCQGNDWSFFFKVVFVLLALSLAG
AISLHSIFVIG
>AtRTNLB20 At2g43420
EKKTFVSFLVLNLFYYWFFFSGNTFTSSAAQLLFIFAVALYGVSFVPSKIFGFQVNK
IPPWRFEISESAVRDLSSDIVVVWNQGVRSFKSLSSGGDWIKFFKIAGSLYLLKLIV
SRSLAAFLFTV
>AtRTNLB21 At5g58000
RSTLVFGFGTFLIISSSYANDLNFSFISVVAYMGLIYLGLMFVLKSLIHRGMVEEER
HKVVGVREEDVKRMLRLIMPYLNESLHQLRALFSGDPSTTLKMGVVLFVLARCGSSI
TLWNLAKFG

Figure S1 For legend, see next page

All authors contributed equally to this review.
[1]To whom correspondence should be addressed (email c.hawes@brookes.ac.uk).

Physcomitrella patens

>PpRTNLB1 PPP_5258_C1
CPGMNFNKAXRFSRNVALGNDFKLFFKVVTLLWVVSTVASWFNLLTLIWIG
>PpRTNLB2 PPP_939_C1
PVELWAVRRSSGXLLEKSGYTFLTLVCNILLFVVVILFVWSNVATLINRPGPPVPEL
SLSENFVMNTANLIRIEVNKALHIARTVALGKDFKLFLLVVASLYVVSIVGSWFNLL
TCVWIGI
>PpRTNLB3 PPP_2025_C1
KDRNLSAIILGGSTLVWFLLEKSGYTFLTLLSNILMFSVIILFVWANVAALLNRAGP
PVPELSLSEDFVLRTASTVRVELNKALSIARDVALGKDFKLFLKMVVLLWVVSTVTS
WFNFLTCIWIG
>PpRTNLB4 PPP_4062_C1
KYLSAGTLGGSTLIWFLVEKSGYTITTLICNILMLITVVLFVWSNVAALLKRPGPPV
PELSLSEDFVLSTASVFRNEVNKALSAARTVALGKDFKLFFIVIAFLYVVSTVTSWF
NFLTCIWIGI
>PpRTNLB5 PPP_939_C2
DKYLSGGTLFGSTAIWYLLEKSGYTFVTLTCNILMCVIVLLFVWSSIAALLHRAGPP
VPEL
>PpRTNLB6 PPP_4062_C2
LSAGTLGGSTLIWFLLEKSGYTLVTLLCNILLFVIVILFLWSNVASLLHRPGPPFTV
PELTLPEDLVLSTANVVRIEVNKALSVARTVALGKDFKLFFIVIAFLYVVSTVTSWF
NFLTCIWIG
>PpRTNLB7 PPP_76_C1
KSAGLFFALFFFLYSFYSSGTTLVSALTYNLCVALIAVFVYNLLPDPFFQISLPKIP
SSSFEISEDGVKVVALQFDRIGIVSAXILERIVVQRDFSLFFKVMVLLRVVKFFGRF
SFQSLLFMG
>PpRTNLB8 XM_001772054.1
SISANLALCYLAIVFFYRTFLSGSSAQSRSGQLKSSGVTEADFLGLIRFVLPTINLT
LTKSGEVFSGDPAITLRVGSFILIKLYYWSLAVLADLYSF
>PpRTNLB9 XM_001764698.1
AISANLALCYLAVVFFYRTFLHRSVAQSSGGQINSSEVTEADFLGLIQFVLPTINLA
LNKSREIFSGDPATTLRVAIVLWLVSKMGAGVSIWSFLRFG

Selaginella moellendorffii

>SmRTNLB1 gnl|Selmo1|271164 estExt_fgenesh1_kg.C_290002
KHLSASVLGIATLIYVLFEWCGYTVLSVFCNTFLLITIVLFVWSLGASFTNRPPPRI
PELQLSEKTVQDVAHTVQLQFNNAVGAFRSIVLERNYVLFLKAAAGLWLLSTVGSWT
SLLTLLYIGVIVAH
>SmRTNLB2 gnl|Selmo1|421735 fgenesh2_pg.C_scaffold_53000092
GGILLGATVSYVLFEWCGYTLLSIASNALLFLVLILFTWSNLAALLDKPPPPIPEIQ
LSEEMVENIAQTLRLELNRALGIIHMIALGKDFMLCVEVIAGLWIFSLVGGWCHFLT
LLYFVVVLAH
>SmRTNLB3 gnl|Selmo1|179628 estExt_Genewise1Plus.C_540349
TSLLVGSTVAWFLFEWSGYTLLSLVCNVLLFLIVILFLWATIASLLHRPPPPIPEIV
LTEEMVHDSAATLRVEINKALLAAHDVAIGKDFRVFLKVTVVLWILSKLGAWFNFIT
LVYILVVGAH
>SmRTNLB4 gnl|Selmo1|136377 e_gw1.147.83.1
IGILGGSTLVWFIFEWSGYTLISLVANIVLFLLIALFAWANLAALVNRPLPPVPEVQ
LSDEKSNKIAKRVAKEVNGVLNYARSLSTGKDFPMLLKTCLMLWVLGNVGQWFSLLT
LIYLGVIGTL
>SmRTNLB5 gnl|Selmo1|405772 fgenesh2_pg.C_scaffold_4000346
ALVMNVILWRDFSTSSLIFGAGAFAILSASLMQDIHLNIVTTLSYLALTYLSAVFFR
INILRRAPSSSSDSWKISEAAALELTRGALPAFNAVLFKFSQLFSGDPGTTLKVAAT
LCRMIPYAVAFFGAFLVPKFYVSYTA

Chlamydomonas reinhardtii

>CrRTNLB1 XP_001698908
KVRSTFYFVAGLLAWVVVRAVSKSDTTLFTGLCYVLLASLFWNFLRAAMAPAYAARC
TWAHSAVTRFLVASATATLNAAAALHDRHLHGIDPLHTLEVGLGLWVLSLLGRALPF
VTLLLLL

Saccharomyces cerevisiae

>RTN1p YEAST
PVQTGKYFGGSLLALLILKKVNLITFFLKVAYTILFTTGSIEFVSKLFLGQGLITKY
GPKECPNIAGFIKPHIDEALKQLPVFQAHIRKTVFAQVPKHTFKTAVALFLLHKFFS
WFSIWTIVFVA
>RTN2p YEAST
PSKSGASFAATLVSLLILRNVNVISVLLKIGYMVLFTSFAVELSTKVLFDKGVVSRF
GMQESPDLVGVLKPHIDRELDRLPALEDRIRKLVFAHRTRNNFTIGVSLYFLHGLFA
IFSMNTVLIMTT

Figure S1 RHD sequences used for phylogenetic analysis

The sequences are shown in FASTA format. The accession numbers for each individual sequence are listed after the RTNLB numbers.

Received 21 July 2009; accepted 4 August 2009
Published on the Internet 25 September 2009, doi:10.1042/BJ20091113

Five plant reticulon isoforms share ER location, topology and membrane shaping properties.

I. Sparkes[1], N. Tolley[2], I. Aller[1,4], J. Svozil[1,5], A. Osterrieder[1], S. Botchway[3], C. Mueller[4], L. Frigerio[2*], C. Hawes[1*]

[1] School of Life Sciences, Oxford Brookes University, Gipsy Lane, Oxford, OX3 0BP.

[2] Department of Biological Sciences, University of Warwick, Coventry, CV4 7AL, UK

[3] Central Laser Facility, STFC Harwell Science Innovation Campus, Didcot, Oxon. OX11 0QX, UK

[4] Institute for Plant Sciences, Heidelberg University, 69120 Heidelberg, Germany.

[5] Institute of Plant, Animal and Agroecosystem Sciences, ETH (Swiss Federal Institute of Technology) Zurich, Universitätstrasse 2, 8092 Zurich, Switzerland.

Running title: Characterisation of plant reticulons

Keywords: Endoplasmic reticulum, reticulon, confocal microscopy

Estimated length: 10 pages

*Corresponding authors: lfrigerio@warwick.ac.uk, chawes@brookes.ac.uk

The authors responsible for distribution of materials integral to the findings presented in this article in accordance with the policy described in the Instructions for Authors (www.plantcell.org) are: Chris Hawes (chawes@brookes.ac.uk) and Lorenzo Frigerio (l.frigerio@warwick.ac.uk).

Abstract

The cortical endoplasmic reticulum (ER) in tobacco epidermal cells is a network of tubules and cisternae undergoing dramatic rearrangements. Reticulons are integral membrane proteins involved in shaping ER tubules. Here, we have characterised the localisation, topology, effect and interactions of 5 Arabidopsis reticulons (RTN), isoforms 1-4 and 13, in the cortical ER. Our results indicate that like RTNLB13, RTNLB1-4 co-locate to and constrict the tubular ER membrane. All 5 RTNs preferentially accumulate on ER tubules and are excluded from ER cisternae. All isoforms share the same transmembrane topology, with N and C termini facing the cytosol and 4 transmembrane domains. We show by FRET/FLIM that several RTNs have the capacity to interact with themselves and each other and we suggest that oligomerization is responsible for their residence in the ER membrane. We also show that a complete reticulon homology domain (RHD) is required for both RTN residence in high-curvature ER membranes and ER tubule constriction, yet it is not necessary for homotypic interactions.

Introduction

The endoplasmic reticulum (ER) is the port of entry into the secretory pathway. The plant ER is an extremely dynamic organelle with a unique architecture consisting of a network of membrane tubules and sheets (cisternae) connected by three-way junctions (for a recent review see Sparkes *et al.*, 2009b). In cells of vegetative tissues, the cortical ER is predominantly tubular with small cisternal patches. This shape is independent of the ER being attached to a functional cytoskeleton (Boevink *et al.*, 1998; Dreier and Rapoport, 2000), indicating that factors within the membrane itself must be responsible for conferring its curvature. Recently, a class of ER membrane proteins named the reticulons (RTN) was shown to be sufficient to induce ER tubulation in yeast, mammalian cells (Voeltz *et al.*, 2006) and in artificial proteoliposomes (Hu *et al.*, 2008). It is assumed that these curvature-inducing properties result from the wedge-like transmembrane topology of the conserved structural motif of these proteins (the reticulon homology domain, RHD), which includes two large hydropobic segments (Shibata *et al.*, 2009).

The *RTN* gene family is much larger in higher plants than it is in mammals, with Arabidopsis having 21 *RTN* genes (Oertle *et al.*, 2003; Nziengui *et al.*, 2007; Nziengui and Schoefs, 2009; Sparkes *et al.*, 2009b). This suggests that the numerous RTN isoforms may perform plant-specific functions. Very little functional information is however available on plant RTNs. RTNLB1, 2 and 4 were isolated in a screen for agrobacterial pilin interacting proteins, and a direct correlation between the level of RTNLB1 and plant susceptibility to Agrobacterium transformation was documented (Hwang and Gelvin, 2004). We have recently shown that the smallest plant reticulon isoform, RTNLB13, localises to the ER membrane and, when overexpressed, can dramatically affect ER morphology by causing constrictions in the ER tubules (Tolley *et al.*, 2008). These constrictions reduce diffusion within the ER lumen but do not cause major anterograde trafficking defects. The ability of a surfeit of RTN to cause constrictions fits the hypothesis that RTNs do individually bend the membrane but can also form multimeric, arc-like structures (Shibata *et al.*, 2008; Shibata *et al.*, 2009) which may ultimately shape and determine the diameter of ER tubules (Hu *et al.*, 2008). It is not known whether the properties of RTNLB13, which contains the conserved RHD but has small soluble N- and C- terminal domains and is predicted to be expressed in seeds (Supplementary figure 1 on line1, Winter *et al.*, 2007), are shared by

the more ubiquitously expressed members of the RTN family such as RTNLB1, 2, 3 and 4 (Supplementary figure 1 on line). Here, we characterised the location, topology, ER-shaping function and interactions of these five isoforms. We report that all five proteins share the same topology and general properties, indicating that these are likely to be shared by the other, less abundant isoforms. We also show that homo- and heterotypic interactions between RTN are responsible for their residence in the ER membrane.

Results

RTNLB1-4 localise to the ER membrane and remodel the ER lumen

RTNLB1-4 were cloned from Arabidopsis seedling cDNA and fluorescent fusions were transiently expressed in tobacco epidermal cells by agroinfiltration (Sparkes *et al.*, 2006), owing to the extremely high transformation efficiency of this system and its prior use to characterise RTNLB13 (Tolley *et al.*, 2008).

Both N- and C- terminal fusions to full length RTNLB1-4 genes resulted in localisation patterns similar to ER. Coexpression of these fusions with an ER marker, GFP-HDEL, confirmed their ER location, and also indicated that all isoforms can induce constriction of ER tubules, similar to that previously observed with both untagged and YFP-tagged RTNLB13 overexpression (Fig. 1A-L).

Reticulons are enriched in the tubular ER

By virtue of their topology, mammalian and yeast reticulon/YOP proteins are predicted to insert preferentially into high-curvature membranes, i.e. tubules rather than cisternae (Shibata *et al.*, 2009). We tested whether this is also true for our selected plant RTN isoforms. As the cortical ER in leaf epidermal cells exists predominantly in tubular rather than cisternal form, we used two strategies in order to induce the formation of ER sheets. First, it has been previously shown that the overexpression of the transmembrane domain of the single-spanning ER membrane protein GFP-calnexin (GFP-CXN) (Runions *et al.*, 2006) has the effect of dilating ER membranes and inducing cisternae. When RTNLB1-eYFP was co-expressed with GFP-CXN, RTNLB1 localisation appeared to be limited to the ER tubules and cisternal rims (Fig. 2, A-C), while GFP-CXN was enriched in the cisternal regions of the membrane (Fig. 2, A-C, asterisk). Similar results were observed for RTNLB2, 3 and 4 fusions (Fig. 2, panels D to L). RTN-eYFP fusions occasionally located to tubular structures which traversed and perforated ER cisternae indicating substructure within cisternae (Fig. 2, arrows). Additionally, all full length RTN fusions collocated to the ER contiguous with the nuclear envelope (Supplementary figure 2 on line).

Treatment with brefeldin A causes reabsorption of Golgi membranes into the ER and induction of extensive ER cisternae, (Boevink *et al.*, 1999). Figure 2 (panels M-O) shows that when cells coexpressing RTNLB13-eYFP and GFP-HDEL were treated with BFA, extensive cisternal sheets were produced but RTNLB13-eYFP remained mostly excluded from them and inhabited only the rims of the sheets and the rest of the tubular network (Fig. 2, M-O).

Taken together, these results indicate that all the plant reticulons under study have a preference for locating to tubular ER.

RTNLB1-4 and 13 share the same transmembrane topology

Topology prediction with TOPCONS (Bernsel *et al.*, 2008) indicates that all 21 Arabidopsis RTN genes have the same 'W' topology, with N and C termini in the cytosol and the central loop between transmembrane domains (TMDs) 2 and 3 also in the cytosol (Supplementary figure 3 on line). The only experimental determination of RTN topology available to date was performed on mammalian Rtn4c (Voeltz *et al.*, 2006) and it is not known whether this topology is shared by the whole family of RTN proteins. We experimentally assessed the topology of Arabidopsis RTNLB1-4 and 13 using three methods: redox-sensitive GFP (roGFP2; Schwarzlander *et al.*, 2008; Brach *et al.*, 2009), protease-protection assays and bimolecular fluorescence complementation (Zamyatnin *et al.*, 2006).

RoGFP2, a mutagenised form of GFP, interacts with the intracellular glutathione pool and detects differences in the glutathione redox potential (E_{GSH}), which is generated by reduced glutathione (GSH) and its oxidised form GSSG. roGFP2 has differing excitation spectra dependent on the local E_{GSH} and allows ratiometric analyses, which can be exploited for determination of membrane protein topology in membranes separating a steep E_{GSH} gradient (Meyer *et al.*, 2007; Brach *et al.*, 2009). A more negative E_{GSH}, as found in the cytosol, results in higher excitation at 488 nm, whereas 405 nm is more efficient at exciting roGFP2 in an environment with less negative E_{GSH} such as the ER lumen. Therefore, RTN N- and C- terminal fusions to roGFP2 indicate whether termini face the ER lumen or the cytosol.

To prevent movement and remodelling of the ER during sequential 405/488 nm image capture samples were incubated in latrunculin B to disrupt the actin cytoskeleton (Sparkes *et al.*, 2009a). Fast scans, at lower resolution, of untreated cells expressing the roGFP2 RTN fusions were also taken to minimise the effects of ER movement on ratiometric analysis. Both sets of data gave similar results with both N and C terminal fusions giving low 405/488 nm fluorescence ratios indicating a reducing environment close to that measured for the cytosolic control. Therefore, both N and C termini of RTNLB1, 4 and 13, and the C termini of RTNLB2 and 3 face the cytosol (Fig. 3). Data for roGFP2-RTNLB2/3 were not taken as the fusions did not express.

In parallel with these experiments, we performed protease protection assays on microsomes purified from leaf sectors infiltrated with eYFP-tagged versions of RTNLB1-4 and 13 (Fig 4). Incubation of microsomes with proteinase K resulted in the loss of the eYFP moiety from all RTN constructs, as revealed by immunoblotting with GFP antisera (Fig 4A). Both N- and C-terminally appended eYFP was suceptible to protease digestion, indicating that the N and C termini of all the RTN isoforms analysed are exposed to the cytosol. As a control, in microsomes from leaf sectors expressing GFP-CXN, with GFP facing the ER lumen, the GFP moiety was indeed protected from protease digestion (Fig. 4B). Protection was lost when the microsomal membranes were solubilised with the detergent Triton X-100 (Fig. 4, panels A and B).

Both sets of results confirm that N and C termini of RTNLB1-4 and 13 are cytosolic, but do not discriminate between a 'V' configuration of TMDs, where the large hydrophobic segments of the RHD only span the membrane twice, with a connecting hydrophilic luminal loop, and a 'W' configuration, where each hydrophobic region would form a hairpin structure resulting in four membrane-spanning regions and a cytosolic connecting

loop. The latter topology is predicted by TOPCONS (Supplementary figure 3 on line). In order to discriminate between these two possibilities, we adopted two strategies: i) expression of roGFP2 fusions to RTN truncations lacking the second hydrophobic stretches in the RHD (RTN truncations 1, schematised in Fig 6A), and ii) bimolecular fluorescence complementation (BiFC). This technique is based on the co-expression of proteins fused to either the N or C-terminal half of YFP. It has been recently shown that, when overexpressed, the two halves interact, and therefore yield a fluorescent YFP, if they are located in the same subcellular compartment (Zamyatnin *et al.*, 2006). Thus this technique is useful for the determination of plant membrane protein topology.

RoGFP2 fusions to the N terminal half of RTNLB1-4 lacking the second hydrophobic segment were generated (Fig 3A, see Fig 6A schematic truncation 1). Ratiometric imaging indicated a cytosolic location for the roGFP2, thus suggesting a 'W' shaped topology as a 'V' topology would result in the probe residing on the luminal face of the ER membrane.

For BiFC, we generated an expression construct where the C-terminal half of YFP was co-translationally fused between Val91 and Val92 of the predicted central loop of RTNLB13 (RTNLB13YC_{loop}) (Fig. 4C). We then coexpressed RTNLB13YC_{loop} in tobacco leaf cells with the complementary N-terminal half of YFP, targeted either to the cytosol (YN_{cyt}) or to the ER lumen (YN_{ER}) (Zamyatnin *et al.*, 2006). Figure 4C shows that complementation of YFP and therefore fluorescence was clearly detectable with the coexpression of YN_{cyt}. Moreover, the interaction of the two YFP halves clearly highlighted the ER network (Fig. 4C). This result corroborates the roGFP2 results and strongly suggests that the RHD loop may be located in the cytosol, therefore confirming the TOPCONS prediction of a W topology. This prediction is also maintained for RTNLB13YC_{loop} (Supplementary figure 3 on line) indicating that the addition of the C-terminal half-barrel of YFP is unlikely to affect membrane insertion of this construct. We also used BiFC to further test the topology of the N and C termini of RTNLB13. The results confirm the protease protection assays and roGFP2 fusion data, and indicate that both ends of RTNLB13 are cytosolic (Supplementary figure 4 on line).

The dilysine ER retrieval signal is not required for ER residence of RTNLB13

Eighteen out of 21 Arabidopsis RTN isoforms are predicted to contain the C-terminal ER retrieval dilysine motif (KKXX; Nziengui *et al.*, 2007). To test whether the dilysine motif is necessary in the context of the full-length protein, we generated a deletion mutant of RTNLB13 lacking the last four C-terminal residues (ΔKKSE). When expressed in tobacco epidermal cells, this mutant both showed complete ER location and maintained the ability to constrict the ER lumen (Fig. 5). We therefore conclude that this motif is not essential for ER retention. In addition, expression of the first half of RTNLB1-4 as an eYFP fusion (truncation 1, Fig. 6A), shows that the first large hydrophobic region (i.e. the first two predicted transmembrane domains) alone is sufficient to afford ER residence (Fig. 6B). This further indicates that an alternative mechanism is responsible for the ER retention of the reticulons under study.

RTNLB1-4 require complete RHDs to efficiently constrict the ER and constrain RTN to tubules and cisternal rims

In order to determine the minimal structure of RTN that is capable of constricting ER tubules, we tested the requirement for the number of transmembrane domains. The topology experiments described above indicate that all the 5 RTN proteins under study contain 4 TMDs. Therefore, we generated RTN truncations containing two rather than four TMDs and monitored both their location and effect on tubular ER morphology (Fig. 6).

Truncations containing either the first 2 TMDs, the first 2 TMD plus cytosolic loop, the last 2 TMDs or the last 2 TMDs plus cytosolic loop were generated (Figure 6A). In general, RTN truncation fusions lacking two of the four TMDs still localised to the ER but failed to induce tubule constrictions (Figure 6B RTNLB1, RTNLB2-4 data not shown). This was irrespective of whether the N-proximal or the C-proximal TMD pair was removed, and also independent of the presence of a full-length cytosolic loop domain. Remarkably, however, the location of truncated RTNs on the ER membrane was no longer limited to tubules and cisternal rims (as shown in Fig. 2) but became evenly spread over the ER membrane, including cisternal surfaces (Figure 6B). Similar results were obtained for RTNLB13 fusion lacking the C-proximal TMD pair (data not shown).

We therefore conclude that both localisation of RTN to high-curvature ER regions and their capacity to constrict ER tubules requires a complete RHD, ie all four TMDs and intervening loop. Targeting to the ER is however independent of the presence of the complete RHD, with only two TMD being sufficient for ER localisation.

Occasionally, eYFP-RTNLB2 truncations 3 and 4 were observed to constrict the ER in very few cells (Supplementary figure 5 on line).The resulting phenotype indicated that the cisternal ER was undergoing constriction producing small pockets of the luminal ER marker, GFP-HDEL, on cisternae (Supplementary figure 5 on line). This was not observed with an ER membrane marker.

RTNLB1 and RTNLB13 can form both homo- and heterotypic interactions

If deletion of the C-terminal KKXX does not result in loss of RTN, what then is anchoring the protein in the ER membrane? Shibata *et al.* (2008) showed that mammalian Rtn4a and yeast Rtn1 have the ability to form oligomers in the ER membrane. It is possible such oligomerisation prevents the proteins from escaping from the ER while enhancing their ability to induce membrane curvature. We therefore decided to test homo- and heterotypic RTN association using fluorescence resonance energy transfer (FRET) measured by donor excited state fluorescence life time imaging (FLIM). FRET-FLIM measures the reduction in the life time of GFP (donor) fluorescence when an acceptor fluorophore, in this case mRFP, is close enough for FRET to occur, thus indicating interactions between the protein fusions (Osterrieder *et al.*, 2009). Limitations in the speed of photon counting in the FLIM system required us to monitor a region of the ER with relatively low mobility such as ER associated with the nuclear envelope (Supplementary figure 2 A-B on line).

Combinations of eGFP- (donor) and mRFP- (acceptor) RTN fusions were transiently coexpressed in tobacco leaf epidermal cells and interactions assessed through FRET-FLIM. Previous FRET-FLIM studies have shown that Golgi targeted fusion pairs STGFP/STmRFP (ST being the signal anchor sequence of a rat sialyl

transferase, Boevink et al. 1998), do not interact, whereas AtGRIP-GFP/mRFP-ARL1 do interact (AtGRIP being a *trans*-Golgi matrix protein and ARL1 a small Rab-like GTPase). These pairs showed respective life times for GFP as and were used as negative and positive controls for the system (Osterrieder *et al.*, 2009, data not shown). Figure 7 shows lifetime images of RTNLB1-eGFP expressed alone (A-C) and RTNLB1-eGFP coexpressed with mRFP-RTNLB1 (D-H). The pseudocoloured lifetime map (A, D) reflects the lifetime values of each point within the region of interest. The distribution of lifetimes within the region of interest is depicted (B, E) where blue shades represent higher eGFP fluorescence lifetimes than those in green. Representative decay curves (C,F) of a single point highlight an optimal single exponential fit (where points with χ^2 values from 0.9-1.4 were taken). Hence, RTNLB1 homodimerises as the lifetime values for the eGFP/mRFP fusion pair (Fig 7) are lower than those for the eGFP fusion alone. The range of lifetimes for each RTN pair are shown in Table 1. The average of the range indicates at least a 0.2 ns decrease in lifetime of the pairs compared to the control donor expressed alone. Therefore, all combinations of full-length RTN and truncations tested appeared to oligomerise (Table 1). The fact that homotypic interactions (at least the ones we tested for RTNLB1 and RTNLB13, Table 1) were also observed for the truncated constructs indicates that the two C-terminal TMDs are not necessary for RTN to interact.

Discussion

The cortical ER network in plants is extremely dynamic with regular tubule outgrowth and transitions between tubules and cisternae being common. Based on several observations, a functional role of ER remodelling in secretion has been proposed. Actively growing and dividing cells have been shown to contain more cisternal ER than non-dividing mature cells (Ridge *et al.*, 1999) and heavily secreting root cap cells show an abundance of cisternal ER (Stephenson and Hawes, 1986). Hence, cisternalisation may increase the surface area and consequently the capacity of the ER for secretion. Therefore, characterisation of the key cellular players in ER remodelling, in particular those controlling tubulation versus cisternalisation of the ER could have important biotechnological implications.

The relative roles of the cytoskeleton, several myosins (XIK and XIJ myosin tail domains) and Golgi bodies on these processes were recently addressed (Sparkes *et al.*, 2009c; Sparkes *et al.*, 2009a). In order to further understand the factors which control the physical constrictive process resulting in ER tubule formation over cisternae, we carried out the comprehensive study on RTNs presented here. Previously we have shown that RTNLB13 locates to the ER membrane and, on transient expression, constricts the cortical ER (Tolley *et al.*, 2008). Here, we have shown that other members of the family, RTNLB1-4, have a similar effect on the ER and locate to ER tubules, but are constrained to the rims of ER cisternae.The ER location for RTNLB2 and 4 is in agreement with previous studies (Nziengui *et al.*, 2007), however these authors also reported that RTNLB4 labelled motile puncta which could reflect a difference between the tissue types (mesophyll derived protoplasts versus epidermal cells) under study. As truncated forms of the reticulons are no longer confined to tubules but label the whole ER network, including the cisternae we conclude that a complete RHD, comprising all four transmembrane domains, is required for both efficient ER constriction and for partitioning to tubules and cisternal rims. This indicates that these transmembrane regions, and not the N and C terminal cytosolic regions, may be directly implicated in conferring the wedge-like shape that is likely to promote membrane curvature.

Thus, given that all 21 Arabidopsis RTN isoforms share a highly conserved RHD (Nziengui *et al.* 2007; Nziengui and Schoefs, 2009; Sparkes *et al.*, 2009b), the remaining members of this family are also likely to be ER tubule-dwelling proteins. However, in the case of RTNLB2 RHD truncations 3 and 4, which have a similar localisation pattern to the other RTN truncations and overlie the entire ER cisternae, they also, on rare occasions, have a propensity to constrict the cisternal ER into nodular clumps (Supplementary figure 5 on line). Since we have not tested RTNLB2 homotypic interactions, this could reflect differing levels of RTN interaction in the cell.

The requirement for a high level of membrane curvature is not restricted to the ER. Many organelles can have tubular extensions as seen in the case of plastid stromules (Kwok and Hanson, 2004), and peroxules and matrixules on peroxisomes and mitochondria (Scott *et al.*, 2007; Sinclair *et al.*, 2009, reviewed in Shibata *et al.*, 2009). Golgi cisternae also demonstate high degrees of curvature. Such curvature can be generated by a number of mechanisms (Shibata *et al.*, 2009) including the action of enzymes that bend membranes into tubules as suggested for plant dynamins at the phragmoplast (Fujimoto *et al.*, 2008). Proteins lying on the surface of a membrane, such as Bar domain proteins, can form crescent-shaped dimers on the bi-layer thereby curving the membrane (Suetsugu *et al.*, 2009). Others such as phospholipase A are thought to modify phospholipids into a wedge shape and insertion of these into in the outer leaflet of membranes such as the rims of Golgi cisternae increase the surface area of the outer leaflet as opposed to the inner thus inducing curvature (San Pietro *et al.*, 2009). It could be envisaged that the reticulons work by a similar mechanism (Voeltz *et al.*, 2006; Shibata *et al.*, 2009). This could result from the unusual length of each of their 4 transmembrane domains. Each of the four TMDs in the RHD most likely exceeds 20 amino acid residues in length (e.g. 24 residues for RTNLB13), which is at odds with the observed average TMD length of 17 residues for proteins that locate to the ER membrane (Brandizzi *et al.*, 2002). It is tempting to speculate that the extra length of the RTN membrane-spanning helices causes them to insert at an angle, ultimately conferring RTN the wedge-like topology that results in curvature.

We have shown that in the proteins studied here the C-terminal ER retention motif which is necessary for the retrieval of many escaped ER membrane proteins is not required for ER residence of RTN and further shown that the presence of the N-terminal half of the RHD is sufficient for ER localisation. Our FRET-FLIM data seem to indicate a general mechanism for ER retention that may depend on interactions between reticulons. The capacity of RTNLB1 to interact with itself, RTNLB2 and RTNLB4 has been previously inferred by yeast-2-hybrid assay and shown to require an intact RHD (Hwang and Gelvin, 2004). Our FRET/FLIM data extend and rationalise these findings *in vivo* in the context of RTN function and localisation. Homotypic interactions of RTNLB1 and RTNLB13 do not require a complete RHD, indicating that the presence of only a subset of TMD is sufficient for interaction and ER residence. However, as only full length reticulons are restricted to areas of high curvature and truncations even if they oligomerise, can insert into flat sheets, we hypothesise that the "W" topology combined with homo or heterotypic interactions are necessary for the induction of membrane curvature. However, the full role of RTN oligomerisation in plants remains to be addressed.

In summary our data distinguish between the capacity of RTN to localise to the ER, which does not require a complete RHD but may depend on RTN-RTN interactions, and the membrane-shaping properties of RTN,

which depend on the full RHD and also result in RTN partitioning to high-curvature ER membranes. Our data indicate a conserved location, topology, function and mechanism of residence for the five most abundantly expressed members of the Arabidopsis *RTN* gene family. Downregulation of RTNLB1, 2 or 4 by t-DNA insertion, antisense RNA or RNAi resulted in plants being less susceptible to Agrobacterium infection, but no obvious plant growth phenotype was observed, likely indicating high functional redundancy between these isoforms (Hwang and Gelvin, 2004). Accordingly, only a triple knockout of rtn1p, rtn2p (the two yeast RTN) and the structurally similar yop1p resulted in detectable loss of ER tubules in yeast (Shibata *et al.*, 2008). Even by invoking redundancy, however, it is somewhat difficult to explain the unique expansion of the RTN family in higher plants (Sparkes *et al.*, 2009b). It is tempting to speculate that, aside from the abundant, ubiquitously expressed RTNs we described in this work, less abundant isoforms are involved in shaping specific ER subdomains in particular tissues or cell types. Only the detailed mapping of the expression of these isoforms will shed light on this issue.

Materials and methods

Generation of RTN clones

The complete list of primers used in this study is shown in supplementary Table 1 on line.

RTNLB1-4 were cloned by RT-PCR using Superscript III one step RT-PCR platinum Taq HiFi kit (Invitrogen) from total RNA extracted from various Arabidopsis tissues using the Nucleospin RNA II kit (Macherey-Nagel). Using Gateway technology (Invitrogen) all cloned products were subsequently cloned into pDONOR 207 and then their respective binary vectors; eYFP fusions required pCAMBIA 1300 derived vectors (Sparkes *et al.*, 2005), roGFP2 fusions required pSS01 (Brach *et al.*, 2009) and pCM01 for N- and C-terminal fusions respectively. A new destination vector for N-terminal fusions to target proteins was created by PCR amplifying roGFP2 thereby adding a 5'-*SpeI* and a 3'-*EcoRV* restriction site. eGFP was replaced by roGFP2 in pK7WGF2,0 to give pCM01. N and C terminal mRFP (pB7WGR2, pB7RWG2) and eGFP (pB7WGF2, pB7FWG2) fusions required the respective vectors as listed here (Karimi *et al.*, 2002). RTNLB1-4 truncations were amplified from the respective pDONOR clone using primers detailed in supplementary Table 1 on line and then subsequently recombined into pDONOR 207 and then the destination vector. Binary clones were transformed into Agrobacterium tumefaciens *GV3101*.

The construction of RTNLB13-YFP has already been described (Tolley *et al.*, 2008). Deletion of the ER retention signal KKSE to generate RTNLB13ΔKKSE was performed by QuickChange mutagenesis using the primers described in supplementary Table 1 on line. All RTNLB13 constructs for BiFC analysis were generated in the vectors described by (Zamyatnin *et al.*, 2006) using the primers indicated in supplementary. Table 1 on line.

Plant material and transient expression system

Nicotiana tabacum (cv Petit Havana SR1) were grown as described (Sparkes *et al.*, 2005). Transient expression was carried out as described (Sparkes *et al.*, 2006). The final optical density at OD_{600} for GV3101 - containing Agrobacterium were as follows; GFP-HDEL 0.04, N and C terminal eYFP fusions to RTN 0.05, roGFP2 RTN

fusions 0.05 and 0.1, roGFP2 cytosolic and HDEL controls both at 0.03 and 0.05, GFP-CXN 0.04, CFP-SKL 0.04. All BiFC constructs were infiltrated at OD_{600} 0.05.

Sample preparation and imaging

Imaging was performed on a Zeiss LSM 510 (Meta) and on a Leica TCS SP5 using 63x or 100x oil immersion objective lenses. eYFP and GFP dual imaging was performed as described (Sparkes *et al.*, 2009a).

The roGFP2 used was as described in (Schwarzlander *et al.*, 2008; Brach *et al.*, 2009). Its oxidised and reduced form excited differently at 405/488nm, which correspond to the intracellular redox environment generated by glutathione. Ratiometric imaging was performed using a Zeiss LSM510 Meta confocal microscope with 63x oil immersion object lens. The roGFP2 was excited at 488nm and 405nm in multi-track mode with frame switching. Ratiometric analysis was performed using a custom written MATLAB script (kindly provided by Mark Fricker, Oxford University). The signal of each pixel from 405nm images was divided by the 488nm signal and the ratio was pseudo-colour coded to enable direct binary readout of the respective localisation of the roGFP2-tag in the cytosol or the ER lumen. As it is known that roGFP2 is reduced in the cytosol and oxidized in the lumen of ER, the calculated ratio of roGFP2-HDEL and free cytoplasmic roGFP2 were used to calibrate the scale (Meyer *et al.*, 2007; Brach *et al.*, 2009).

Leaf tissue was excised and approximately $5mm^2$ pieces were incubated in latrunculin b (2.5 or 25µm as stated, 1M stock dissolved in DMSO) or BFA (50 µg/ml, 5 mg/ml stock dissolved in DMSO) as stated.

Protease protection assay

4 - 8 Agrobacterium-infiltrated tobacco leaf sectors expressing the relevant construct were ground with a chilled mortar and pestle in 4 ml extraction buffer (10 mM KCl, 1 mM $MgCl_2$, 0.4 mM sucrose, 0.4% PVP, 40 mM HEPES.KOH, pH 7.5) for 3 minutes. The homogenate was transferred to two pre-chilled 2 ml Eppendorf tubes. The samples were centrifuged at 1000 ×g for 5 minutes at 4°C, and the supernatants transferred to a fresh tube on ice.A sucrose pad was set up in 4 ml ultracentrifuge tube. 750 µl of 20% (w/v) sucrose in extraction buffer was layered on top of 750 µl of 60% (w/v) sucrose in extraction buffer. Finally, 2 ml of sample was carefully added to the sucrose pad, and centrifuged at 55,000 rpm for 30 minutes at 4°C in a Beckman TL-100 ultracentrifuge.

The microsomes form an interphase between the 20% and 60% sucrose layers. The majority of the upper phase were removed by aspiration, and 200 µl of the microsomes recovered and gently re-suspended in a fresh tube. 25µl of the sample was pre-incubated with 20 mM $CaCl_2$, PK buffer (50 mM Tris.HCl pH 8.0, 1 mM $CaCl_2$) and Triton X-100 for 15 minutes on ice to ensure membranes are disrupted (Ma *et al.*, 2006), before adding the Proteinase K, and incubating at 30°C for 30 minutes. To terminate the reaction, one Complete-mini protease inhibitor cocktail tablet (Roche) was dissolved in 1ml sterile distilled water and 10 µl of this was added to each reaction tube. 60 µl of loading dye was added and the samples were boiled for 5 minutes before loading on a 15% SDS-PAGE. Immunoblot was performed with rabbt polyclonal anti-GFP antibodies (Clontech).

Bimolecular fluorescence complementation

Fusions were made of either residues 1 – 154 of YFP (termed YN) or residues 155 – 239 (termed YC) to either the N- or C-terminus, or the loop of RTNLB13 using conventional PCR, using pLH-YN, pLH-YC (Zamyatnin *et al.*, 2006) and myc-RTNLB13 (Tolley *et al.*, 2008) as templates. Primers were designed to add the restriction sites XhoI to the 5' end and XbaI to the 3' end of each construct (Supplementary Table 1 on line). For the insertion of YC in the loop region of RTNLB13, a fusion was made of residues 155 – 239 of YFP (termed YC) in between Val91 and Val92 of the central loop region of RTNLB13 using fusion PCR, using pLH-YC and myc-RTNLB13 as a template, respectively. Amplified fragments were cloned into the plant binary vector pLH7000 (Hausmann and Töpfer, 1999). The binary vector was then transformed in *Agrobacterium* strain C58 harbouring the pSoup helper plasmid (Hellens *et al.*, 2000). Reciprocal clones of each BiFC construct were also created, in order to test the efficiency of expression, yielding YN-RTN, YC-RTN, RTN-YN, RTN-YC and RTN-YC-RTN.

FRET-FLIM data acquisition

Tobacco leaf epidermal samples were excised and FRET-FLIM data capture was performed according to Osterrieder *et al.* using a 2-photon microscope at the Central Laser facility of the Rutherford Appleton laboratory with slight modifications (Osterrieder *et al.*, 2009). Briefly, a 2-photon microscopy was constructred around a Nikon TE2000-U inverted microscope using custom made XY galvanometers (GSI Lumonics) for the scanning system. Laser light at a wavelength of 920 ± 5 nm was obtained from a mode-locked titanium sapphire laser (Mira, Coherent Lasers Ltd) producing 180 fs pulses at 75 MHz, pumped by solid state continuous wave 532nm laser (Verdi V18, Coherent Laser Ltd). The laser beam was focused to a diffraction-limited spot through a water-immersion objective (Nikon VC x60, NA 1.2) and specimens illuminated at the microscope stage. Fluorescence emission was collected without descanning, bypassing the scanning system, and passed through a BG39 (Comar) filter to block the near infrared laser light. Line, frame and pixel clock signals were generated and synchronized with an external fast microchannel plate photomultiplier tube (MCP-PMT, Hamamatsu R3809U) used as the detector. These were linked via a Time-Correlated Single Photon Counting (TCSPC) PC module SPC830 (Becker and Hickl, Germany) to generate the raw FLIM data. Prior to FLIM data collection, the eGFP and mRFP expression levels in the plant samples within the region of interest (ROI) were confirm using a Nikon eC1 confocal microscope with excitation at 488nm and 543nm respectively. A 633nm interference filter was used to significantly minimise the contaminating effect of chlorophyll autofluorescence emission that would otherwise obscure the mRFP emission as well as that of eGFP.

Data was analysed by obtaining excited state lifetime values of a region of interest (ROI) on the nucleus were calculated using the SPCImage analysis software (Becker and Hickl). The distribution of lifetime values within the ROI were generated and displayed as a curve. Only values which had a χ^2 between 0.9-1.4 were taken. The median lifetime value and minimum and maximum values for a quarter of the median lifetime values from the curve were taken to generate the range of lifetimes per sample. At least 8 nuclei per RTN combination were analysed and the average of the ranges taken. Results are from two independent experiments.

Acknowledgements

We are grateful to Dr E.I. Savenkov for the gift of his BiFC vectors collection, and Dr. M. Fricker for the MATLAB script. IAS was funded on Leverhulme grant (F/00 382/G), IA and JS were funded on an Erasmus scheme from Heidelberg University and AO by BBSRC grant number BB/F008147/1. Work in the LF lab was supported in part by the European Union (LSH-2002-1.2.5-2 "Recombinant Pharmaceuticals from Plant for Human Health –Pharma-Planta") and by the Leverhulme Trust (grant F/00215/AP). NT was supported by a BBSRC studentship. Access to the Confocal Microscopy Laboratory at the Central Laser Facility, CCLRC Rutherford Appleton Laboratory, was made possible through a STFC Programme Access grant to CH.

Figure Legends

Figure 1. RTNLB1-4 colocalise to and constrict tubular ER

RTNLB1-eYFP (A-C, magenta), RTNLB2-eYFP (D-F, magenta), RTNLB3-eYFP (G-I) and RTN 4-eYFP (J-L) were transiently coexpressed with the ER lumenal marker GFP-HDEL (green) in tobacco leaf epidermal cells. All RTN isoforms constrict the ER resulting in pockets of lumenal content (arrowhead). Scale bar 2μm.

.

Figure 2. RTNLB1-4 and RTNLB13 preferentially localise to high-curvature ER membranes

A-L: RTN 1-eYFP (A-C, magenta), RTN 2-eYFP (D-F, magenta), RTNLB3-eYFP (G-I) and RTN 4-eYFP (J-L) were transiently coexpressed with GFP-CXN (green) in tobacco leaf epidermal cells. While RTN was present on ER tubules (arrowhead), the vast majority of it was confined to the rims of ER cisternae (asterisk). On occasion there seemed to be low levels or / and parallel tubules of RTN over the sheets (arrow). Unlike coexpression with an ER luminal marker, occasional fine tubular connections containing the ER membrane marker (GFP-CXN) were observed (arrowhead). Scale bars 2μm.

M-O: tobacco epidermal cells co-expressing RTNLB13-YFP (magenta) and GFP-HDEL were treated with 50 μg/ml BFA for 30 min. Note that RTNLB13 is enriched in ER tubules and in the rim of the BFA-induced ER sheets. Scale bar 5μm.

Figure 3. Determination of RTNLB1-4 and 13 topology through ratiometric imaging of roGFP2 fusions.

RoGFP2 fusions to RTNLB1-4 and 13 were transiently expressed in tobacco leaf epidermal cells and imaged with 405nm and 488nm to detect oxidised and reduced forms respectively. Ratiometric analysis of the reduced/oxidised forms are presented in the histogram where control for ER lumen and cytosol are indicated alongside the ratiometric scale bar (A). Representative ratiometric images for controls and RTNLB13 fusions are shown (B). Note, where T1 and T2 refer to truncations 1 and 2 (see Fig. 6a); RTNLB1 T1 (1-153aa), RTNLB2 T1 (1-150aa), RTNLB3 T1 (1-127aa), RTNLB4 T1 (1-132aa), RTNLB13 T1(1-93aa), RTNLB13 T2 (1-131aa).

Figure 4. Determination of RTNLB1-4 and 13 topology through protease protection

A-B: microsomes from tobacco epidermal leaves expressing the indicated constructs were subjected to proteinase K treatment in the presence or absence of Triton X-100. Microsomal proteins were solubilised,

resolved by SDS-PAGE and subjected to immunoblot with GFP antiserum. Numbers indicate molecular size in kDa.

C: tobacco epidermal cells were agroinfiltrated with the indicated expression construct combinations and visualised by confocal microscopy. Scale bar, 20 μm

The cartoons depict topological orientations of N and C terminal fusions for the protein fusion(s) under study.

Figure 5. RTNLB13 location to the ER is not dependent on its dylisine ER retention signal.

Tobacco epidermal cells were agroinfiltrated with RTNLB13ΔKKSE (magenta) and GFP-HDEL (green). Scale bar, 20 μm

Figure 6. RTN require a fully functional RHD to constrict the ER and constrain it to cisternal rims.

Truncations of RTNLB1-4 were generated containing either the amino terminus with the first stretch of hydrophobic sequence (two black boxes) without (truncation 1) or with (truncation 2) the predicted loop domain, or only the carboxy terminus with the second stretch of hydrophobic sequence with (truncation 3) or without (truncation 4) the predicted loop domain. The truncations were fused to eYFP (pink star) and the amino acids of each RTN fusion are shown (A). Note, each stretch of hydrophobic sequence is predicted, and has been shown experimentally here, to contain two TMD (black box). Images of tobacco leaf epidermal cells coexpressing RTNLB1 truncations 1-4 (T1-T4) with GFP-CXN are depicted (B). Scale bar 2μm.

Figure 7. FRET-FLIM analysis of RTNLB1 dimerisation in tobacco leaf epidermal cells.

RNLB1-eGFP (A-C) and coexpression with mRFP-RTNLB1 (D-H) in tobacco leaf epidermal cells were tested for interaction through FRET-FLIM. A region of interest on the ER continuous with the nuclear envelope was selected (A,D, see inset) based on the lifetime decay curves of points within the region having a χ^2 value between 0.9-1.4 (C,F). The lifetimes of the points within the selected region are diplayed (B,E) and psuedocoloured accordingly in A and D. Confirmation of coexpression of eGFP and mRFP RTNLB1 fusions are shown (G,H). The lifetime of the combination is more than 0.1ns lower than the donor fusion by itself indicating RTNLB1 dimerisation. Scale bar 5μm.

Table 1. FRET-FLIM lifetimes of RTN pairs.

Donor	Acceptor	Range of FLIM lifetimes (ns)	Average FLIM lifetime (ns)
RTNLB1-eGFP	-	2.3-2.4	2.35
RTNLB1-eGFP	mRFP-RTNLB1	2.1-2.2	2.15
RTNLB1-eGFP	RTNLB1-mRFP	2.1-2.2	2.15
eGFP-RTNLB1	-	2.3-2.5	2.4
eGFP-RTNLB1	mRFP-RTNLB1	2.1-2.2	2.15
eGFP-RTNLB1	RTNLB1-mRFP	2.1-2.3	2.2
RTNLB1 T1-eGFP	-	2.3-2.5	2.4
RTNLB1 T1-eGFP	RTNLB1 T1-mRFP	2.1-2.2	2.15
eGFP-RTNLB13	-	2.2-2.5	2.3
eGFP-RTNLB13	mRFP-RTNLB13	1.9-2.0	1.95
RTNLB13 T1-eGFP	-	2.3-2.4	2.35
RTNLB13 T1-eGFP	RTNLB13 T1-mRFP	2.0-2.2	2.1
eGFP-RTNLB1	mRFP-RTNLB3	2.1-2.3	2.2
eGFP-RTNLB1	mRFP-RTNLB4	2.1-2.3	2.2
eGFP-RTNLB13	mRFP-RTNLB3	2.1-2.2	2.15
eGFP-RTNLB13	mRFP-RTNLB4	2.0-2.1	2.05

References

Bernsel, A., Viklund, H., Falk, J., Lindahl, E., von Heijne, G., and Elofsson, A. (2008). Prediction of membrane-protein topology from first principles. Proc Natl Acad Sci USA **105,** 7177-7181.

Boevink, P., Martin, B., Oparka, K., Santa Cruz, S., and Hawes, C. (1999). Transport of virally expressed green fluorescent protein through the secretory pathway in tobacco leaves is inhibited by cold shock and brefeldin A. Planta **208,** 392-400.

Boevink, P., Oparka, K., Santa Cruz, S., Martin, B., Batteridge, A., and Hawes, C. (1998). Stacks on tracks: the plant Golgi apparatus traffics on an actin/ER network. Plant J. **15,** 441-447.

Brach, T., Soyk, S., Muller, C., Hinz, G., Hell, R., Brandizzi, F., and Meyer, A.J. (2009). Non-invasive topology analysis of membrane proteins in the secretory pathway. Plant J **57,** 534-541.

Brandizzi, F., Frangne, N., Marc-Martin, S., Hawes, C., Neuhaus, J.M., and Paris, N. (2002). The Destination for Single-Pass Membrane Proteins Is Influenced Markedly by the Length of the Hydrophobic Domain. Plant Cell **14,** 1077-1092.

Dreier, L., and Rapoport, T.A. (2000). In Vitro Formation of the Endoplasmic Reticulum Occurs Independently of Microtubules by a Controlled Fusion Reaction. J. Cell Biol. **148,** 883-898.

Fujimoto, M., Arimura, S., Nakazono, M., and Tsutsumi, N. (2008). Arabidopsis dynamin-related protein DRP2B is co-localized with DRP1A on the leading edge of the forming cell plate. Plant Cell Rep **27,** 1581-1586.

Hausmann, L., and Töpfer, R. (1999). Entwicklung von Plasmid-Vektoren. Pflanzenzücht **45,** 155-172.

Hellens, R.P., Edwards, E.A., Leyland, N.R., Bean, S., and Mullineaux, P.M. (2000). pGreen: a versatile and flexible binary Ti vector for Agrobacterium-mediated plant transformation. Plant Mol Biol **42,** 819-832.

Hu, J., Shibata, Y., Voss, C., Shemesh, T., Li, Z., Coughlin, M., Kozlov, M.M., Rapoport, T.A., and Prinz, W.A. (2008). Membrane proteins of the endoplasmic reticulum induce high-curvature tubules. Science **319,** 1247-1250.

Hwang, H.-H., and Gelvin, S.B. (2004). Plant proteins that interact with VirB2, the Agrobacterium tumefaciens pilin protein, mediate plant transformation. Plant Cell **16,** 3148-3167.

Karimi, M., Inze, D., and Depicker, A. (2002). Gateway vectors for Agrobacterium-mediated plant transformation. Trends in Plant Science **7,** 193-195.

Kwok, E.Y., and Hanson, M.R. (2004). Stromules and the dynamic nature of plastid morphology. J Microsc **214,** 124-137.

Ma, B., Cui, M.L., Sun, H.J., Takada, K., Mori, H., Kamada, H., and Ezura, H. (2006). Subcellular localization and membrane topology of the melon ethylene receptor CmERS1. Plant Physiol **141,** 587-597.

Meyer, A.J., Brach, T., Marty, L., Kreye, S., Rouhier, N., Jacquot, J.P., and Hell, R. (2007). Redox-sensitive GFP in Arabidopsis thaliana is a quantitative biosensor for the redox potential of the cellular glutathione redox buffer. Plant J **52,** 973-986.

Nziengui, H., Bouhidel, K., Pillon, D., Der, C., Marty, F., and Schoefs, B. (2007). Reticulon-like proteins in Arabidopsis thaliana: structural organization and ER localization. FEBS Lett **581,** 3356-3362.

Nziengui, H. and Schoefs, B. (2009). Functions of reticulons in plants: What we can learn from animals and yeasts. Cell Mol Life Sci **66**, 584-595

Oertle, T., Klinger, M., Stuermer, C.A.O., and Schwab, M.E. (2003). A reticular rhapsody: phylogenic evolution and nomenclature of the RTN/Nogo gene family. FASEB J. **17,** 1238-1247.

Osterrieder, A., Carvalho, C.M., Latijnhouwers, M., Johansen, J.N., Stubbs, C., Bothchway, S., and Hawes, C. (2009). Fluorescence lifetime imaging of interactions between Golgi tethering factors and small GTPases in plants. Traffic **10,** 1034-1046.

Ridge, R.W., Uozumi, Y., Plazinski, J., Hurley, U.A., and Williamson, R.E. (1999). Developmental transitions and dynamics of the cortical ER of Arabidopsis cells seen with green fluorescent protein. Plant & cell physiology **40,** 1253-1261.

Runions, J., Brach, T., Kuhner, S., and Hawes, C. (2006). Photoactivation of GFP reveals protein dynamics within the endoplasmic reticulum membrane. J Exp Bot **57,** 43-50.

San Pietro, E., Capestrano, M., Polishchuk, E.V., DiPentima, A., Trucco, A., Zizza, P., Mariggio, S., Pulvirenti, T., Sallese, M., Tete, S., Mironov, A.A., Leslie, C.C., Corda, D., Luini, A., Polishchuk, R.S. (2009). Group IV phospholipase A(2)alpha controls the formation of inter-cisternal continuities involved in intra-Golgi transport. PLoS Biol **7**, e1000194.

Schwarzlander, M., Fricker, M.D., Muller, C., Marty, L., Brach, T., Novak, J., Sweetlove, L.J., Hell, R., and Meyer, A.J. (2008). Confocal imaging of glutathione redox potential in living plant cells. Journal of microscopy **231,** 299-316.

Scott, I., Sparkes, I.A., and Logan, D.C. (2007). The missing link:inter-organellar connections in mitochondria and peroxisomes? Trends in Plant Science **12,** 380-381.

Shibata, Y., Hu, J., Kozlov, M.M., and Rapoport, T.A. (2009). Mechanisms shaping the membranes of cellular organelles. Annual Review of Cell and Developmental Biology **25,** 329-354.

Shibata, Y., Voss, C., Rist, J.M., Hu, J., Rapoport, T.A., Prinz, W.A., and Voeltz, G.K. (2008). The reticulon and DP1/Yop1p proteins form immobile oligomers in the tubular endoplasmic reticulum. J Biol Chem **283,** 18892-18904.

Sinclair, A.M., Trobacher, C.P., Mathur, N., Greenwood, J.S., and Mathur, J. (2009). Peroxule extension over ER-defined paths constitutes a rapid subcellular response to hydroxyl stress. Plant J **59,** 231-242.

Sparkes, I.A., Hawes, C., and Baker, A. (2005). AtPEX2 and AtPEX10 are targeted to peroxisomes independently of known endoplasmic reticulum trafficking routes. Plant Physiol **139,** 690-700.

Sparkes, I.A., Runions, J., Kearns, A., and Hawes, C. (2006). Rapid, transient expression of fluorescent fusion proteins in tobacco plants and generation of stably transformed plants. Nat Protoc **1,** 2019-2025.

Sparkes, I.A., Runions, J., Hawes, C., and Griffing, L. (2009a). Movement and remodelling of the endoplasmic reticulum in nondividing cells of tobacco leaves. Plant Cell**,** 10.1105/tpc.1109.072249.

Sparkes, I.A., Frigerio, L., Tolley, N., and Hawes, C. (2009b). The plant endoplasmic reticulum: a cell-wide web. Biochem J **423,** 145-155.

Sparkes, I.A., Ketelaar, T., Ruijter, N.C., and Hawes, C. (2009c). Grab a Golgi: laser trapping of Golgi bodies reveals in vivo interactions with the endoplasmic reticulum. Traffic **10,** 567-571.

Stephenson, J.L.M., and Hawes, C.R. (1986). Stereology and stereometry of endoplasmic reticulum during differentitation in the Maize root cap. Protoplasma **131,** 32-46.

Suetsugu, S., Toyooka, K., and Senju, Y. (2009). Subcellular membrane curvature mediated by the BAR domain superfamily proteins. Semin Cell Dev Biol. 10.1016/j.semcdb.2009.12.002

Tolley, N., Sparkes, I.A., Hunter, P.R., Craddock, C.P., Nuttall, J., Roberts, L.M., Hawes, C., Pedrazzini, E., and Frigerio, L. (2008). Overexpression of a plant reticulon remodels the lumen of the cortical endoplasmic reticulum but does not perturb protein transport. Traffic **9,** 94-102.

Voeltz, G.K., Prinz, W.A., Shibata, Y., Rist, J.M., and Rapoport, T.A. (2006). A class of membrane proteins shaping the tubular endoplasmic reticulum. Cell **124,** 573-586.

Winter, D., Vinegar, B., Nahal, H., Ammar, R., Wilson, G.V., and Provart, N.J. (2007). An 'Electronic fluorescent pictograph' browser for exploring and analyzing large-scale biological data sets. PLoS one **2,** e718.

Zamyatnin, A.A., Jr., Solovyev, A.G., Bozhkov, P.V., Valkonen, J.P., Morozov, S.Y., and Savenkov, E.I. (2006). Assessment of the integral membrane protein topology in living cells. Plant J **46,** 145-154.

FIG 1 Sparkes et al

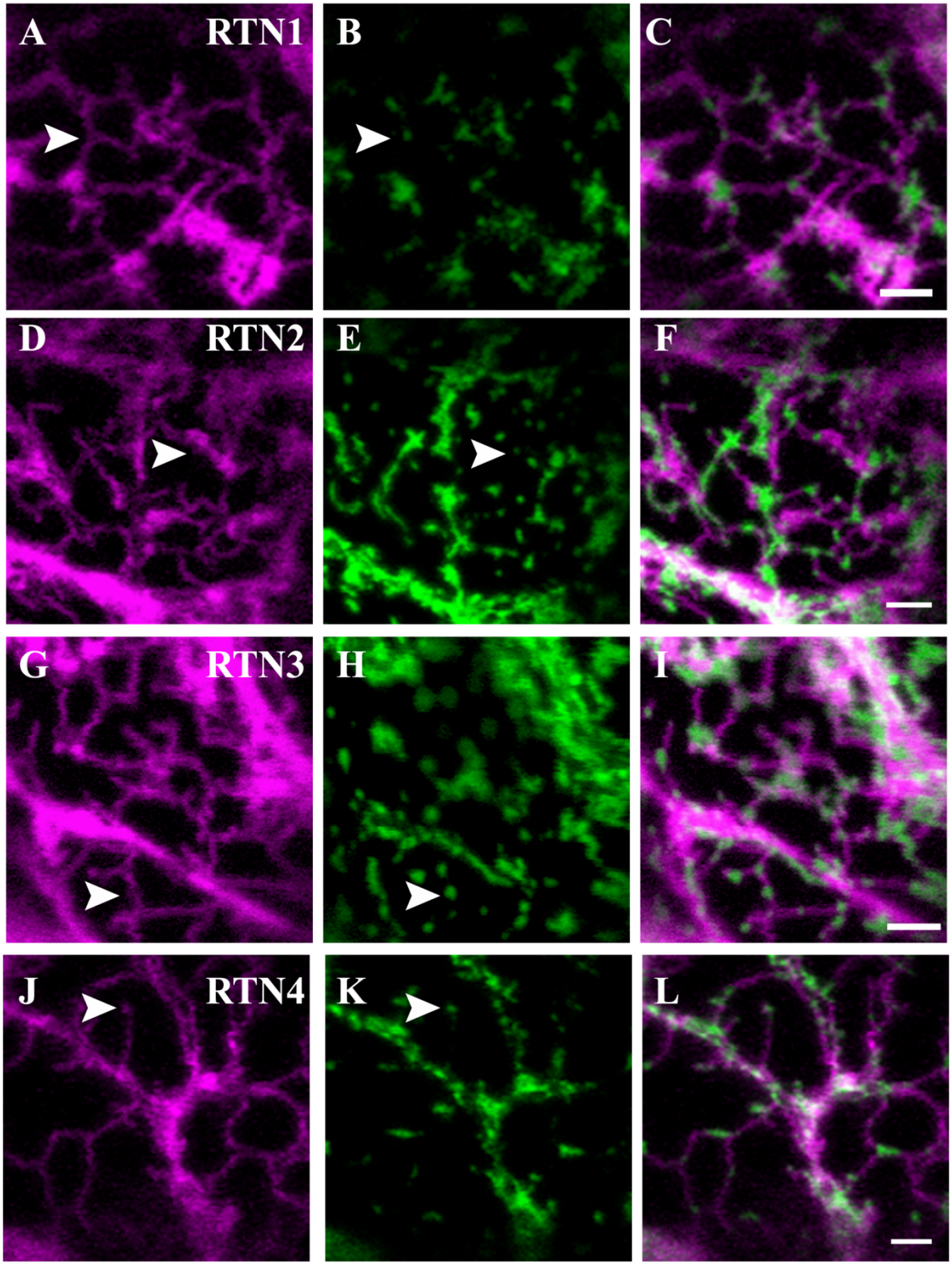

FIG 2 Sparkes et al

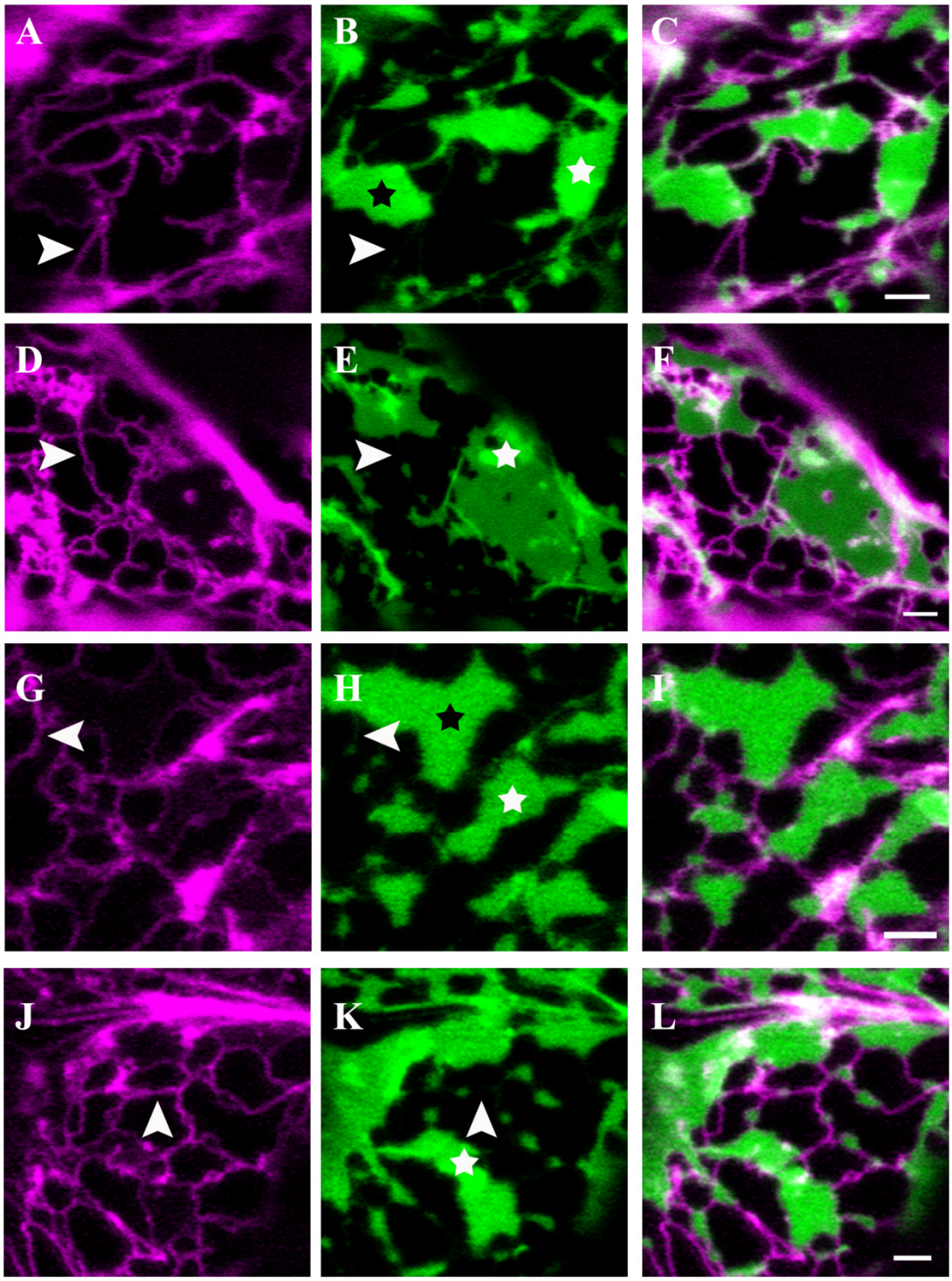

Figure 3 Sparkes et al

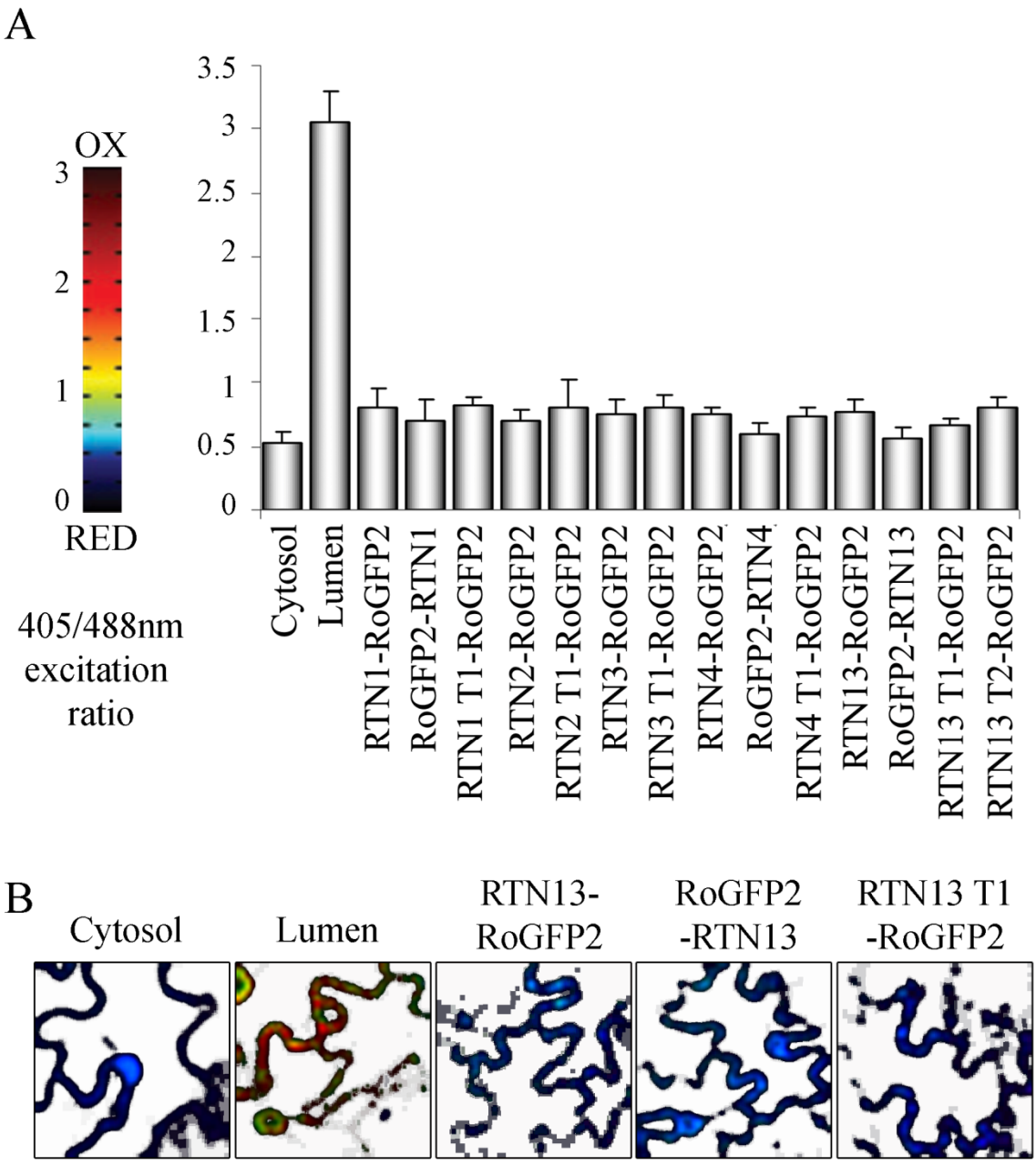

Figure 4 Sparkes et al

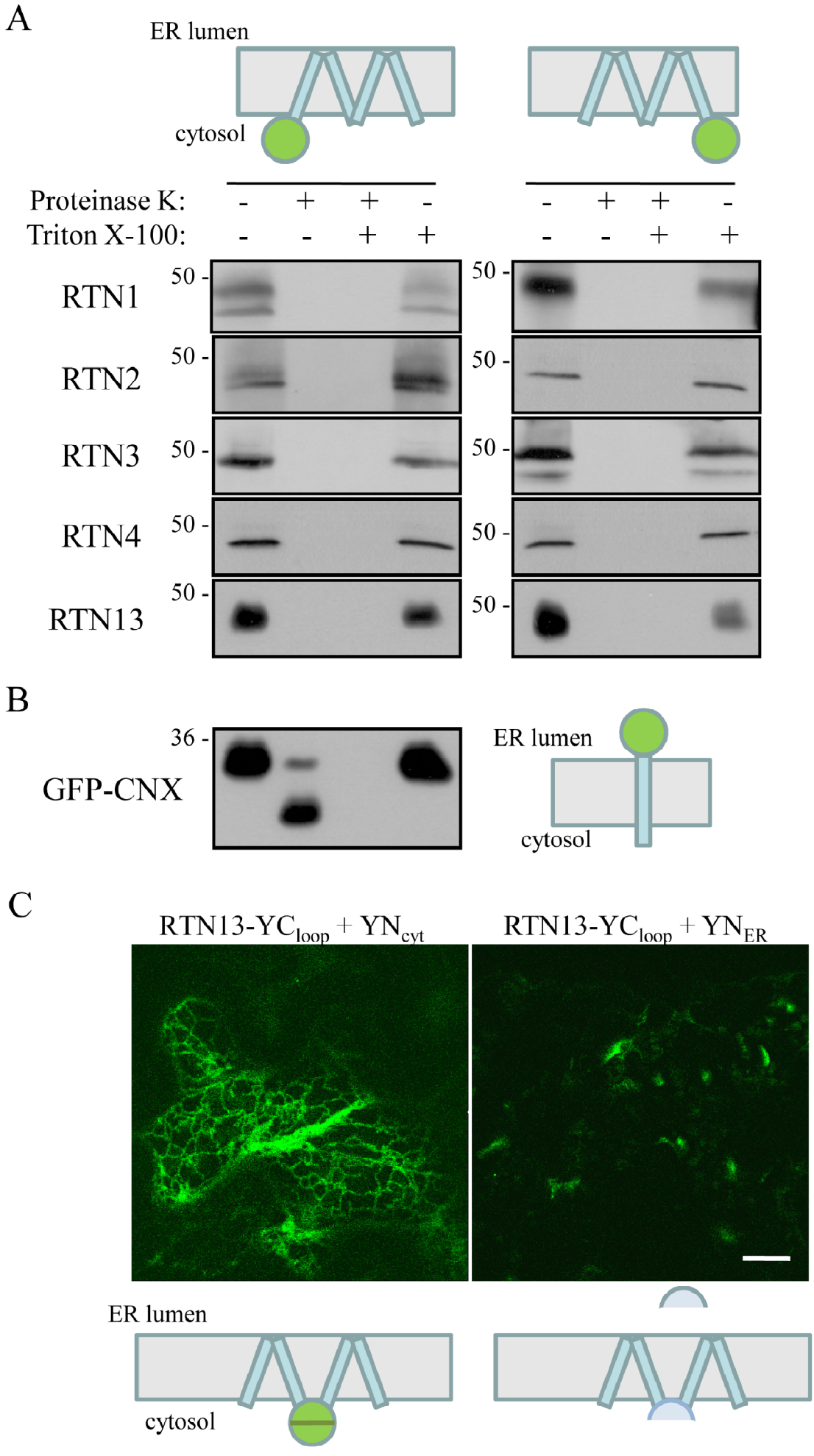

Figure 5 Sparkes et al

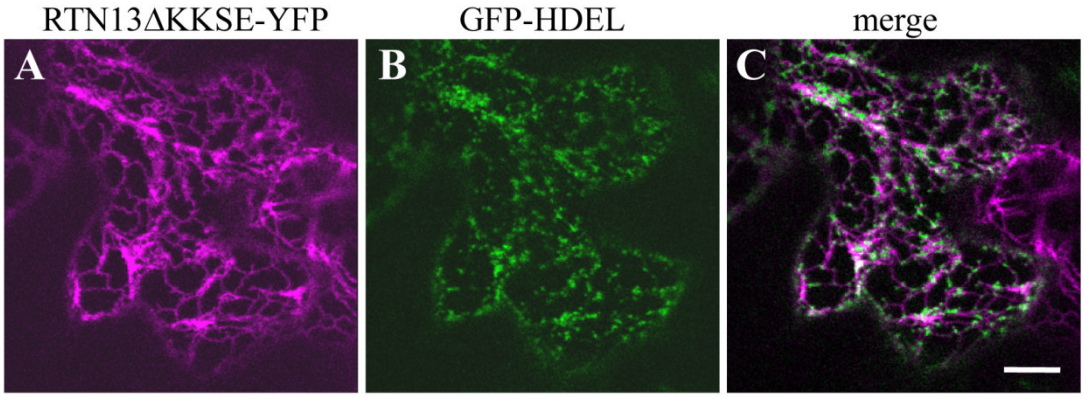

Figure 6 Sparkes et al

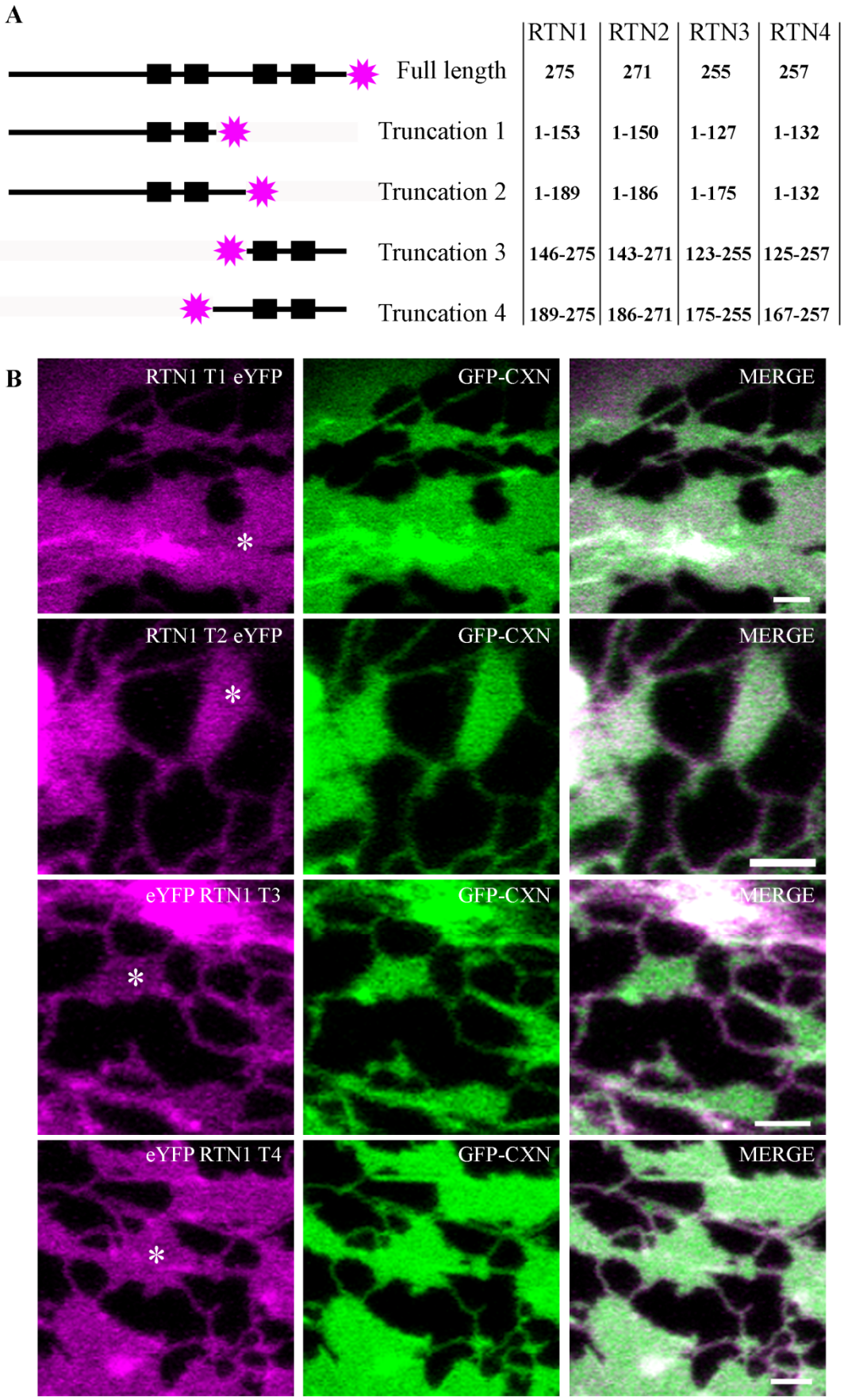

Figure 7 Sparkes et al